HOMOGENEOUS CATALYSTS FOR THE SYNTHESIS OF OXYGENATED POLYMERS

Arnaud Aurélien Thevenon

A thesis submitted in partial fulfilment of the requirements for the degree of Doctor of Philosophy in Inorganic Chemistry

Trinity College

Department of Inorganic Chemistry

University of Oxford

November 2017

“Nullum magnum ingenium sine mixtura dementiae fuit”

Seneca

To all my family and friends

Declaration

The work presented in this thesis was conducted in the Department of Chemistry, Imperial College London, between July 2014 - September 2016 and in the Department of Inorganic Chemistry, University of Oxford, between September 2016 - November 2017. This is the work of the author unless otherwise stated.

Abstract

This thesis describes the synthesis and characterisation of novel mono and dinuclear homogenous [Zn(II)] and [In(III)] metal complexes. Their applications as catalysts for CO_2/epoxide or epoxide/anhydride ring opening copolymerisation and lactide ring opening polymerisation to generate polycarbonates and polyesters, respectively, are also reported.

Chapter 3 reports the first indium phosphasalen catalysts for CO_2/cyclohexene oxide ring opening copolymerization. The catalysts are active at 1 bar pressure of CO_2 and are most effective without any co-catalyst. It is also possible to use the complexes to isolate and characterise the key intermediates in the catalytic cycle. Kinetic and spectroscopic analyses show that polymerisation proceeds via a rare *cis*-mononuclear coordination-insertion mechanism.

Chapter 4 describes a series of mono and dinuclear zinc macrocycle catalysts with very high activities for the *racemic* lactide ring opening polymerisation. In most cases, the dinuclear zinc catalysts significantly out-perform the mono-zinc homologue. In addition, kinetic and spectroscopic investigations suggest a role for the ligand conformation in mediating rate. The catalysts perform very well under immortal conditions and operate at low catalyst loading, whilst conserving high activities.

Chapter 5 presents four dinuclear zinc acetate salen catalysts for the ring opening copolymerisation of CO_2/cyclohexene oxide and phthalic anhydride/cyclohexene oxide. The catalysts show moderate activities for CO_2/epoxide copolymerisation but are highly active for epoxide/anhydride copolymerisation. Structure/activity relationship studies reveal that the more flexible and electron donating ligand displays the highest activity. Poly(ester-*b*-carbonate)s are also afforded using the most active catalyst in terpolymerisations of anhydride/epoxide/CO_2.

Acknowledgements

First of all and foremost, I would like to thank my supervisor, Prof Charlotte Williams, for giving me the opportunity to work in her group over the past three years. I could not have wished for a better mentor. She has always trusted in my capacity of carrying out research and has provided me the support to thrive professionally. Her daily advices on my research and my future professional career have been invaluable and will form the basis of my scientific career.

The success of this thesis would not have being possible without the amazing post-docs and D-Phil team of the Williams group (past and present). A special thanks to Dr Charles Romain who has played the "*avocat du diable"* during all my D-Phil to provide constructive criticism of my work. Your help was invaluable. I would also like to express my gratitude to Dr Jenni Garden, Dr Anish Cyriac and Dr Valentin Poirier for all their expertise, supervision and whom I really enjoyed working with. Thanks to the rest of the post doc team: Sumesh, Andrés, Giulia, Chris, Frank, Guun, Prabhjot, Clare, Dom, Seb, Leticia, Jason, Neil and Yoni, you all have been great colleagues. Also a huge thanks to the rest of the Williams group, especially to all the members of the CO_2/epoxide catalysts development sub-group, I am so grateful for your support. Thanks to Gemma, Arron, Charlie, Alice, Peck, Ni, Jameel, Tim, Tom, Rachel, Matt, Shyeni, Said and Greg. I am going to miss you all as well as the tea breaks, cakes, evening drinks, squash games and cross fit training.

I am also grateful to a number of other people who have made uncountable contributions to the work presented in this thesis. First of all, I would like to thanks Prof Sally Brooker, Hannah Davidson and Michael Bennington for the exceptional collaboration, I really enjoyed working with you. I am also grateful to Dr Andrew White who analysed and

solved all my crystals at Imperial College London and to Dr Amber Thompson and Dr Kirsten Christensen for teaching me the “art” of running single crystal X-ray crystallography experiments and solving the structures at the University of Oxford. I would also like to thanks Dr Peter haycock and Dr Nick Rees who have helped me with countless NMR experiments over the years. I am also grateful to Dr Lisa Haigh for her help in mass spectrometry and Stephen Boyer for elemental analyses.

A massive thank to all my family and friends who have been there for me and supported me throughout my D-Phil. Particularly to my lovely girlfriend, Nicole, who took the difficult choice to follow me to London and later to Oxford. You have always encouraged me to pursue my dreams and cheered my every day. I am so grateful for your support and will never forget what you did for me. Thanks to my grand-parents papy-Paul, Simone and papy-Jean, my parents Patrick and Marie-Andrée, my brother Julien and his family: Faustine, Nathael, Lucien and “future numéro 3” for always being present and believing in me. Finally to all my friends, especially to Nicolas, Pascal, Stephen, Charles “Belge”, Alexandre, Leonard, Mickaël and people from the MCR of Trinity College for all the fun times during the past three years.

Finally, I would like to acknowledge the funding and support from Climate-KIC in carrying out this research. Climate-KIC is supported by the European Institute of Innovation and Technology (EIT), a body of the European Union.

List of publications

Publications in Peer-Reviewed Journals

1. *Di-Zinc Macrocycles: CO_2 Insertion and Structure/Selectivity Relationship in Oxygenated Polymerization Catalysis*
   A. Thevenon; C. Romain; G. Rosetto; H. J. Davidson; A. J. P. White; S. Brooker; C. K. Williams; *Dalton Trans.* (in preparation)

2. *Indium Phosphasalen Catalysts for Low-Pressure CO_2/Epoxide Copolymerization: Evidence of an Unexpected Mononuclear Pathway?*
   A. Thevenon; A. Cyriac; D. Myers; A. J. P. White; C. B. Durr; C. K. Williams; *J. Am. Chem. Soc.* (submitted)

3. *Comparing Yttrium phosphasalen and salen initiators for stereoselective rac-lactide polymerizations*
   A. Cyriac; D. Myers; G. Trott; C. Coleman; A. Thevenon; A. J. P. White; C. K.Williams., *Chem. Sci.* (submitted)

4. *Dizinc Lactide Polymerization Catalysts: Hyperactivity by Control of Ligand Conformation and Metallic Cooperativity*
   A. Thevenon; C. Romain; M. S. Bennington; A. J. P. White; H. J. Davidson; S. Brooker; C. K. Williams; *Angew. Chem. Int. Ed.*, **2016**, 55, 8680-8685.

5. *Dinuclear Zinc Salen Catalysts for the Ring Opening Copolymerization of Epoxides and Carbon Dioxide or Anhydrides*
   A. Thevenon; J. A. Garden; A. J. P. White; C. K. Williams; *Inorg. Chem.* **2015**, 54, 24, 11906-11915.

Additional Publications:

1. *Dinuclear metal complex-mediated formation of CO_2-based polycarbonates*
   C. Romain, A. Thevenon, P. K. Saini and C. K. Williams, *Topics in Organometallic Chemistry: Carbon Dioxide and Organometallics*, **2015**, 101-141.

List of Abbreviations

Ad	adamentane
Ar	aryl
ATR-FTIR	fourier transform infra-red
BDI	β-diiminate
BnOH	benzyl alcohol
CHD	cyclohexan-1,2-diol
CHO	cyclohexene-oxide
CHC	cyclic cyclohexene carbonate
COSY	correlated spectroscopy
COPO	meso-3,4-epoxy tetrahydrofuran
Conv.	conversion
CPO	cyclopentene oxide
CTA	Chain Transfer Agent
CXO	4-dimethyl-3,5,8-trioxabicyclo[5.1.0]octane
D	diffusion coefficient
Đ	dispersities
1D	one-dimensional
2D	two-dimensional
3D	three-dimensional
DCM	dichloromethane
$\Delta G^{\neq}$	activation Gibbs energy
DFT	density functional theory
dipp	2,6-diisopropylphenyl
DMAP	4-dimethylaminopyridine

DMC	double metal cyanide
DMSO	dimethyl sulfoxide
DOSY	diffusion-ordered spectroscopy
$\overline{DP}$	degree of polymerisation
ee	enantiomeric excess
ε-CL	ε-caprolactone
equiv.	equivalent
Et	ethyl
η	viscosity
[Et_4NX]	tetraethylammonium salt
[$EtPh_3PX$]	methyltriphenylphosphonium salt
ESI	electronspray analysis
EtOH	ethanol
GPE	glycydil phenyl ether
HMBC	heteonuclear multiple-bond coherence
HSQC	heteronuclear single quantum coherence
I	iso dyad
IPA	isopropanol
^{i}Pr	isopropyl
IR	infrared
k_b	Boltzmann constant
k_{ex}	exchange rate constant
k_i	initiation rate constant
k_{iso}	isomerisation rate constant
K_m	Michaelis constant

k_{obs}	observed rate constant
k_p	propagation constant
L	ligand
λ	wave length
LA	lactide
LC-MS	liquid chromatography mass spectrometry
LHS	left hand side
LO	limonene oxide
m	meso dyad
M	Lewis acidic metal center
MALDI-ToF	Matrix-Assisted Laser Desorption/Ionisation - Time of Flight
Me	methyl
MeCN	acetonitrile
MeOH	methanol
M_n	number of average molar mass
$M_{n(cld)}$	calculated number of average molar mass
$M_{n(exp)}$	experimental number of average molar mass
MS	mass spectrometry
M_w	mass average molar mass
MW	molecular weight
n	number of mol
N-MeBzIm	1-methylbenzimidazole
N-MeIm	N-methyl imidazole
NMR	Nuclear Magnetic Resonance
NOE	nuclear Overhauser effect

NO_3	nitrate
Nu	nucleophile
OAc	acetate
OMe	methoxy
o-vanillin	ortho-vanillin
PC	polycarbonate
PCHC	poly(cychlohexene carbonate)
PCL	poly(ε-caprolactone)
Ph	phenyl
P_i	probability of isotactic enchainment
PLA	polylactide
Pm	probability to have a meso-centred tetrad
PPC	Poly(propylene carbonate)
ppm	party per million
[PPN-X]	bis(triphenylphosphine)iminium salt
Pr	propyl
PTMC	poly(trimethylene carbonate)
Pyr	pyridine
r	hydrodynamic radius
rac	racemic
R.d.s	rate determining step
RHS	right hand side
ROP	ring opening polymerisation
ROCOP	ring opening copolymerisation
ROESY	rotating frame overhause effect Spectroscopy

s	hetero dyad
sec	second
SEC	size exclusion chromatography
SO	styrene oxide
t	time
T	temperature
τ	structural parameter
^{t}Bu	tert-butyl
THF	tetrahydrofuran
TMC	trimethylcarbonate
ToF	time of flight
TOF	turnover frequencies
TON	turnover number

List of Figures, Schemes and Tables

Chapter 1

Chapter 2

Chapter 3

Chapter 4

Table of Contents

CHAPTER 1

Introduction

1.1. Introduction to Bio-Derived Polymers

Polymers are ubiquitous throughout society. Their properties are highly varied and can be tuned to meet the requirements for a range of applications. They are used in packaging, automotive, aeronautics, consumer goods, construction, textiles, agriculture, medical, electrical and many more industries. The global production of polymer worldwide has been estimated to have exceeded 300 million metric tonnes in 2015, with growth expected at 1.5 - 3.5 % per annum (Figure 1.1).[1]

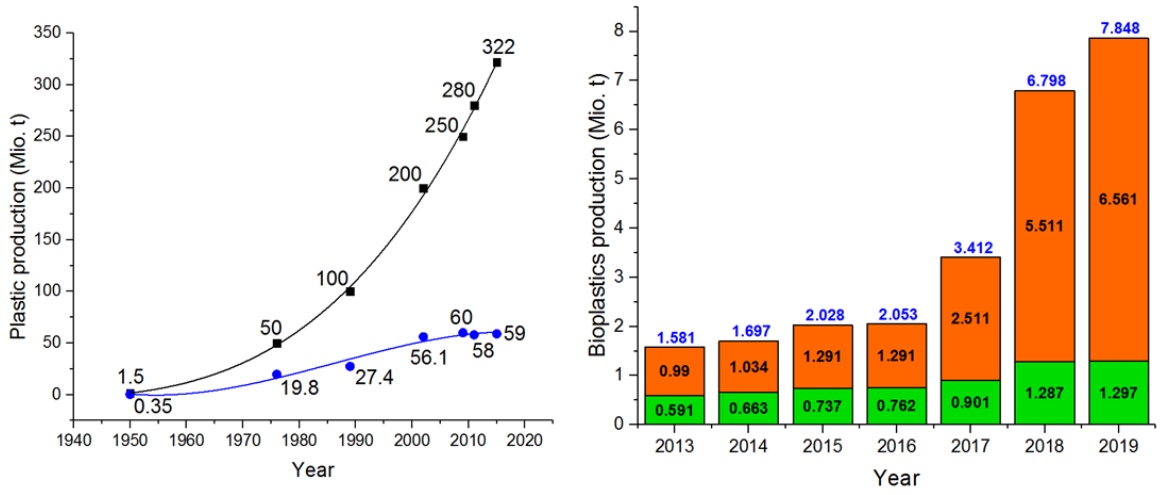

Figure 1.1. LHS: world global plastic production (■) and European global plastic production (●);[1a] RHS: total bio-derived polymer production in 2013 and 2014 and the expected growth. The lower part (green) of the stacked column represents the production of biodegradable bio-based polymers and the upper part (orange) represents the production of non-biodegradable bio-based polymers.[1b]

From an environmental point of view, the production of many existing materials is not particularly sustainable.[2] Most of the starting materials are petrochemically-derived. The proportion of oil and gas used in the polymer industry is low (~ 8 % in Europe) compared to the transport industry (~ 65 %).[3] Nevertheless, with the depletion of oil, it is likely important to increase the use of renewable feedstocks. Additionally, there are major concerns about the end-life fate of conventional plastics: most waste plastics end in landfill where they are bulky and pervasive, whilst only a small portion of plastics can be recycled.[2] A global analysis of total plastics production (from production to use, and to end life) have come to the conclusion that out of the 8300 millionmetric tons (Mt) of

plastics produced between 1905 and 2015, 2500 Mt are currently in use, 4900 Mt have been discarded (either in landfills or the natural environment), 800 Mt have been incinerated, and only 600 Mt have been recycled (~ 9 % of the global plastic production).[4] Almost all current plastics are non-biodegradable and this is a major cause of pollution across the world. Their impact on the earth's geology and ecosystems is potentially irreversible. There is, therefore, an urgent need for the development of alternative that deliver equivalent properties but with a managed end-of-life pathway.[5]

The demand of bio-derived polymers is rapidly growing. Bio-derived polymers are defined as polymers made using monomers derived from biomass.[2] They may be bio-derived but non-biodegradable or bio-derived and biodegradable. Biodegradable polymers have the properties suitable for single applications where recycling is not feasible (e.g. packaging, disposal medical products, disposable consumer goods). A number of biodegradable polymers, such as polylactide (PLA), are already commercially available.[6]

On the other hand, there is also a rapid growth of the so called "drop in" plastics such as bio-polyethylene and bio-polyethylene terephthalate to move away from petrochemically derived monomers.[7] It is worth emphasising that these polymers are not biodegradable but are made from renewable resources. Current estimation foresees that by 2020, ~ 80 % of polymers will be bio-derived but non-biodegradable.[1b]

1.2. Polycarbonate

1.2.1 Generality

Polycarbonates contain repeating carbonate [-C-C(O)-O-] linkages (Scheme 1.1). They are an important class of polymers used in a variety of commodity products such as rigid plastics (e.g. in furniture, automotive, packaging etc.), elastomers (clothing, films, adhesives) and fibres (textile).[8] The major product derives from bis(phenol) A and is industrially produced on a 5 Mt scale every year. More generally, polycarbonates can be divided into two groups: bis(phenol) A based polycarbonates (BAPC) and aliphatic polycarbonates.

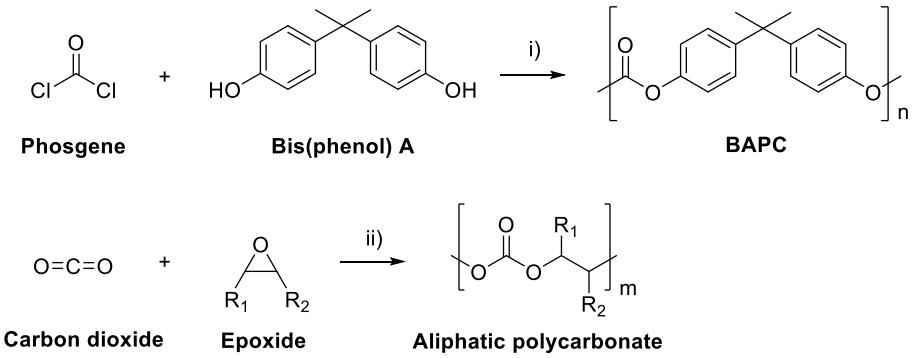

Scheme 1.1. Illustration of the two different families of polycarbonates and their corresponding polymerisation reaction. i) NaOH; ii) catalyst.

BAPC are important industrially and are made from the copolymerisation of bis(phenol) A and phosgene, often using a base catalyst (NaOH). On the other hand, the industrial production of aliphatic carbonate is very much smaller.[9] This may be due, in part, to difficulties in polymers synthesis. Recently, the development of efficient catalysts for CO_2/epoxide ring opening polymerisation (ROCOP),[10] cyclic carbonate ring opening polymerisation (ROP)[11] and polycondensation[6] may facilitate the controlled synthesis of aliphatic polycarbonates.

The production of aliphatic polycarbonate from CO_2/epoxide ROCOP has attracted considerable attention due to the potential economic and environmental benefits by the

adding value to the waste CO_2.[12] Life cycle analysis indicates that there are clear advantages to using these materials compared to polyether polyols, including reductions of ~ 20 % in fossil fuels and carbon dioxide emissions with only 40 % CO_2 uptake.[13] Additionally, carbon dioxide capture from flue gas and CO_2 contaminated gas stream can successfully be applied in the polymerisation.[14]

Within the class of CO_2-based polycarbonate, the copolymerisation of carbon dioxide with the commodity chemical propylene oxide (PO) receives significant of industrial interest.[15] Its mechanical and thermal properties make it an elastomer (*vide infra)*: poly(propylene carbonate) (PPC) is already produced at a 100 000 ton/year scale.[15] Poly(cyclohexene carbonate) (PCHC) is only produced on a small scale industrially and has properties typical of a rigid plastic.[16] The monomer, CHO, is produced on a large scale industrially but is consumed by the chemical industry as an important intermediate in agrochemicals and other sectors.[17] Thus CHO is not currently available on the scale (or cost) of PO.

1.2.2 Properties of CO_2 Based Polycarbonate

The macroscopic properties of CO_2-derived polycarbonates can be controlled by the CO_2 content, the nature of epoxide, the molecular weight of the polymer and the regio/ stereocontrol.[18] Table 1.1 compares the general properties of the two most common CO_2-based polycarbonates (PPC and PCHC) with a fully renewable CO_2-based polycarbonate [poly(limonene carbonate), PLimC] and BAPC.

Table 1.1. General properties of BAPC, PPC, PCHC and poly(limonene carbonate) (PLimC).

Property	**MW** (kDa)	***Đ***	T_g (°C)	**Young's Modulus** (MPa)	**Tensile strength** (MPa)	**Elongation at break** (%)	T_d**-5 %** (°C)
BAPC[19]	45	-	145	2500	65	125	458
PPC[12c]	50-360	1.7-2.8	30-41	700-1400	7-30	330	200-240
PCHC[16]	42	6.0	112-115	3600	43	2	240-280
PLimC[a,19]	25-109	1.1-1.2	130	950	55	15	240

PPC and PCHC are usually amorphous polymers with a glass transition temperatures (T_g) of 30-40 ^{o}C (PPC) and 80-115 ^{o}C (PCHC) and a decomposition temperature (T_d-5 %) of ~ 230 ^{o}C and ~ 300 ^{o}C, respectively.[12c] The T_g is highly dependent on the carbonate content and proportion of ether linkages. Higher T_g values are achieved with iso-enriched PCHC (P_m = 0.82, T_g = 125 ^{o}C).[20] Changing the epoxide to indene oxide or dimethyl substituted dioxaepoxide (CXO) results in significant improvement of the thermal properties of the resulting polycarbonate (T_g = 134 ^{o}C and T_g = 140 ^{o}C, respectively) approaching that of the polycarbonate prepared form bis(phenol) A (T_g = 145 ^{o}C).[20a, 21] For the CXO, an isotactic polymer (PCXC) with > 99 % enantioselectivity and high crystallinity was prepared, exhibiting a melting temperature (T_m) of 340 ^{o}C.[20a, 21]

The mechanical properties of CO_2-based polycarbonate also depend on the microstructure of the polymer and vary to a large extent depending on the catalyst and the conditions used during the polymerisation.[12c] For example, a PPC with M_n = 50 kDa and a T_g = 40 ^{o}C exhibits a Young's modulus, at room temperature, of 830 MPa with an elongation at break of 330 % and a tensile strength of 21 MPa.[22] On the other hand, PCHC is a rigid plastic with an elongation at break of 1-2 % but its Young's modulus at room temperature (3,600 MPa) is much higher than the corresponding value for BAPC (2,400 MPa).[16]

1.2.3 Applications

PPC has a moderate/high elongation at break and is an elastomer. It has been applied as a (inorganic) fillers or in blends with other polymers for use in packaging, without loss of toughness.[23] BASF and Siemens developed an alternative to the widely used styrene-based acrylonitrile-butadiene-styrene (ABS) by blending polyhydroxybutyrate with PPC.[23] Empower Materials is using PPC as a sacrificial binder for high quality products in powder metals, sealing glasses and advanced ceramics.[23] PPC has also been investigated as a packaging material and adhesive,[24] an organic filler in containers,[12c] as

a flame-retardant materials via incorporation of phosphorous groups,[25] and medical in dressings and as a tissue scaffold material.[26]

PCHC has a more limited range of applications, but α,ω-hydroxyl-terminated PCHCs show significant promise in dry powder coatings as a scratch resistant coating with high transparency.[27]

Hydroxyl-end capped polycarbonates are most commonly used as macro-initiators for the synthesis of polyurethane (PU).[28] In the case of PPC, its low molecular weight polyol acts as soft blocks in PU. Synthesis is particularly important for the production of rigid and flexible foams.[28]

Post modifications of polycarbonates bearing terminal (at the end of the polymer chain)[29] or pendant (along the backbone) functional groups (e.g. alkenyl, carbonate or hydrophilic group)[30] have recently been investigated by both academic and industrial research groups. These polymers have shown promising performances as coating resins,[27, 31] polymeric nanoparticles,[32] electronic[32] and biomedical materials.[10b]

1.2.4 Bio-based Epoxides

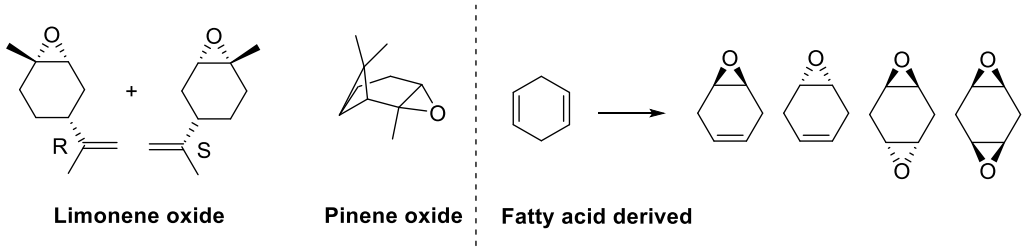

Figure 1.2. Illustration of some bioderived epoxides used for CO_2/epoxide copolymerisation.

Fully renewable polycarbonates can be synthesised from epoxides that are derived from the terpene family such as from limonene or pinene (Figure 1.2, LHS).[6, 33] PLimC has properties showing promise as a resistant and hard dry-powder coating (by crosslinking the pendant alkene functional group of the limonene moiety).[34] Highly crystalline

stereocomplexes from PLimC have better thermal properties [higher degradation temperature (265 °C)] than analogues of lower crystallinity.[35]

Our group, in collaboration with the group of Meier, have reported the preparation of various epoxides derived from vegetable oils containing unsaturated groups and their copolymerisation with CO_2 to prepare fully bio-based functionalised polycarbonates (Figure 1.2, RHS).[36]

1.3 CO_2/Epoxide ROCOP

The copolymerisation reaction between CO_2 and epoxide requires a catalyst to lower the activation barrier and enable selective polymerisation.[37] Catalysts for CO_2/epoxide ROCOP generally consist of a Lewis acidic metal halide, carboxylate or alkoxide coordinated by an ancillary ligand. The elementary catalytic steps of CO_2/epoxide ROCOP can be separated into four steps: initiation, propagation, chain transfer and termination (Scheme 1.2).

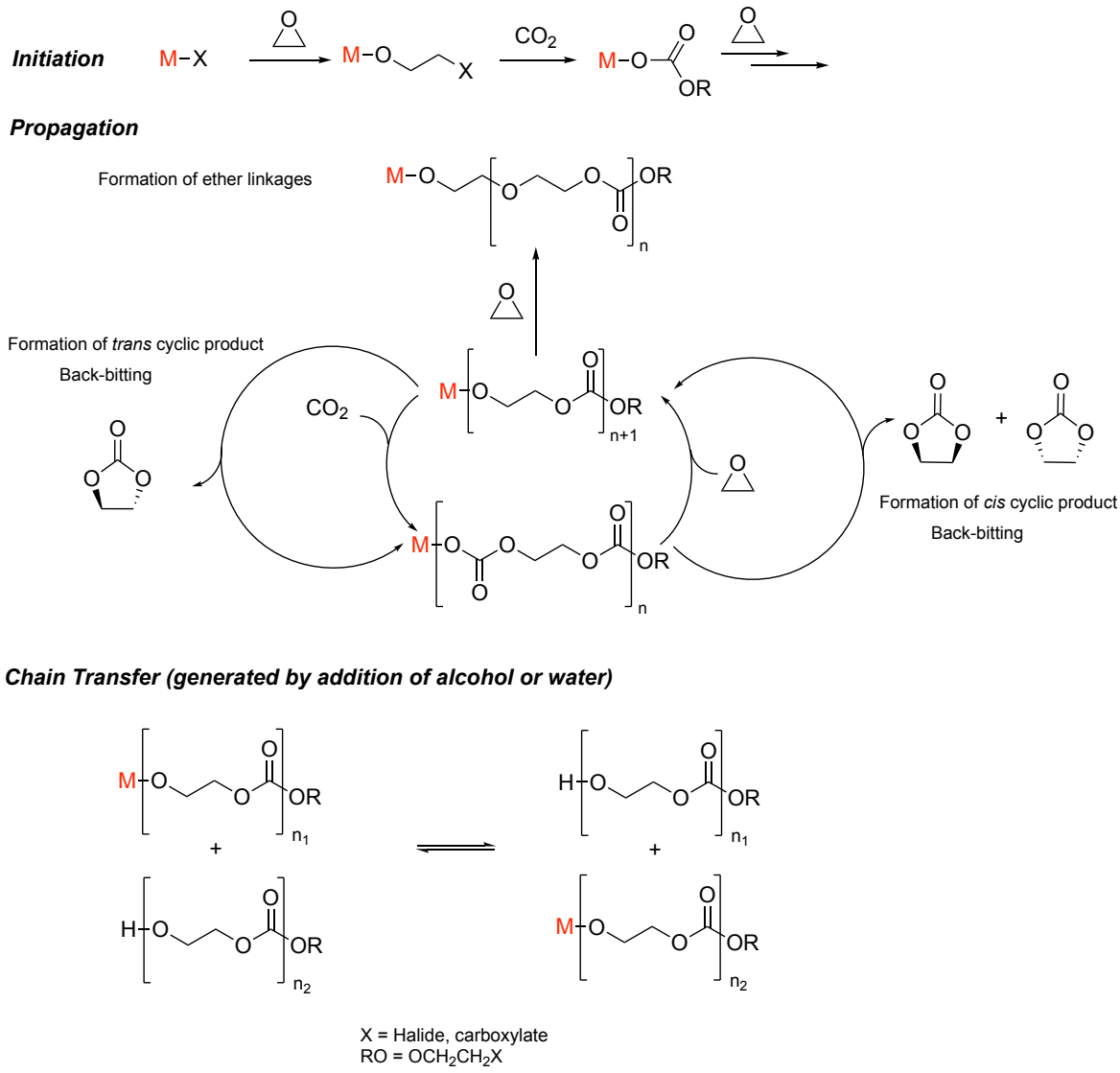

Scheme 1.2. Illustrates the elementary steps occurring during copolymerisation, including initiation, propagation and chain transfer processes.

The *initiation* step corresponds to the first monomer insertion (epoxide and/or CO_2) at the metal centre and the initiator. As a consequence, the initiating group (X) is incorporated as a chain end group on the polymer.

During *propagation,* the catalyst alternates between metal-alkoxide and metal-carbonate intermediates. The interconversion occurs via insertion of CO_2 into a metal-alkoxide intermediate and the epoxide ring opening by the metal-carbonate intermediate. Catalysts exhibiting controlled behaviour typically enable the chain length, and molecular weights, to be predicted and controlled. Experimental features of such control include an inverse relationship between catalyst concentration and molecular weight (at constant monomer conversion) and a linear increase in molecular weight as the polymerisation conversion increases.

During propagation, there are two common side reactions: the sequential enchainment of epoxides, leading to ether linkages in the polymer backbone and the formation of cyclic carbonate by-products. These cyclic carbonates are stable five membered rings and are the thermodynamically product of CO_2/epoxide coupling. The selectivity for polycarbonate is maintained by performing the polymerisation under kinetic control, frequently achieved either by selection of the catalyst or by control over the reaction conditions (most commonly the temperature). It should be noted that the five-membered rings cyclic carbonates generally cannot re-enter into polymerisation cycles as their ring-opening polymerisation is thermodynamically unfavourable. Nonetheless, one exception was reported by Guillaume and co-workers, where they demonstrated that the polymerisation of the highly strained *trans*-cyclohexene carbonate was thermodynamically possible.[38]

In many cases, the polymerisations also operate under immortal conditions,[39] whereby very rapid exchange between the growing polymer chain (alkoxide group) and protic

compounds leads to reversible alcoholysis known as *chain transfer*. It is rather common that such chain transfer processes occur more rapidly than propagation, signalled by narrow molecular weight distributions (polydispersities) and molecular weights which depend on the quantity of protic compound(s), as well as the catalyst concentration. Chain transfer reactions with protic compounds can lead to bimodal molecular weight distributions, particularly if a mixture of telechelic and monofunctional chains propagate concurrently.[40] In this scenario, chain transfer also results in mixtures of chain end groups, as detected by several polymer populations in MALDI-ToF spectra.

The polymerisations are typically terminated by exposure of the mixture to acids/aqueous conditions which hydrolyse the growing chains from the residual catalyst and prevent any further propagation. It is important to note that basic conditions should be avoided due to the propensity for base catalysed degradation of polycarbonates.

1.4. Early Catalyst Developments and Heterogeneous Catalysts

The first example of CO_2/PO copolymerisation was reported by Inoue, in 1969.[41] Sluggish activities were obtained using a mixture of [$ZnEt_2$] and water at 80 °C and high CO_2 pressure (50-60 bar). Since this discovery, several groups have studied the copolymerisation of CO_2/PO with mixtures of organometallic zinc reagents and hydric sources (water, methanol, amine).[42] Heterogeneous mixtures of carboxylic acids and [$Zn(OH)_2$] also showed promising activities.[42b] These studies led, several years later, to a new type of heterogeneous catalyst: zinc glutarate.[43] This species was easily prepared by reaction between zinc oxide and glutaric acid and were either isolated as crystalline or amorphous materials. The crystalline structures showed higher activity (~ 300 g poly(propylene carbonate) (PPC) / g [Zn]) and produced polymers with high molecular weight.[44]

Double Metal Cyanides (DMCs) are another major class of heterogeneous catalysts.[45] DMCs have a general stoichiometry of [$Zn_3\{M(CN)_6\}_2$] where M = [Fe(III)] or [Co(III)]. These catalysts are highly active for CO_2/epoxide ROCOP and are extensively reported in the patent literature.[46] Their activity and selectivity is highly dependent on the synthetic protocol but typically produce copolymers with high ether content and require high CO_2 pressure. Several academic studies were performed to increase the formation of carbonate linkages by synthesising well-defined homogeneous analogues of the DMC structures. Reasonable activities (TON: ~ 1860 g PO/ g Co, at 130 °C and 54.4 bar of CO_2) and carbonate linkages (> 85 %) could be achieved.[47]

There are very few reports concerning the possible mechanisms for the heterogeneous catalysts.[43b, 48] In 2011, Reiger and co-workers reported a mechanistic study on zinc dicarboxylate catalysts.[49] Experimental and calculation results highlighted that a large

proportion of Zn-Zn surface couples separated by 4.3-5 Å seems to correlate with high activity. Interestingly, this metal-metal distance matches closely with other mechanistic studies using homogenous di-zinc catalysts (*vide infra*). The results also indicated that, for heterogeneous zinc dicarboxylates, a dinuclear mechanism may be operative (Scheme 1.3).

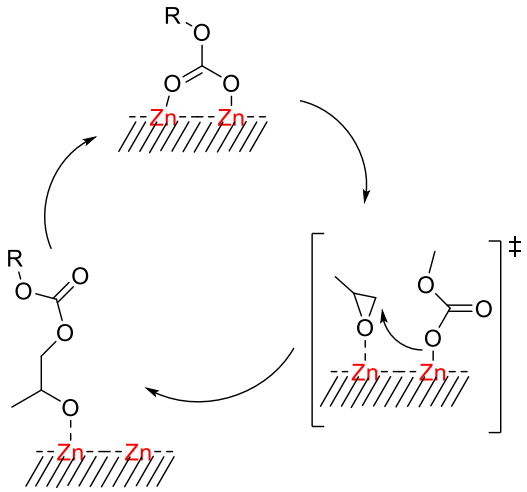

Scheme 1.3. Illustration of the proposed dinuclear catalytic cycle operating on the surface of heterogeneous zinc dicarboxylate catalysts.[49]

1.5 Early Development of Homogenous Catalysts

1.5.1 Bicomponent Catalysts

The first homogeneous copolymerisation catalyst, reported in 1970, was an aluminium tetraphenyl-porphyrin complex **1a** (Figure 1.3) which was active, for CO_2/cyclohexene oxide (CHO) ROCOP, only if an equimolar amount of methyltriphenylphosphonium bromide ($[EtPh_3P^+]Br^-$) was used as a cocatalyst.[50]

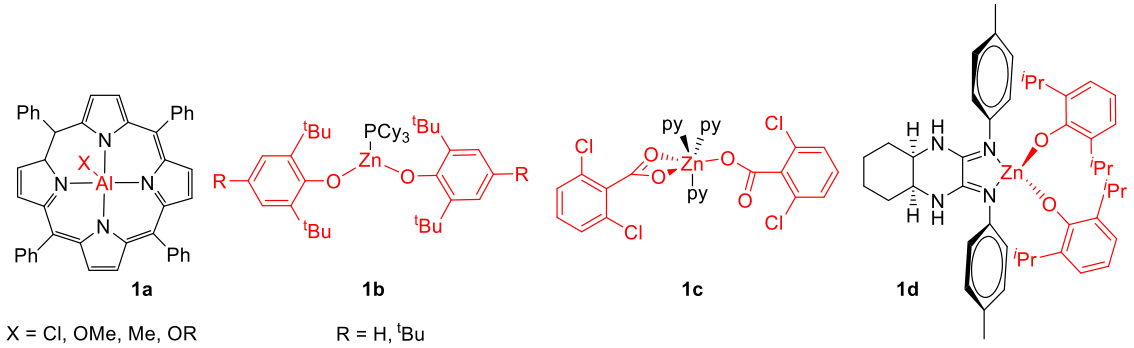

Figure 1.3. Examples of some of the early homogeneous catalysts.[42a, 51]

Almost 30 years later, a series of zinc bis(phenoxides) (including **1b**) was developed by Darensbourg and co-workers, and showed good activity but produced polydispersed polymers.[51-52] Structural variation at the phenoxy moieties did not affect the activity or significantly improve the quality of the polymer.[52] Soon after, the same group reported a zinc benzoate complex, **1c**, showing TOF of ~ 8 h^{-1} in CHO/CO_2 copolymerisation.[53] Similar activities were achieved with a quinoxaline derived zinc alkoxide complex, **1d,** developed by Hampel *et al*.[54] It is important to point out that an important aspect of this earlier work was that most of the successful zinc catalysts exhibit di- or multi-nuclear structures, providing early pointers towards dinuclear polymerisation pathways.

1.5.2 Zinc β-Diiminate Catalysts: Dimeric Catalysts

It was not until 1998 that Coates and co-workers reported a ground-breaking series of zinc β-diiminate (BDI) catalysts (**2**) which showed significantly higher activities (TOF = 917 h^{-1}) and selectivities (> 99 % carbonate linkages) at 50 °C and only 7 bar of CO_2 pressure.[55]

The structure/activity relationship of the catalysts was extensively studied and revealed the importance of the *ortho*-substituents on the phenyl rings of the BDI ligand (Figure 1.4, LHS) and of the initiating group. Furthermore, these structure activity studies revealed the subtleties of "catalyst design". It was discovered that if the phenyl rings in the ligand were substituted with sterically hindered groups, the complexes formed monomeric structures which were inactive or of low activity. On the other hand, if substituents with low steric hindrance were applied the resulting complexes formed tightly bound dimers which were also of lower activity/inactive. The best catalysts were formed from ligands with medium steric hindrance (R_1 = R_3 = Et, R_4 = H) which resulted in the formation of loosely associated dimeric structures. Electron withdrawing substituents attached to the backbone of the BDI zinc complexes (e.g. R_2 = CN) also improved activities.[55-56] Kinetic and mechanistic studies strongly implicated two zinc metal centres in the copolymerisation catalytic cycle. It was proposed that the epoxide coordinates to one zinc metal centre, whilst the other metal centre provides the nucleophile to attack and ring opens the epoxide (Figure 1.4 RHS). More recently, isotactic PCHC was produced using C_1 symmetric [Zn-BDI] catalysts (*ee* > 90 %).[18b] Earlier this year, Rieger *et al*. also reported similar [Zn-BDI] complex as a switchable catalyst able to synthesise multiblock copolymers from a mixture a monomers.[57] This result followed from earlier work by our group developing this reaction (*vide infra*).

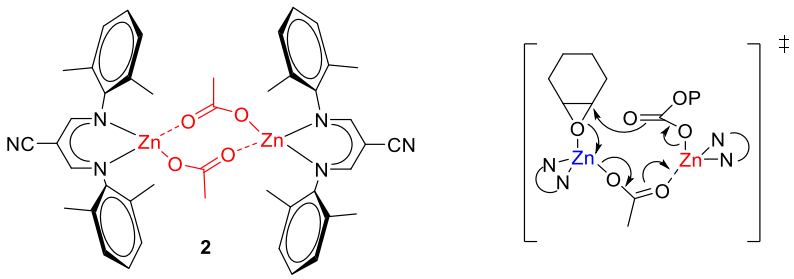

Figure 1.4. Highly active dimeric [Zn-BDI] catalyst (LHS) and the proposed transition state involving two metal centres for the ring opening of the CHO (RHS).[56a]

1.5.3 Salen Catalysts: Bifunctional Catalytic Systems

One of the most widely researched classes of catalysts for this copolymerisation are metal salen complexes (Figure 1.5).

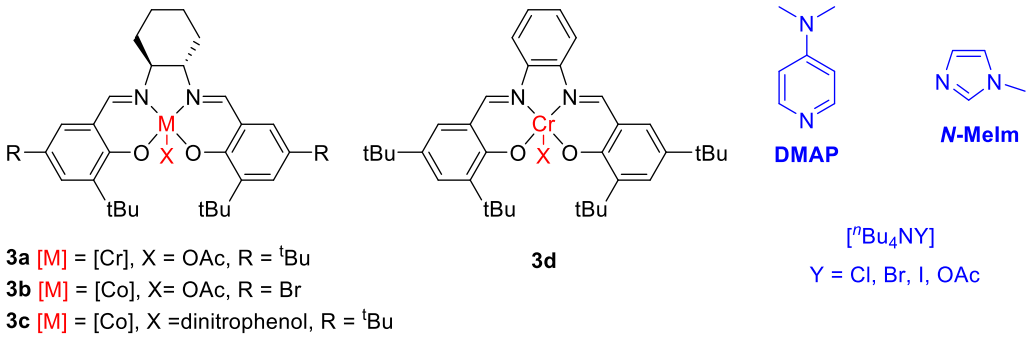

Figure 1.5. Various metal salen complexes, and cocatalysts, which are applied together in a bifunctional catalytic system.[58]

The first detailed report of metal salen catalysts came from Darensbourg and co-workers who showed that the [Cr(III)] salen complex **3a**, in conjunction with various Lewis bases (*N*-MeIm or DMAP) gave a TOF = 32 h^{-1} (80 ºC, 58.5 bar of CO_2).[58a] Shortly afterwards, a closely related [Cr(III)] salphen complex, **3d**, was reported by Rieger and co-workers in conjunction with DMAP, as a PPC catalyst.[58c] [Co(III)] salen complexes, such as **3b**, were established to be effective for PO/CO_2 copolymerisation,[58b, 59] without requiring any cocatalyst[58b] (TOF = 70 h^{-1} at 55 bar of CO_2, 30 ^{o}C). Lu *et al.* reported activity > 5 times higher using a similar [Co(III)] salen complex **3c** (TOF = 370 h^{-1}), at lower CO_2 pressure (20 bar), by using anionic cocatalysts ([$^{n}Bu_4Y$], Y = Cl, Br, I, OAc) emphasising the importance of the cocatalyst to achieve high activities.[60] Despite these promising results, a major limitation of this first generation of salen catalysts is that their activities were compromised at low catalyst loading.

Since the early discoveries, a significant amount of research has been carried out on metal salen complexes, including studies of the influence of the metals, ligands, cocatalysts and reactions conditions, as well as expanding the scope with various different epoxides.[8, 61] These studies highlighted the key role of the cocatalysts. Cocatalysts (neutral and anionic)

are proposed to coordinate to the metal centre at a site *trans* to the initiating group to form an octahedral intermediate (neutral, or negatively charged in presence of an anionic cocatalyst).[58a, 62] It is believed that the *trans* coordination of the cocatalyst causes the [M-OR] bond to weaken ("OR" being the growing polymer chain). This, therefore, promotes the ring opening of an epoxide molecule and CO_2 insertion. There is also evidence that cocatalysts may be involved in initiation: MALDI-ToF spectra of polymers show both the initiating group and the cocatalyst as end groups. It was proposed that initiation by the cocatalyst may occur by off metal nucleophilic attack on epoxide by the cocatalyst (Scheme 1.4).[8, 61]

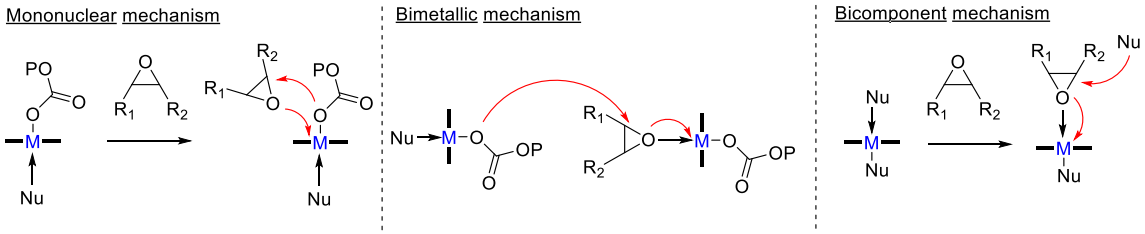

Scheme 1.4. Proposed mechanism for the ring opening of epoxide catalysed by metal salen complexes. Nu can either be the initiating group, a propagating polymer chain or the cocatalyst.[62]

Based on these studies, three mechanisms were proposed (Scheme 1.4).[58a, 58b] The first is a monometallic pathway, similar to the coordination-insertion mechanism proposed for lactone ROP. It was rapidly rejected due to the evidence that the cocatalyst was essential for effective polymerisation. It was also not consistent with kinetic results obtained for a wide range of salen catalysts which all show a non-integer order in catalyst concentration (1.2-1.8 depending on the catalysts and on the conditions).[58c, 62] The bimetallic mechanism is similar to the mechanism proposed by Jacobsen for the asymmetric epoxide hydroxylation. It is a dinuclear mechanism where the epoxide is activated by one catalyst and the nucleophilic attack occurs from a second catalyst.[62] The last mechanism is a bicomponent mechanism involving the dissociated cocatalyst or propagating polymer chain attacking the coordinated epoxide.[63] There are still lots of uncertainty on the real

active species during catalysis. Nevertheless, the results from mechanistic studies have led to the development of dinuclear salen catalysts consisting of two salen complexes covalently linked (to enhance the proposed bimetallic mechanism) and to the tethering of the cocatalyst on to the salen catalyst (to enhance the proposed bicomponent mechanism) (*vide-infra)*.

1.6 Dinuclear Catalysts

The results from kinetic and mechanistic studies performed on both homogeneous and heterogeneous catalysts have spurred the development of dinuclear complexes.[56b, 64] Within this class of catalysts, there are three commonly occurring structures:

i) Dinucleating ligands enabling dinuclear complexes

ii) Dimerisation of the monometallic complexes (e.g. [Zn-BDI] catalysts)

iii) Tethering two monometallic complexes together.

1.6.1 Dinucleating Ligands

The first successful example of a deliberately dinuclear catalyst was reported by Lee and co-workers and consisted of a di-zinc anilido-aldimine catalyst (**4**, Figure 1.6).[64a, 65] These catalysts showed high activities (TON: 2860 h^{-1}) at low catalyst loading (0.006 mol%), selectivities for carbonate linkages (85-96 %) and produced very high molecular weight polymer (M_n = 90-280 kg/mol) with broad distribution. Other dinuclear catalysts were reported by Xiao and co-workers, which include a series of di-zinc and di-magnesium phenolate catalysts (**5**, Figure 1.6).[66] These were the first example of catalysts showing low activities at 1 bar of CO_2 pressure albeit with high catalyst loading (5 mol%).[67]

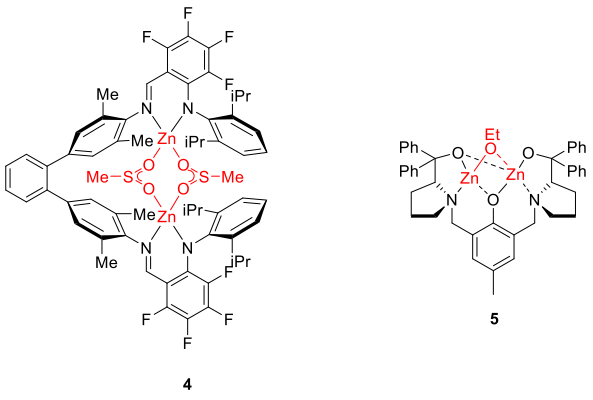

4 **5**

Figure 1.6. LHS: di-zinc anildo-aldimine catalyst reported by Lee and co-workers.[64a] RHS: di-zinc phenolate complex reported by Xiao and co-workers.[66]

Since 2009, our group (Williams and co-workers) has applied a symmetrical diphenolate macrocyclic ligand which coordinates two metal centres (Figure 1.7).[36, 64b-d, 68] All

catalysts show good activity at only 1 bar of CO_2 pressure, conditions under which many other catalysts are inactive. The high activity of these complexes was attributed to the macrocyclic ligand as well as the dinuclear structure. In addition, the catalyst allows the synthesis of multiblocks copolymer from a mixture of monomer feedstocks.[69]

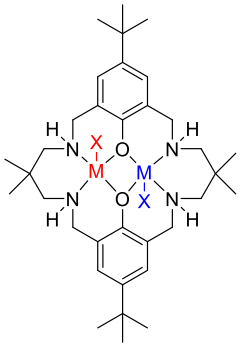

6a, [M] = [M_2] =[Zn], X = OAc
6b, [M] = [M_2] = [Mg], X = OAc
6c, [M] = [M_2] = [Co], X = OAc
6d, [M_1] = [M_2] = [FeCl], X = Cl
6e, [M_1] = Zn, [M_2] = Mg, X = Br

Figure 1.7. Dinuclear complexes supported by a macrocyclic diphenolate ligand reported by Williams and co-workers.[64b, 68b, 68e, 68h]

The selection of the metals is of key importance in controlling the catalytic performance (Table 1.2). [36, 64b-d, 68a-g, 70] The activity was enhanced 7 times by changing the metal centres from zinc (**6a**, TOF = 13 h^{-1}, at 100 °C) to magnesium (**6b**, TOF = 76 h^{-1}, at 100 °C). The activity of the [bis-Co(II)] complex was approximately nine times higher than the zinc analogue, under the same conditions (**6c**, TOF = 86 h^{-1}, at 80 °C). We also reported the first di-iron catalyst (**6d**, TOF = 100 h^{-1}). Furthermore, under optimised reaction conditions and with high rates of stirring, very high activities (TOF up to 5400 h^{-1}) were achieved with **6b**.[14b] All catalysts produce polycarbonates with > 99 % of carbonate linkages, and > 99 % selectivity towards copolymer (**6a** shows slightly lower values).

Table 1.2. Copolymerisation of CHO/ CO_2, catalysed by macrocylic dinuclear catalysts.

Cat	T (°C)	TON[a]	TOF[b] (h^{-1})	% PCHC[c]	% carbonate[c]	M_n[d] (g/mol)	Đ[e]	Ref
6a	80	220	9.2	96	> 99	6200	1.19	[68h]
6a	100	264	13	94	> 99	7360	1.21	[68h]
6b	80	261	18	> 99	> 99	13 300	1.03	[64b]
6b	100	229	76	> 99	> 99	11 800	1.03	[64b]
6b[f]	125	26 900	5400	> 99	> 99	7200	1.06	[14b]
6c	80	170	86	> 99	> 99	5100	1.26	[68f]
6d[f]	80	145	47	> 99	> 99	11 400	1.13	[68e]
6e	80	344	34	> 99	> 99	3100	1.14	[71]
6e[g]	120	3118	624	> 99	> 99	18 000	1.05	[71]
						7300	1.10	

All copolymerisations were carried out at 1 bar of CO_2 at a loading of catalyst/CHO of 1:1000; [(a)]TON = moles CHO consumed per mole of metal; [(b)]TOF = TON per hour; [(c)]Determined by ^{1}H-NMR spectroscopy; [(d,e)]determined by SEC in THF, using narrow polystyrene standards; [(f)]10 bar of CO_2 pressure; [(g)]50 bar of CO_2 pressure.

The copolymerisation reaction was extensively studied by Density Functional Theory (DFT) calculations, detailes kinetic studies and *in-situ* attenuated total reflectance infra-red (ATR-IR) experiments to interrogate the mechanism.[40, 64c] The results indicate a dinuclear chain shuttling mechanism where the rate determining step is the nucleophilic attack of the coordinated epoxide. During catalysis, each metal is proposed to have a specific role: one metal activates the epoxide and the second provides the carbonate group.[71] Although two carboxylate initiating groups are present in the catalyst, the detailed spectroscopic investigation results suggest an unusual propagation pathway in which one carboxylate group serves as an initiating group and the other as a spectator co-ligand.[40, 64c]

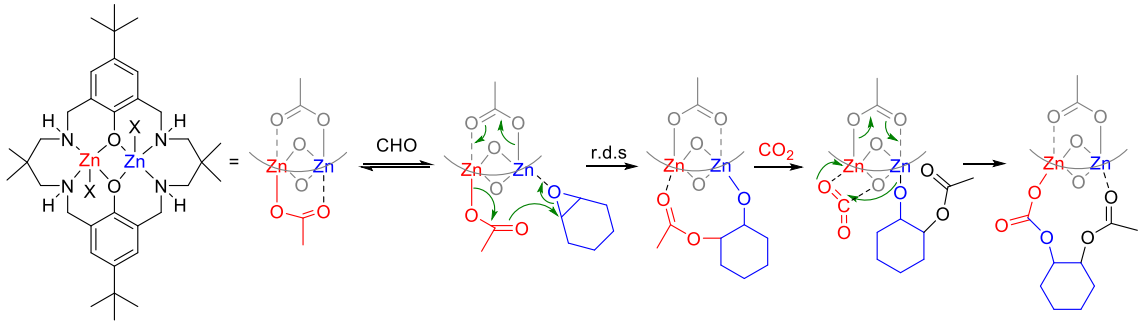

Scheme 1.5. Proposed mechanism occurring during copolymerisation catalysed by **6a** highlighting the role of each metal centre during catalysis.[64c]

The proposed mechanism for these dinuclear macrocyclic catalysts, based on all the experimental and theoretical evidence, is illustrated in Scheme 1.5. It begins with coordination of an epoxide to the di-zinc catalyst. The epoxide is attacked and ring-opened by an acetate group coordinated at the other zinc centre. The initiation step leads to the formation of a zinc bound alkoxide species. According to the DFT calculations, a CO_2 molecule approaches the di-zinc intermediate but is not directly coordinated by the zinc centres. Rather a zwitterionic intermediate forms by attack of the zinc alkoxide on the carbon dioxide molecule. This intermediate rapidly forms a zinc carbonate intermediate,

bound at the other zinc site. The polymerization propagates by the alternation of these steps.

During polymerisation, it is proposed that the growing chain 'shuttles', or switches its formal coordination site, between the two zinc centres. It changes its coordination site with both epoxide ring-opening and CO_2 insertion steps. In total, therefore, it switches twice with every propagation cycle (Scheme 1.5). According to this mechanism, the carboxylate (acetate) ligand plays a dual role in catalysis: one acetate group is an initiating/propagating site, whilst the other is retained during catalysis as a spectator co-ligand. The spectator acetate ligand serves to counterbalance the polymer chain 'shuttling' by balancing the charge and coordination number at alternating zinc sites as the polymer chain grows. This unusual feature for the carboxylate ligand is supported by experimental results which reveal a dependence of the catalyst activity (TOF) depending on the co-ligand. Such an effect should not occur if the carboxylate ligand only serves as an initiating group (assuming initiation is relatively fast). [64c, 64d]

A logical extension of the chain shuttling mechanism was the development of hetero-dinuclear catalysts, i.e. containing two different metals.[68a, 70-71] Such complexes are challenging due to the symmetry of the macrocyclic ligand and the potential for the metals to exchange. Indeed preliminary studies demonstrated that a mixture of compounds, including **6a**, **6d** and **6e** was more efficient than either homodinuclear catalyst (**6a** or **6d**), either alone, or mixed together. The mixture showed activity which is greater than the sum of its parts (TOF = 79 ± 5 h^{-1}, at 80 °C and 1 bar of CO_2).[68a] These encouraging results prompted the synthesis of a pure heterodinuclear [Zn/Mg] catalyst which was achieved from the reaction of [$MgBr_2$] with a mono-Zn intermediate.[71] Its activity was more than 5 times higher than that obtained using a 1:1 molar ratio mixture of its homodinuclear counterparts. The activity enhancement with the heterodinuclear complex was even greater

for phthalic anhydride (PA)/CHO ROCOP. In this case, the catalyst was 20 times more active than the corresponding di-zinc catalyst and 10 times more active than di-magnesium.

Lin and co-workers have reported multidendate bis(benzotriazole iminophenol) dinuclear complexes [Zn(II)], [Ni(II)] and [Co(II)] (Figure 1.8).[72] Whereas the di-zinc complex **7a** mainly yields cyclic carbonate (66 % vs polymer), the di-nickel and di-cobalt complexes, **7b-c**, show good selectivity for polymer formation (94; > 99 %f or **7c**; **7b**, respectively) and carbonate linkages (> 99 %). Under optimal conditions (T = 120 °C, P_{CO2} = 21 bar, 0.0625 mol% catalyst), **7b** and **7c** exhibit TOFs of 40 h^{-1} and 53 h^{-1}, respectively. Higher activities were achieved with a di-nickel trifluoroacetate catalyst (TOF = 432 h^{-1}). The catalyst also shows promising activities with vinyl-CHO (TOF = 208 h^{-1}) and cyclopentene oxide (CPO) (TOF = 17 h^{-1}).[73]

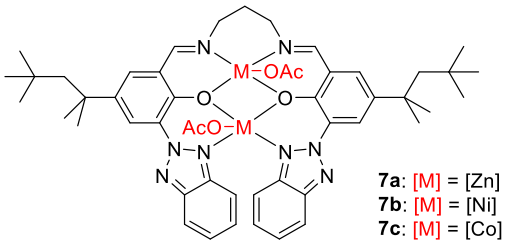

Figure 1.8. Dinuclear [Zn(II)], [Co(II)] and [Ni(II)] catalysts, as reported by Lin and co-workers.[72]

1.6.2 Dimeric and Multimeric Structures

Various dimeric, and even trimeric, structures have been reported for epoxide/CO_2 catalysts. Most of these structures feature Schiff base ligands or multi-*N*, *O* donor ligands that dimerise via formation of oxo bridge, either as part of the ligand scaffold or from exogenous co-ligands (e.g. alkoxides or carboxylates). Complex **8** and **9** are particularly interesting due to their straightforward synthesis and they capability to produce stereocontrolled polycarbonate.

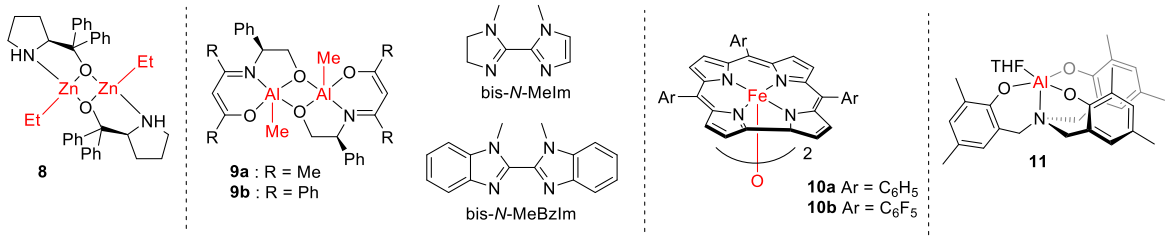

Figure 1.9. From left to right: first dimeric catalysts (**8**), reported by Nozaki and co-workers;[74] schiff-base dimeric aluminium complexes (**9**), reported by Sugimoto and co-workers[75]; iron corrole catalyst (**10**), reported by Nozaki and co-workers;[18d] aluminium trisphenolate catalyst (**11**), reported by Kleij *et al.*[33a]

Nozaki and co-workers reported the stereocontrolled copolymerisation of CHO/CO_2 using various chiral dimeric zinc complexes such as **8** (Figure 1.9).[74, 76] Catalyst **8** showed ~ 70 % *ee*. The mechanism proposed invoked a dinuclear pathway, where initiation occurs by insertion of CO_2 into the amino ligand creating a monomeric zinc species which is the chiral propagating species.

Sugimoto and co-workers investigated various dimeric BDI and Schiff-base aluminium complexes, including **9a/b** (Figure 1.9).[75] Complexes **9a/b**, in the presence of [Et_4NOAc], showed good selectivity (carbonate linkages > 98 %), moderate activity (TOF < 13 h^{-1}) and low enantioselectivity (*ee* ~ 25 %). The *ee* was improved (*ee* ~ 62 %) by adding various Lewis bases, most especially with bis-*N*-MeIm or bis-*N*-MeBzIm. The influence of the cocatalysts may suggest a two-component mechanism.

In 2013, Nozaki and co-workers reported a dimeric iron-corrole complex, **10a**, for the copolymerisation of CHO, PO and glycydil phenyl ether (GPE) with CO_2 (Figure 1.9).[18d] The series showed excellent selectivity for polymer formation (> 99 % vs cyclic carbonate) with a good activity in the case of PO (TOF > 1000 h^{-1}) in presence of a cocatalyst (e.g. bis(triphenylphosphine)iminium chloride, PPN-Cl). However, the polymers have low contents of carbonate linkages, up to 29 % and 22 % for PO and GPE, respectively. Crystalline materials were achieved when GPE was copolymerised with CO_2.

Kleij *et al.* reported an aluminium amino-trisphenolate catalyst (**11**) which have promising activities for the challenging limonene oxide (LO)/CO_2 copolymerisation reaction, in presence of PPN-Cl (Figure 1.9).[33a] The catalyst was fully selective for polycarbonate formation at 42 ^oC and 10 bar of CO_2 and produced polycarbonate with > 99 % carbonate linkages. Although the complex is monomeric, mechanistic and DFT studies highlighted a dinuclear mechanism.[33a]

1.6.3 Tethered Mononuclear Catalysts

Driven by the high activities reported for single ligand dinuclear catalysts, several groups synthesised dinuclear complexes by tethering successful mononuclear catalysts including [Zn-BDI], metal salen and porphyrin complexes.[77] The common strategies have been to link together two ligands, using covalent bonds, and then to coordinate two metal centres to produce dinuclear catalysts.

1.6.3.1 Linked Dinuclear BDI Catalysts

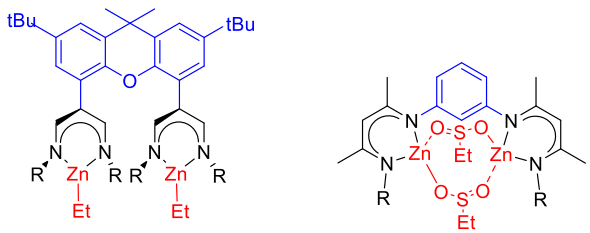

Figure 1.10. Two examples of tethered of dinuclear [Zn-BDI] catalysts reported by Ziemer *et al.* (**12a**), and Harder and co-worker (**12b**), respectively.[78]

Given the excellent performance of [Zn-BDI] catalysts and the mechanistic findings from Coates and co-workers, it was a natural next step to investigate tethered [Zn-BDI] catalysts. Ziemer *et al* reported tethered BDI ligand where the two zinc site parallel to each other (Figure 1.10, **12a**).[78b] The reported distance between the two zinc atoms was 4.92 Å, but the resulting catalyst showed a worse performance than conventional [Zn-BDI] dimers (TOF = 9 h^{-1}), possibly due to steric factors. An improved catalyst was obtained by

bridging two BDI ligands via *para*- and *meta*-substituted phenyl groups (Figure 1.10, **12b**).[78a] Complex **12b** showed a reduced [Zn-Zn] distance (3.79 Å) and showed a good activity (TOF = 262 h^{-1}), at 10 bar of CO_2 and 60 °C. The selectivity was excellent (> 99 % carbonate linkages), yielding PCHC of high molecular weights (M_n: 45–100kg/mol).

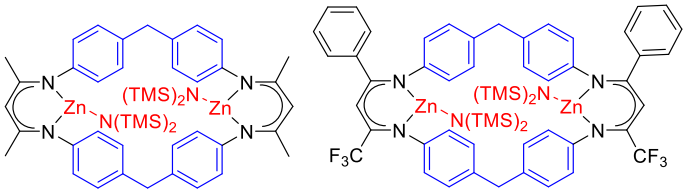

13a 13b

Figure 1.11. Tethered dinuclear [Zn-BDI] catalysts by Reiger and co-workers.[64e]

In 2013, Rieger and *al.* reported a series of di-zinc complexes featuring BDI moieties linked through the phenyl rings (Figure 1.11).[64e] The kinetic and DFT studies on **13a** suggested a change in the rate-determining step, depending on the CO_2 pressure. Below 25 bar pressure, the rate law was proposed to be first order dependent on CO_2 pressure and zero order in epoxide concentration, suggesting CO_2 insertion is rate limiting. In contrast, above 25 bar pressure, the rate law was interpreted as first order in epoxide and zero order in CO_2, suggesting epoxide ring opening is rate limiting. In 2014, the same group reported the highest active catalyst, **13b**, for CO_2/CHO ROCOP with an impressive TOF = 155 000 h^{-1} at 30 bar of CO_2 and 100 °C with fairly high carbonate linkages (88 %) and high selectivity for PCHC (> 99 %).[79] It is worth noting that the TOF values were reported differently to standard method. Surprisingly, the same catalyst was almost inactive for PO/CO_2 ROCOP due to the formation of a thermodynamically stable metallocyclic intermediate which stops the propagation regime.[80]

1.6.3.2 Linked Dinuclear Salen Complexes

In 2010, Nozaki and co-workers reported various linked dinuclear cobalt(III) salen complexes for the PO/CO_2 copolymerisation (Figure 1.12).[81] Dinuclear complexes showed improved activities compared to their mononuclear homologue, especially at low

catalyst loading, and did not require the addition of exogenous cocatalyst (for [PO]/[Co] = 3000, TOF = 120 h^{-1} and 20 h^{-1} for **14a** and **14d**, respectively). In addition, the relative configurations of the two metal salen units influenced the activity. The (*R,R*)-(*S,S*)-**14a** was more than three times more active than (*R,R*)-(*R,R*)-**14a** (TOF = 120 h^{-1} vs. 40 h^{-1}, respectively). Finally, the length of the spacer group affected the activity and selectivity with smaller linker giving higher activities. These important results provide further support for a dinuclear mechanism.

Later, Rieger observed similar results with a tethered di-chromium catalyst (Figure 1.12).[82] **15a** was 12 times faster than **15b** at low catalyst loading ([PO]/[Cr] = 20 000), whilst similar activities were obtained at higher catalyst loading ([PO]/[Cr] = 2000). Again, mechanistic and kinetic studies suggested a dinuclear mechanism with both catalysts in absence of cocatalyst and most probably to a bicomponent mechanism in presence of onium salts.

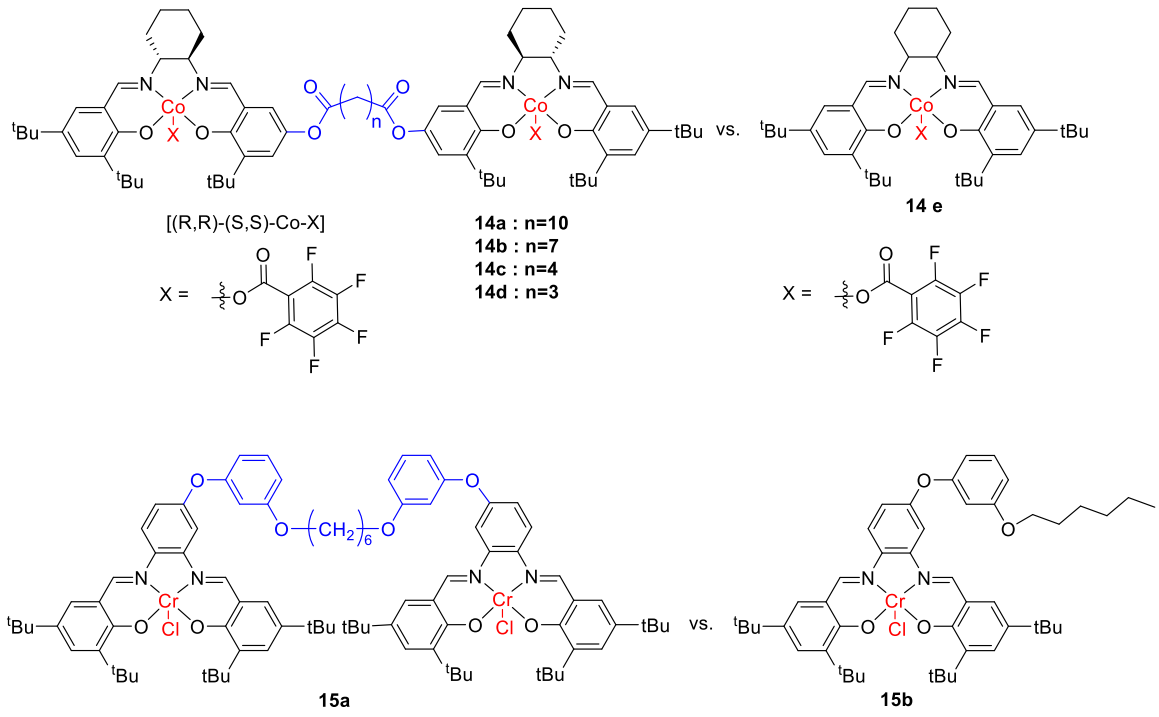

Figure 1.12. Dinuclear salen complexes reported by Nozaki *et al.* (complexes **13a-e**)[81] and by Rieger and co-workers (complexes **14a-b**).

The field was once again inspired by the pioneering work of Jacobsen,[83] on the steroselective epoxide ROP[84] and applied similar dinuclear salens complexes for the enantioselective CO_2/epoxide ROCOP.

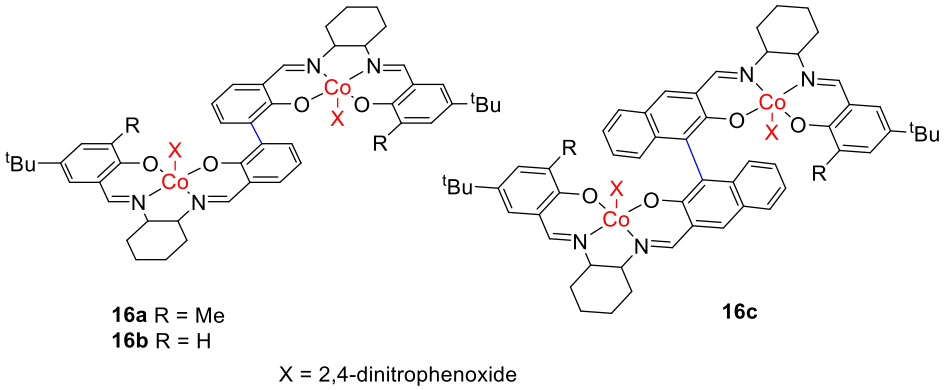

Figure 1.13. Dinuclear [Co(III)] salen catalysts reported by Lu and co-workers.[18c]

Lu and co-workers reported a series of dinuclear catalysts for the enantioselective CO_2/epoxide ROCOP (Figure 1.13).[18c] The series was highly active for CO_2/CPO ROCOP (TOF = ~ 200 h^{-1}) and were highly enantioselective (*ee* > 99 %). It also operates at only 1 bar of CO_2 pressure whilst, retaining excellent enantioselectivity (*ee* = 96 %). Under optimal conditions (0 ºC, in the presence of toluene), catalyst **16b** affords highly isotactic semi-crystalline PCHC (M_n = 35.6 kg/mol, Đ = 1.35, *ee* = 98 %), showing a high melting temperature of 272 ºC. Similar results were achieved by copolymerising meso-3,4-epoxy tetrahydrofuran (COPO) with CO_2 (M_n = 15.4 kg/mol, Đ = 1.14, *ee* > 99 %, T_m = 271 °C).[20b] Semicrystaline thermoplastic polycarbonates were achieved from terpolymerisation of CPO/(COPO)/ CO_2. Stereocomplex polycarbonates were also produced using a racemic mixture of **16a** (R,R,R,R and S,S,S,S) using *meso*-CHO and *meso*-4-dimethyl-3,5,8-trioxabicyclo[5.1.0]octane (CXO), opening a new strategy for preparing various intramolecular stereocomplex with enhanced thermal stability.[20a] Interestingly, in the absence of cocatalyst, **16a-b** showed only very low activities and enantioselectivities for either CHO/CO_2 or CPO/CO_2 copolymerisation. Similarly, the dinuclear cobalt complex **16c**, which is an effective catalyst for the enantioselective

homopolymerisation of epoxide,[18e, 85] showed a low activity (TOF < 10 h^{-1}) and a poor enantioselectivity (*ee* < 33 %) for CPO/CO_2 copolymerisation.

1.6.3.3 Dinuclear Porphyrin Catalysts

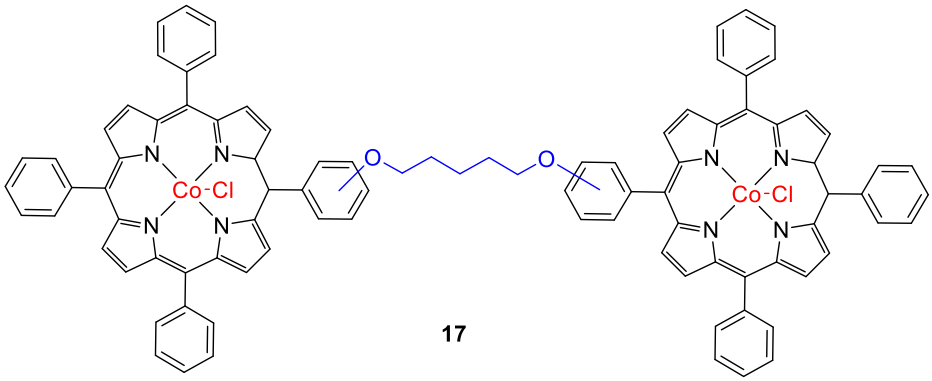

Figure 1.14. Dinuclear porphyrin catalyst reported by Rieger and co-workers.[64f]

Later, Rieger and co-workers studied a series of linked bis-porpyhrin complexes, **17**, comparing them to a monometallic cobalt porphyrin (Figure 1.14).[64f] However, in this case the dinuclear porphyrin showed lower productivities (TON = 300 – 696, depending on the linker position) than the monometallic counterparts (TON = 983). The presence of cocatalyst was essential to both initiation and propagation steps. Mechanistic and kinetic studies suggest that instead of a dinuclear mechanism, a bicomponent mechanism, similar to the previously described for salen catalyst, may operate for metal porphyrins. The study also suggests that the poor performance of the dinuclear catalyst was potentially due to catalyst deactivation, by reduction of [Co(III)] to [Co(II)], which was faster in the case of the dinuclear catalyst.[64f, 86]

1.6.4 Bicomponent Catalysts

1.6.4.1 Ionic Cocatalysts

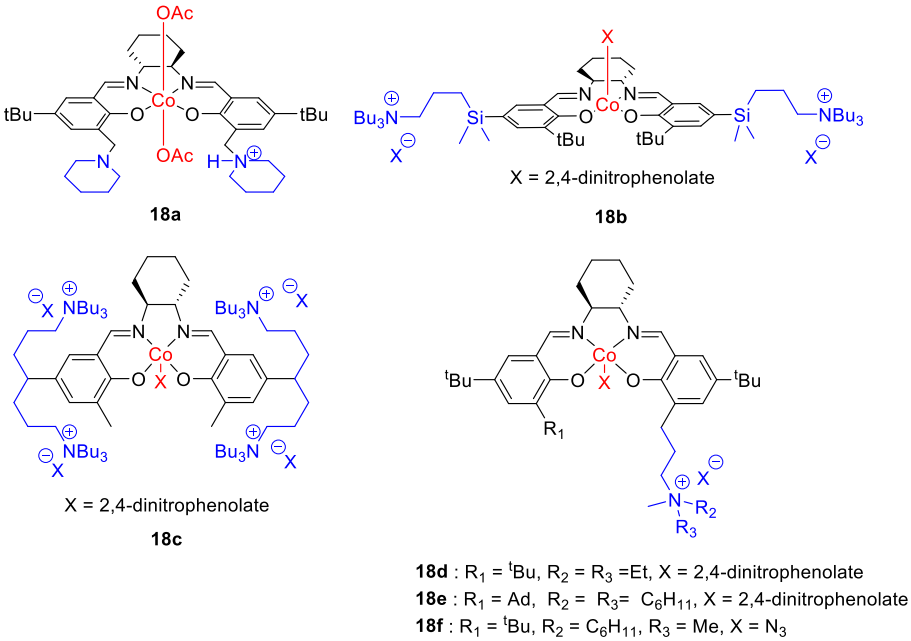

Figure 1.15. Two-component catalysts reported by Nozaki, Lu, Lee and Darensbourg.[21, 87]

Another strategy adopted to enhance the catalytic activity salen catalysts was to tether the cocatalyst on the ligand backbone (Figure 1.15). The hypothesis was that it would stop the reduction of the catalytic activity at low catalyst loading by preventing the dissociation of the catalyst/cocatalyst ion pair. It would also favour the bicomponent mechanism.

Accordingly, Nozaki and co-workers reported the first two components catalyst (**18a**, Figure 1.15).[87b] The catalyst, bearing a piperidinium moiety tethered to the ligand, showed high selectivity (> 99 %) and activity (TOF = 250 h^{-1}) for PPC formation at 14 bar of CO_2 and 25 ºC, in absence of additional cocatalyst. The tethered piperidinium moiety efficiently suppressed the formation of cyclic carbonate, allowing the reaction to be heated to 60 ºC (TOF = 680 h^{-1}) whilst retaining high polymer selectivity (~ 90 %).

Later, Lee and co-workers reported a [Co(III)] metal salen complex featuring two tethered ammonium arm for PO/CO_2 copolymerisation (**18b**, Figure 1.15).[87c] The complex was thermally robust and showed high activity (3500 h^{-1}), at 90 ºC, whilst retaining good

polymer selectivity (~ 90 %). In addition, the enantiopure catalyst **18b**, featuring a bulky substituent, afforded isotactic poly(chloropropylene carbonate).[88] Under the same conditions, an analogous catalyst/cocatalyst combination showed low activity and poor selectivity for polymer.[89] This was proposed to be due to the ammonium salt, tethered to the salen backbone, ensuring that any dissociated polycarbonate chains remain in "close proximity" to the metal. Moreover, the enhanced selectivities of the bifunctional catalyst over the binary systems were likely due to higher activation energy barriers to cyclic by-products.

Shortly after, Lee reported a series of [Co(III)] metal salen complexes bearing tethered ammonium groups for PO/CO_2 copolymerisation.[90] Thus, complex **18c**, bearing four – onium substituents, was the most active and afforded PPC, at 70 ºC, with excellent polymer selectivity (> 99 %) and with very impressive productivities (TON > 20 000) and activities (TOF > 20 000 h^{-1}). In addition, the catalyst could be separated from the polymer (by column chromatography on a small-scale) and re-used, without significant loss of catalytic performance.[91] Further kinetic and mechanistic investigations have implicated cobaltate intermediates and various coordination geometries as important for good activity.[92] Additionally, the catalysts have been applied to prepare various polymers, with variable composition and architectures.[25, 93] Thus, telechelic PPC has been synthetised and used to prepare of block copolymers and polyurethanes.[94]

Darensbourg *et al.* applied **18d** to the copolymerisation of other epoxides, including cyclopropene oxide and indene oxide (Figure 1.15). Such monomers had previously proven very difficult to copolymerise (low selectivities/catalysts). The bifunctional catalysts showed improved activities and selectivity compared to previous analogous catalyst/cocatalyst combination.[21, 95] Beside, the study highlighted that poly(cyclopentene

carbonate) could undergo facile depolymerisation to regenerate epoxide/CO_2, a very unusual finding as most polycarbonates depolymerise to cyclic carbonates.[96]

1.6.4.2 Neutral Lewis-Base Cocatalysts

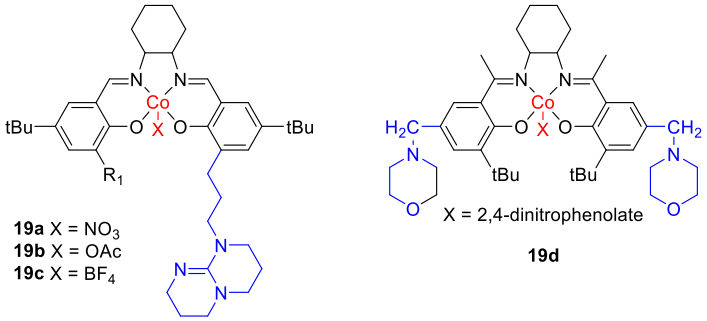

Figure 1.16. Bicomponent cobalt(III) salen complexes bearing Lewis bases.[59, 61e, 87a, 97]

Applying a similar strategy, Lu and co-workers also designed various new salen ligands with tethered neutral Lewis bases (Figure 1.16).[61e, 61f, 87a] The catalyst with an anchored TBD group, **19a-c**, was highly active (TOF up to 10 000 h^{-1}) and selective (> 97 %), even at high temperatures (up to 100 ºC), for CHO, PO and styrene oxide (SO)/CO_2 copolymerisation.[89, 98] In addition, the catalyst afforded epichlorohydrin/CO_2 copolymers (> 99 % carbonate linkages). A decrease in the reaction temperature, from 25 ºC to 0 ºC, enabled a high selectivity for polymer formation (> 99 % vs. cyclic carbonate), whereas under the same conditions, a binary cobalt salen/PPN-X system led to only 66 % selectivity for polymer.[99]

Morpholine moieties were also successfully tethered to salen backbone (Figure 1.16). Firstly reported by Wang *et al.*, the [Co(III)] catalyst showed promising activities for PO/CO_2 copolymerisation in absence of catalyst.[60] Nui and co-workers reported a closely related catalyst **19d** having high activity (TOF = 633 h^{-1}) and selectivity (> 99 % carbonate linkages).[97] The catalyst was also applied in various terpolymerisations.

1.6.4.3 Metal Free Bicomponent Catalysts

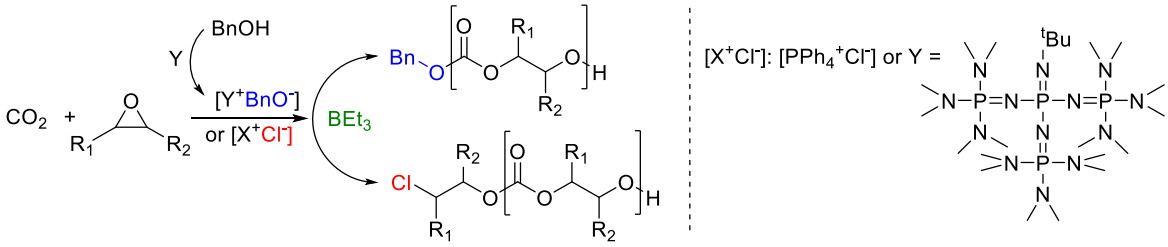

Scheme 1.6. Bicomponent metal free system reported by Feng.[100]

In 2016, Feng and co-workers reported a metal-free catalyst for CO_2/CHO and CO_2/PO copolymerisation (Scheme 1.6).[100] Using Lewis acidic BEt_3 in the presence of a cocatalyst and with added alcohol, polycarbonate with > 99 % of carbonate linkages was formed, at 10 bar of CO_2, and 60 ^oC. The selectivity for polycarbonate against cyclic carbonate was dependent on the co-catalyst used but was high most cases (> 82 %). Darensbourg *et al.* used a similar approach to successfully copolymerise PO with carbonyl sulphide (COS), at ambient temperature, starting from BEt_3 and a quaternary ammonium salt.[101] Perfectly alternating copolymer with > 99 % head-to-tail selectivity were achieved and the catalyst system showed good activities (TOF = 119 h^{-1}, 25 ^oC, COS:PO = 2:1, molar ratio).

1.7 *rac*-Lactide Ring Opening Polymerisation

1.7.1 Generality

Polylactide (PLA) is an aliphatic polyester composed of lactic acid repeating units (Scheme 1.7). It has attracted much attention as it is fully renewable and biodegradable polymers, undergoing hydrolysis to produce lactic acid, which can be metabolised both in vivo and in the environment.[102] Three common methods are used to prepare PLA: polycondensation of lactic acid,[103] ring opening polymerisation (ROP) of lactide[104] and ROP of lactic acid *O*-carboxyanhydride.[105] Within the field of lactide ROP, the release of the ring strain upon ring opening of the monomer serve as a thermodynamic driving force for the polymerisation.[106] The ROP can be initiated by metal complexes,[107] organic/cationic compounds,[108] or enzymes with or without alcohol,[109] to yield PLA with high molecular weight in excellent conversion and low dispersity. Metal complexes are desirable because of their good control over polymerisation reactions as well as their high activity and stability even in the presence of protic impurities.[110] Metal complexes also allow the straightforward synthesis of block copolymers.[10a, 107a] The most common initiators are metal alkoxides or amides, which are especially useful due to their tolerance, selectivity, rate, and lack of side reactions.[107c]

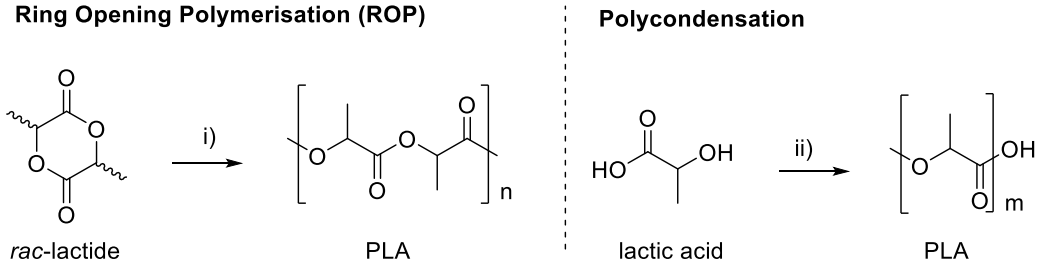

Scheme 1.7. Illustration of the lactide ROP and lactic acid polycondensation to form PLA. i) catalyst; ii) heat.

1.7.2 Properties and Applications

The detailed physical, rheological, and processing properties of PLA have been the subject of a number of good reviews and the reader is referred to these for a detailed account.[111] The physical properties of PLA are often compared to polystyrene; it has a high modulus and strength but low toughness. PLA exhibits a crystallinity that depends on the stereochemistry of the polymer, isotactic poly(L-lactide) is a crystalline thermoplastic with a T_g of approximately 60 ^oC and a T_m of 170–180 ^oC, whilst atactic PLA is an amorphous material.[112] The improvement on the thermal properties of isotactic PLA has driven the development of catalysts able to synthesise such stereoblocks or stereocomplexes from a *racemic* mixture of lactide.[113] Althought this field of PLA catalysts development is relevant to the field, it is not further developed in this thesis.

Amorphous PLA has good oil resistance, good barrier properties to aromas and low temperature heat sealability, making it a useful material for packaging applications.[111d] Furthermore, PLA can be processed by injection molding, melt fibre spinning, film casting and thermoforming.[111d]

1.7.3 Mechanisms

There are two general mechanisms of the polymerisation: the coordination-insertion mechanism for metal complexes[114] and the activated monomer mechanism for organo-cationic initiators.[115] It is worth noting that the two mechanisms have different initiation/propagation profile but typically show a living polymerisation behaviour (i.e linear increase of the polymer molecular weight over the conversion). As only metal complexes will be used in this thesis, only the coordination-insertion will be described (Scheme 1.8). According to the mechanism, the Lewis acidic metal centre loosely binds and activates the lactide. The metal alkoxide group attacks the lactide to form a tetrahedral intermediate. The intermediate undergoes acyl bond cleavage of the lactide ring to regenerate a new metal alkoxide species and a growing chain, which is end capped with an

ester or amide group. A wide range of metal complexes have been tested with nearly all the Lewis acidic metals centres in the periodic table.[90, 107c, 116] Catalysts for *rac*-LA ROP have been extensively reviewed in the literature and the reader is referred to these for a detailed account.[90, 107c, 113d, 116] In this thesis Zn(II) catalysts are investigated and a relevant introduction to the prior literature is provided in Chapter 4.

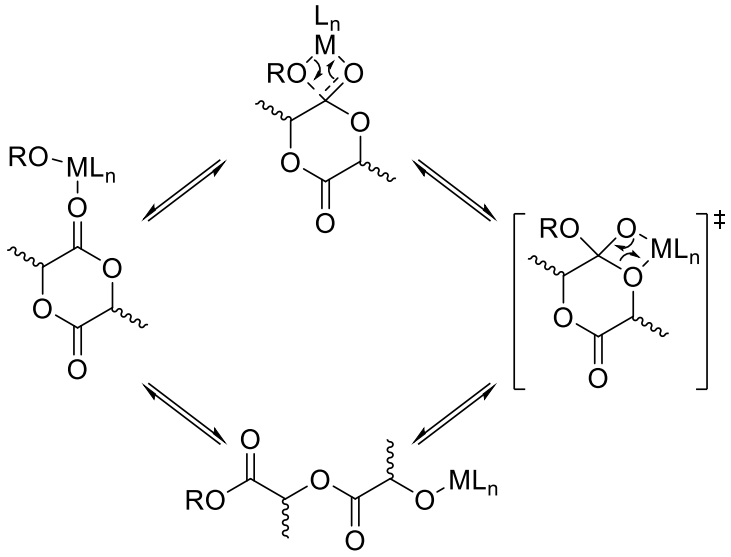

Scheme 1.8. The coordination-insertion mechanism.

1.8 Outlook

This chapter reviews the advances in CO_2/epoxide copolymerisation catalysis. The activity/selectivity of catalysts has improved significantly and is underpinned by mechanistic studies which point to both dinuclear and bicomponent mechanisms. The chapter also introduces the field of lactide ring opening polymerisation and describes the coordination-insertion mechanism typically observed for metal catalysed polymerisation.

The enthusiasm for polymers sourced from biomass, or CO_2, continues to grow. In order to broaden scope and application for these materials, products, processes and catalyts that improve efficiency and reduce costs are needed. This, of course, should occur in parallel with material development and polymer chemistry, as there is a strong link between polymer synthesis and its properties.

There are still fundamental challenges in this field, including a need for improved insight into mechanisms and intermediates on the polymerisation catalysis, as well as the need to increase active and tolerance to impurities (i.e. air and moisture stability). Despite the successes achieved so far, it is remarkable how limited the range of catalysts for ROCOP remains. There is still a considerable lack of understanding of the requirements for a good ligand (electronic/steric considerations), active site (metal) and initiator. For both ROCOP and ROP, there are clearly opportunities to introduce new catalysts, including the development of new ligands, metals and combinations so as to improve performance.

There is also a need for fine control of polymerisation, specifically to control the regio-chemistry and stereochemistry of polymerisation, so as to enable new polymer tacticities and microstructures. Thus, although the fields of ROCOP and ROP catalysis were discovered some decades ago, there remain exciting future opportunities and significant new challenges to be overcome.

1.9 Aims and Objectives

The broad aims of this thesis can be summarised as follow:

1. To study new ancillary ligands. This includes the study of coordination geometry of the ligand during catalysis and also to correlate its overall conformation with the catalyst activity. In addition, structure/activity relationships will be investigated to rationalise observed electronic/steric substituent effects on the polymerisation rate and selectivity.
2. To study the influence of the metal centre (size, Lewis acidity) on the polymerisation reaction. The kinetics of the reaction will be investigated to deduce the rate law (mononuclear or dinuclear mechanism) and to propose a rate determining step. In addition, attempts will be made to isolate catalytic intermediates.
3. To investigate the influence of the initiating group (steric bulk, nucleophilicity, basicity) on the rate and the selectivity of the polymerisation reaction. Currently, it is not clear what effect, if any, this group should exert. On the one hand, theory dictates initiation should be irrelevant to catalysis, but on the other hand several reports observed improved activity/selectivity by changing the initiator.[68d] It is, therefore, important to understand better its role in catalysis.
4. To explore the concept of intermetallic cooperativity during polymerisation. To investigate whether there is any link between metal-metal distance and catalytic activities. This will be investigated by comparing the activity of several dinuclear catalysts against their mononuclear homologue.

For each chapter, the main objectives can be described as:

Objectives of chapter 3:

1. To design and to synthesis a novel class of mononuclear indium salen catalysts for low CO_2 pressure, epoxide ROCOP.
2. To understand the effects of different ligands (with different electronic or steric properties) and different initiator on the activity and the selectivity of the polymerisation.
3. To perform a mechanistic study of the best catalyst by isolation of catalytic intermediates and kinetic studies of the reaction (order in monomers and catalyst).
4. To rationalise a mechanism in accordance with the mechanistic study results.

Objectives of chapter 4:

1. To develop new highly active dinuclear zinc macrocycle catalysts for lactide ROP.
2. To understand the link between metal-metal distance and cooperativity effect by synthesising macrocycles differing in size and comparing activities with a monometallic homologue.
3. To investigate the link between the type of initiators and the kinetic profile of the polymerisation (order in monomer).
4. To correlate the hyper activity of the series with structural information to understand the requirements for a highly active ROP catalyst.

Objectives of Chapter 5:

1. To synthesis and characterise a new series of dinuclear zinc salen catalysts from *o*-vanillin with different backbone for CO_2/epoxide ROCOP.
2. To test the series for CO_2/epoxide ROCOP and to draw a conclusion on the structure/activity relationship for these complexes.

3. To form block copolymers from cyclic anhydride/CO_2/epoxide ROCOP.

1.10 References

[1] a) https://www.statista.com/statistics/282732/global-production-of-plastics-since-1950/*, visited: 2017*, last update: **2017**; b) http://ifbb.wp.hs-hannover.de/downloads/index.php?site=Statistics&nav=5-1-0-0-0*, visited: 2017*, last update: **2015**.

[2] S. Lambert, M. Wagner, *Chem. Soc. Rev.* **2017**.

[3] R. C. Thompson, S. H. Swan, C. J. Moore, F. S. vom Saal, *Phil. Trans. R. Soc. B Biol. Sci.* **2009**, *364*, 1973-1976.

[4] R. Geyer, J. R. Jambeck, K. L. Law, *Sci. Adv.* **2017**, *3*.

[5] J. F. Patrick, M. J. Robb, N. R. Sottos, J. S. Moore, S. R. White, *Nature* **2016**, *540*, 363-370.

[6] Y. Zhu, C. Romain, C. K. Williams, *Nature* **2016**, *540*, 354-362.

[7] F. Aeschelmann, M. Carus, *Indus. Biotechnol.* **2015**, *11*, 154-159.

[8] D. J. Darensbourg, *Chem. Rev.* **2007**, *107*, 2388-2410.

[9] J. Xu, E. Feng, J. Song, *J. Appl. Polym. Sci.* **2014**, *131*, 39822-39838.

[10] a) S. Paul, Y. Zhu, C. Romain, R. Brooks, P. K. Saini, C. K. Williams, *Chem. Commun.* **2015**, *51*, 6459-6479; b) G. Trott, P. K. Saini, C. K. Williams, *Phil. Trans. R. Soc. A Math. Phys. Engin. Sci.* **2016**, *374*.

[11] a) M. Helou, O. Miserque, J.-M. Brusson, J.-F. Carpentier, S. M. Guillaume, *Chem. Eur. J.* **2008**, *14*, 8772-8775; b) N. Ajellal, J.-F. Carpentier, C. Guillaume, S. M. Guillaume, M. Helou, V. Poirier, Y. Sarazin, A. Trifonov, *Dalton Trans.* **2010**, *39*, 8363-8376; c) S. M. Quan, P. L. Diaconescu, *Chem. Commun.* **2015**, *51*, 9643-9646.

[12] a) C. Romain, A. Thevenon, P. Saini, C. Williams, Springer Berlin Heidelberg, **2015**, pp. 1-41; b) G. W. Coates, D. R. Moore, *Angew. Chem. Int. Ed.* **2004**, *43*, 6618-6639; c) G. A. Luinstra, *Polym. Rev.* **2008**, *48*, 192-219.

[13] N. von der Assen, A. Bardow, *Green Chem.* **2014**, *16*, 3272-3280.

[14] a) D. J. Darensbourg, W.-C. Chung, K. Wang, H.-C. Zhou, *ACS Catal.* **2014**, *4*, 1511-1515; b) A. M. Chapman, C. Keyworth, M. R. Kember, A. J. J. Lennox, C. K. Williams, *ACS Catal.* **2015**, *5*, 1581-1588.

[15] Y. Qin, X. Wang, *Biotechno. J.* **2010**, *5*, 1164-1180.

[16] C. Koning, J. Wildeson, R. Parton, B. Plum, P. Steeman, D. J. Darensbourg, *Polymer* **2001**, *42*, 3995-4004.

[17] J.-M. Sauer, J. Bao, R. L. Smith, T. D. McClure, M. Mayersohn, U. Pillai, M. L. Cunningham, I. G. Sipes, *Drug Metab. Dispos.* **1997**, *25*, 371-378.

[18] a) M. I. Childers, J. M. Longo, N. J. Van Zee, A. M. LaPointe, G. W. Coates, *Chem. Rev.* **2014**, *114*, 8129-8152; b) W. C. Ellis, Y. Jung, M. Mulzer, R. Di Girolamo, E. B. Lobkovsky, G. W. Coates, *Chem. Sci.* **2014**, *5*, 4004-4011; c) Y. Liu, W.-M. Ren, J. Liu, X.-B. Lu, *Angew. Chem. Int. Ed.* **2013**, *52*, 11594-11598; d) K. Nakano, K. Kobayashi, T. Ohkawara, H. Imoto, K. Nozaki, *J. Am.Chem. Soc.* **2013**, *135*, 8456-8459; e) R. M. Thomas, P. C. B. Widger, S. M. Ahmed, R. C. Jeske, W. Hirahata, E. B. Lobkovsky, G. W. Coates, *J. Am. Chem. Soc.* **2010**, *132*, 16520-16525.

[19] O. Hauenstein, S. Agarwal, A. Greiner, **2016**, *7*, 11862.

[20] a) Y. Liu, W.-M. Ren, W.-P. Zhang, R.-R. Zhao, X.-B. Lu, *Nat. Commun.* **2015**, *6*; b) Y. Liu, W.-M. Ren, K.-K. He, X.-B. Lu, *Nat. Commun.* **2014**, *5*.

[21] D. J. Darensbourg, S. J. Wilson, *Macromolecules* **2013**, *46*, 5929-5934.

[22] a) L. Du, B. Qu, Y. Meng, Q. Zhu, *Compos. Sci. Technol.* **2006**, *66*, 913-918; b) W. Chen, M. Pang, M. Xiao, S. Wang, L. Wen, Y. Meng, *J. Reinf. Plast. Compos.* **2010**, *29*, 1545-1550; c) X. L. Wang, R. K. Y. Li, Y. X. Cao, Y. Z. Meng, *Polym. Test.* **2005**, *24*, 699-703.

[23] M. Taherimehr, P. P. Pescarmona, *J. Appl. Polym. Sci.* **2014**, *131*, 41141-41158.

[24] G. Flodberg, I. Helland, L. Thomsson, S. Bodil Fredriksen, *Eur. Polym. J.* **2015**, *63*, 217-226.

[25] A. Cyriac, S. H. Lee, J. K. Varghese, J. H. Park, J. Y. Jeon, S. J. Kim, B. Y. Lee, *Green Chem.* **2011**, *13*, 3469-3475.

[26] A. Welle, M. Kröger, M. Döring, K. Niederer, E. Pindel, I. S. Chronakis, *Biomaterials* **2007**, *28*, 2211-2219.

[27] C. E. Koning, R. J. Sablong, E. H. Nejad, R. Duchateau, P. Buijsen, *Prog. Org. Coat.* **2013**, *76*, 1704-1711.

[28] a) J. Langanke, A. Wolf, J. Hofmann, K. Bohm, M. A. Subhani, T. E. Muller, W. Leitner, C. Gurtler, *Green Chem.* **2014**, *16*, 1865-1870; b) D. Wang, G. Zhang, Y. Zhang, Y. Gao, Y. Zhao, C. Zhou, Q. Zhang, X. Wang, *J. Appl. Polym. Sci.* **2007**, *103*, 417-424; c) H. Blattmann, M. Fleischer, M. Bähr, R. Mülhaupt, *Macromol. Rapid Commun.* **2014**, *35*, 1238-1254.

[29] a) M. Kröger, C. Folli, O. Walter, M. Döring, *Adv. Synth. Catal.* **2006**, *348*, 1908-1918; b) G.-P. Wu, D. J. Darensbourg, X.-B. Lu, *J. Am. Chem. Soc.* **2012**, *134*, 17739-17745; c) D. J. Darensbourg, G.-P. Wu, *Angew. Chem. Int. Ed.* **2013**, *52*, 10602-10606; d) M. R. Kember, J. Copley, A. Buchard, C. K. Williams, *Polym. Chem.* **2012**, *3*, 1196-1201.

[30] a) Y. Liu, M. Wang, W.-M. Ren, K.-K. He, Y.-C. Xu, J. Liu, X.-B. Lu, *Macromolecules* **2014**, *47*, 1269-1276; b) J. Geschwind, F. Wurm, H. Frey, *Macromol. Chem. Phys.* **2013**, *214*, 892-901; c) A. Dag, M. Aydin, H. Durmaz, G. Hizal, U. Tunca, *J. Polym. Sci., Part A Polym. Chem.* **2012**, *50*, 4476-4483; d) J.-F. Zhang, W.-M. Ren, X.-K. Sun, Y. Meng, B.-Y. Du, X.-H. Zhang, *Macromolecules* **2011**, *44*, 9882-9886.

[31] a) T. Stöβer, C. Li, J. Unruangsri, P. K. Saini, R. J. Sablong, M. A. R. Meier, C. K. Williams, C. Koning, *Polym. Chem.* **2017**, *8*, 6099-6105; b) G.-Q. Chen, M. K. Patel, *Chem. Rev.* **2012**, *112*, 2082-2099.

[32] J. Geschwind, H. Frey, *Macromol. Rapid Commun.* **2013**, *34*, 150-155.

[33] a) C. J. Whiteoak, N. Kielland, V. Laserna, F. Castro-Gómez, E. Martin, E. C. Escudero-Adán, C. Bo, A. W. Kleij, *Chem. Eur. J.* **2014**, *20*, 2264-2275; b) C. M. Byrne, S. D. Allen, E. B. Lobkovsky, G. W. Coates, *J. Am. Chem. Soc.* **2004**, *126*, 11404-11405.

[34] C. Li, R. J. Sablong, C. E. Koning, *Eur. Polym. J.* **2015**, *67*, 449-458.

[35] F. Auriemma, C. De Rosa, M. R. Di Caprio, R. Di Girolamo, W. C. Ellis, G. W. Coates, *Angew. Chem. Int. Ed.* **2015**, *54*, 1215-1218.

[36] M. Winkler, C. Romain, M. A. R. Meier, C. K. Williams, *Green Chem.* **2015,** *17*, 300-306.

[37] D. J. Darensbourg, A. D. Yeung, *Macromolecules* **2013**, *46*, 83-95.

[38] W. Guerin, A. K. Diallo, E. Kirilov, M. Helou, M. Slawinski, J.-M. Brusson, J.-F. Carpentier, S. M. Guillaume, *Macromolecules* **2014**, *47*, 4230-4235.

[39] S. Inoue, *J. Polym. Chem., Part A: Polym. Chem.* **2000**, *38*, 2861-2871.

[40] F. Jutz, A. Buchard, M. R. Kember, S. B. Fredrickson, C. K. Williams, *J. Am. Chem. Soc.* **2011**, *133*, 17395–17405.

[41] S. Inoue, H. Koinuma, T. Tsuruta, *J. Polym. Sci. Part B: Polym. Lett.* **1969**, *7*, 287-292.

[42] a) S. Inoue, H. Koinuma, Y. Yokoo, T. Tsuruta, *Makromol. Chem.* **1971**, *143*, 97-104; b) M. Kobayashi, S. Inoue, T. Tsuruta, *J. Polym. Chem., Part A Polym. Chem.* **1973**, *11*, 2383-2385; c) T. Hirano, S. Inoue, T. Tsuruta, *Makromol. Chem.* **1975**, *176*, 1913-1917; d) T. Hirano, S. Inoue, T. Tsuruta, *Makromol. Chem.* **1976**, *177*,

3237-3243; e) Y. Hasebe, T. Tsuruta, *Makromol. Chem.* **1987**, *188*, 1403-1414; f) Y. Hasebe, T. Tsuruta, *Makromol. Chem.* **1988**, *189*, 1915-1926; g) N. Yoshino, C. Suzuki, H. Kobayashi, T. Tsuruta, *Makromol. Chem.* **1988**, *189*, 1903-1913; h) M. Ishimori, T. Hagiwara, T. Tsuruta, Y. Kai, N. Yasuoka, N. Kasai, *Bull. Chem. Soc. Jpn.* **1976**, *49*, 1165-1166; i) M. Kobayashi, Y.-L. Tang, T. Tsuruta, S. Inoue, *Makromol. Chem.* **1973**, *169*, 69-81.

[43] a) R. Eberhardt, M. Allmendinger, M. Zintl, C. Troll, G. A. Luinstra, B. Rieger, *Macromol. Chem. Phys.* **2004**, *205*, 42-47; b) J. S. Kim, M. Ree, S. W. Lee, W. Oh, S. Baek, B. Lee, T. J. Shin, K. J. Kim, B. Kim, J. Lüning, *J. Catal.* **2003**, *218*, 386-395; c) S. J. Wang, L. C. Du, X. S. Zhao, Y. Z. Meng, S. C. Tjong, *J. Appl. Poly. Sci.* **2002**, *85*, 2327-2334; d) Y. Z. Meng, L. C. Du, S. C. Tiong, Q. Zhu, A. S. Hay, *J. Polym. Chem., Part A Polym. Chem.* **2002**, *40*, 3579-3591.

[44] M. Ree, J. Y. Bae, J. H. Jung, T. J. Shin, *J. Polym. Sci., Part A Polym. Chem.* **1999**, *37*, 1863-1876.

[45] a) S. Chen, G.-R. Qi, Z.-J. Hua, H.-Q. Yan, *J. Polym. Chem., Part A: Polym. Chem.* **2004**, *42*, 5284-5291; b) I. Kim, M. J. Yi, S. H. Byun, D. W. Park, B. U. Kim, C. S. Ha, *Macromol. Symp.* **2005**, *224*, 181-192.

[46] a) W. Hinz, E. M. Dexheimer, E. Bohres, G. H. Grosch, BASF Corporation, **2004**; b) W. Hinz, J. Wildeson, E. M. Dexheimer, BASF Corporation, **2007**; c) W. Hinz, J. Wildeson, E. M. Dexheimer, R. Neff, BASF Corporation, **2004**; d) W. J. Kruper, D. J. Swart, The Dow Chemical Company, **1985**; e) J. Kuyper, P. W. Lednor, G. A. Pogany, Shell Oil Company, **1989**; f) J. Kuyper, P. W. Lednor, G. A. Pogany, Shell Oil Company, **1989**; g) J. Kuyper, P. W. Lednor, G. A. Pogany, Shell Oil Company, **1989**.

[47] a) D. J. Darensbourg, M. J. Adams, J. C. Yarbrough, *Inorg. Chem.* **2001**, *40*, 6543-6544; b) D. J. Darensbourg, M. J. Adams, J. C. Yarbrough, A. L. Phelps, *Inorg. Chem.* **2003**, *42*, 7809-7818; c) N. J. Robertson, Z. Qin, G. C. Dallinger, E. B. Lobkovsky, S. Lee, G. W. Coates, *Dalton Trans.* **2006**, 5390-5395.

[48] M. Ree, Y. Hwang, J.-S. Kim, H. Kim, G. Kim, H. Kim, *Catal. Today* **2006**, *115*, 134-145.

[49] S. Klaus, M. W. Lehenmeier, E. Herdtweck, P. Deglmann, A. K. Ott, B. Rieger, *J. Am. Chem. Soc.* **2011**, *133*, 13151-13161.

[50] N. Takeda, S. Inoue, *Makromol. Chem.* **1978**, *179*, 1377-1381.

[51] a) D. J. Darensbourg, M. W. Holtcamp, *Macromolecules* **1995**, *28*, 7577-7579; b) D. J. Darensbourg, M. W. Holtcamp, G. E. Struck, M. S. Zimmer, S. A. Niezgoda, P. Rainey, J. B. Robertson, J. D. Draper, J. H. Reibenspies, *J. Am. Chem. Soc.* **1998**, *121*, 107-116.

[52] D. J. Darensbourg, J. R. Wildeson, J. C. Yarbrough, J. H. Reibenspies, *J. Am. Chem. Soc.* **2000**, *122*, 12487-12496.

[53] D. J. Darensbourg, J. R. Wildeson, J. C. Yarbrough, *Inorg. Chem.* **2002**, *41*, 973-980.

[54] O. Hampel, C. Rode, D. Walther, R. Beckert, H. Görls, *Naturforsch. B.* **2002**, *57*, 946-956.

[55] M. Cheng, E. B. Lobkovsky, G. W. Coates, *J. Am. Chem. Soc.* **1998**, *120*, 11018-11019.

[56] a) M. Cheng, D. R. Moore, J. J. Reczek, B. M. Chamberlain, E. B. Lobkovsky, G. W. Coates, *J. Am. Chem. Soc.* **2001**, *123*, 8738-8749; b) D. R. Moore, M. Cheng, E. B. Lobkovsky, G. W. Coates, *J. Am. Chem. Soc.* **2003**, *125*, 11911-11924.

[57] a) S. Kernbichl, M. Reiter, F. Adams, S. Vagin, B. Rieger, *J. Am. Chem. Soc.* **2017**, *139*, 6787-6790; b) M. Reiter, S. Vagin, A. Kronast, C. Jandl, B. Rieger, *Chem. Sci.* **2017**, *8*, 1876-1882.

[58] a) D. J. Darensbourg, J. C. Yarbrough, *J. Am. Chem. Soc.* **2002**, *124*, 6335-6342; b) Z. Qin, C. M. Thomas, S. Lee, G. W. Coates, *Angew. Chem. Int. Ed.* **2003**, *42*, 5484-5487; c) R. Eberhardt, M. Allmendinger, B. Rieger, *Macromol. Rapid Commun.* **2003**, *24*, 194-196.

[59] C. T. Cohen, T. Chu, G. W. Coates, *J. Am. Chem. Soc.* **2005**, *127*, 10869-10878.

[60] X.-B. Lu, Y. Wang, *Angew. Chem. Int. Ed.* **2004**, *43*, 3574-3577.

[61] a) W.-M. Ren, T.-J. Yue, X. Zhang, G.-G. Gu, Y. Liu, X.-B. Lu, *Macromolecules* **2017**, *50*, 7062-7069; b) E. Hosseini Nejad, C. G. W. van Melis, T. J. Vermeer, C. E. Koning, R. Duchateau, *Macromolecules* **2012**, *45*, 1770-1776; c) M. E. Fieser, M. J. Sanford, L. A. Mitchell, C. R. Dunbar, M. Mandal, N. J. Van Zee, D. M. Urness, C. J. Cramer, G. W. Coates, W. B. Tolman, *J. Am. Chem. Soc.* **2017**; d) D. J. Darensbourg, in *Adv. Inorg. Chem., Vol. 66* (Eds.: M. Aresta, R. van Eldik), Academic Press, **2014**, pp. 1-23; e) X.-B. Lu, D. J. Darensbourg, *Chem. Soc. Rev.* **2012**, *41*, 1462-1484; f) X.-B. Lu, W.-M. Ren, G.-P. Wu, *Acc. Chem. Res.* **2012**, *45*, 1721-1735.

[62] T. Ohkawara, K. Suzuki, K. Nakano, S. Mori, K. Nozaki, *J. Am. Chem. Soc.* **2014**, *136*, 10728-10735.

[63] K. Devaine-Pressing, C. M. Kozak, *ChemSusChem* **2017**, *10*, 1266-1273.

[64] a) B. Y. Lee, H. Y. Kwon, S. Y. Lee, S. J. Na, S.-i. Han, H. Yun, H. Lee, Y.-W. Park, *J. Am. Chem. Soc.* **2005**, *127*, 3031-3037; b) M. R. Kember, C. K. Williams, *J. Am. Chem. Soc.* **2012**, *134*, 15676-15679; c) A. Buchard, F. Jutz, M. R. Kember, A. J. P. White, H. S. Rzepa, C. K. Williams, *Macromolecules* **2012**, *45*, 6781-6795;

d) F. Jutz, A. Buchard, M. R. Kember, S. B. Fredriksen, C. K. Williams, *J. Am. Chem. Soc.* **2011**, *133*, 17395-17405; e) M. W. Lehenmeier, S. Kissling, P. T. Altenbuchner, C. Bruckmeier, P. Deglmann, A.-K. Brym, B. Rieger, *Angew. Chem. Int. Ed.* **2013**, *52*, 9821-9826; f) C. E. Anderson, S. I. Vagin, M. Hammann, L. Zimmermann, B. Rieger, *ChemCatChem* **2013**, *5*, 3269-3280; g) S. Klaus, M. W. Lehenmeier, C. E. Anderson, B. Rieger, *Coord. Chem. Rev.* **2011**, *255*, 1460-1479.

[65] T. Bok, H. Yun, B. Y. Lee, *Inorg. Chem.* **2006**, *45*, 4228-4237.

[66] Y. Xiao, Z. Wang, K. Ding, *Macromolecules* **2005**, *39*, 128-137.

[67] Y. L. Xiao, Z. Wang, K. L. Ding, *Chem. Eur. J.* **2005**, *11*, 3668-3678.

[68] a) P. K. Saini, C. Romain, C. K. Williams, *Chem. Commun.* **2014**, *50*, 4164-4167; b) M. R. Kember, F. Jutz, A. Buchard, A. J. P. White, C. K. Williams, *Chem. Sci.* **2012**, *3*, 1245-1255; c) A. Buchard, C. M. Bakewell, J. Weiner, C. K. Williams, in *Organometallics and Renewables, Vol. 39* (Eds.: M. A. R. Meier, B. M. Weckhuysen, P. C. A. Bruijnincx), **2012**, pp. 175-224; d) M. R. Kember, A. Buchard, C. K. Williams, *Chem. Commun.* **2011**, *47*, 141-163; e) A. Buchard, M. R. Kember, K. G. Sandeman, C. K. Williams, *Chem. Commun.* **2011**, *47*, 212-214; f) M. R. Kember, A. J. P. White, C. K. Williams, *Macromolecules* **2010**, *43*, 2291-2298; g) M. R. Kember, A. J. P. White, C. K. Williams, *Inorg. Chem.* **2009**, *48*, 9535-9542; h) M. R. Kember, P. D. Knight, P. T. R. Reung, C. K. Williams, *Angew. Chem. Int. Ed.* **2009**, *48*, 931-933.

[69] a) Y. Zhu, C. Romain, C. K. Williams, *J. Am. Chem. Soc.* **2015**, *137*, 12179-12182; b) C. Romain, C. K. Williams, *Angew. Chem. Int. Ed.* **2014**, *53*, 1607-1610; c) C. Romain, Y. Zhu, P. Dingwall, S. Paul, H. S. Rzepa, A. Buchard, C. K. Williams, *J. Am. Chem. Soc.* **2016**, *138*, 4120-4131; d) S. Paul, C. Romain, J. Shaw, C. K. Williams, *Macromolecules* **2015**, *48*, 6047-6056.

[70] J. A. Garden, A. J. P. White, C. K. Williams, *Dalton Trans.* **2017**, *46*, 2532-2541.

[71] J. A. Garden, P. K. Saini, C. K. Williams, *J. Am. Chem. Soc.* **2015**, *137*, 15078-15081.

[72] C.-H. Li, H.-J. Chuang, C.-Y. Li, B.-T. Ko, C.-H. Lin, *Polym. Chem.* **2014**, *5*, 4875-4878.

[73] L.-S. Huang, C.-Y. Tsai, H.-J. Chuang, B.-T. Ko, *Inorg. Chem.* **2017**, *56*, 6141-6151.

[74] K. Nakano, T. Hiyama, K. Nozaki, *Chem. Commun.* **2005**, 1871-1873.

[75] K. Nishioka, H. Goto, H. Sugimoto, *Macromolecules* **2012**, *45*, 8172-8192.

[76] K. Nakano, K. Nozaki, T. Hiyama, *J. Am. Chem. Soc.* **2003**, *125*, 5501-5510.

[77] a) N. D. Harrold, Y. Li, M. H. Chisholm, *Macromolecules* **2013**, *46*, 692-698; b) C. Chatterjee, M. H. Chisholm, A. El-Khaldy, R. D. McIntosh, J. T. Miller, T. Wu, *Inorg. Chem.* **2013**, *52*, 4547-4553; c) A. Bernard, C. Chatterjee, M. H. Chisholm, *Polymer* **2013**, *54*, 2639-2646; d) C. Chatterjee, M. H. Chisholm, *Inorg. Chem.* **2012**, *51*, 12041-12052; e) C. Chatterjee, M. H. Chisholm, *Inorg. Chem.* **2011**, *50*, 4481-4492; f) M. H. Chisholm, Z. Zhou, *J. Am. Chem. Soc.* **2004**, *126*, 11030-11039.

[78] a) D. F. J. Piesik, S. Range, S. Harder, *Organometallics* **2008**, *27*, 6178-6187; b) M. F. Pilz, C. Limberg, B. B. Lazarov, K. C. Hultzsch, B. Ziemer, *Organometallics* **2007**, *26*, 3668-3676.

[79] S. Kissling, M. W. Lehenmeier, P. T. Altenbuchner, A. Kronast, M. Reiter, P. Deglmann, U. B. Seemann, B. Rieger, *Chem. Commun.* **2015**, *51*, 4579-4582.

[80] S. Kissling, P. T. Altenbuchner, M. W. Lehenmeier, E. Herdtweck, P. Deglmann, U. B. Seemann, B. Rieger, *Chem. Eur. J.* **2015**, *21*, 8148-8157.

[81] K. Nakano, S. Hashimoto, K. Nozaki, *Chem. Sci.* **2010**, 369-373.

[82] S. I. Vagin, R. Reichardt, S. Klaus, B. Rieger, *J. Am. Chem. Soc.* **2010**, *132*, 14367-14369.

[83] a) R. G. Konsler, J. Karl, E. N. Jacobsen, *J. Am. Chem. Soc.* **1998**, *120*, 10780-10781; b) J. M. Ready, E. N. Jacobsen, *Angew. Chem. Int. Ed.* **2002**, *41*, 1374-1377.

[84] P. C. B. Widger, S. M. Ahmed, G. W. Coates, *Macromolecules* **2011**, *44*, 5666-5670.

[85] W. Hirahata, R. M. Thomas, E. B. Lobkovsky, G. W. Coates, *J. Am. Chem. Soc.* **2008**, *130*, 17658-17659.

[86] S. Klaus, S. I. Vagin, M. W. Lehenmeier, P. Deglmann, A. K. Brym, B. Rieger, *Macromolecules* **2011**, *44*, 9508-9516.

[87] a) W.-M. Ren, Z.-W. Liu, Y.-Q. Wen, R. Zhang, X.-B. Lu, *J. Am. Chem. Soc.* **2009**, *131*, 11509-11518; b) K. Nakano, T. Kamada, K. Nozaki, *Angew. Chem. Int. Ed.* **2006**, *45*, 7274-7277; c) E. K. Noh, S. J. Na, S. S, S.-W. Kim, B. Y. Lee, *J. Am. Chem. Soc.* **2007**, *129*, 8082-8083.

[88] G.-P. Wu, P.-X. Xu, X.-B. Lu, Y.-P. Zu, S.-H. Wei, W.-M. Ren, D. J. Darensbourg, *Macromolecules* **2013**, *46*, 2128-2133.

[89] W.-M. Ren, X. Zhang, Y. Liu, J.-F. Li, H. Wang, X.-B. Lu, *Macromolecules* **2010**, *43*, 1396-1402.

[90] R. H. Platel, L. M. Hodgson, C. K. Williams, *Polym. Rev.* **2008**, *48*, 11-63.

[91] S. S, J. K. Min, J. E. Seong, S. J. Na, B. Y. Lee, *Angew. Chem. Int. Ed.* **2008**, *47*, 7306-7309.

[92] a) S. J. Na, S. S, A. Cyriac, B. E. Kim, J. Yoo, Y. K. Kang, S. J. Han, C. Lee, B. Y. Lee, *Inorg. Chem.* **2009**, *48*, 10455-10465; b) A. Cyriac, J. Y. Jeon, J. K. Varghese, J. H. Park, S. Y. Choi, Y. K. Chung, B. Y. Lee, *Dalton Trans.* **2012**, *41*, 1444-

1447; c) J. Yoo, S. J. Na, H. C. Park, A. Cyriac, B. Y. Lee, *Dalton Trans.* **2010**, *39*, 2622-2630.

[93] a) J. E. Seong, S. J. Na, A. Cyriac, B.-W. Kim, B. Y. Lee, *Macromolecules* **2009**, *43*, 903-908; b) A. Cyriac, S. H. Lee, B. Y. Lee, *Polym. Chem.* **2011**, *2*, 950-956.

[94] a) A. Cyriac, S. H. Lee, J. K. Varghese, E. S. Park, J. H. Park, B. Y. Lee, *Macromolecules* **2010**, *43*, 7398-7401; b) S. H. Lee, A. Cyriac, J. Y. Jeon, B. Y. Lee, *Polym. Chem.* **2012**, *3*, 1215-1220.

[95] D. J. Darensbourg, W.-C. Chung, S. J. Wilson, *ACS Catal.* **2013**, *3*, 3050-3057.

[96] D. J. Darensbourg, S.-H. Wei, A. D. Yeung, W. C. Ellis, *Macromolecules* **2013**, *46*, 5850-5855.

[97] H. Li, Y. Niu, *Polym. J.* **2011**, *43*, 121-125.

[98] a) W.-M. Ren, Y. Liu, G.-P. Wu, J. Liu, X.-B. Lu, *J. Polym. Sci., Part A Polym. Chem.* **2011**, *49*, 4894-4901; b) G.-P. Wu, S.-H. Wei, X.-B. Lu, W.-M. Ren, D. J. Darensbourg, *Macromolecules* **2010**, *43*, 9202-9204.

[99] G.-P. Wu, S.-H. Wei, W.-M. Ren, X.-B. Lu, T.-Q. Xu, D. J. Darensbourg, *J. Am. Chem. Soc.* **2011**, *133*, 15191-15199.

[100] D. Zhang, S. K. Boopathi, N. Hadjichristidis, Y. Gnanou, X. Feng, *J. Am. Chem. Soc.* **2016**, *138*, 11117-11120.

[101] J.-L. Yang, H.-L. Wu, Y. Li, X.-H. Zhang, D. J. Darensbourg, *Angew. Chem. Int. Ed.* **2017**, *56*, 5774-5779.

[102] a) A. J. Ragauskas, C. K. Williams, B. H. Davison, G. Britovsek, J. Cairney, C. A. Eckert, W. J. Frederick, J. P. Hallett, D. J. Leak, C. L. Liotta, J. R. Mielenz, R. Murphy, R. Templer, T. Tschaplinski, *Science* **2006**, *311*, 484-489; b) M. Hong, E. Y. X. Chen, *Green Chem.* **2017**, *19*, 3692-3706; c) S. Mecking, *Angew. Chem. Int. Ed.* **2004**, *43*, 1078-1085.

[103] M. H. Hartmann, in *Biopolymers from Renewable Resources* (Ed.: D. L. Kaplan), Springer Berlin Heidelberg, Berlin, Heidelberg, **1998**, pp. 367-411.

[104] Y. Sarazin, J.-F. Carpentier, *Chem. Rev.* **2015**, *115*, 3564-3614.

[105] B. Martin Vaca, D. Bourissou, *ACS Macro Letters* **2015**, *4*, 792-798.

[106] A. Duda, S. Penczek, in *Polymers from Renewable Resources, Vol. 764*, American Chemical Society, **2001**, pp. 160-198.

[107] a) X. Wang, A. Thevenon, J. L. Brosmer, I. Yu, S. I. Khan, P. Mehrkhodavandi, P. L. Diaconescu, *J. Am. Chem. Soc.* **2014**, *136*, 11264-11267; b) X. Wang, J. L. Brosmer, A. Thevenon, P. L. Diaconescu, *Organometallics* **2015**, *34*, 4700-4706; c) O. Dechy-Cabaret, B. Martin-Vaca, D. Bourissou, *Chem. Rev.* **2004**, *104*, 6147-6176.

[108] N. E. Kamber, W. Jeong, R. M. Waymouth, R. C. Pratt, B. G. G. Lohmeijer, J. L. Hedrick, *Chem. Rev.* **2007**, *107*, 5813-5840.

[109] a) R. A. Gross, A. Kumar, B. Kalra, *Chem. Rev.* **2001**, *101*, 2097-2124; b) S. Kobayashi, *Macromol. Symp.* **2006**, *240*, 178-185.

[110] A. Thevenon, C. Romain, M. S. Bennington, A. J. P. White, H. J. Davidson, S. Brooker, C. K. Williams, *Angew. Chem. Int. Ed.* **2016**, *55*, 8680-8685.

[111] a) A. Södergård, M. Stolt, *Prog. Polym. Sci.* **2002**, *27*, 1123-1163; b) W. Amass, A. Amass, B. Tighe, *Polym. Int.* **1998**, *47*, 89-144; c) J. Lunt, *Polym. Degrad. Stab.* **1998**, *59*, 145-152; d) R. E. Drumright, P. R. Gruber, D. E. Henton, *Adv. Mater.* **2000**, *12*, 1841-1846; e) A.-C. Albertsson, I. K. Varma, *Biomacromolecules* **2003**, *4*, 1466-1486.

[112] a) D. Myers, A. J. P. White, C. M. Forsyth, M. Bown, C. K. Williams, *Angew. Chem. Int. Ed.* **2017**, *56*, 5277-5282; b) N. Nomura, R. Ishii, M. Akakura, K. Aoi,

J. Am. Chem. Soc. **2002**, *124*; c) N. Nomura, R. Ishii, Y. Yamamoto, T. Kondo, *Chem. Eur. J.* **2007**, *13*, 4433-4451.

[113] a) Z. Zhong, P. J. Dijkstra, J. Feijen, *J. Am. Chem. Soc.* **2003**, *125*, 11291-11298; b) K. Nakano, N. Kosaka, T. Hiyama, K. Nozaki, *Dalton Trans.* **2003**, 4039-4050; c) P. B. Smith, R. A. Gross, H. N. Cheng, in *ACS Symp. Ser., Vol. 1192*, American Chemical Society, **2015**, p. 0; d) M. J. Stanford, A. P. Dove, *Chem. Soc. Rev.* **2010**, *39*, 486-494; e) C. M. Thomas, *Chem. Soc. Rev.* **2010**, *39*, 165-173.

[114] a) P. Dubois, C. Jacobs, R. Jerome, P. Teyssie, *Macromolecules* **1991**, *24*, 2266-2270; b) H. R. Kricheldorf, M. Berl, N. Scharnagl, *Macromolecules* **1988**, *21*, 286-293; c) J. L. Eguiburu, M. J. Fernandez-Berridi, F. P. Cossío, J. S. Román, *Macromolecules* **1999**, *32*, 8252-8258; d) A. Kowalski, A. Duda, S. Penczek, *Macromolecules* **2000**, *33*, 7359-7370; e) E. L. Marshall, V. C. Gibson, H. S. Rzepa, *J. Am. Chem. Soc.* **2005**, *127*, 6048-6051.

[115] a) E. F. Connor, G. W. Nyce, M. Myers, A. Möck, J. L. Hedrick, *J. Am. Chem. Soc.* **2002**, *124*, 914-915; b) D. Bourissou, B. Martin-Vaca, A. Dumitrescu, M. Graullier, F. Lacombe, *Macromolecules* **2005**, *38*, 9993-9998; c) A. P. Dove, R. C. Pratt, B. G. G. Lohmeijer, R. M. Waymouth, J. L. Hedrick, *J. Am. Chem. Soc.* **2005**, *127*, 13798-13799.

[116] A. Sauer, A. Kapelski, C. Fliedel, S. Dagorne, M. Kol, J. Okuda, *Dalton Trans.* **2013**, *42*, 9007-9023.

CHAPTER 2

Methodology

2.1 Nuclear Magnetic Resonance (NMR) Spectroscopy

One and two dimensional multinuclear (^{1}H, ^{31}P and ^{13}C) NMR spectroscopy was routinely used for the characterisation of new compounds.

2.1.1 Characterisation of Polymers

Polymerisation reactions were monitored by ^{1}H NMR spectroscopy (Table 2.1). Conversions were determined through relative integration of distinct monomer and polymer resonances. It is worth mentioning that T_1 has not been optimised for any polymer characterisations. For copolymerization reactions, the percentage of carbonate/ester linkages was determined through relative integration of distinct polycarbonate/polyester and polyether resonances. The selectivity in CO_2/cyclohexene oxide (CHO) ring opening copolymerisation (ROCOP), i.e. polycarbonate vs. cyclic carbonate, was determined through relative integration of the polycarbonate resonances against the cyclic carbonate resonance.

Table 2.1. ^{1}H NMR chemical shifts of the monomers and polymers/side products reported in this thesis.

	Poly(CHO/CO_2)[a]	**Poly(PA/CHO)**[b]	**Poly(CHO)**[a]	**Polylactide**[a]	**Cyclic carbonate**[a]
Monomer (ppm)	3.09	8.20-8.00	3.09	5.10-5.02	3.09
Polymer (ppm)	4.75-4.55[1]	7.70-7.50[1]	3.40-3.20[2]	5.28-5.14[3]	4.08-4.00[1]

[a]Measured in $CDCl_3$ at 298 K; [b]measured in DMSO at 298 K.

Taking the example illustrated in Figure 2.1, the conversion, % carbonate linkages and the polymer/cyclic carbonate selectivity were determined as follow:

$$\textit{Conversion} = \frac{\int H_{Polycarbonate} + \int H_{Cyclic\ carbonate} + \int H_{Polyether}}{\int H_{Polycarbonate} + \int H_{Cyclic\ carbonate} + \int H_{Polyether} + \int H_{CHO}}$$

With:

$$\int H_{Polycarbonate} = H_a + H_b + H_c = 62 + 1 + 0.5 = 63.5$$

$$\int H_{Cyclic\ carbonate} = H_d = 4.5$$

$\int H_{Polyether} = 0$

$\int H_{CHO} = H_e = 29$

$Conversion = \frac{63.5+4.5+0}{63.5+4.5+0+29} = 0.7$ → The conversion of the polymerization is **70 %**.

$$\% \textbf{\textit{Carbonate linkages}} = \frac{\int \boldsymbol{H_{Polycarbonate}} + \int \boldsymbol{H_{Cyclic\ carbonate}}}{\int \boldsymbol{H_{Polycarbonate}} + \int \boldsymbol{H_{Cyclic\ carbonate}} + \int \boldsymbol{H_{Polyether}}}$$

$\%\ \textbf{\textit{Carbonate linkages}} = \frac{\mathbf{63.5+4.5}}{\mathbf{63.5+4.5+0}} = \mathbf{1}$ → The % carbonates linkages are **> 99%**.

$$\% \textbf{\textit{Selectivity}} = \frac{\int H_{Polycarbonate}}{\int H_{Polycarbonate} + \int H_{Cyclic\ carbonate}}$$

$\%\ Selectivity = \frac{\mathbf{63.5}}{\mathbf{63.5+4.5}} = 0.93$ → The selectivity (polycarbonate vs. cyclic) is **93 %**.

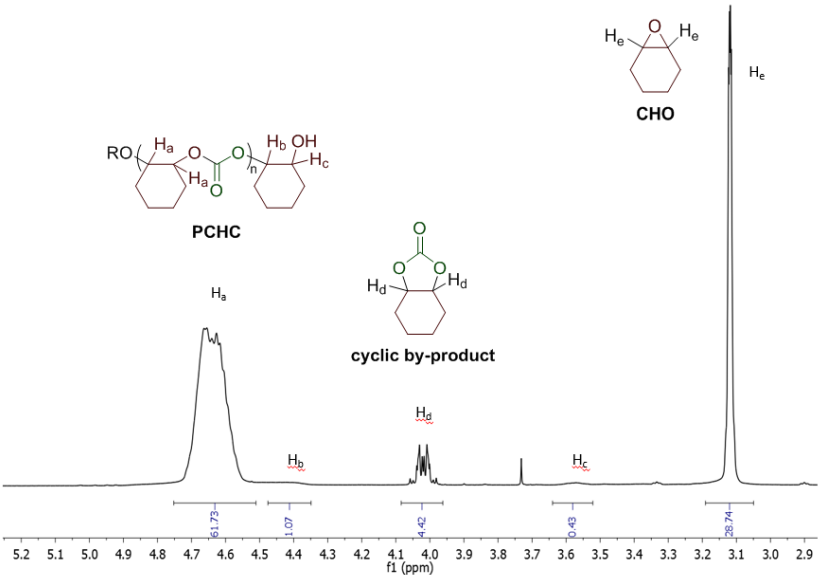

Figure 2.1. Example of ^{1}H NMR spectrum, in $CDCl_3$ (298 K), of an aliquot taken during CO_2/epoxide ROCOP. Peak H_a (4.65 ppm) is assigned to carbonate linkages, peak H_b (4.45 ppm) and H_c (3.60 ppm) are assigned to methyne groups on the end group $OCHC_4H_8CHOH$, peak H_d is assigned to the trans-cyclic carbonate species (δ = 4.00 – 4.08). Peak H_e (3.09 ppm) is the monomer resonance. The absence of ether linkages is confirmed by the lack of any peak at 3.45 ppm.

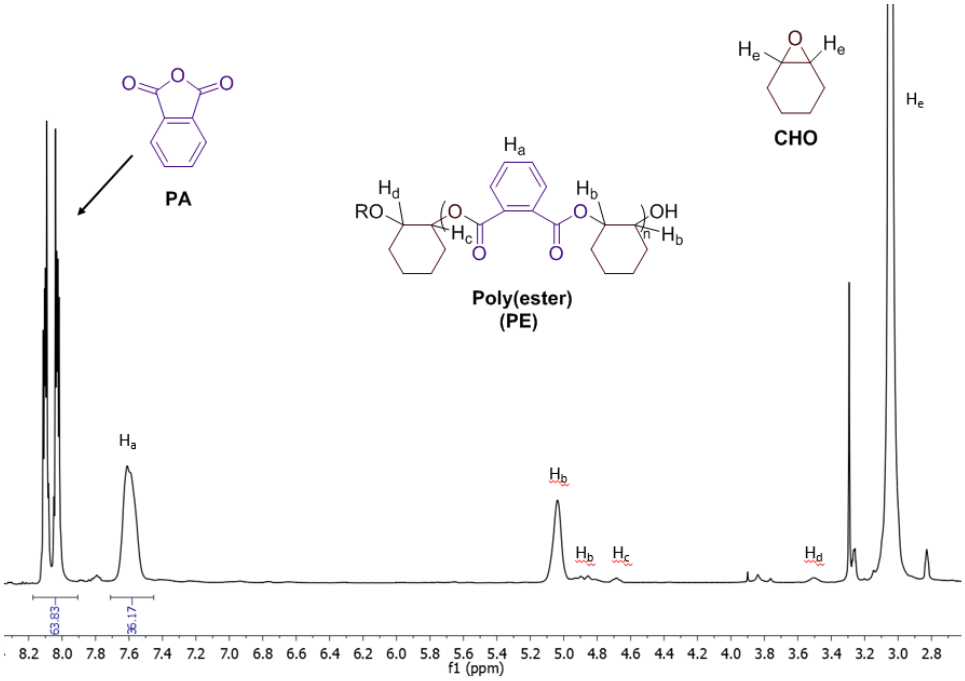

Figure 2.2. Example of ^{1}H NMR spectrum, in d_6-DMSO (298 K), of an aliquot taken during PA/CHO ROCOP. The PA monomer resonance is located at 8.06 ppm. Peak H_a (7.60 ppm) is assigned to the phenyl moiety of PA, peak H_b (5.03 ppm and 4.87 ppm) correspond to methyne groups, peak H_c (4.67 ppm) and H_d (3.50 ppm) are assigned to the end group $OCHC_4H_8CHOR$. Peak H_e (3.09 ppm) is the CHO resonance. The absence of ether linkages is confirmed by the lack of any peak at 3.62 ppm.

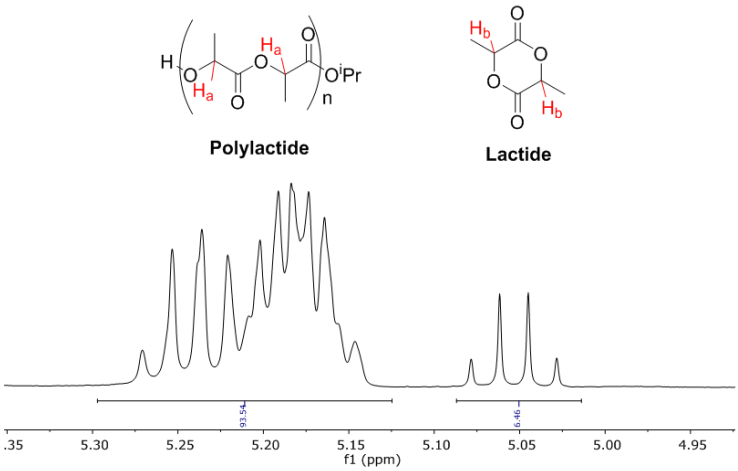

Figure 2.3. Example of ^{1}H NMR spectrum, in $CDCl_3$ (298 K), of an aliquot taken during lactide polymerization. Peak H_a (5.28-5.14 ppm) is assigned to the methine of the polylactide, peak H_b (5.05 ppm) is assigned to methyne group of the lactide monomer.

2.1.2 ^{31}P NMR{^{1}H} NMR Spectroscopy

In the chapter 3 of this thesis, the synthesis of ligands and complexes were monitored by $^{31}P\{^{1}H\}$ NMR spectroscopy (as all ligands/complexes incorporate phosphines).[4] Figure 2.4 show an example of a three step complexation of a proligand salt monitored by

$^{31}P\{^{1}H\}$ NMR spectroscopy (without the need for removal non-deuterated solvents). At each stage, the $^{31}P\{^{1}H\}$ NMR spectrum shows a singlet with a distinct chemical shift.

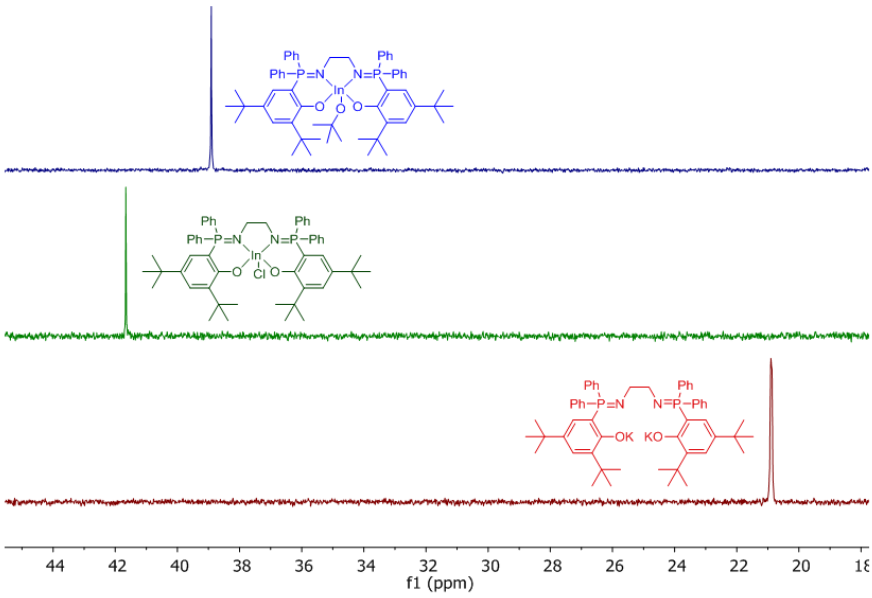

Figure 2.4. Stacked $^{31}P\{^{1}H\}$ NMR spectra (C_6D_6, 298 K) for the synthesis of an indium phosphasalen initiator.

2.1.3 Two-Dimensional (2D) NMR Spectroscopy Techniques

2D NMR spectroscopy was used for the full assignment of all ^{1}H and $^{13}C\{^{1}H\}$ NMR spectra. In addition, 2D NMR spectroscopy was used to gain additional structural data. Table 2.2 summarizes the key methods used in this thesis.

Table 2.2. Summary and comparison of 2D NMR spectroscopy techniques used.

	Nucleus	Correlation	Range
COSY	^{1}H-^{1}H	Through-bond	2-4 bonds
HSQC	^{1}H-^{13}C	Through-bond	1 bond
HMBC	^{1}H-^{13}C	Through-bond	Entire spin system
ROESY	^{1}H-^{1}H	Through-space	Up to ~5 Å

Multiple couplings in ^{1}H and $^{13}C\{^{1}H\}$ NMR were generally assigned using COSY, HSQC and HMBC. ROESY NMR was used to examine the proximity of different groups "through-space" using the *nuclear Overhauser effect* (NOE). Cross-peak signals are observed in ROESY NMR if two protons are close in space, but lack direct connectivity.

2.1.4 Diffusion Ordered NMR Spectroscopy (DOSY)

A useful technique to probe the solution state nuclearity of organometallic complexes is DOSY NMR. DOSY provides useful information on aggregation states, solvent phenomena and multicomponent solutions. DOSY may separate resonances according to the species solution diffusion coefficient. As the diffusion coefficient is directly linked to the hydrodynamic radius (via the Stokes-Einstein equation), the aggregation state can be extracted from DOSY experiment. Using the Stokes-Einstein equation, assuming each components of the solution can be described as spherical and under high dilution, there is a linear correlation between the logarithm of diffusion coefficient and the logarithm of the molecular weight (MW).[5] Therefore, a compound's molecular weight can be estimated using a linear calibration obtained from the diffusion coefficients of standard compounds (the calibration plots used in this thesis are presented in the experimental chapter).[1, 6]

$$D = \frac{k_B T}{n\pi\eta r}$$

Stoke-Einstein equation: k_b is the Boltzmann constant, T the temperature, η the solvent viscosity, and r the hydrodynamic radius.

$$D = A(MW)^{\alpha}$$

$$log(D) = \alpha\, log(MW) + log\ (A)$$

Where A and α are intrinsic constants of the deuterated solvent used.

It is worth mentioning that DOSY has been used in this thesis to roughly estimates the molecular weight of complexes. The error between the calculated and the theoretical molecular weight can be consequent therefore this method was primary used to investigate the aggregation state of complexes in solution (monomer vs. dimer).

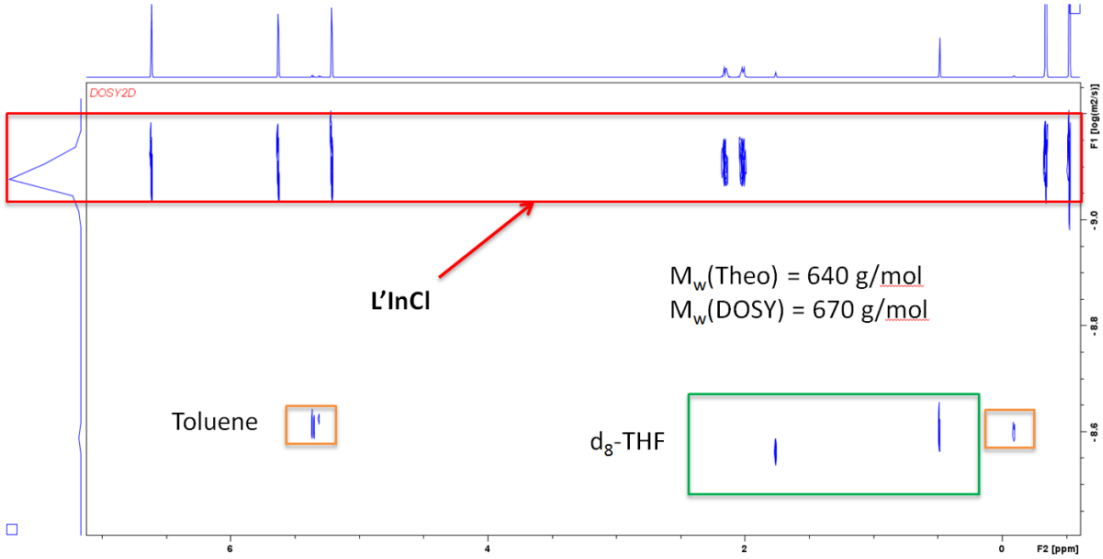

Figure 2.5. Example of a DOSY NMR spectrum in d_8-THF (298 K) of a complex used in this thesis.

Taking the example illustrated in Figure 2.5, the molecular weight of the complex was determined using the following procedure:

The linear calibration plot obtained in d_8-THF gives $\alpha = -0.5626$ and $\log(A) = -7.505$

$$\log(D) = -7.505 - 0.5626 * \log(MW)$$

$$\boldsymbol{MW = 10^{\left(\frac{7.505+\log(D)}{-0.5626}\right)}}$$

$$MW = 10^{\left(\frac{7.505-9.095}{-0.5626}\right)} = \boldsymbol{670\ g/mol}$$

2.2 Single Crystal X-ray Diffraction

Single crystal X-ray diffraction is a non-destructive analytical technique which provides the lattice of a crystalline substance. In this thesis, single crystal X-ray diffraction was mostly used in the characterisation of inorganic complexes to determine bond lengths, bond angles, metal geometries and ligands coordination modes.

An X-ray diffractometer consists of three basic elements, an X-ray tube, a sample holder, and an X-ray detector. X-rays are used because the wavelength is on the same order of magnitude as a carbon-carbon bond distance. The monochromic X-rays source is produced by filtering X-ray beam, generated from accelerated electrons impacting a metal surface (generally molybdenum or copper surface). The interaction of the incident x-rays with the sample produces constructive interference (and a diffracted beam) according to the Bragg's equation:

$$Bragg's\ equation: \quad n\lambda = 2dsin\theta$$

Where n is a positive integer, λ (nm) is the wavelength of incident ray, d (nm) is the interplanar spacing of the crystal units, and θ is the angle between the incident ray and the surface of the crystal.

Constructive interferences produce intense peaks which appear as reflection spots in the diffraction pattern. Information about the position and the relative intensity are obtained for each reflection. It is then possible to determine the distribution of electron density throughout the crystal by acquiring the relative intensities of thousands of unique reflections at multiple crystal orientations.

For all the molecular structures of metal-coordinated complexes described in the thesis, the geometry at the metal centre was determined. Across all compounds, only tetra, penta and hexacoordinated structures were observed (Figure 2.6).

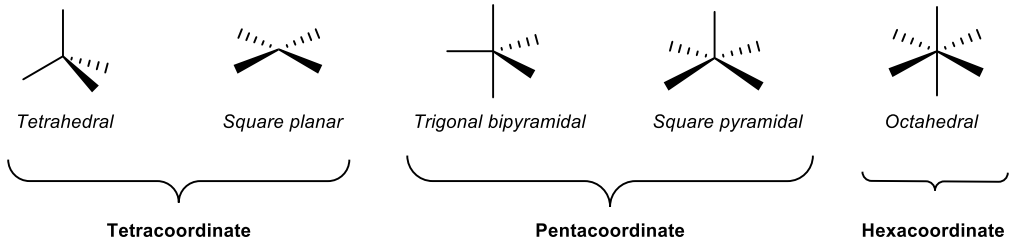

Figure 2.6. Illustration of key coordination geometries observed in this thesis.

For tetracoordinate structures, a structural parameter (τ_4') was used to determine whether the geometry at the metal centre was best described as tetrahedral or square planar.[7]

$$\tau_4' = \frac{\beta - \alpha}{360^\circ - \theta} + \frac{180^\circ - \beta}{180^\circ - \theta}$$

Where $\beta > \alpha$ are the two greatest valence angles at the coordination centre and $\theta = \cos^{-1}(-1/3) \approx 109.5^\circ$. For an ideal tetrahedron, $\tau_4' = 1$ and for an ideal square plan, $\tau_4' = 0$.

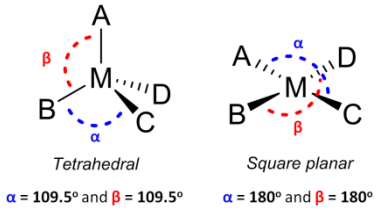

Figure 2.7. Illustration of tetrahedral and square planar coordination geometries with key bond angles, α and β, for determination of the structural parameter τ_4'.

For pentacoordinate structures, a structural parameter (τ) was used to assess whether the geometry at the metal centre best described as square pyramidal or a trigonal bipyramidal.[8]

$$\tau = \frac{\beta - \alpha}{60^\circ}$$

Where β > α are the two greatest valence angles at the coordination centre. For an ideal trigonal bipyramid, τ = 1 and for an ideal square pyramid, τ = 0.

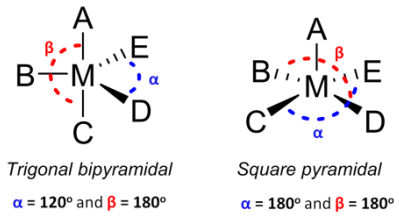

Figure 2.8. Illustration of trigonal bipyramidal and square pyramidal coordination geometries with key bond angles, α and β, for determination of the structural parameter τ.

For octahedral metal complexes coordinated by a tetradentate ligand (e.g. O,N,N,O-type) and two monodentate co-ligands (X and Y), three general configurations are possible: *trans*, *cis-α* and *cis-β* (Figure 2.9).[9]

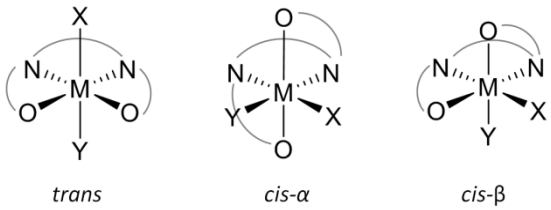

Figure 2.9. Illustration of the three possible octahedral metal complex geometries comprised of a tetradentate salen-type ligand and two monodentate co-ligands.

In the *trans* configuration, the two monodentate co-ligands are in *trans* configuration. For *cis-α*, the two monodentate co-ligands are *cis* to one another and the two O atoms of the [O,N,N,O] ligand are in a *trans* configuration. Finally, for *cis-β*, the two monodentate co-ligands, two O atoms and two N atoms of the [O,N,N,O] ligand are in a *cis* configuration.

2.3 Mass Spectrometry (MS)

Mass spectrometry measures the masses of charged isotopes, molecules and molecular fragments. The basic principle of mass spectrometry is to ionise the sample with an ionisation source to form a charged species (mainly cationic, although a number of types of ionisation mode exist). These charged species are accelerated in an electromagnetic field which separates ions based on their mass/charge (*m/z*) ratio.

In this thesis, MS was mostly used to characterize polymers. Matrix Assisted Lased Desorption/Ionisation Time of Flight (MALDI-ToF) analysis is a soft ionisation technique particularly useful for the analysis of macromolecules such as proteins, polymers and metal complexes (600 Da < MW < 10'000 Da). The preparation method used for MALDI-ToF samples is quite important in being able to observe any signals. Firstly, the matrix needs to be carefully chosen according to the sample properties (Table 2.3). Secondly, the sample needs to be uniformly mixed with an excess of the matrix. Additives, such as potassium salts, are added, to facilitate the ionisation of the sample, if needed.

Table 2.3. Types of matrices and additives used in this thesis.

Matrix	**Full name**	**Substrate**
Dithranol	1,8-Dihydroxy-9(10H)-anthracenone	Synthetic polymers
DCTB	*Trans*-2-[3-(4-*tert*-butylphenyl)-2-methyl-2-propenylidene]malononitrile	Metal complexes
Additives	**Full name**	**Substrate**
NaOAc	Sodium acetate	Metal-acetate complexes
KTFA	potassium trifluoroacetate	Synthetic polymers

In a polymer samples, a MALDI-ToF spectrum displays one or several series of peaks corresponding to polymer chains. The difference in *m/z* between each peak, within a given series, should be equivalent to the mass of the repeating unit of the polymer. Each series of peaks will reflect a different population of polymers (e.g. bearing different end groups, detected with different counter cation…). The initiating group (ideally corresponding to

the end group of the polymer) within one series is determined empirically by solving the following equation:

$$MW_{initiator} = MW_{signal} - (n.MW_{repeating\ unit} + MW_{counter\ cation} + MW_{hydrogen})$$

Where MW_{signal} is the MW of one peak being part of the series of interest; n is the number of repeating unit; $MW_{counter\text{-}cation}$ is generally the MW of sodium or potassium.

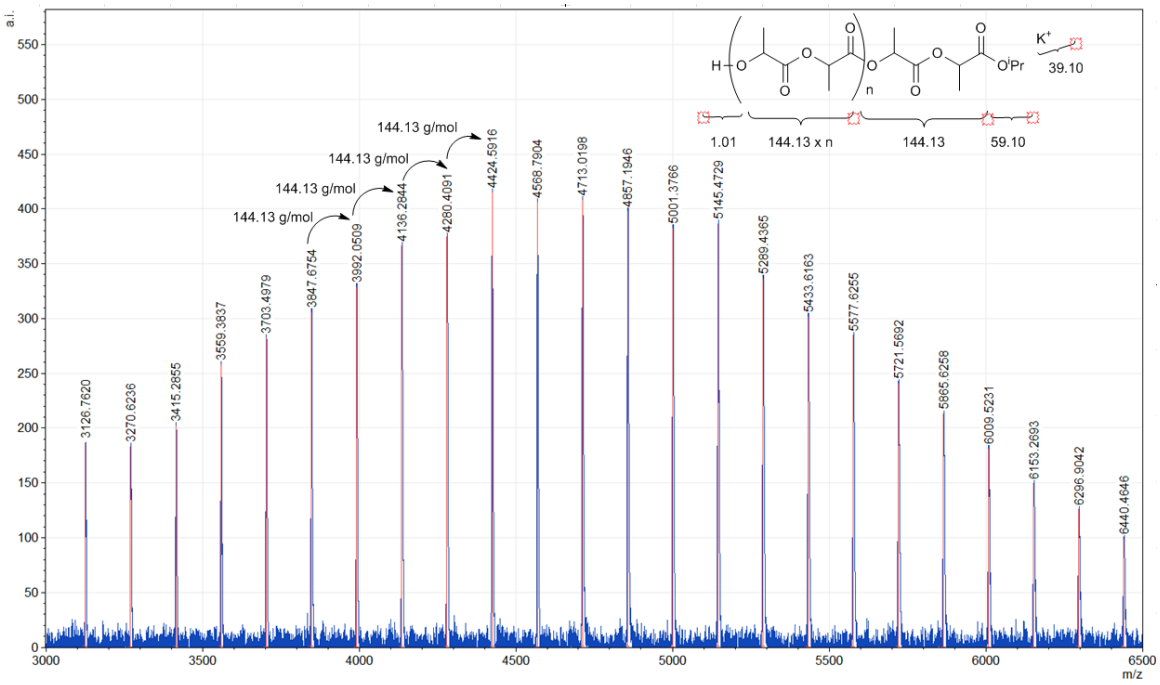

Figure 2.10. Example of a MALDI-ToF spectrum obtained for a polymer sample. The present spectrum illustrates the MALDI-ToF of polylactide initiated by an isopropoxide moiety.

2.4 Size Exclusion Chromatography (SEC)

SEC is an analytical technique which separates macromolecules based on hydrodynamic radii. It is particularly useful in polymer chemistry as a way to determine molecular weights (M_n = number average molecular weight; M_w = weight average molecular weight) and dispersity ($Đ = M_w / M_n$).

The SEC columns are filled with a porous medium. For example, the THF-SEC column used for all polymers described in this thesis is made of highly cross-linked polystyrene-divinylbenzene copolymer matrix. In a general SEC experiment, the dissolved polymer sample will have specific interactions with the column depending on its hydrodynamic radius. Smaller species will penetrate further into the pores compared to larger species. Consequently, larger molecules will elute from the column first, followed by smaller molecules. It is therefore important to ensure that the polymer is fully dissolved in the solvent media and adopts a random coil (i.e. the polymer should be dissolved at least 12 h before SEC analysis). Polymers do not show a random coil configuration have a smaller hydrodynamic radii, therefore, the MW obtained by SEC analysis will be under-estimated.

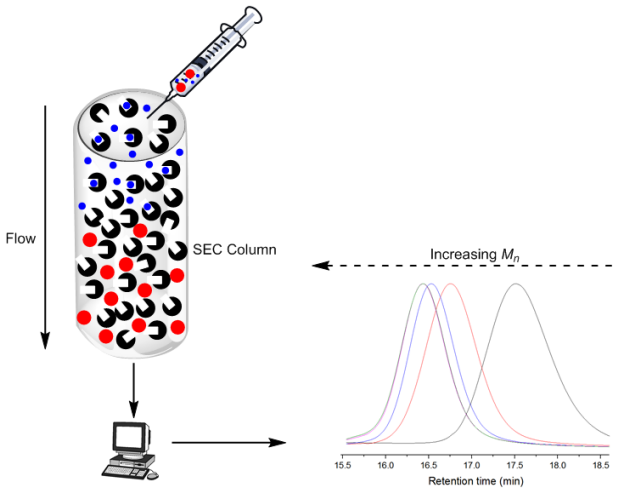

Figure 2.11. Illustration of the basic principle of SEC.

There is usually a linear correlation between the retention time of a polymer sample and its hydrodynamic radius. By using polymer standards with known MW values (in this case, the standard used was polystyrene), it is possible to determine a calibration plot and hence to estimate the MW of an unknown polymer. In an ideal system, the polymer to be studied does not interact with the solvent and behaves in similar manner as the standard. Here the polymers cannot be assumed to behave identically to polystyrene. Therefore, absolute molecular weights were obtained for polylactide using a correction factor of 0.58 (refer to experimental part for more details).[10] For other polyesters and polycarbonates, only the relative molecular weights against polystyrene standard were reported.

2.5 Kinetic Studies

The general rate law for the copolymerization of two monomers is expressed as:[11]

$$Rate = k_p[catalyst]^x[monomer_1]^y[monomer_2]^z$$

Where x, y and z are the orders in catalyst, the monomer$_1$ and the monomer$_2$, respectively.

2.5.1 CO_2/Epoxide ROCOP

For CO_2/epoxide copolymerization, the rate law is expressed as:

$$Rate = k_p[catalyst]^x[CHO]^y[CO_2]^z$$

The isolation method (pseudo first order) was used to study the order of each species. The method assumes that the other reactants are present in large excess and therefore their concentration remains constant throughout the course of the reaction. This enables a pseudo-order rate law, used to determine a particular reaction order.[11]

a. Order in CHO

To determine the order in CHO, an integrated rate law method was applied. Using the isolation method, the rate of reaction in CHO is expressed as:[11]

$$Rate = k_{obs}[CHO]^y$$

$$k_{obs} = k_p[catalyst]^x \rho {CO_2}^z$$

The order of CHO is determined by measuring the change in concentration over time over the full course of the polymerization. This rate of consumption of monomer is expressed as:

$$\frac{d[CHO]}{dt} = -k_{obs}[CHO]^\alpha$$

For polymerization reactions, α is generally either 1 or 0. The equation is easily integrated for the two values of α to give:

For α = 0, $[\mathrm{CHO}] = -kt$

For α = 1, $\ln\left(\frac{[CHO]}{[CHO]_0}\right) = -kt$

Therefore, the order in CHO can be determined by plotting the consumption of CHO over time. If a linear relationship is obtained the order of CHO is 0. On the other hand, if the relationship follows a semi-logarithmic plot, the order in epoxide will be 1 and a straight line will be obtained by plotting $\ln\left(\frac{[CHO]}{[CHO]_0}\right)$ over time.

b. Order in catalyst

The order in catalyst concentration is determined by an initial rates method over conversion from 0-20 %. The initial rate of the reaction is determined at a range of different catalyst concentration. The order in catalyst is obtained from the plot of initial rate vs. catalyst concentration. A horizontal line is indicative of a zero order whilst a linear relationship indicates a first order in catalyst concentration. A polynomial fit would indicate a second or higher order in catalyst concentration.

c. Order in CO_2 pressure

The polymerization initial rate was determined over a range of pressure (1-40 bar of CO_2). The turn over frequencies (TOF, in h^{-1}) of the catalyst was calculated using the following equation:

$$TOF = \frac{[CHO]_t}{[catalyst] * t}$$

Where $[CHO]_t$ correspond to the concentration of CHO when the reaction was stopped; [catalyst] is the concentration of catalyst; t is the reaction time.

An approximation for the order in CO_2 pressure was determined by plotting the variation of TOF with CO_2 pressure.

2.5.2 Lactide Ring Opening Polymerization (ROP)

In the case of lactide ROP, the polymerization rate is simplified to:

$$Rate = k_p[catalyst]^x[lactide]^y$$

The order in monomer and catalyst concentration are determined using integrated rate law treatments in both cases.[11]

2.5.3 The Michealis-Menton Kinetic Model

In chapter 4, the Michealis-Menton kinetic model will be invoked to study the kinetic of the ROP of *rac*-LA catalysed by a series of dinuclear catalysts. The model is widely used for kinetic studies of enzymatic process and has been applied to polymerisation catalysts to illustrate a reversible slow bonding of the substrate on the active site.

A polymerisation reaction can be modelled as:

$$[L_nM(OR)] + [LA] \underset{k_{-1}}{\overset{k_1}{\rightleftharpoons}} [L_nM(OR).LA] \xrightarrow{k_2} [L_nM(OR)] + [PLA]$$

Where $[L_nMOR]$ is the catalyst concentration, [LA] is the monomer concentration (in this case, rac-lactide), $[L_nMOR.LA]$ correspond to adduct formed from the coordination of the monomer on the metal centre, [PLA] is the concentration of polymer formed (in this case, polylactide), k_1, k_{-1} and k_2 are the rates constant associated with each process.

The rate of the polymerisation is determined from:

$$\frac{d[PLA]}{dt} = k_2[L_nM(OR).LA]$$

[$L_nM(OR).LA$] can easily be determined using the steady state approximation which stipule that if a reactive is present at low and constant concentration through the course of the reaction, then its concentration variation is null:

$$\frac{d[L_nM(OR).LA]}{dt} = k_1[L_nM(OR)][LA] - k_{-1}[L_nM(OR)] - k_2[L_nM(OR).LA] = 0$$

$$[L_nM(OR).LA] = \frac{k_1[L_nM(OR)][LA]}{k_{-1} + k_2}$$

In addition, if the total catalyst concentration of catalyst is $[L_nM(OR)]_0$, then the amount of free catalyst has to be: $[L_nM(OR)] = [L_nM(OR)]_0 - [L_nM(OR).LA]$. Substituting this into the previous equation gives:

$$[L_nM(OR).LA] = \frac{k_1\{[L_nM(OR)]_0 - [L_nM(OR).LA]\}[LA]}{k_{-1} + k_2}$$

Which rearranges to give:

$$[L_nM(OR).LA] = \frac{k_1[L_nM(OR)]_0[LA]}{k_{-1} + k_2 + k_1[LA]} = \frac{[L_nM(OR)]_0[LA]}{K_M + [LA]}$$

where $K_M = \frac{k_2 + k_{-1}}{k_1}$ *is called the Michaelis constant.*

The overall rate of reaction is therefore:

$$\frac{d[PLA]}{dt} = k_2 \frac{[L_nM(OR)]_0[LA]}{K_M + [LA]}$$

When [LA] >> K_M, then the overall rate is independent of the monomer concentration. This is because there is so much monomer present that its concentration remains essentially constant as the reaction proceeds. Under these conditions, the rate of reaction is a maximum and the catalyst is saturated with monomer.

2.6 Bernoulian Statistical Model

In Chatper 3, the Bernoulian statistical model will be used to quantify the isoselectivity of catalysts for CO_2/epoxide ring opening copolymerisation. Bernoulian statistics are based on a chain-end control mechanism, and defines probabilities in terms of either racemic (P_r) or meso (P_m) enchainment (also called r and m centred tetrads, respectively). By using this statistical model, the probability of each tetrad is calculated and compared with the experimental values (determined by integration of the corresponding tetrad resonance from the quantitative ^{13}C NMR spectrum of the pure polymer). The Bernoulian (chain-end control) equations for tetrad sequences are the following:[12]

$$[mmm] = P_m^4 + (1\text{-}P_m)^4$$

$$[mmr] = P_m[(1\text{-}P_m)(1\text{-}2P_m\text{+}2P_m^2)]$$

$$[rmm] = P_m[(1\text{-}P_m)(1\text{-}2P_m\text{+}2P_m^2)]$$

$$[mrr] = P_m[(1\text{-}P_m)(1\text{-}2P_m\text{+}2P_m^2)]$$

$$[rrm] = P_m[(1\text{-}P_m)(1\text{-}2P_m\text{+}2P_m^2)]$$

$$[mrm] = 2P_m^2(1\text{-}P_m)^2$$

$$[rmr] = 2P_m^2(1\text{-}P_m)^2$$

$$[rrr] = 2P_m^2(1\text{-}P_m)^2$$

$$P_m + P_r = 1$$

P_m = m centred tetrads; P_r = r centred tetrads

The value of P_m is determined by rearrangement these equations using the experimental integral values. Taking the example of an *iso*-enriched poly(cyclohexene carbonate), the

most intense resonance at 153.8 ppm corresponds to the [*mmm*] and [*mmr*] tetrads. Therefore P_m is determined by the rearrangement of:

$$[mmm] + [mmr] = x$$

where x is the relative integral of the 153.8 ppm resonance

Wich is rearranged to:

$$P_m^4 + (1-P_m)^4 + P_m[(1-P_m)(1-2P_m+2P_m^2)] = x$$

The previous equation is easily simplified to:

$$3P_m^2 - 3P_m + 1 = x$$

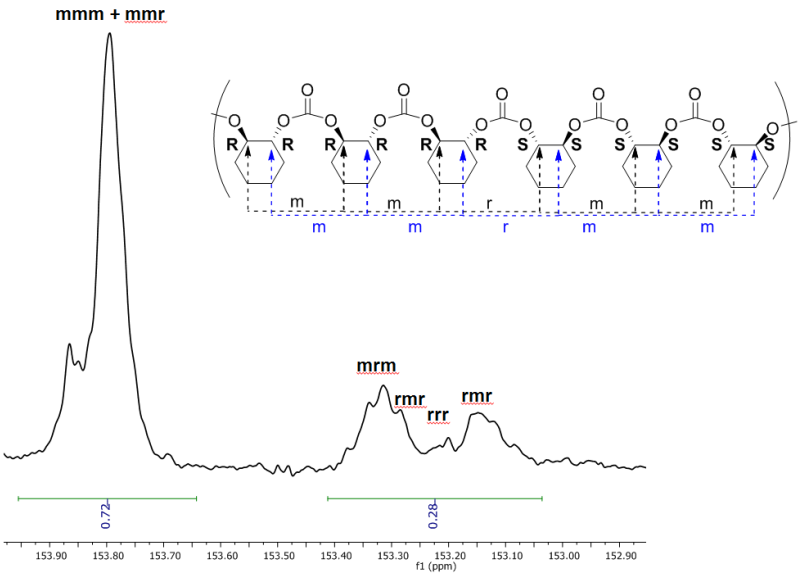

Figure 2.12. Example of a $^{13}C\{^1H\}$ NMR spectrum of PCHC (298 K, $CDCl_3$) zoomed in the carbonyl region ($CDCl_3$, 298 K).

Taking the example illustrated in Figure 2.12, x = 0.72 and the last equation is solved with P_m = 0.92. Based on this value, the other tetrad probabilities are calculated and compared with normalised experimental integrals. If the values are close, the statistical model used is appropriate and a chain-end-control mechanism is assigned.

In addition, the accuracy of the model can be tested using the Bernoulian Test Equation which is a means to assess the accuracy of the model. The Bernoulian Test Equation is expected to provide a value close to 1, when the Bernoulian model is a suitable model for the system studied.[12a, 13]

$$\mathrm{B} = \frac{4\,P_m^2(1-P_m)^2}{[2P_m(1-P_m)]^2}$$

In the example illustrated in Figure 2.12, B = 1.

2.7 References

[1] A. Thevenon, J. A. Garden, A. J. P. White, C. K. Williams, *Inorg. Chem.* **2015**, *54*, 11906-11915.

[2] S. Kissling, M. W. Lehenmeier, P. T. Altenbuchner, A. Kronast, M. Reiter, P. Deglmann, U. B. Seemann, B. Rieger, *Chem. Commun.* **2015**, *51*, 4579-4582.

[3] A. Thevenon, C. Romain, M. S. Bennington, A. J. P. White, H. J. Davidson, S. Brooker, C. K. Williams, *Angew. Chem. Int. Ed.* **2016**, *55*, 8680-8685.

[4] a) D. Myers, A. J. P. White, C. M. Forsyth, M. Bown, C. K. Williams, *Angew. Chem. Int. Ed.* **2017**, *56*, 5277-5282; b) C. Bakewell, A. J. P. White, N. J. Long, C. K. Williams, *Angew. Chem. Int. Ed.* **2014**, *53*, 9226-9230; c) C. Bakewell, T.-P.-A. Cao, X. F. Le Goff, N. J. Long, A. Auffrant, C. K. Williams, *Organometallics* **2013**, *32*, 1475-1483; d) T.-P.-A. Cao, A. Buchard, X. F. Le Goff, A. Auffrant, C. K. Williams, *Inorg. Chem.* **2012**, *51*, 2157-2169.

[5] a) C. S. Johnson, *Prog. Nucl. Magn. Reson. Spectrosc.* **1999**, *34*, 203-256; b) E. R. Johnson, S. Keinan, P. Mori-Sánchez, J. Contreras-García, A. J. Cohen, W. Yang, *J. Am. Chem. Soc.* **2010**, *132*, 6498-6506.

[6] J. A. Garden, P. K. Saini, C. K. Williams, *J. Am. Chem. Soc.* **2015**, *137*, 15078-15081.

[7] A. Okuniewski, D. Rosiak, J. Chojnacki, B. Becker, *Polyhedron* **2015**, *90*, 47-57.

[8] A. W. Addison, T. N. Rao, J. Reedijk, J. van Rijn, G. C. Verschoor, *J. Chem. Soc., Dalton Trans.* **1984**, 1349-1356.

[9] a) X. Wang, A. Thevenon, J. L. Brosmer, I. Yu, S. I. Khan, P. Mehrkhodavandi, P. L. Diaconescu, *J. Am. Chem. Soc.* **2014**, *136*, 11264-11267; b) A. Cyriac, J. Y. Jeon, J. K. Varghese, J. H. Park, S. Y. Choi, Y. K. Chung, B. Y. Lee, *Dalton Trans.* **2012**, *41*, 1444-1447.

[10] A. Kowalski, A. Duda, S. Penczek, *Macromolecules* **1998**, *31*, 2114-2122.

[11] P. Atkins, J. d. Paula, *Elements of Physical Chemistry*, W. H. Freeman and Company, New York, **2005**.

[12] a) F. A. Bovey, *Pure Appl. Chem.* **1967**, *15*, 349-368; b) M. Sepulchre, *Makromol. Chem.* **1988**, *189*, 1117-1131.

[13] C. G. Jaffredo, Y. Chapurina, S. M. Guillaume, J.-F. Carpentier, *Angew. Chem. Int. Ed.* **2014**, *53*, 2687-2691.

CHAPTER 3

Indium Phosphasalen Catalysts for Low CO_2 Pressure/Epoxide Copolymerisation: Evidence of an Unexpected Mononuclear Pathway?

Abstract

In this chapter, the first indium phosphasalen catalysts for CO_2/epoxide ROCOP are described. In contrast to other reported metal salen catalysts, the indium catalysts work best without any co-catalysts and are active at 1 bar pressure of carbon dioxide. The catalysts show moderate activities (TOF = 16 h^{-1}, 80 °C, 1 bar), high selectivity for carbonate linkages (> 99 %) and produce iso-enriched poly(cyclohexene carbonate) (P_m = ~70 %). The series of new complexes, featuring different ligand and metal substituents, are isolated and fully characterised, including in some cases by X-ray crystallography. Solid state structural analysis combined with solution and *in-situ* spectroscopic analyses provide insights into the possible catalytic active sites and intermediates.

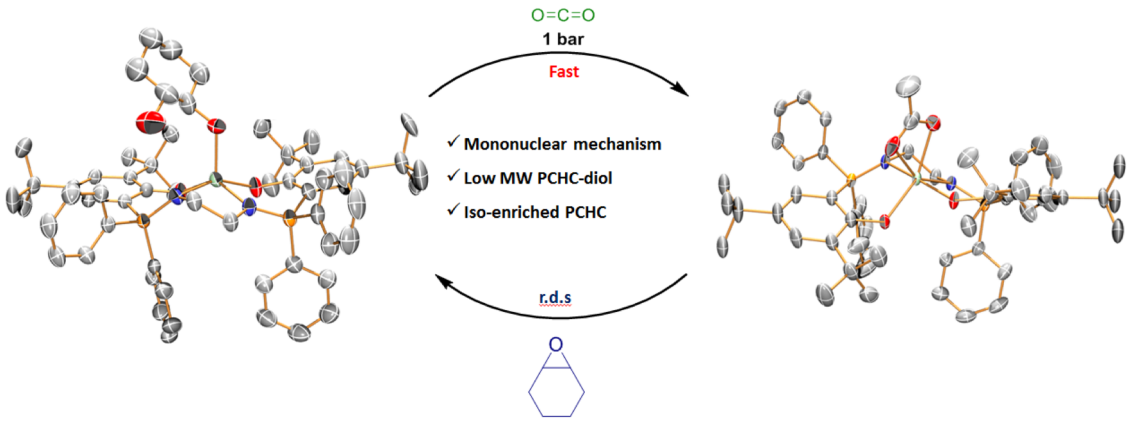

3.1 Introduction

The development of new CO_2/epoxide catalysts requires detailed understanding of the reaction pathway(s) and is ultimately dependent upon a high selectivity for the kinetic reaction product (polymer).[1] In order to maximise carbon dioxide uptake, the catalyst must maintain high alternation between alkoxide and carbonate intermediates, however, control of both reactivity and selectivity for these intermediates remains poorly understood. In terms of the catalytic cycle, there are two common pathways: 1) dinuclear (or dimeric) mechanisms or 2) bi-component mechanisms involving metal catalyst(s) activated by ionic or Lewis basic co-catalysts (Figure 3.1).[2] The two mechanisms share common features such as the activation of the epoxide by the Lewis acidic metal catalyst, followed by attack by a second metal carbonate complex, or free carbonate anion, to form a metal alkoxide intermediate. Carbon dioxide inserts into the metal alkoxide bond to (re)form the carbonate intermediate.

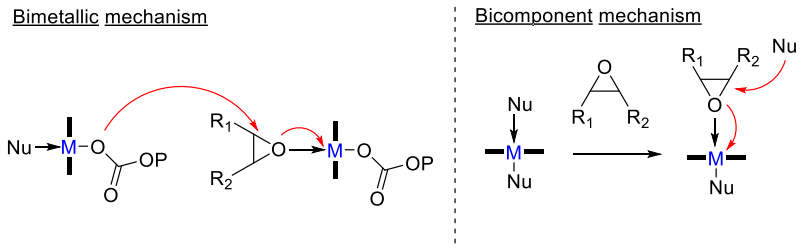

Figure 3.1. The two different nucleophilic ring opening mechanisms reported in the literature. "Nu" can either be the initiating group, a propagating polymer chain or the cocatalyst.

Metal salen catalysts are particularly widely studied as they show good activity, high selectivity and polymerisation control.[1a, 3] Catalysts featuring cobalt(III),[3a-d, 3g, 3i-k, 3o, 4] or chromium(III)[1a, 3h, 3n, 5] are most common, but there is a report of a low activity aluminium(III) catalyst.[6] The most highly active metal salen catalysts feature ligands with the ionic co-catalyst covalently attached and/or dinuclear salens which both allow better activity at lower catalyst loadings.[3e, 3f, 3i, 3o, 4a, 5a, 7] Typically, the metal salen catalysts are applied at higher CO_2 pressures, usually above 20 bar, and cobalt salens typically require

lower temperatures, often 25-40 °C, so as to avoid irreversible reduction (to [Co(II)]) which occurs at higher temperatures.[4a, 8] Under such conditions, kinetic investigations showed fractional orders in catalyst concentration, typically between 1 and 2, indicative of dinuclear mechanisms.[4b, 5c, 9] Studies into the ratio of metal salens:cocatalysts concluded that the best systems featured equimolar ratios, consistent with the formation of ion pairs.[3m, 5h] Indeed, it is worth noting quite how similar the metal salen ROCOP mechanisms are compared to earlier work, by Jacobsen and co-workers, using closely related metal salen catalysts in epoxide kinetic resolutions.[10] Despite the popularity of these metal-salen polymerisation catalysts, fundamental questions still remain regarding the structures, and hence reactivity, of nearly all the proposed catalytic intermediates. These studies are hindered by a general lack of well-characterised [Cr(III)] or [Co(III)] alkoxide complexes, the redox instability of [Co(III)] at higher temperatures, the paramagnetism of nearly all the intermediates, uncertainties regarding whether structures are ionic or covalent and the requirement for high CO_2 pressures complicating *in situ* spectroscopic studies.

In contrast to salen catalysts, the closely related phosphasalen catalysts, bearing two iminophosphorane moieties (P=N, Figure 3.2), have never been studied for CO_2/epoxide ROCOP. Phosphasalen ligands are interesting alternatives to traditional salen as they combine strong σ- and π-donation.[11] Therefore, the Lewis acidity of the metal centre is proposed to be reduced upon coordination compared to salen analogues. Previous studies have suggesed that decreasing the Lewis acidity of the metal centre is important to achieve high carbonate linkage selectivity.[12] The phosphorous moieties also enable new sites for ligand modifications (steric/electronic). Previous and current studies by our group, and others have demonstrated that phenyl substituents and bulky *ortho*-phenol moieties are detrimental to selectivity (tacticity) and activity in *rac*-lactide (*rac*-LA) ring opening

polymerisation (ROP).[13] A recent study comparing yttrium salen/phosphasalen complexes, also for *rac*-LA ROP, highlights that the phosphasalen yttrium complexes have lower activity (perhaps due to a more congested active site) but afford mainly isotactic poly(lactide) (PLA) while the salen analogue produced heterotactic PLA.*

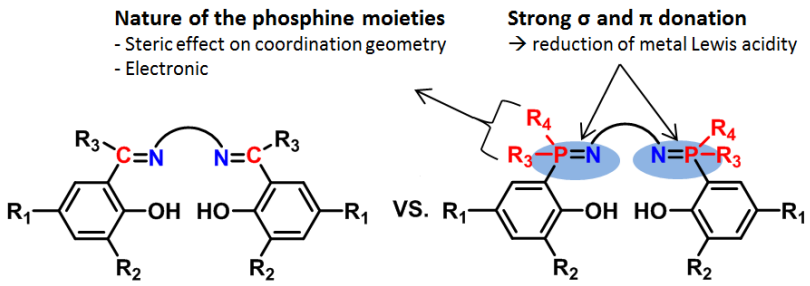

Figure 3.2. Comparison between salen and phosphasalen ligands.

In this study complexes of salen and phosphasalen ligands are compared as ROCOP catalysts.[13b, 14] Indium(III) was chosen as the metal centre due to its improved performance in ROP of *rac*-LA compare to the more Lewis acidic aluminium(III) metal centre.[15] In addition, indium is diamagnetic, mechanistic studies using NMR spectroscopy are feasible. Surprisingly, only few papers describe the use of indium in CO_2 reactions – these are restricted to two reports on CO_2 insertion into an indium-alkyl and one on CO_2/epoxide coupling reaction using [In(III)Br_3].[16]

* A. Cyriac; D. Myers; G. Trott; C. Coleman; A. Thevenon; A. J. P. White; C. K.Williams, manuscript in preparation

3.2 Comparative Study of Salen and Phosphasalen Initiators

3.2.1 Ligand Syntheses

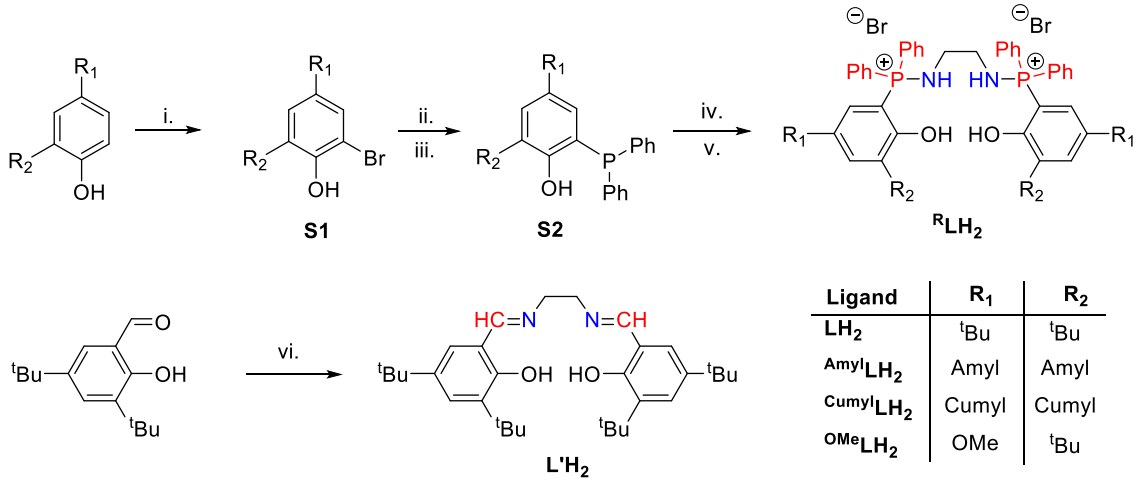

Ligand	R_1	R_2
LH_2	^{t}Bu	^{t}Bu
$^{Amyl}LH_2$	Amyl	Amyl
$^{Cumyl}LH_2$	Cumyl	Cumyl
$^{OMe}LH_2$	OMe	^{t}Bu

Figure 3.3. Synthetic procedure to $^{R}\mathbf{LH_2}$ and $\mathbf{L'H_2}$. i. NBS, CH_3CN, 18 h, 90 %; ii. 1.7 M n-BuLi, -78 °C, Et_2O, 4 h; iii. PPh_2Cl, -78 °C, Et_2O, 18 h, 80 %; iv. Br_2 (1 equiv.), CH_2Cl_2, -78 °C, 2 h; v. Bu_3N (1 equiv.), $NH_2(CH_2)_2NH_2$ (0.5 equiv.), -78 °C, 18 h, 70 %; vi. $NH_2(CH_2)_2NH_2$ (0.5 equiv.), MeOH, 18 h, 25 °C, 100 %.

The phosphasalen ($^{R}\mathbf{LH_2}$) and salen ($\mathbf{L'H_2}$) ligands were synthesised according to previous reported literature procedures.[14] $^{R}\mathbf{LH_2}$ required a three step synthesis and was isolated in high yield (~ 70 %) (Figure 3.3). The first step was a bromination of the corresponding commercially available 2,4-di-substituted-phenol (*tert*-butyl, amyl or cumyl) with *N*-bromo-succinamide (NBS) to afford 2-bromo-4,6-di-substituted-phenol ($^{R}\mathbf{S1}$), in almost quantitative yield. A phosphorylation reaction of $^{R}\mathbf{S1}$, using n-BuLi, and subsequent reaction with chlorodiphenylphosphine, at -78 °C, gave $^{R}\mathbf{S2}$ in good yield (~ 80 %). $^{R}\mathbf{LH_2}$ was obtained as a hydrobromide salt, after carrying out the Kirsanov reaction. The last step was monitored by ^{31}P NMR spectroscopy, where the singlet at -30.1 ppm corresponding $^{R}\mathbf{S2}$ shifted to ~ 40 ppm ($\mathbf{LH_2}$: 40.3 ppm, $^{Amyl}\mathbf{LH_2}$: 39.9 ppm, $^{Cumyl}\mathbf{LH_2}$: 39.4) upon completion of the reaction. The salen ($\mathbf{L'H_2}$) ligand was isolated, in quantitative yield, by amination of 3,5-di-*tert*-butyl-1-hydroxobenzaldehyde with ethylene-diamine in methanol (Figure 3.3). The reaction was monitored by ^{1}H NMR spectroscopy with the disappearance of the aldehyde resonance, at 10.19 ppm, and the evolution of the HC=N resonance, at 8.39 ppm being particularly diagnostic. All reactions were successfully achieved on a

multi-gram scale. Ligands were fully characterised by multinuclear NMR spectroscopy and elemental analysis. The ethylenediamine backbone was chosen based on a previously reported study using aluminium salen complexes which showed moderate activities for CO_2/CHO ROCOP.[6]

3.2.2 Synthesis and Characterisation of [LInCl] and [L'InCl]

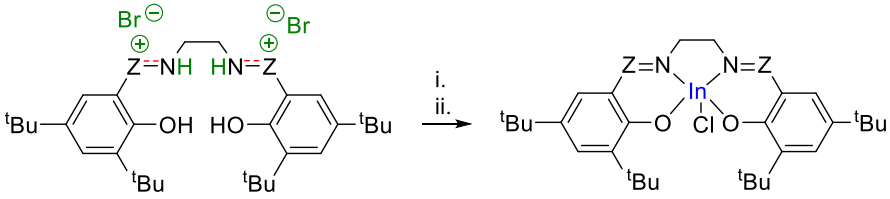

Scheme 3.1. Complexation reactions of $\mathbf{LH_2}$ and $\mathbf{L'H_2}$. i. $KN(SiMe_3)_2$ (4 eq for $\mathbf{LH_2}$ and 2 equiv. for $\mathbf{L'H_2}$), THF, 18 h, 25 °C; ii. $[InCl_3]$ (1 equiv.), THF, 18 h, 25 °C, (84 % and 86 % respectively).

Firstly, indium halide complexes were investigated using $\mathbf{LH_2}$ and $\mathbf{L'H_2}$, that each feature *ortho*- and *para*- *tert*-butyl phenolate substituents and an ethylene backbone linker (Scheme 3.1).[14c] Other ligands ($^{\mathbf{R}}\mathbf{LH_2}$) complexation reactions will be described in Section 3.4. The indium halide complexes were synthesised by deprotonation of the ligands, by reaction with potassium bis(trimethylsilyl)amide $[KN(SiMe_3)_2]$, followed by reaction with $[InCl_3]$. Both complexes were isolated in high yields (> 80 %) and were fully characterised by multinuclear NMR spectroscopy and elemental analyses. Single crystals of the salen complex **[L'InCl]**, were grown by the slow diffusion of hexane into a concentrated solution of **[L'InCl]** in toluene (Figure 3.4). X-ray diffraction experiments reveal a distorted square pyramidal geometry at indium (τ = 0.37),[17] with the ligand coordinated in the equatorial positions and the chloride coordinated in the axial position.

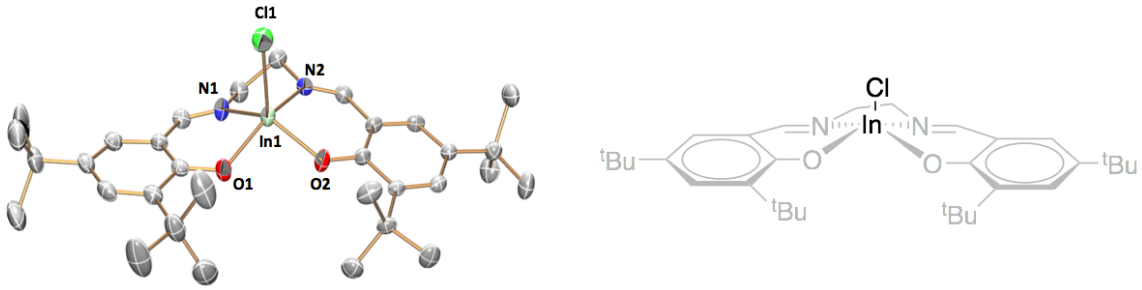

Figure 3.4. LHS: molecular structure of **[L'InCl]** with thermal ellipsoids at the 50 % probability level, hydrogen atoms and a hexane molecule omitted for clarity (refer to appendix for complete data set). RHS: schematic representation of the molecular structures.

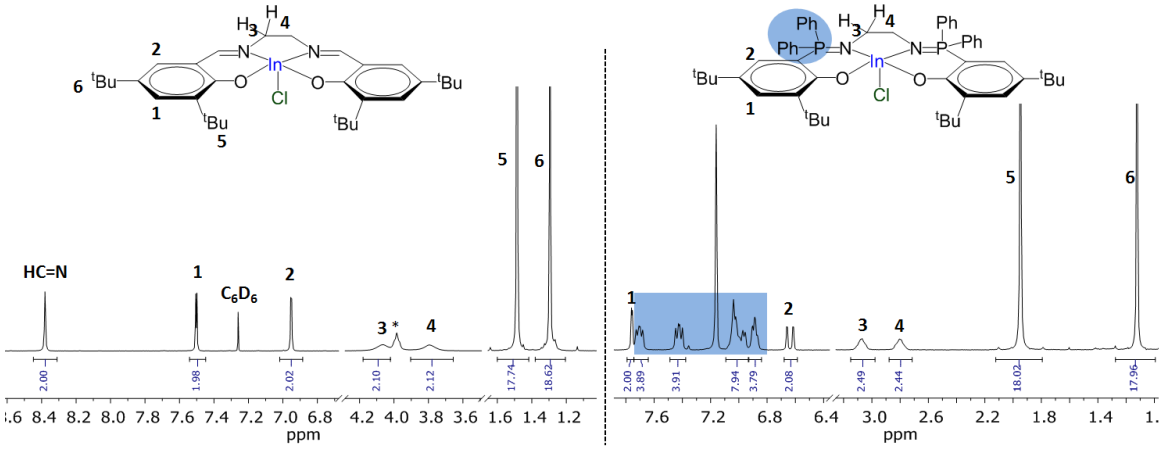

Figure 3.5. ^{1}H NMR spectra of **L'InCl** (L.H.S) and **LInCl** (R.H.S), in C_6D_6, at 298 K. *Residual THF.

The ^{1}H NMR spectra, in C_6D_6, at 25 ^{o}C, of **[L'InCl]** and **[LInCl]** are very similar (Figure 3.5). In both cases, ligand resonances are shifted upfield consistent with metal coordination. Two diasterotopic signals assigned to the methylene backbone protons (resonances labelled 3 and 4 in Figure 3.5) are observed which is also consistent with metal coordination. For **[LInCl]**, the complexation reaction was monitored by ^{31}P NMR, in C_6D_6, which showed a clear shift in signals from 40.3 ppm to 25.4 ppm upon deprotonation, and to 42.1 ppm upon complexation with [$InCl_3$]. DOSY NMR spectroscopy was conducted in d_8-THF, so as to mimic conditions in catalysis and shows that both complexes are monomeric - an important finding given that dimeric and higher order aggregates are known for other indium alkoxide complexes.[18]

3.2.3 CO_2/Epoxide ROCOP Catalysis

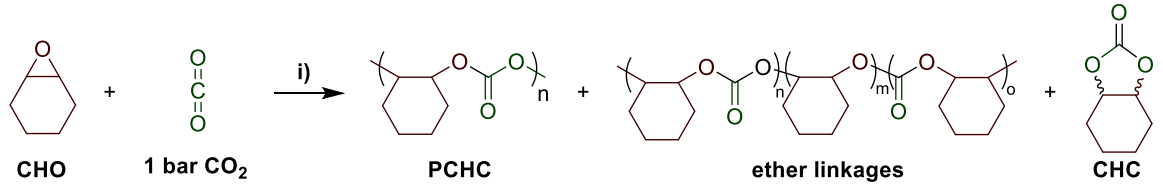

Scheme 3.2. Copolymerisation of CHO and CO_2 i) **[In]** = 0.1 mol%, 1 atm CO_2, 60 °C, neat CHO (9.89 M).

[L'InCl] and **[LInCl]** were tested in catalysis using a standard set of reaction conditions: neat cyclohexene oxide (9.89 M), 1 bar pressure of CO_2 and 0.1 mol% of catalyst, at 60 °C. The results of the polymerisations are summarised in Table 1.1.

Table 1.1. Polymerisation results for **[LInCl]** and **[L'InCl]** without and in presence of co-catalyst.

Catalyst	Co-catalyst	Conversion (%)[a]	% Carbonate linkages[a]	% Selectivity PCHC[a]	% cis/trans CHC[a]	M_n (g/mol)[b]	Đ[b]
[LInCl]	-	14	73	94	0/100	197000	2.0
						7500	1.3
						700	1.2
[L'InCl]	-	21	< 1	< 1	0/100	416000	1.2
						10400	2.5
[LInCl]	PPN-Cl	8	> 99	0	73/27	-	-
[L'InCl]	PPN-Cl	26	> 99	43	79/21	4300	1.2
[LInCl]	DMAP	10	> 99	72	0/100	600	1.2
[L'InCl]	DMAP	trace	-	-	-	-	-

Copolymerisation conditions: **[In]** = 0.1 mol%, 60 °C, 48 h, **[In]**/[co-cat] = 1. [a]Determined by ^{1}H NMR by comparison of the integrals of signals arising from the methylene protons due to copolymer carbonate linkages (δ = 4.65 pmm), ether linkages (δ = 3.45 ppm), and the cyclic carbonate (δ = 4.00 ppm). [b]Determined by SEC, in THF, at 40 °C, calibrated using polystyrene standards.

The salen catalyst produced only polyether, in line with previous studies of [Cr(III)] or [Co(III)] salen catalysts applied at low CO_2 pressures.[3n] On the other hand, the phosphasalen catalyst, afforded polycarbonates with a high carbonate linkages (~73 % CO_2 incorporation) and high polymer selectivity (94 %). However, the molecular weight showed a multimodal distribution consistent with a slow initiation compared to propagation.[13b, 14a-c] The result was rather unexpected since other metal salen catalysts cannot operate at 1 bar pressure of carbon dioxide and generally require an excess of 20 bars for effective catalysis.[3n, 5m, 16a, 19] These known metal salen catalysts also operate best when an equivalent a co-catalyst is used – it is proposed to bind *trans* to the active site and accelerate insertions.[20] To understand the influence of co-catalysts, the indium catalysts

were tested with the addition of an equivalent of 4-dimethylaminopyridine (DMAP) and bis(triphenyl phosphoranylidene)ammonium chloride (PPN-Cl). In contrast to all salen catalysts, addition of DMAP and PPN-Cl resulted in severe reductions to both catalyst activity and selectivity.

3.3 Optimisation of the Initiation Reactions

3.3.1 Synthesis of [LInX] (X = Br, O^{t}Bu, OAc, NO$_3$)

As the best results were obtained using the phosphasalen indium catalyst (without co-catalyst), a series of other complexes were prepared featuring different initiating groups. These complexes were targeted to overcome the initiation problems observed with **[LInCl]** and to allow the production of monomodal molecular weight distribution polycarbonate. Thus, complexes of the type **[LInX]** were prepared, where X = Br, O^{t}Bu,[13b] OAc and NO$_3$ (Scheme 3.3).

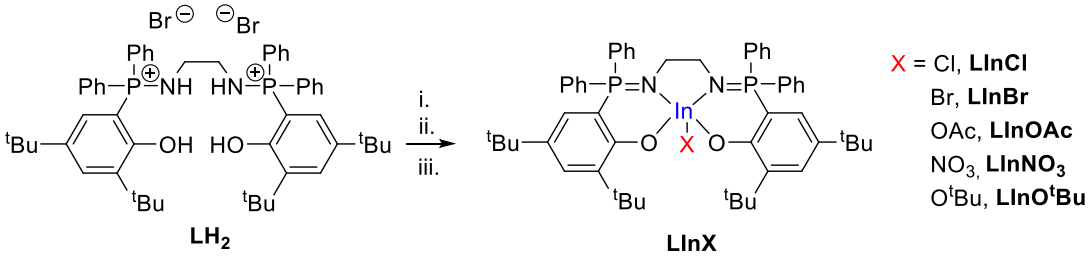

Scheme 3.3. Complexation reactions. Reaction conditions: i. KN(SiMe$_3$)$_2$ (4 equiv.), THF, 18 h, 25 °C; ii. [InCl$_3$] or [InBr$_3$] (1 equiv.), THF, 18 h, 25 °C, (84 % and 89 % respectively); iii. KOAc, AgNO$_3$ or KO^{t}Bu (1 equiv.), THF, 18h (72 %, 68 % and 63 %, respectively).

Complexation reactions were monitored by ^{31}P NMR, in C$_6$D$_6$. **[LInBr]** (^{31}P{^{1}H} NMR signal at 41.9 ppm) was synthesised by deprotonation, using [KN(SiMe$_3$)$_2$], and reaction with [InBr$_3$]. **[LInNO$_3$]** (^{31}P{^{1}H} NMR signal at 40.9 ppm) and **[LInOAc]** (^{31}P{^{1}H} NMR signal at 38.7 ppm) were obtained from reaction of **[LInBr]** with [AgNO$_3$] or [KOAc], respectively. **[LInO^{t}Bu]** (^{31}P{^{1}H} NMR signal at 40.3 ppm) was afforded by reaction between **[LInCl]** and [KO^{t}Bu]. All the complexes were isolated in good yield and were fully characterised, including by single crystal X-ray crystallography, multinuclear NMR spectroscopy and elemental analyses.

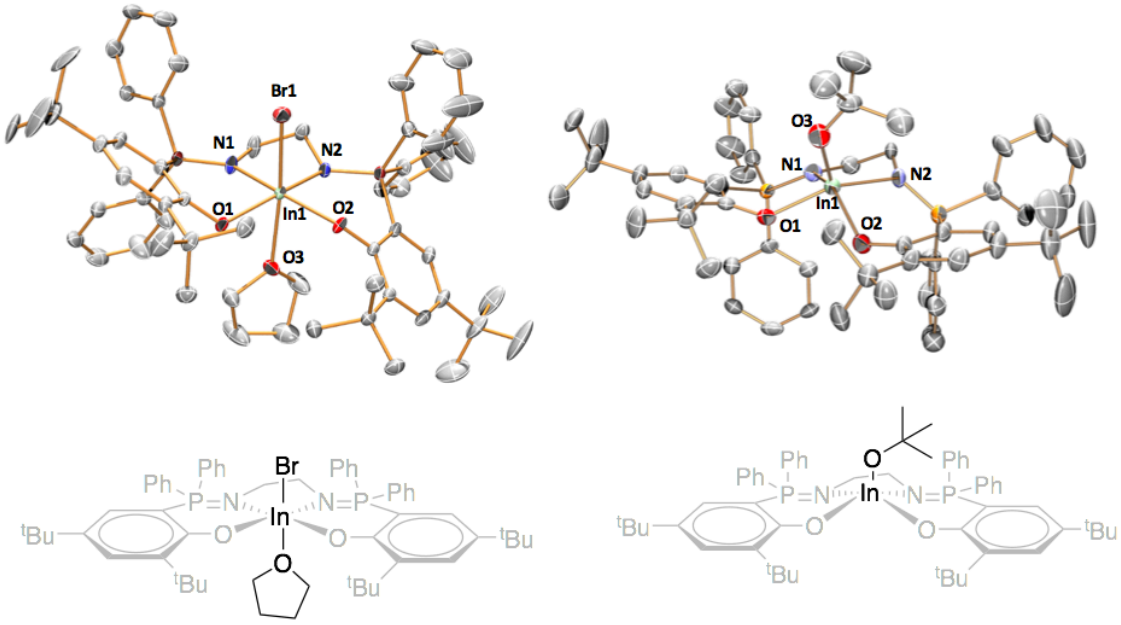

Figure 3.6. Molecular structure of **[LInBr]** (LHS) and **[LInO^{t}Bu]** (RHS) with thermal ellipsoids at the 50 % probability level, hydrogen atoms omitted for clarity (refer to appendix for complete data set). Below is a schematic representation of the molecular structures.

The molecular structure of **[LInBr]** is monomeric and has an octahedral geometry at indium. In octahedral salen complexes, the ligand can coordinate resulting in three different isomers: *cis*-α, *cis*-β and *trans* complexes (refer to the methodology chapter for more details).[21] In the present case, **LInBr** adopts a *trans* conformation where a THF molecule is coordinated *trans* to the bromide co-ligand and the phosphasalen ligand completes the coordination sphere at the metal centre. The ^{1}H NMR spectrum, in C_6D_6, of **[LInBr]** consists in a series of sharp resonances corresponding to half the total number of protons of the complex, indicating a C_s symmetric complex in solution. Interestingly, the ^{1}H NMR spectrum, in C_6D_6 with a slight excess of THF, reveals that THF is not coordinating in solution. DOSY NMR, in d_8-THF, also shows that **[LInBr]** is isostructural to **[LInCl]** (i.e. five coordinated complex) and is monomeric under the polymerisation conditions. The solution and the solid state structure of **[LInO^{t}Bu]** have already been reported by Dr. Dominic Myers but are briefely described here to aid understanding of polymerisation behaviours.[13b] **[LInO^{t}Bu]** is monomeric under the polymerisation

conditions and exhibits a distorted square pyramidal coordination geometry ($\tau = 0.33$).[13b, 17] It is also isostructural to **[LInCl]**.

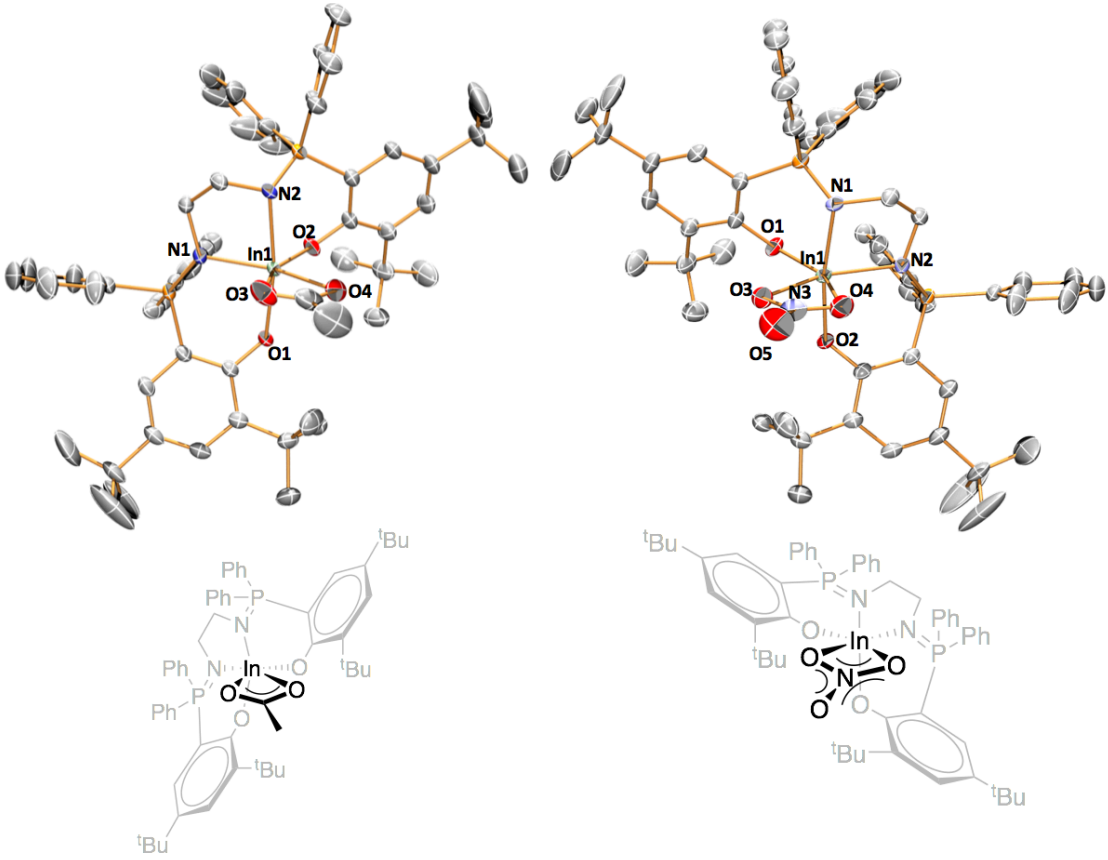

Figure 3.7. Molecular structures of **[LInOAc]** (LHS) and **[LInNO$_3$]** (RHS) with thermal ellipsoids at the 50 % probability level, hydrogen atoms omitted for clarity (refer to appendix for complete data set). Below is a schematic representation of the molecular structures.

In contrast, the molecular structures of **[LInOAc]** and **[LInNO$_3$]** are also monomeric but each show a distorted octahedral geometry at indium. The co-ligands adopt chelating κ^2 coordination modes (Figure 3.7). The similarities between the length of the two C-O bonds [1.249(4) and 1.294(5)] and the N-O bonds [1.270(4) and 1.294(5)], indicate that the charge is delocalised across the chelate. In each case, the phosphasalen ligand coordinates in a *cis*-β fashion. It's relevant to note that a few highly active [Co(III)] salen catalysts also adopt a *cis*-β coordination modes,[22] but the majority of other metal salen catalysts adopt *trans* coordination mode.[5f] Nonetheless, more recent studies using a series of highly active [Co(III)] salen catalysts has suggested that the ligand coordination mode alone may

not be so directly responsible for controlling activity.[3f] Both **[LInOAc]** and **[LInNO$_3$]** were investigated by DOSY NMR**,** in d_8-THF at 298 K, and the results indicate that the monomeric structures are maintained in solution. The ^{1}H NMR spectra (C_6D_6 or d_8-THF) show two broadened resonances for the phosphorus phenyl substituents (Figure 3.8). In contrast, the pentacoordinate indium complexes show 4 sharp resonances for the same substituents. Comparing the aromatic regions of the spectra shows that for **[LInO^{t}Bu]** two distinct multiplets (7.72, 7.41 ppm) are assigned to the *ortho*-phenyl groups, whereas for **[LInOAc]** a single broad resonance (7.55 ppm) is assigned to the same groups. For the octahedral complexes, the peak broadening is tentatively attributed to the equilibration between two *cis*-β conformers (Scheme 3.4). VT-NMR shows that temperatures below 173 K, the broad peak resolves to two well-defined sets resonances which might be due to two distinct conformers. The key observation is that both the relative chemical shifts and multiplicities of the phenyl signals in the ^{1}H NMR spectra enable differentiation between octahedral and square pyramidal coordination. The correlation between the ^{1}H NMR spectra and the coordination geometry around indium may be very useful to characterise catalytic intermediates (*vide infra*).

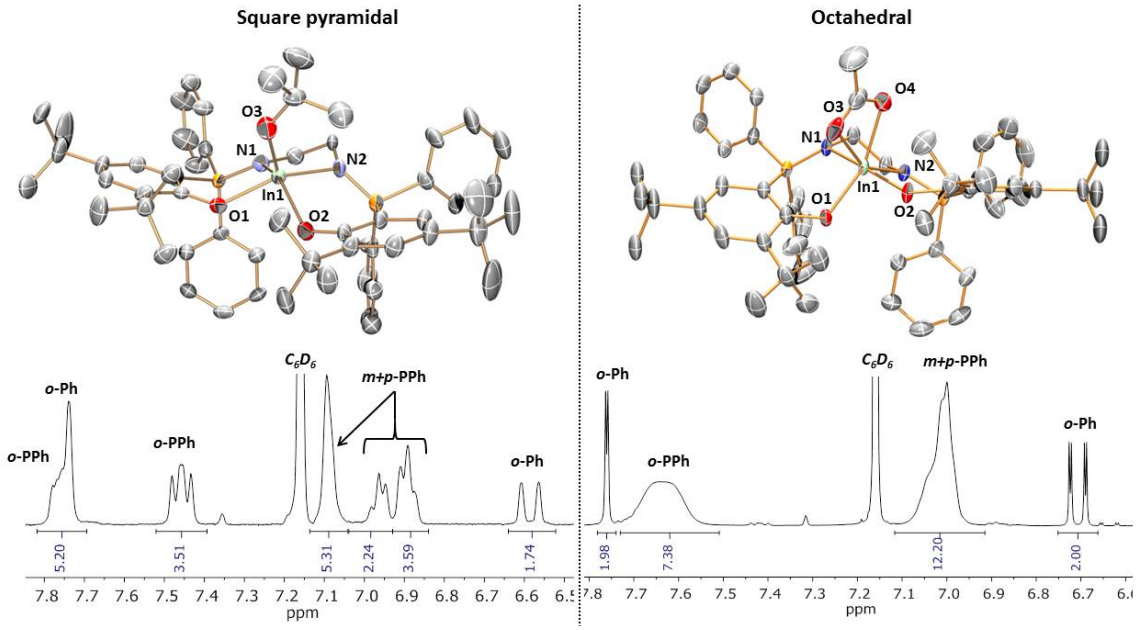

Figure 3.8. Molecular structures of **[LInO^{t}Bu]**[13b] (top LHS) **[LInOAc]** (top RHS) with thermal ellipsoids at the 50 % probability level. ^{1}H NMR (C_6D_6, 298 K) spectra of **[LInO^{t}Bu]** (bottom LHS) and of **[LInOAc]** (bottom RHS) zoomed in the phenyl region.

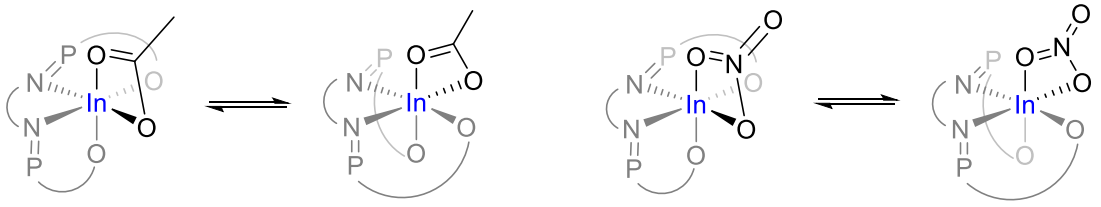

Scheme 3.4. Illustration of the possible equilibrium between the two *cis*-β ligand conformers proposed for **[LInOAc]** and **[LInNO$_3$]**.

3.3.2 CO_2/CHO ROCOP

The series of complexes were each tested, under the same polymerisation catalysis conditions, and performances compared to **[LInCl]** (Table 3.2).

Table 3.2. CO_2/CHO ROCOP catalysed by **[LInX]** (X = Cl, Br, O^{t}Bu, OAc, NO_3).

Catalyst	% Conversion[a]	% Carbonate linkages[a]	% Selectivity PCHC[a]	TOF[b] (h^{-1})	M_n[c] (g/mol)	Đ[c]
[LInCl]	14	73	94	3	197 000 7500	2 1.3
[LInBr]	3	> 99	60	0.6	-	-
[LInO^{t}Bu]	14	> 99	83	3	1410	1.23
[LInOAc]	3	> 99	85	0.6	-	-
[LInNO$_3$]	16	64	80	3.5	7500 900	1.44 1.16

Copolymerisation conditions: **[In]** = 0.1 mol%, 60 °C, 48 h, 1 bar CO_2. [a]Determined by ^{1}H NMR by comparison of the integrals of signals arising from the methylene protons due to copolymer carbonate linkages (δ = 4.65 pmm), ether linkages (δ = 3.45 ppm), and the cyclic carbonate (δ = 4.00 ppm). [b]TOF = (number of moles of epoxide consumed per mole of catalyst)/time (h). [c]Determined by SEC, in THF, at 40 °C, calibrated using polystyrene standards.

Compared to **[LInCl]**, the bromide complex, **[LInBr]**, showed significantly worse performance and evolved cyclic carbonate as the major product. This observation is tentatively attributed to the better leaving group ability of bromide compared to chloride, which accelerates elimination, and cyclic formation, during the first monomer insertion reactions (Scheme 3.5). The finding is also in line with previous reports that [$InBr_3$] efficiently catalyses the formation of cyclic carbonate from CHO/CO_2 mixtures.[16a]

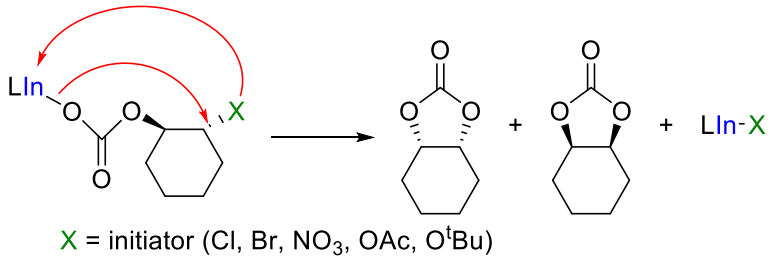

Scheme 3.5. Backbiting reaction observed when the chain end features a good leaving group.

In contrast, the alkoxide derivative, **[LInO^{t}Bu]**, showed much better catalytic performance yielding highly alternating polycarbonate with a high selectivity for polymer (93 %). The polycarbonate showed predictable (low) molecular weight, considering that cyclohexene diol (CHD) is present as a chain transfer agent (see section 3.5), and a monomodal molecular weight distribution.

Surprisingly, the acetate derivative, **[LInOAc],** show negligible activity. Indeed, its ^{1}H NMR spectrum**,** in d_8-THF, remained unchanged both after the addition of one equivalent of CHO and even after two days heating at 60 ^{o}C. On the other hand, the iso-structural nitrate derivative, **[LInNO$_3$]**, showed equivalent activity to the alkoxide catalyst, but formed polymers with lower carbonate linkages (64 %). It is tentatively proposed that these results relate to the difference between the propensity for dissociation of the indium acetate and nitrate co-ligand. Metal-nitrate dissociation in solution of coordinating solvent is a well-known phenomenon, previously reported for several [Co(III)] salen catalysts.[22b, 23] Thus, on the one hand it is proposed that acetate is strongly coordinated to indium

preventing initiation. On the other hand, it is hypothesised that free nitrate anion, may catalyse polyether formation, perhaps by anionic epoxide ROP routes, and concurrently initiation from the indium nitrate catalyst is expected to furnish polycarbonate. As a control experiment, $AgNO_3$ was tested, under similar conditions, and showed only low activity for epoxide ROP leading to polyether formation. It is relevant to note that **[LInNO$_3$]** is not contaminated by $AgNO_3$ (which was used in its synthesis) as it passed elemental analysis.

3.4. Structure/Activity Study

3.4.1 Synthesis and Characterisation of [^{R}LInO^{t}Bu] (y = Amyl, Cumyl or OMe)

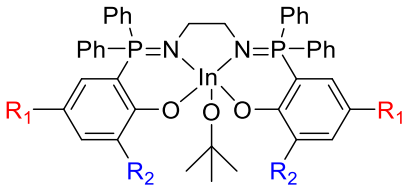

Complex	R_1	R_2
LInO^{t}Bu	^{t}Bu	^{t}Bu
^{Amyl}LInO^{t}Bu	Amyl	Amyl
^{Cumyl}LInO^{t}Bu	Cumyl	Cumyl
^{OMe}LInO^{t}Bu	OMe	^{t}Bu

Scheme 3.6. Indium phosphasalen catalysts featuring ligands with different R_1 and R_2 substituents.

The low activity of **[LInO^{t}Bu]** prompted the structure/activity investigation. The phosphasalen ligand has a range of sites for modification (e.g. phosphorous substituents, *para* and *ortho*-phenolate or the diamine backbone). As described in section 3.1, the influence of *para* and *ortho*-phenolate sites are targeted first. Recently, phosphasalen indium catalysts for lactide ROP showed the highest rates using sterically hindered substituents at this site – a counter-intuitive finding but which may also be relevant to ROCOP catalysis.[13b] Three complexes bearing OMe, amyl or cumyl moieties were synthesised (by modification of the route described in section 3.3.1), and were fully characterised (Scheme 3.6).

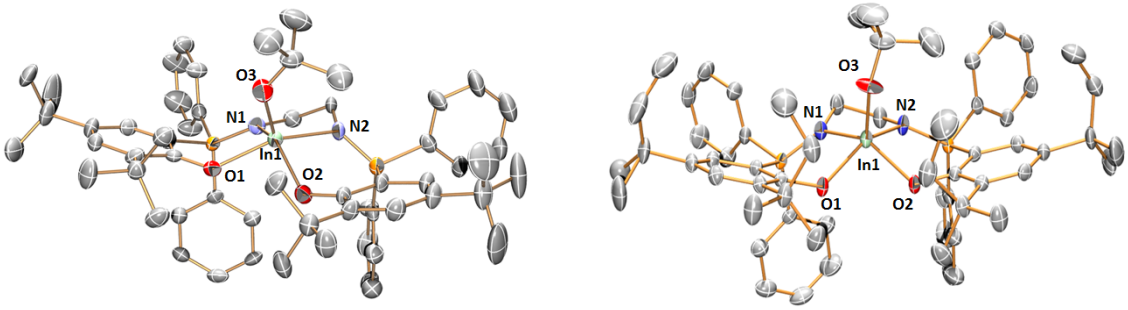

Figure 3.9. Molecular structures of **[LInO^{t}Bu]** (LHS) and **[^{Amyl}LInO^{t}Bu]** (RHS) with thermal ellipsoids at the 50 % probability level, hydrogen atoms omitted for clarity (refer to appendix for complete data set).†

The molecular structure of **[^{Amyl}LInO^{t}Bu]** shows formation of a monomeric, distorted square pyramidal indium geometry with similar bond distances and bond angles to **[LInO^{t}Bu]** (Figure 3.9). ^{1}H NMR, in C_6D_6, and DOSY NMR spectra, in d_8-THF, at 298 K,

† Both structures were obtained by Dr. Dominnic Myers.

of **[^{Amyl}LInO^{t}Bu]** indicates that the solid state geometry is retained in solution. Resonances for the amyl substituents are particularly interesting as two resonances corresponding to the two methyl moieties of the *ortho*-substituents are observable while only one is present for the *para*-substituent (Figure 3.10). This suggests there is restricted rotation at the *ortho* site, which is probably caused by steric hindrance at indium.

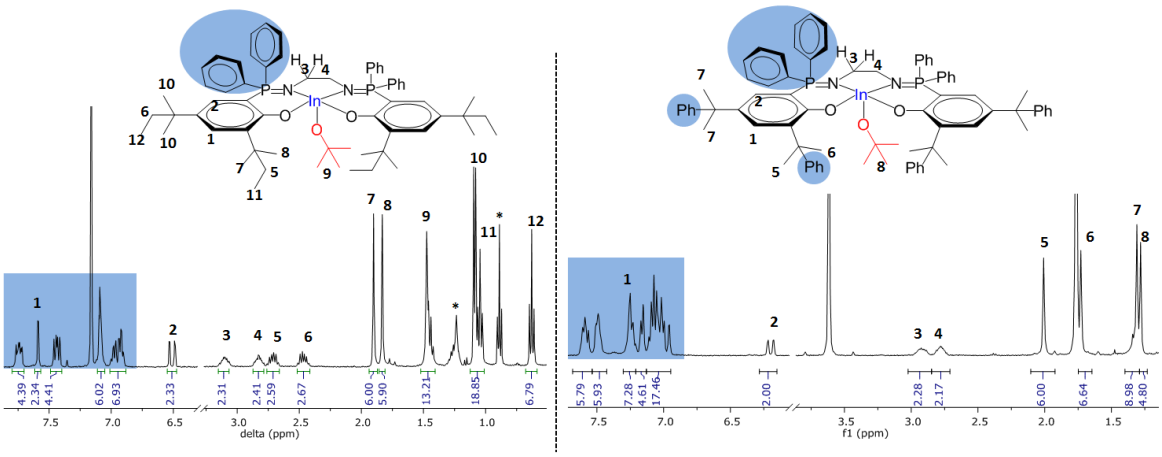

Figure 3.10. ^{1}H NMR spectra of **[^{Amyl}LInO^{t}Bu]** (L.H.S) and **[^{Cumyl}LInO^{t}Bu]** (R.H.S), in C_6D_6, at 298 K.

The solution structures of **[^{OMe}LInO^{t}Bu]** and **[^{Cumyl}LInO^{t}Bu]** are similar to **[LInO^{t}Bu],** with equivalent sharp resonances observed in the ^{1}H NMR spectra in C_6D_6. Once again, the two methyl resonances of *ortho*-substituents are inequivalent (2.37 ppm and 2.10 ppm), indicating there is restricted rotation at the active site. Finally, the DOSY NMR spectra of **[^{Cumyl}LInO^{t}Bu]** and **[^{OMe}LInO^{t}Bu]**, in d_8-THF, at 298 K, indicate that both complexes are monomeric under the polymerisation conditions.

3.4.2 CO_2/CHO ROCOP

The complexes were each tested, under the same polymerisation conditions described previously and performances are compared to **[LInO^{t}Bu]** (Table 3.3).

Table 3.3. CO_2/CHO ROCOP catalysed by **[^{R}LInO^{t}Bu]** (y = ^{t}Bu, amyl, cumyl).

Catalyst	% Conversion[a]	% Carbonate linkages[a]	% Selectivity PCHC[a]	TOF[b] (h^{-1})	M_n[c] (g/mol)	Đ[c]	P_m[d]
[LInO^{t}Bu]	14	> 99	83	3	1410	1.23	0.76
[^{OMe}LInO^{t}Bu]	0	-	-	-	-	-	-
[^{Amyl}LInO^{t}Bu]	16	> 99	85	3.5	1600	1.23	0.78
[^{Cumyl}LInO^{t}Bu]	28	> 99	90	6	2900	1.16	0.86

Copolymerisation conditions: **[In]** = 0.1 mol%, 60 °C, 48 h, 1 bar CO_2. [a]Determined by ^{1}H NMR by comparison of the integrals of signals arising from the methylene protons due to copolymer carbonate linkages (δ = 4.65 pmm), ether linkages (δ = 3.45 ppm), and the cyclic carbonate (δ = 4.00 ppm). [b]TOF = (number of moles of epoxide consumed per mole of catalyst)/time (h). [c]Determined by SEC, in THF, at 40 °C, calibrated using polystyrene standards. [d]Determined by $^{13}C\{^1H\}$ NMR ($CDCl_3$, 125.8 MHz).

[^{OMe}LInO^{t}Bu] was totally inactive, likely because it was unstable and decomposed even upon storage under an inert atmosphere over three weeks to a mixture of products. The higher sensitivity of this complex compared to analogues, which were stable over several months under similar storage conditions, is probably due to increased electron donation of the OMe which destabilises the [In-O^{t}Bu] bond. Under polymerisation conditions, traces of water are present (ppm or ppb levels from for CO_2, *vide infra*), and it is proposed that **[^{OMe}LInO^{t}Bu]** decomposes quickly. The amyl-substituted complex showed equivalent activity to **[LInO^{t}Bu]**, but, the cumyl-substituted complex, **[^{Cumyl}LInO^{t}Bu],** showed approximately twice the activity**.**

All catalysts resulted in high carbonate linkage content and the polycarbonates showed low molecular weights, with monomodal molecular weight distributions, and narrow dispersity. Surprisingly, the polymer $^{13}C\{^1H\}$ NMR spectra also showed the catalysts were isoselective, with the carbonyl region showing an intense resonance assigned to the [*mmm*] tetrad.[24] The iso-selectivity increased in the order **[LInO^{t}Bu]** (rel. intensity = 76 %), < **[^{Amyl}LInO^{t}Bu]** (rel. intensity = 78 %) < **[^{Cumyl}LInO^{t}Bu]** (rel. intensity = 86 %). In order to understand the stereocontrol mechanism, the stereoerrors were analysed. In an

enantiomorphic-site control mechanism, [*mrr*] and [*mmr*] tetrads are expected to be the most common stereoerrors with much smaller contributions from remaining [*rrr*], [*rmr*] and [*mrm*].[3d] However, signals for these errors were essentially absent from the spectrum suggesting a chain end control isoselectivity mechanism. To further confirm the operating mechanism, Bernoulian statistical methods were applied and the calculated values for each tetrad were close to experimental values indicating a chain end control mechanism (see section 3.7.4).[25]

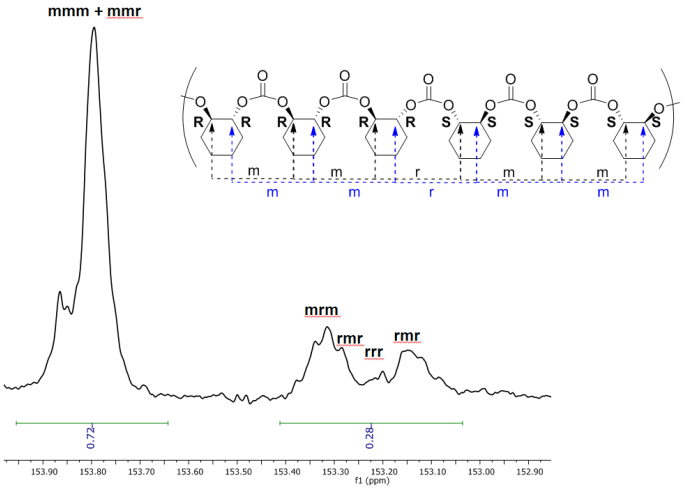

Figure 3.11. $^{13}C\{^{1}H\}$ NMR spectrum of PCHC (298 K, $CDCl_3$) catalysed by **[^{cumyl}LInO^{t}Bu]** zoomed in the carbonyl region ($CDCl_3$, 298 K).

3.4.3 Optimisation of the Polymerisation Conditions

Next the potential to further enhance activity by changing reactions parameters (e.g. temperature and pressure) was investigated.

Table 3.4. Polymerisation data for **[^{R}LInO^{t}Bu]**, at temperatures from 60 °C to 100 °C (at 1 bar of CO_2) and pressures from 1 bar to 40 bars (at 80 °C).

Catalyst	P_{CO2} (bar)	T (°C)	% Carbonate linkages[a]	% Selectivity PCHC[a]	TOF[b] (h^{-1})	M_n[c] (g/mol)	Đ[c]
[LInO^{t}Bu][d]	1	60	> 99	83	3	1400	1.23
[LInO^{t}Bu]	1	80	> 99	84	6.5	2600	1.55
[LInO^{t}Bu]	1	100	> 99	86	7	600	1.20
[^{Cumyl}LInO^{t}Bu]	1	80	> 99	95	16	3400	1.32
[LInO^{t}Bu]	10	80	> 99	87	5.5	12 600	1.94
[LInO^{t}Bu]	20	80	> 99	71	5	4 000	1.15
						11 000	1.05
[LInO^{t}Bu]	30	80	> 99	72	4.5	6500	2.21
[LInO^{t}Bu]	40	80	> 99	75	4	10 600	1.89

Copolymerisation conditions: **[In]** = 0.1 mol%, 24 h. [a]Determined by ^{1}H NMR by comparison of the integrals of signals arising from the methylene protons due to copolymer carbonate linkages (δ = 4.65 pmm), ether

linkages (δ = 3.45 ppm), and the cyclic carbonate (δ = 4.00 ppm). [b]TOF = (number of moles of epoxide consumed per mole of catalyst)/time (h). [c]Determined by SEC, in THF, at 40 °C, calibrated using polystyrene standards. [d]Polymerisation run for 48 h.

When **[LInO^{t}Bu]** was tested at 80 °C, the rate was approximately doubled. The more hindered catalyst, **[^{Cumyl}LInO^{t}Bu]**, also performed well under these conditions and achieved a TOF of 16 h^{-1}, whilst maintaining high selectivity for polymer and a high percentage of carbonate linkages (Table 3.4). Indeed the performance of **[^{Cumyl}LInO^{t}Bu]** is approximately equivalent to the first generation of di-zinc macrocyclic catalysts, which were early examples of catalysts able to operate at 1 bar carbon dioxide pressure.[26] It shows lower activities compared to most aluminium porphyrin catalysts (10 h^{-1} < TOF < 50 h^{-1}, at 40 bar of CO_2, and 60 °C) but activity in the same range as aluminium salen catalysts (5 h^{-1} < TOF < 28 h^{-1}, at 34 bar of CO_2, and 80 °C).[27] It is worth noting that the previously reported **[L'AlCl]** aluminium catalyst is inactive at 80 °C, 50 bar of CO_2 in presence one equivalent of PPN-Cl.[6] Overall, in this field of catalysis the activity is low to modest, particularly compared to highly active zinc[28] or cobalt catalysts,[3o, 7b] but the ability to use catalysts at 1 bar pressure, with higher selectivity and activity in absence of co-catalyst, is unusual and warrants further analysis.

3.5. ROCOP Kinetics

The reaction kinetics were studied using **[LInO^{t}Bu]** and showed that the reaction rate (TOF) is not strongly influenced by the carbon dioxide pressure over the range 1 to 40 bar pressure (Figure 3.12, LHS). This finding is indicative of a zero order in carbon dioxide pressure in the rate law. In contrast, other metal salen catalysts require reaction pressures in excess of 20 bar for activity which is generally supposed to correlate with the rate determining step involving carbon dioxide insertion.[5f]

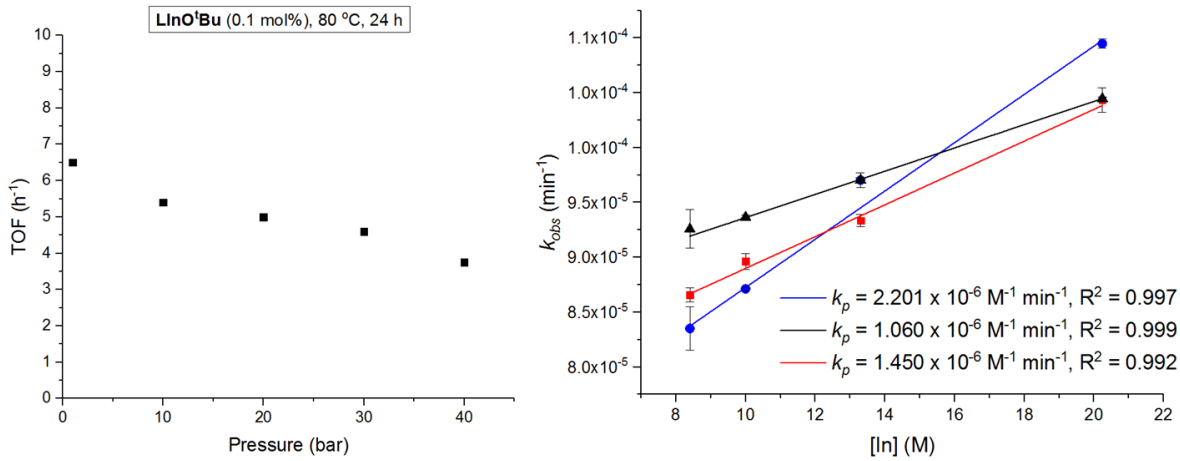

Figure 3.12. LHS: plot of the catalyst activity (in h^{-1}) against CO_2 pressure (in bar). RHS: plot of the initial rates, determined at three different polymer stretch [C=O stretch at 1787-1731 cm^{-1} (▲), C-O-C asymmetric stretch at 1239-1176 cm^{-1} (●) and a polymer mode at 1014 cm^{-1} (■)], against the concentration of initiator.

The order in catalyst concentration was determined over the range 0.08-0.2 mol% (1:500 - 1:1250; catalyst:monomer, Figure 3.12, RHS). The polymerisations were all monitored using *in situ* ATR-IR spectroscopy by monitoring the increase in three polycarbonate vibrational modes: the C=O stretch (1787-1731 cm^{-1}), the C-O stretch (O-C=O = 1014 cm^{-1}), and the C-O-C asymmetric stretch (1239-1176 cm^{-1}). The polymerisations all occurred without any induction period, which is in contrast to many other catalysts, likely due to the alkoxide initiator also being a key intermediate in propagation.[1c, 3n] It is notable that, as previously described,[1b] the rate obtained from analysis of the C-O-C asymmetric stretch is twice that of the other two stretches, due to the formation of two C-O-C linkages per repeat unit. The plots of initial rates vs. catalyst concentrations are all linear which is in

line with a first-order dependence on catalyst concentration. It can also be noted that the three curves are crossing the x axis, indicating a limited catalyst concentration under which the catalysis is impossible. This is probably coming from catalyst deactivation due to water impurities under polymerisation conditions.

All attempts to determine the order in monomer concentration were unsuccessful as polymerisations under dilute conditions (diethylcarbonate solvent) resulted in increased formation of cyclic carbonate by-products.

Overall, a zeroth order in carbon dioxide pressure and a first order in catalyst concentration are suggested. The rate limiting step seems likely to involve either epoxide coordination or insertion. In summary, the rate law for the process seems likely to be best expressed by the following equation:

$$\text{Initial rate} = \nu_0 = k[\text{CHO}]^x[\text{CO}_2]^0[\mathbf{LInO^tBu}]^1$$

3.6. Mechanistic Studies

3.6.1 Initiation reactions

A useful tool to investigate the initiation of polymerisation is by analysing the polymer by Matrix Assisted Laser Desorption/Ionisation Time of Flight (MALDI-ToF) spectrometry (refer to Chapter 2 for more details). When performing CHO/CO_2 co-polymerisation reactions in presence of **[^{R}LInO^{t}Bu]** as the catalyst, the MALDI-ToF spectrum of the resulting PCHC co-polymer clearly showed only one series of chains initiated from CHD (Figure 3.13).

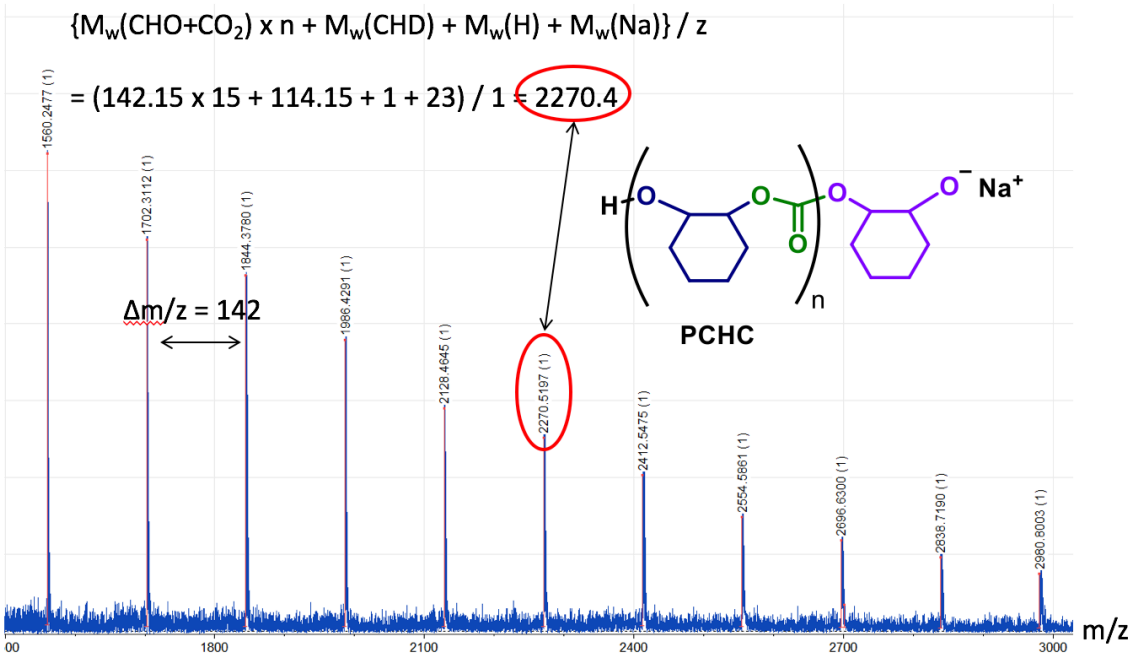

Figure 3.13. MALDI-ToF spectrum of PCHC catalysed by **[^{cumyl}LInO^{t}Bu]**.

To better understand the initiation process, **[LInO^{t}Bu]** was reacted with one equivalent of *trans*-1,2-cyclohexane diol and the reaction progress monitored by ^{1}H NMR spectroscopy (in C_6D_6, at 298 K, Figure 3.14). Immediate appearance of a signal assigned to ^{t}BuOH was observed, alongside with a shift to lower field of the CHD resonances. DOSY analysis of the reaction mixture was in agreement with the formation of a monomeric complex. In particular, CHD resonances have a slightly lower diffusion coefficient than those corresponding to the phosphasalen indium complex, while the diffusion coefficient of the

t-butanol signal had a slightly higher value than expected. Additionally, mixing between CHD and butanol signals was observed – this mixing is a phenomenon typically observed in dynamic equilibrium systems (also described as "out of equilibrium" in the literature).[29] Overall, the observations suggest that ^{t}BuOH/CHD exchange is reversible. However, under polymerisation conditions, it is proposed that the equilibrium is entirely shifted towards the formation of **[LInCHD]** due to the higher relative concentration of CHD vs. alkoxide complex in the bulk reaction mixture.

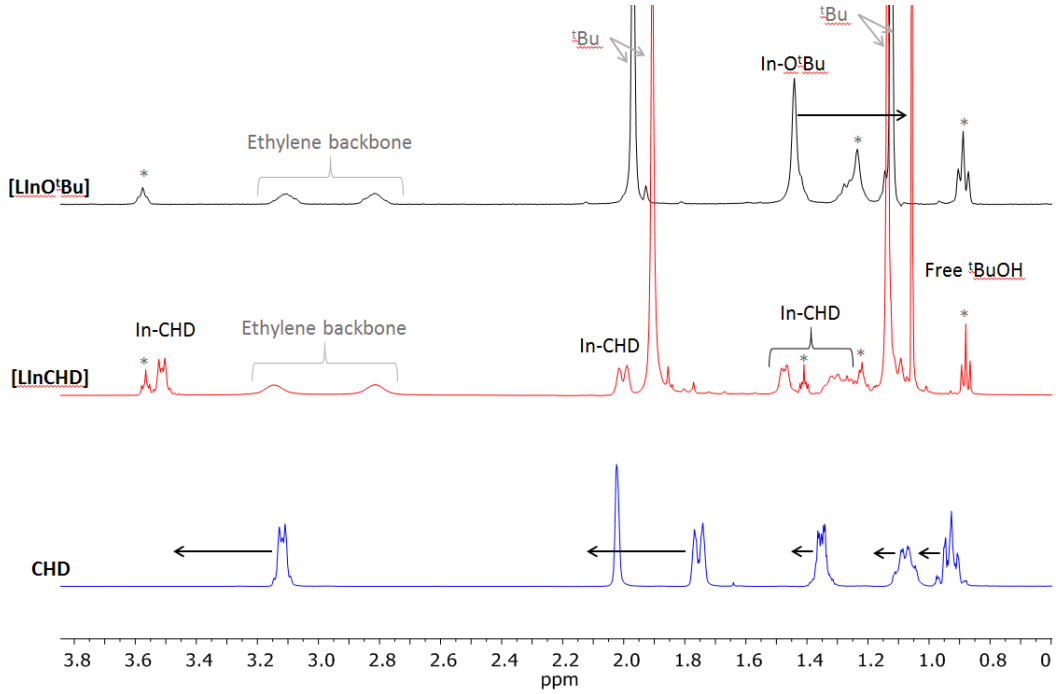

Figure 3.14. Overlay of the ^{1}H NMR spectra (C_6D_6, 298 K) expanded between 0-4 ppm, **[LInO^{t}Bu]** (top), **[LInCHD]** (middle) and CHD (bottom). The middle spectrum shows the formation of ^{t}BuOH and indicates coordination of CHD to form **[LInCHD]**. *Residual THF and hexane.

Crystals suitable for X-ray diffraction were isolated from the mixture by slow diffusion of hexane (Figure 3.15). The molecular structure shows a rare example of a metal-cyclohexanediol complex, **[LInCHD],** with CHD coordinated as an indium-alkoxide (with an In-CHD bond length of [2.068(7) Å]). The coordination geometry at indium is a distorted square pyramidal (τ = 0.28)[17] and the complex is mononuclear. As expected, the observed ligand and alkoxide bond lengths are closely related to those of **[LInO^{t}Bu]** (with an In-O^{t}Bu bond length of [2.023(6) Å]). The crystal lattice also contains a second

uncoordinated diol molecule which is hydrogen bonded to the indium-alkoxide. Both CHD groups are disordered.

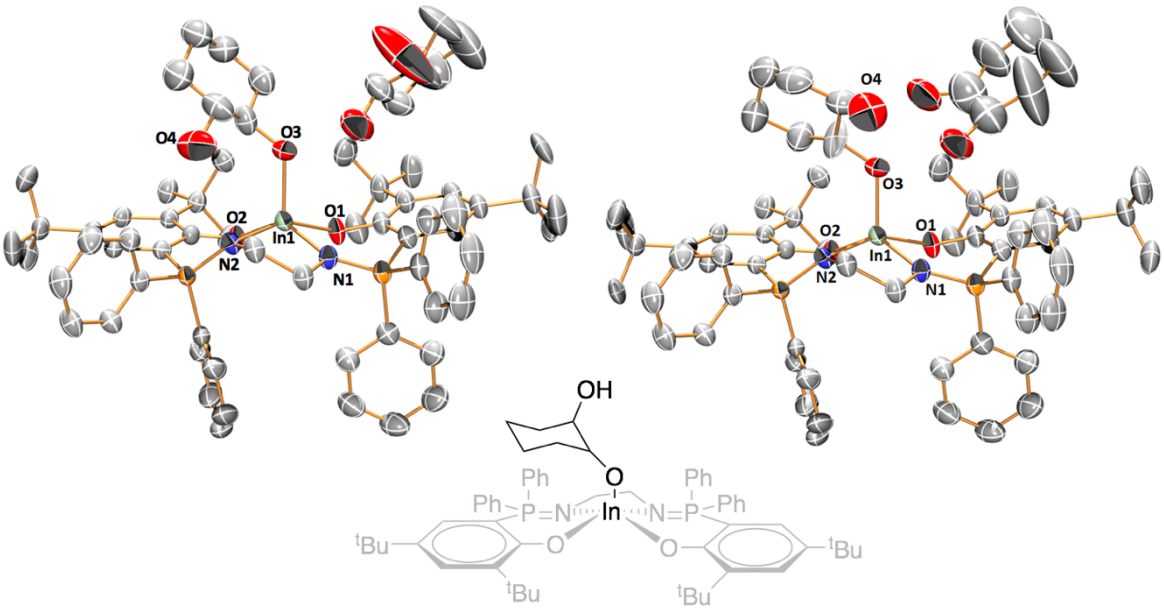

Figure 3.15. Molecular structure of **[LInCHD]** with thermal ellipsoid at the 50 % probability level. The coordinated and free CHD are present in two orientations in the crystal lattice (L.H.S and R.H.S). Hydrogen atoms, a hexane, and a THF molecule have been removed for clarity (refer to appendix for complete data set). Below is a schematic representation of the molecular structures.

The presence of an equilibrium between [In-O^{t}Bu] and [In-CHD] highlights another important phenomenon taking place during polymerisation: the occurrence of chain transfer reactions. The term "chain transfer reactions" refers to the exchange between hydroxyl end-capped dormant polymer chains and alkoxide coordinated growing polymer chains. In all cases, the observed polymer molar masses are lower than theoretical values but dispersities remain narrow. It has been reported in the literature that CHD is known to be an excellent chain transfer agent (CTA).[30] This latter information combined with the previously discussed experimental observations support the occurrence of fast chain transfer reactions, ultimately resulting in polymer molecular weights controlled by the concentration of CHD.

3.6.2 CO_2 Insertion Reaction

In terms of propagation, the insertion of carbon dioxide into the metal alkoxide intermediate is a key reaction. Thus, the CO_2 insertion step was investigated starting from **[LInO^{t}Bu]** and monitored by multinuclear NMR spectroscopy in d_8-THF. Upon the addition of CO_2 to **[LInO^{t}Bu]**, a new signal appeared at 165.0 ppm in the $^{13}C\{^1H\}$ NMR spectrum, in the typical region assigned to carbonate resonances. Moreover, the singlet resonance, in the $^{31}P\{^1H\}$ NMR spectrum, shifts from 40.3 ppm to 38.6 ppm, while in the ^1H NMR spectrum the tert-butoxide resonance shifted from 0.97 ppm (**[LInO^{t}Bu]**) to 1.13 ppm (**[LInO$_2$CO^{t}Bu]**) (Figure 3.16). The resonances associated to the ortho-phenyl protons on the iminophosphorane moieties, showed a series of broad signals (7.77-7.38 ppm), suggesting an octahedral geometry in solution and a κ^2-carbonate coordination mode. Prolonged drying of **[LInO$_2$CO^{t}Bu]** (under vacuum) did not result in detectable changes in the NMR spectrum, nor did the analysis of the product formed after removal of carbon dioxide from the reaction mixture - both findings suggest irreversible CO_2 insertion step to form a stable carbonate intermediate.

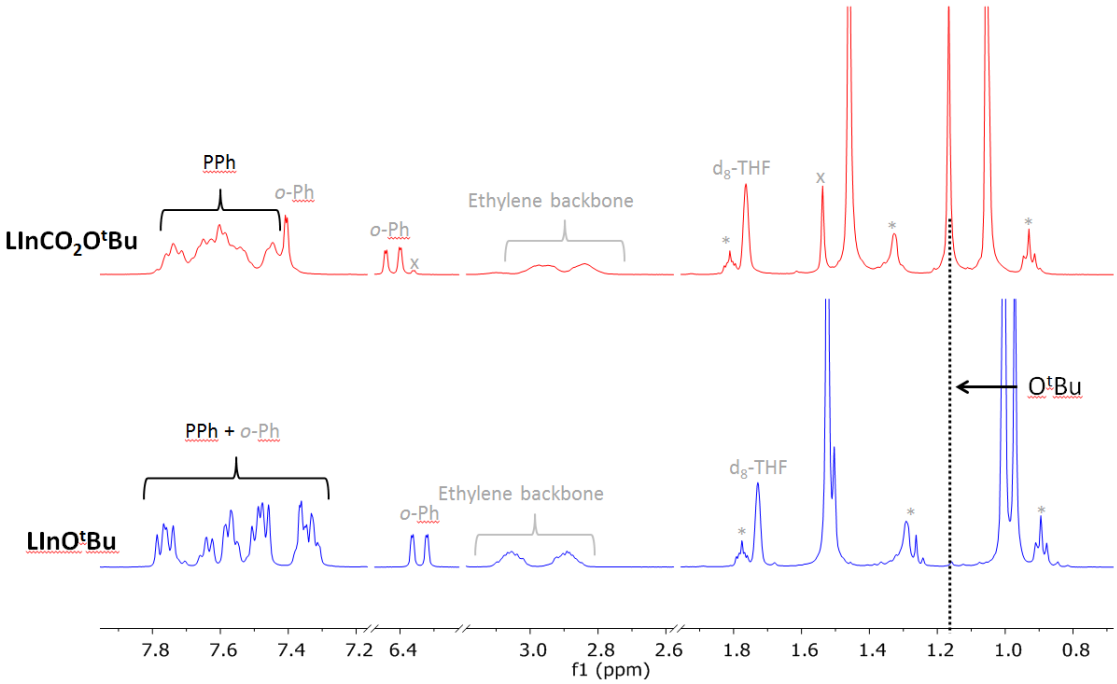

Figure 3.16. Comparison between the ^{1}H NMR spectra of **[LInO$_2$CO^{t}Bu]** (top) and the ^{1}H NMR spectrum of **[LInO^{t}Bu]** (bottom) (d$_8$-THF, 298 K). *: Residual THF and hexane. ^{x}: Side product which has been isolated and fully characterised (*vide infra)*.

To further investigate the coordination mode of the carbonate intermediate, the CO_2 insertion step was also monitored using *in situ* ATR-FTIR spectroscopy. **[LInO^{t}Bu]** was dissolved in THF and 1 bar of CO_2 was added after a freeze-pump-thaw cycle. Carbon dioxide addition resulted in the immediate formation of two new signals assigned to an indium carbonate, at 1560 and 1400 cm^{-1} (Figure 3.17). The signals are assigned as asymmetric and symmetric carbonate stretching modes by analogy of previously reported data for widely studied metal carboxylate complexes.[31] The formation of an indium-carbonate species was proposed as the resonances are at significantly different wavenumbers compared to the typical ones observed for anionic carbonates (e.g. carbonate anions signals are typically observed at 1415 and 1570 cm^{-1}). For metal carboxylate complexes, the difference between the asymmetric and symmetric stretches (Δ) provides a tentative indicator of the coordination mode. Values of Δ < 200 cm^{-1} typically correlate with κ^2-chelation, whilst values of Δ > 200 cm^{-1} are observed for κ^1-coordination.[31] Considering the indium carbonate intermediate (**[LInO$_2$CO^{t}Bu]**), Δ = 160 cm^{-1} and

together with the above mentioned NMR data (in d_8-THF) indicate a κ^2 carbonate chelation mode. Finally, the rate of formation of the carbonate was very fast but can be estimated from ATR-IR data (evolution of the signals at 1400 and 1560 cm^{-1} over time). Nonetheless, a control experiment to determine the rate of carbon dioxide dissolution (monitoring the evolution of the signal at 2346 cm^{-1}, ascribed to the asymmetric stretch of CO_2) reveals a nearly identical rate (Figure 3.18).[32] Thus, it is proposed that the rate of carbon dioxide insertion into the indium-alkoxide bond is likely sufficiently fast to be diffusion limited under the conditions of ATR-IR experiments.

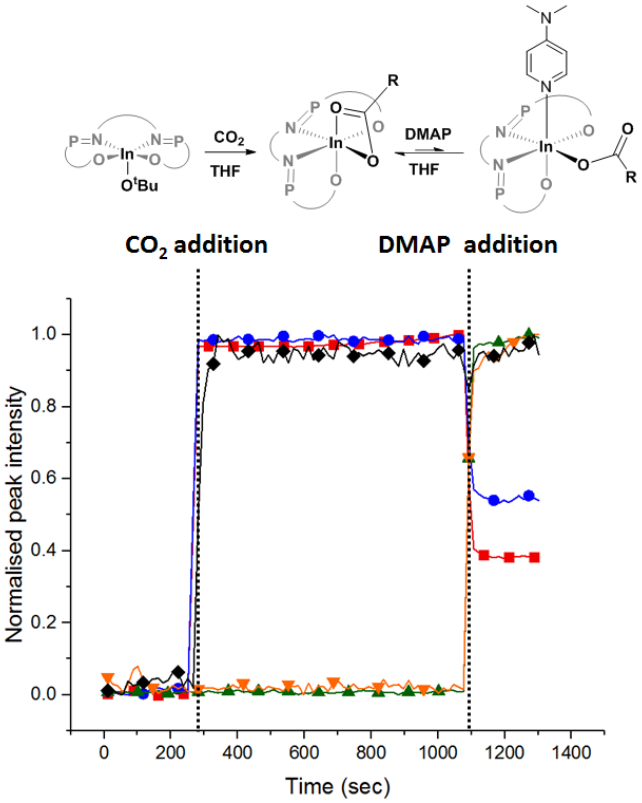

Figure 3.17. Proposed reaction occurring between **[LInO^{t}Bu]**, with CO_2 and DMAP (top) and evolution of selected, normalised IR absorptions against time for the reaction of **LInO^{t}Bu** with: 1) CO_2 and 2) DMAP (bottom). Reaction conditions: i) **LInO^{t}Bu** (0.1 M), THF, CO_2 (1 bar); 2) DMAP (0.2M). Absorptions are monitored at 2346 cm^{-1} (CO_2 band, ◆), 1607 cm^{-1} (DMAP band, ▲), 1387-1410 cm^{-1} (symmetric C-O stretching, ■), 1559-1574 cm^{-1} (asymmetric C-O stretching ●) and 1618 cm^{-1} (terminal C-O stretching, ▼).

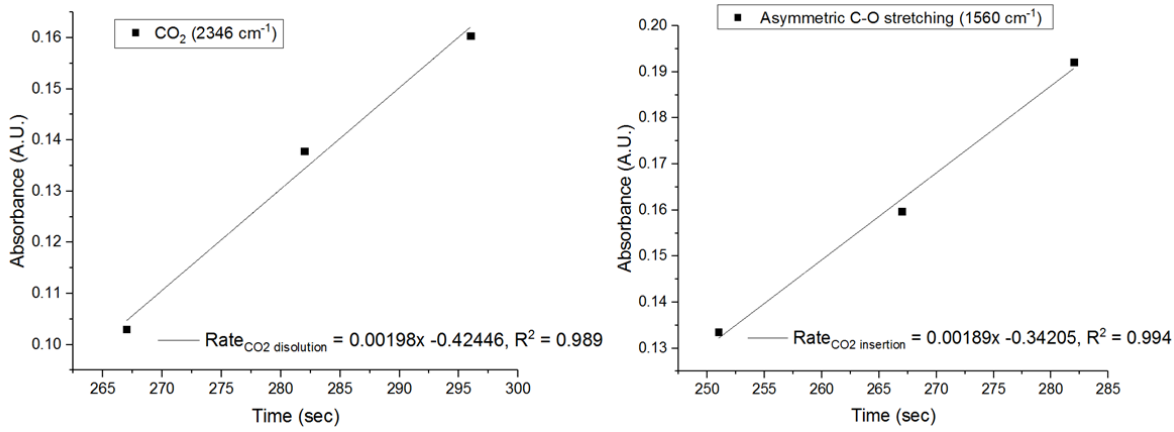

Figure 3.18. Plot illustrating the initial rates of the CO_2 dissolution in THF (resonances are 2346 cm^{-1} corresponding to CO_2, L.H.S) and CO_2 insertion into indium alkoxide bond (resonances at 1560 cm^{-1} corresponding to the asymmetric C-O, R.H.S).

Furthermore, a stable indium-carbonate complex could be isolated when attempting propylene oxide (PO) and CO_2 co-polymerisation. Indeed, **[LInO^{t}Bu]** was not active towards the latter transformation (T = 60 ^oC and 20 bar of CO_2). After the reaction a white crystalline powder, which was insoluble in PO, was isolated and characterised. Single crystal X-ray crystallography diffraction confirmed metal carbonate formation. The complex adopts a dimeric structure with two indium carbonate units bridged by a 1,2-propylenediol (POD) group (**[{LInO$_2$C}$_2$POD]**), presumably formed by CO_2 insertion into both alkoxides groups of 1,2-propylene diol (Figure 3.19). Each indium complex is equivalent and has an octahedral geometry at the indium centre. The phosphasalen ligands adopt a *cis*-β configuration and the carbonates show κ^2 chelation with delocalised charges [C-O distances: 1.220(6), 1.264(6) Å]. Indeed, the lack of ROCOP catalytic activity presumably results from both its high thermodynamic stability and lack of solubility in PO. Solid state ATR-IR and the ^1H NMR spectrum ($CDCl_3$) were consistent with the proposed molecular structure with a Δ = 152 cm^{-1} and the observed broadened resonances for the *ortho*-phenyl substituents in line with the formation of a κ^2 carbonate and octahedral In-complex.

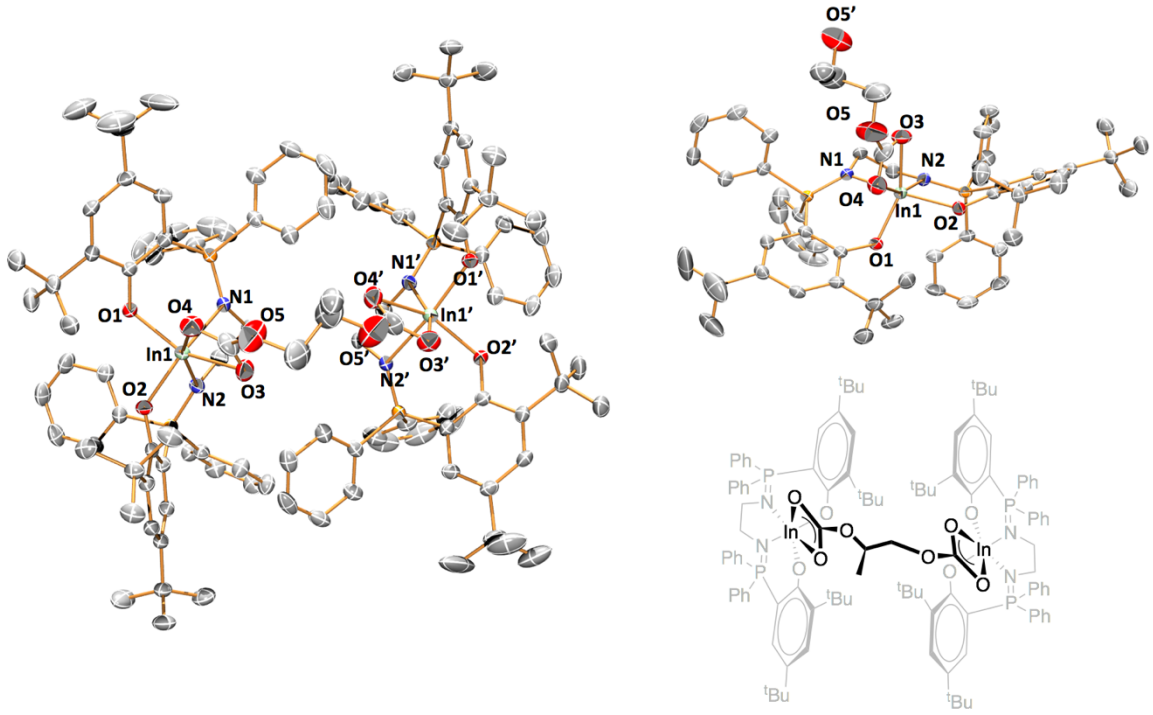

Figure 3.19. Molecular structure of the white crystalline powder, label as **[{LInO$_2$C}$_2$POD]** obtained from the reaction of PO/CO_2 catalysed by **[LInO^{t}Bu]** (LHS) and half of the structure (top RHS), showing the coordination at indium, with thermal ellipsoid at the 50 % probability level. Hydrogen atoms, disorder around the propylene bridge and one PO molecule have been removed for clarity (refer to appendix for complete data set). The bottom RHS scheme represents a schematic representation of **[{LInO$_2$C}$_2$POD]**.

3.6.3 Side Product from CO_2 Insertion into [LInO^{t}Bu]

As mentioned in the previous section, ^{1}H, ^{31}P{^{1}H} and ^{13}C{^{1}H} NMR spectra of **[LInO$_2$CO^{t}Bu]** also showed formation of a side product, which was synthesised quantitatively by reacting **[LInO^{t}Bu]** with wet CO_2 (the CO_2 was used directly from a research grade cylinder without drying columns). Crystals suitable for X-ray diffraction were isolated by slow diffusion of hexane into a saturated solution of the side product in THF (Figure 3.20, LHS). The molecular structure is dimeric with a carbonate group bridging between two indium centres (**[{LIn}$_2$O$_3$C]**). One of the indium has a distorted octahedral geometry with the ligand coordinated in a *cis*-β fashion, while the second one has a distorted square pyramidal geometry ($\tau = 0.36$).[17] Multinuclear NMR spectra of the product were consistent with the molecular structure. ^{1}H NMR spectrum of **[{LIn}$_2$O$_3$C]** showed no resonances corresponding to [In-O^{t}Bu] moieties. On the other hand, ^{13}C{^{1}H} NMR spectrum showed a new resonance at 171.4 ppm assigned to the carbonate group and

$^{31}P\{^{1}H\}$ NMR spectrum consisted in one new singlet at 38.7 ppm. It is proposed that this product is formed by initial alkoxide hydrolysis followed by CO_2 insertion into the hydroxyl species. Indeed, the closely related **[^{Cumyl}LInO^{t}Bu]** was isolated as **[{^{Cumyl}LIn(OH)}$_2$]** probably due to protic impurities present in the crystallisation solvents. The molecular structure of **[{^{Cumyl}LIn(OH)}$_2$]** is also dimeric with two bridging hydroxyl moieties. The two metal complexes were related by an inversion centre and each indium centre displayed an octahedral geometry at indium with a *cis*-β coordinated ligand.

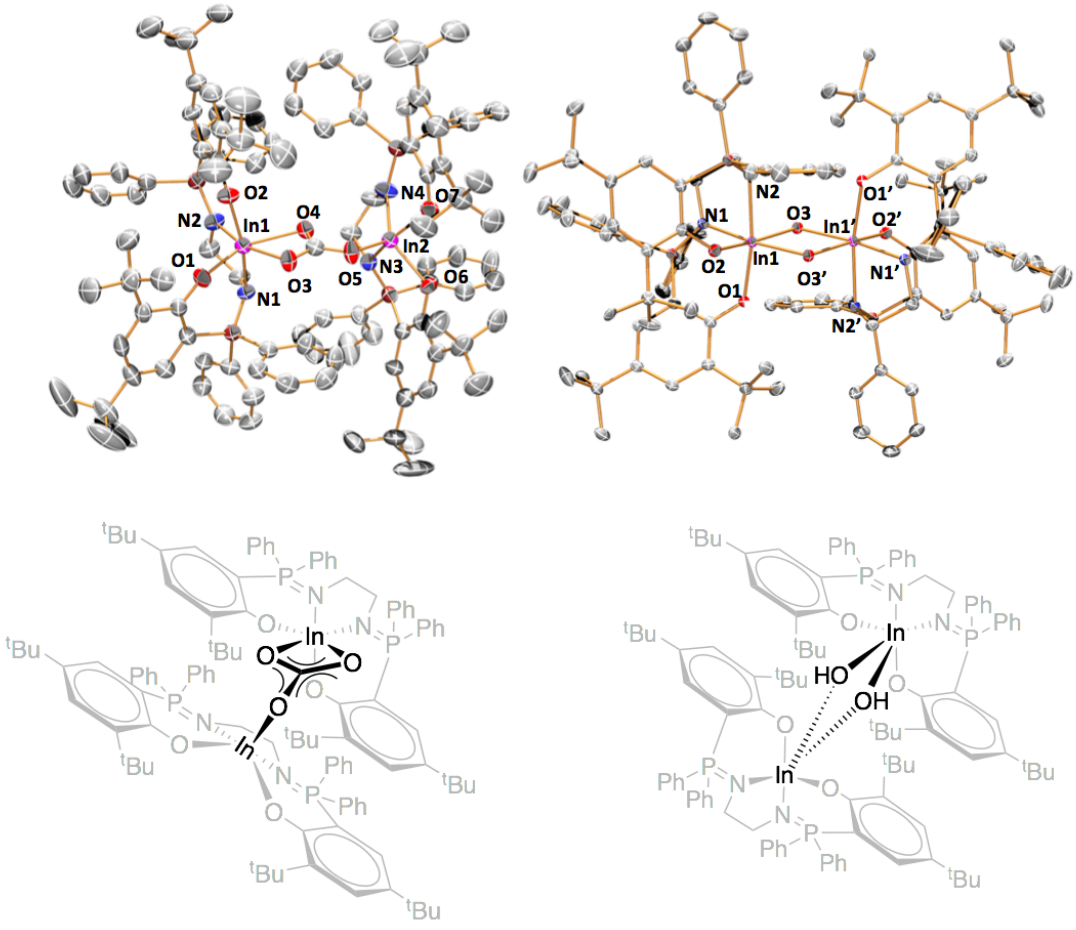

Figure 3.20. L.H.S: Molecular structure of the isolated side product from the reaction **[LInO^{t}Bu]** and CO_2 with thermal ellipsoid at the 50 % probability level. R.H.S: Molecular structure obtained upon crystallisation of **[^{Cumyl}LInO^{t}Bu]** with protic impurities with thermal ellipsoid at the 50 % probability level. Hydrogen atoms have been removed for clarity (refer to appendix for complete data set).

A rationale to explain the formation of these unusual intermediates can be devised for the **[LInO^{t}Bu]** complex. When working with a mixture of CO_2/H_2O (unpurified CO_2), **[LInO^{t}Bu]** reacts first with water to form **[{LIn(OH)}$_2$]**. The dimeric intermediate then

reacts quickly with CO_2, realising a water molecule, to form the thermodynamically stable **[{LIn}$_2$O$_3$C]** intermediate. On the other hand, when working with ultra-dry CO_2, formation of **[LInO$_2$CO^{t}Bu]** occurs exclusively. It is worth reminding the readers that despite using commercially available ultra-high purity carbon dioxide (research grade CO_2 99.9995 % pure), the gas was further purified before being used for co-polymerisation reactions, by flowing it through a series of two drying columns. Still, low levels of residual water may still be present in concentrations sufficient to partially hydrolyse **[LInO^{t}Bu]**. Finally, it is proposed that **[LInO$_2$CO^{t}Bu]** does not react with water to form **[{LIn}$_2$O$_3$C]** as **[LInO$_2$CO^{t}Bu]** is stable to protic impurities.

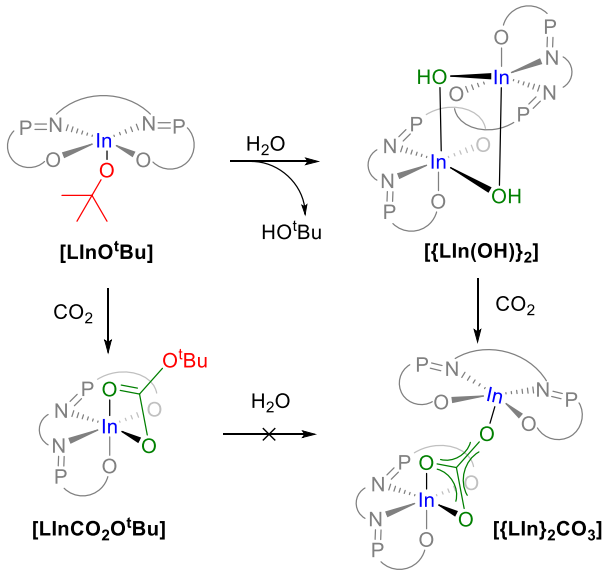

Figure 3.21. Proposed pathway for the formation of **[LInO$_2$CO^{t}Bu]** and the side products **[{LIn(OH)}$_2$]** and **[{LIn}$_2$O$_3$C].**

It is worth noting that even if the formation of **[{LIn}$_2$O$_3$C]** is possible starting from **[LInO^{t}Bu]**, there is no evidence that this side product can be formed starting from **[LInCHD]**, the real polymerisation initiator. This is likely due to the improved stability of the CHD alkoxide intermediate when compared to the terbutoxide one, preventing the formation of the hydrolysed product and the formation of **[{LIn}$_2$O$_3$C]**. Thus, in the optimised CHO/CO_2 copolymerisation conditions catalyst deactivation through formation of **[{LIn}$_2$O$_3$C]** is likely not occurring.

3.6.4 Reaction of [LInO$_2$CO^{t}Bu] with a Lewis Base

In order to investigate the coordination process in more detail, **[LInO$_2$CO^{t}Bu]** was reacted with an equivalent of a strong Lewis base, dimethylaminopyridine (DMAP), selected to study coordination but not subsequent insertion reactions. Thus, the carbonate intermediate was reacted with an equivalent of DMAP and the complexation reaction monitored by *in sit*u ATR-IR spectroscopy (Figure 3.22). Upon addition of DMAP, an immediate decrease in intensity of the two carbonate stretches absorptions at 1560 and 1400 cm^{-1} was observed with simultaneous evolution of a new signal at 1618 cm^{-1}, assigned to a κ^1 carbonate asymmetric stretch (Δ_{max} = 218 cm^{-1}). It is also notable that there is no evidence for carbonate displacement to form an anionic carbonate (the wavenumbers for carbonate stretches for the anion differ). The changes to the IR spectrum occurred immediately after DMAP addition, but did not evolve further over ~1 hour more of reaction monitoring. The final product showed three distinct absorptions, centered at 1618, 1560 and 1400 cm^{-1}, respectively which were assigned to carbonate stretches. This data was tentatively interpreted as the result of an equilibrium between two distinct carbonate intermediates, both characterised by an octahedral coordination geometry: one involving a chelating κ^2-carbonate ligand and the other featuring coordinated DMAP and a terminal κ^1-carbonate ligand (Figure 3.17).

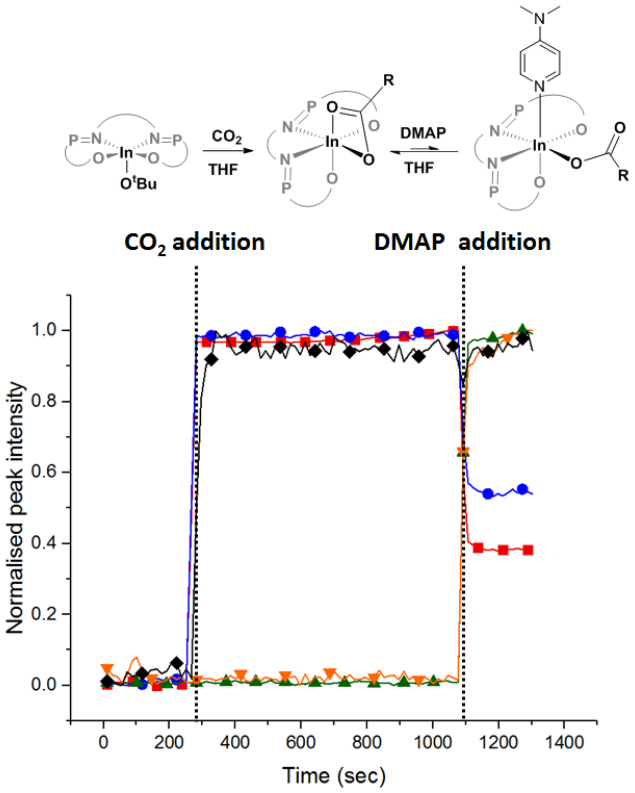

Figure 3.22. Copy of the figure 16: evolution of selected, normalised IR absorptions against time for the reaction of **LInO^{t}Bu** with: 1) Carbon dioxide and 2) DMAP. Reaction conditions: i) **LInO^{t}Bu** (0.1 M), THF, CO_2 (1 bar); 2) DMAP (0.2M). Absorptions are monitored at 2346 cm^{-1} (CO_2 band, ◆), 1607 cm^{-1} (DMAP band, ▲), 1387-1410 cm^{-1} (symmetric C-O stretching, ■), 1559-1574 cm^{-1} (asymmetric C-O stretching ●) and 1618 cm^{-1} (terminal C-O stretching, ▼). Above is a scheme showing the proposed reaction between [LInO^{t}Bu], with CO_2 and DMAP.

The coordination of DMAP to **[LInO$_2$CO^{t}Bu]** was also followed by ^{1}H NMR spectroscopy at different temperatures (d_8-THF). After the addition of 2.5 equiv. of the Lewis base to **[LInO$_2$CO^{t}Bu]**, the ^{1}H NMR spectrum at 298 K stayed unchanged (Figure 3.23, middle spectrum). However, upon cooling the solution to 190 K, coordination of DMAP was observed (Figure 3.23, top spectrum). In particular, the phenyl resonances of the pyridine moiety shifted from 8.11 ppm to 8.28 ppm and from 6.54 to 5.94 ppm, respectively whilst the resonances of the dimethylamino moiety shifted from 2.97 ppm to 2.90 ppm. Accordingly, a new broad resonance appeared at 7.96 ppm for the phosphorus phenyl substituents. Integration of these signals suggests quantitative formation of a **[LInO$_2$CO^{t}Bu·DMAP]** adduct. Warming up the NMR sample to 298 K resulted in the same initial spectrum. Combined with the in situ ATR-IR results, NMR experiments

highlighted the presence of an equilibrium between **[LInO$_2$CO^{t}Bu]** and **[LInO$_2$CO^{t}Bu·DMAP]**. The equilibrium is proposed to be faster than the NMR time-scale at 298 K but could be significantly slowed down at lower temperatures. DOSY NMR analysis showed mixing between DMAP and **[LInO$_2$CO^{t}Bu]** providing further evidence of an equilibrium process.[29]

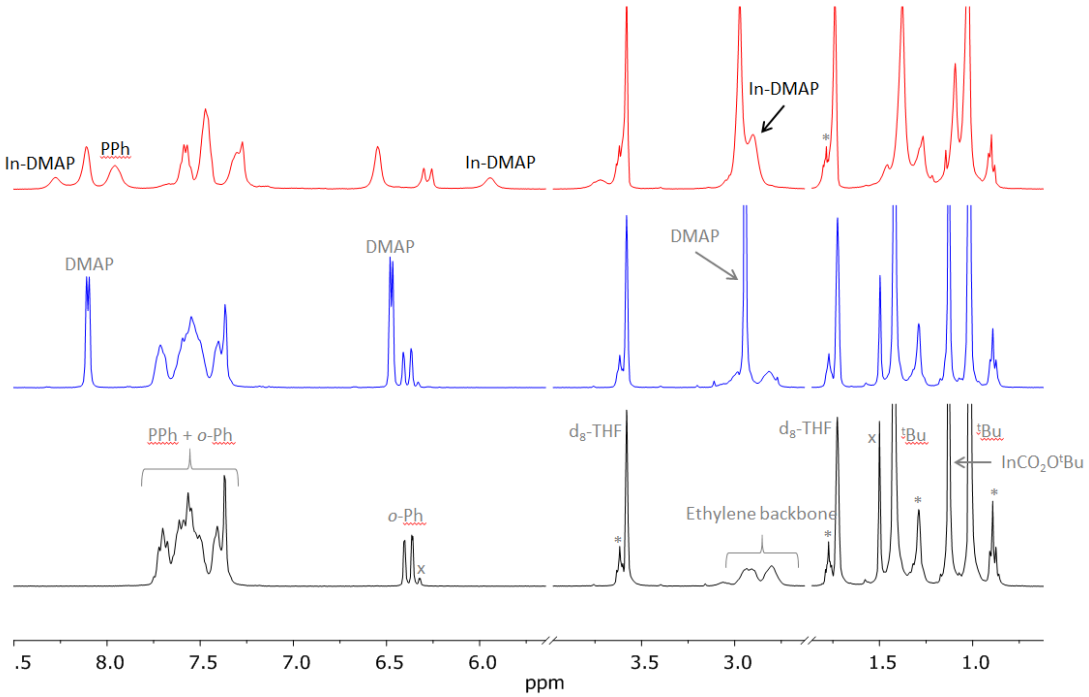

Figure 3.23. ^{1}H NMR spectra (d$_8$-THF) of **[LInO$_2$CO^{t}Bu]** (298 K) before the addition of DMAP (lower spectrum), after the addition of DMAP (middle spectrum, 298 K) and at 190 K (top spectrum).

3.7 Discussion and Proposed Mechanism

Bringing together the structure-activity, kinetic analysis and catalytic intermediate studies, enabled the polymerisation mechanism to be proposed (Figure 3.24).

3.7.1 Initiation and Chain Transfer

MALDI-ToF data showed that polymer chains were exclusively α,ω-dihydroxyl end-capped and SEC analysis of the polymers, showed molar masses values (calibrated with PS standards) were lower than expected on the basis of catalyst concentration/conversions. It is important to emphasise that both the observed chain end-groups and the obtained molar mass data are in agreement with polycarbonates produced by a range of other known catalysts in this field.[3h, 24a, 24b, 26, 33]

The observed results were ascribed to low quantities of CHD present in the initial batch of monomer. The presence of CHD, even after several fractional distillations, is a known problem in the field of CO_2/epoxide ROCOP.[34] Here, **[^{R}LInO^{t}Bu]** (y = ^{t}Bu, amyl or cumyl) catalysts are proposed to form the true initiating alkoxide complex (**[^{R}LInCHD]**) instantaneously upon dissolution of **[LInO^{t}Bu]** into CHO, via an equilibrium with 1,2-cyclohexanediol (CHD). The equilibrium process was studied monitoring the stoichiometric reaction between **[LInO^{t}Bu]** and CHD, and proposed to lie towards formation of **[LInCHD]** under catalytic conditions (e. g. in presence of excess CHD vs. catalyst). The solid state structure of **[LInCHD]** was characterised by X-ray crystallography, surprisingly there are not any equivalent structures reported for any metal centre and so the structure provides rare insight into the true catalytic species proposed for most metal/ligand combinations.

In addition, water contamination, likely resulting from the dynamic gas atmosphere, is also known to facilitate epoxide hydrolysis to form the corresponding diol.[3h, 5l, 33e, 33g, 33h, 35]

Recently, Darensbourg and co-workers studied Cr-salen catalysts for CHO/CO_2 ROCOP when small quantities of water were deliberately added.[51] A range of spectroscopies were used to characterise the formation of 1,2-cyclohexanediol *in situ* during catalysis. Further, they observed that the hydrolysis reaction occurred more rapidly and prior to any polymerisation catalysis, rationalising, in part, the observed initiation periods and the polymer molar mass/end-group results.[51] Overall, in the present case, it is proposed that the low molecular weight of the polycarbonate diol produced could be ascribed to CHD present both in the starting batch of epoxide and formed from epoxide hydrolysis due to water contamination during the polymerisation reaction.

3.7.2 Propagation

[LInCHD] also serves as a close structural model for the indium propagating alkoxide (which features a growing polymer chain in place of the free hydroxyl group). It is important to emphasise the existence of the equilibrium between metal-alkoxide and alcohols because the propagating alkoxide will propagate from both sides of the diol so as to form telechelic, dihydroxyl terminated polymer chains. **[LInCHD]**, and by analogy the propagating alkoxides, has pentacoordinate square-pyramidal indium centre as established by both solid state and solution studies. Further, there was no experimental evidence of formation of an indium-epoxide adduct from **[LInCHD]**, even in the presence of excess epoxide. This lack of reactivity may in part rationalise the very low formation of ether linkages; such linkage formation requires epoxide coordination by the metal alkoxide intermediate. Rather, during polymerisation the indium alkoxide intermediate reacts with carbon dioxide. Indeed the reactivity study revealed that the closely related **[LInO^{t}Bu]** complex reacts very rapidly and irreversibly with carbon dioxide, even at low pressures and under diffusion limited conditions, to form a stable indium carbonate intermediate **[LInO$_2$CO^{t}Bu]**. The isolated **[LInO$_2$CO^{t}Bu]** indium carbonate complex, and by analogy

the propagating indium carbonate intermediate, showed a hexacoordinate structure with an octahedral coordination geometry at indium. It features a chelating (κ^2) carbonate and *cis*-β phosphasalen coordination mode. It is worth comment that most salen complexes are proposed to adopt a trans-coordination of the ligand but highly active bicomponent cobalt salen catalysts showed *cis*-β ligand configurations.[3f, 22a] The extent to which ligand conformation influences reactivity remains an open question since subsequent studies revealed the same conformation for inactive complexes.[3f]

The next catalytically relevant step of the polymerisation requires coordination of an epoxide to the indium carbonate intermediate forming an adduct. On the basis of the stoichiometric reactions carried out using **[LInO$_2$CO^{t}Bu]** with DMAP, monomer coordination is expected to be an equilibrium process shifted towards **[LInO$_2$CO^{t}Bu]**. Further, epoxide coordination resulted in a change in carbonate coordination mode, resulting in formation of a κ^1-carbonate. Monomer coordination is tentatively proposed to occur at a site *cis* to the indium carbonate. Following epoxide coordination, the indium carbonate attacks and ring-opens the coordinated epoxide - a reaction that is inferred to occur by a *cis*-mononuclear mechanism. After epoxide ring-opening the five-coordinate alkoxide intermediate re-forms and the catalytic cycle continued. It is proposed that the catalyst resting-state is the stable indium carbonate species on the basis of the low pressure activity and its observed high stability.

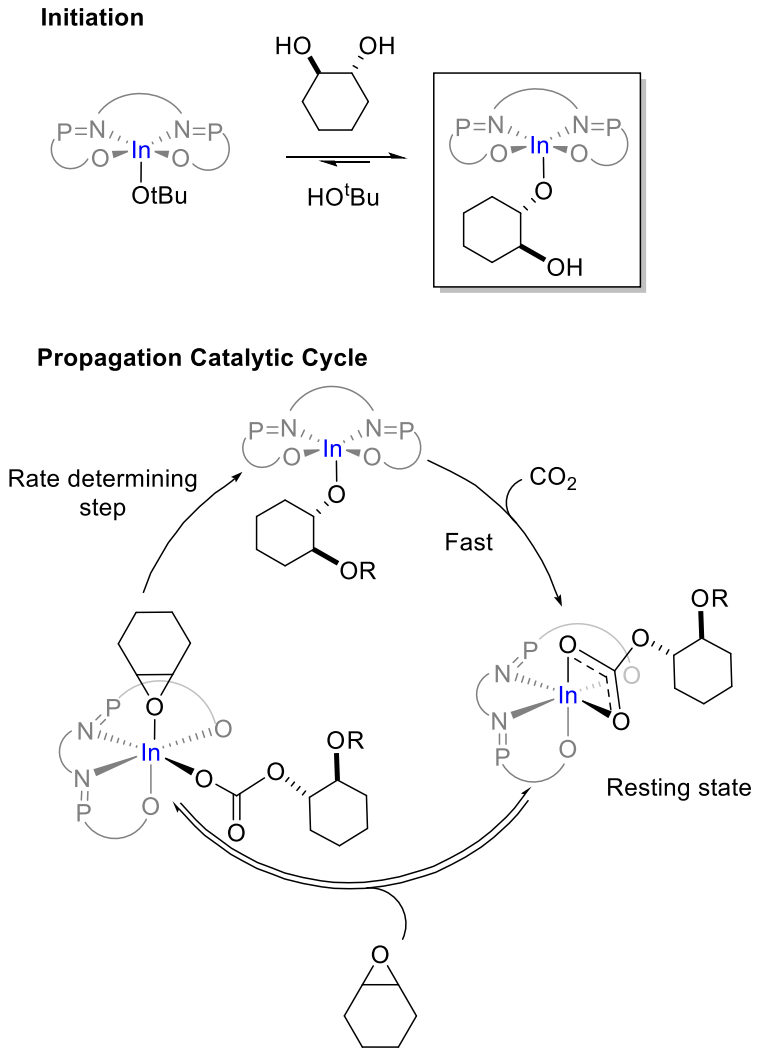

Figure 3.24. Proposed mononuclear mechanism for CO_2/epoxide ROCOP using indium phosphasalen alkoxide catalysts.

3.7.3 Structure-Activity Studies

Given the observed better performance of indium phosphasalens compared to indium salen complex, it is relevant to consider differences between the two ligands. The phosphasalen ligand is known to be a strong σ and π donor and as such is considered to be more electron donating than salen ligands.[11, 14c, 36] Thus, it would be expected that for phosphasalen catalysts, the indium centre shows reduced Lewis acidity (and electrophilicity) compared to the salen analogue. The reduction in Lewis acidity appears to be beneficial for catalysis, perhaps by increasing the lability of the indium alkoxide to insert CO_2 (either through destabilisation of the ground state or by stabilisation of the transition state). Structure-activity studies on phosphasalen ligands revealed that the most active catalysts features

sterically hindered ortho-substituted phenolate substituents. It is proposed that increasing steric hindrance may destabilise the hexacoordinate indium carbonate complex and favour the formation of the pentacoordinate alkoxide complex (after epoxide ring-opening). Future efforts to model the catalytic cycle and transition states using DFT would be useful to test this hypothesis but are beyond the scope of the current study.

Finally, the absolute activity of indium phosphasalen catalysts is only low to moderate and this may relate to the high stability of the indium carbonate intermediate and in particular the κ^2 vs. κ^1 -carbonate coordination modes. In support of this notion, the crystal structure of the carbonate intermediate (formed by reaction between **[LInO^{t}Bu]**/PO/CO_2) shows an additional, uncoordinated propylene oxide molecule in the lattice. The lack of coordination between the indium centre and excess epoxide indicates the relatively high stability of the chelating carbonate intermediate. Future catalyst design strategies should focus on additional means to destabilise the κ^2 carbonate coordination mode and to try to accelerate epoxide attack and ring-opening.

3.7.4 Stereoselectivity

The iso-selectivity of the phosphasalen catalysts is quite unexpected and unusual - especially since the other isoselective ROCOP catalysts are chiral and operate by enantiomorphic site control or hybrid mechanisms.[3d, 3l, 37] Here, the iso-selectivity is increased by substitution of the *ortho*-phenolate site and was attributed to a chain end control mechanism (on the basis of stereoerror analysis). Recently, the closely related catalyst, **[^{Cumyl}LInOEt],** showed high isoselectivity for rac-lactide ROP (P_i = 0.92, THF, 298 K) and also operates by a chain end control mechanism.[13b] It seems likely that **[^{R}LInO^{t}Bu]** catalysts for CHO/CO_2 ROCOP owe the stereoselectivity in part to steric direction by the two ortho-phenolate substituents over epoxide enchainment and/or coordination of the growing polymer chain.

To further confirm this hypothesis, Bernoulian statistics were applied to model the relative tetrads intensities and compared them with the experimental values determined from the $^{13}C\{^{1}H\}$ NMR spectrum of PCHC ($CDCl_3$).[25] Table 3.5 compare the experimental values for several tetrads and the calculated values using the Bernoulian model.

Table 3.5. Comparison of experimental tetrad intensities against the calculated probabilities for iso-enriched PCHC, catalysed by **[^{R}LInO^{t}Bu]** (y = ^{t}Bu, Amyl, Cumyl).

	P_m		[*mmm*]+[*mmr*]		[*mrm*]+[*rrm*]		[*rrr*]		B
	Calc (%)	**Obs** (%)	**Calc** (%)	**Obs** (%)	**Calc** (%)	**Obs** (%)	**Calc** (%)	**Obs** (%)	**Calc** (%)
[LInO^{t}Bu]	0.85	0.76	0.62	0.62	0.13	0.19	0.03	0.05	1.00
[^{Amyl}LInO^{t}Bu]	0.88	0.78	0.66	0.68	0.13	0.18	0.04	0.04	1.00
[^{Cumyl}LInO^{t}Bu]	0.92	0.86	0.80	0.78	0.14	0.14	0.03	0.02	1.00

In all cases, the calculated probabilities were close to the experimental values. In addition, the accuracy of the model was tested using the Bernoulian Test Equation which is a means to assess the accuracy of the model. In all cases, a value of 1 was obtained, indicating a chain end control mechanism.

3.7.5 Comparison with Metal Salen Catalysts

Comparing the indium phosphasalen catalysts with the widely studied Cr/Co salen catalysts revealed clear differences in both rate laws and mechanisms. Firstly, binary metal salen catalysts/co-catalyst systems generally show pressure dependent activities, consistent with carbon dioxide insertion being rate determining, at least up to around 30 bar pressure.[1a, 3a-d, 3g, 3h, 3j, 3m-o, 4, 5b, 5d, 5f, 5h, 5j, 5k, 33b, 38] In contrast, the indium phosphasalen catalysts show activities which are pressure independent over the range 1-40 bar, consistent with rapid carbon dioxide insertion and suggesting a different rate determining step: indium carbonate attack on coordinated epoxide.

Another central difference concerns the addition of co-catalysts. Most metal salen catalysts require the addition of 1-2 equivalents of co-catalyst, preferably PPN-X salt (where X= halide or phenolate in many of the most active systems).[1a, 3a-d, 3g, 3h, 3j, 3m-o, 4, 5b, 5d, 5f, 5h, 5j, 5k,

[33b, 38] The precise role and speciation during catalysis is very complex and kinetic studies using **[Cr-salenX]**/PPN-X catalysts, revealed orders of 1-1.34 for both catalyst *and* co-catalyst (up to ~2-3 equivalents of co-catalyst).[1a, 5c, 5h, 5i] Two independent studies of the rate laws shown by **[Co-salenX]**/PPN-X systems showed orders of 1.57 and 1.61 in catalyst concentration.[4b, 9] Overall, these findings may be rationalised by multiple active sites and are likely to include active ion pairs and dimeric/dinuclear intermediates. Subsequently, catalytic activity was dramatically improved by tethering the ionic co-catalyst to the salen ligand.[3e, 3f, 7b, 22] A kinetic study using such a [Co(III)] catalyst showed a first order dependence on catalyst concentration which was interpreted by mechanisms invoking alkoxide/carbonate dissociation from the metal active site during catalysis.[4b] Another approach to increase activity and selectivity is to use dinuclear [Cr(III)] or [Co(III)] complexes coordinated by two salen ligand tethered together.[3i, 3k, 5a, 37b, 39] Once again, such dinuclear catalysts showed a first order dependence in catalyst concentration, consistent with the rate determing step requiring two metals.[2b, 9, 40] Figure 3.25 illustrates the different mechanisms generally invoked for metal salen catalysts.[2a]

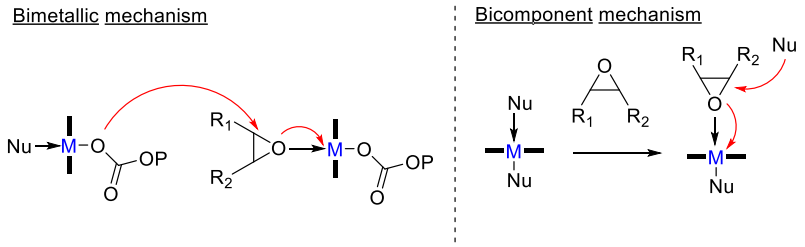

Figure 3.25 Previously reported ROCOP mechanisms.

In contrast, the indium phosphasalen catalysts have improved activity without any co-catalyst and show mononuclear structures with a first order dependence on catalyst concentration. These findings suggest a different operative mechanism and point towards a mononuclear mechanism (Figure 3.24). The mononuclear mechanism is very different to the dinuclear/bicomponent mechanisms in that the epoxide molecule is coordinated at the same indium centre and adjacent (or *cis*) to the indium carbonate (*vide supra*). It seems

unlikely that ionic mechanism/intermediates play a significant role since addition of PPN-Cl completely shuts down polymerisation catalysis favouring of cyclic carbonate formation. Ionic intermediates cannot be completely ruled out and could perhaps form by indium carbonate bond dissociation (resulting in an indium cation and carbonate anion). Nonetheless, at present there is no experimental evidence supporting indium-carbonate (or alkoxide) bond dissociation, but rather it was found that the indium carbonate intermediate is highly stable (*vide supra*). Furthermore, any anionic carbonate intermediate might be expected to result in side products from back-biting (cyclic carbonate) and decarboxylation (ether linkages) reactions and yet polymer is produced with high selectivity and with high carbonate linkage content. Another counter factual in the formation of putative ionic species is that the *in-situ* IR characterisation clearly shows metal-carbonate stretches even after coordination of a strong Lewis base such as DMAP. Therefore, it seems much more likely that a metal based coordination-insertion mechanism is operative. Although the **[LInO$_2$CO^{t}Bu·DMAP]** adduct was not isolated to establish the *cis*-coordination geometry, there is unambiguous experimental evidence supporting the change in indium-carbonate coordination mode (from κ^2 to κ^1) which would be required for the proposed catalytic cycle to occur by a cis-mononuclear mechanism.

Considering why it might be that the indium phosphasalen catalysts operate by a different mechanism, it is appropriate to consider the differences in ionic radius of the central metal. Indium is significantly larger than other metal salen catalysts (r_{ionic} (pm) In(III) = 94; Cr(III): 76, Co(III): 68 and Al(III) = 75 pm).[41] It is tentatively proposed that the larger size of indium may better accommodate *cis*-coordination of epoxide/carbonate and reduce the free energy barrier to indium-carbonate attack at the (coordinated) epoxide. Further support in favour of a *cis*-coordination-insertion mechanism is the unexpected decrease in catalytic activity when a Lewis base co-catalyst is applied. Metal salen catalysts often

show enhanced activity when used with such Lewis base co-catalysts; this was proposed to be due to trans-coordination by the base on the active metal centre, increasing the reactivity of the metal alkoxide bond.[3n, 5c] In contrast, when using indium-phosphasalen catalysts the mononuclear mechanism is inhibited by Lewis base coordination which competes with monomer coordination and hinders catalysis.

The proposed mononuclear mechanism is unexpected in the broader context of other CO_2/epoxide ROCOP catalysts. Generally, a wide range of dinuclear (or dimeric) Zn(II), Mg(II) and other transition metal complexes displayed good activity in this catalysis.[24c, 28a, 33i, 42] Kinetic and mechanistic studies support a dinuclear mechanism requiring two distinct active metal centres.[1b, 1c, 42f] Even heterogeneous metal catalysts, based on zinc glutarate or double metal cyanide surfaces, are proposed to operate by metallic cooperativity and to involve at least two metals in the active site.[43] Thus, compared to the state-of-the-art available in the literature, the current findings on indium-phosphasalen ROCOP catalysis open up new opportunities in this field of study. In particular, using a metal with significantly larger ionic radius enables access to a distinct mononuclear polymerisation pathway presents an opportunity to test other large metal centres, for example lanthanides or heavier main group elements, which so far do not have equivalent precedent in this field of catalysis.

3.8 Conclusions and outlook

3.8.1 Conclusions

The first indium catalysts for selective CO_2/CHO ROCOP are presented, with catalysts showing activity at 1 bar pressure of carbon dioxide. The phosphasalen ligand is important to performance with, an indium salen analogue producing mostly polyether. Thus, by controlling the ligand chemistry it is possible to ensure quantitative and rapid carbon dioxide insertion. The optimised catalyst, **[^{Cumyl}LInO^{t}Bu]**, yielded alternating iso-enriched polycarbonate polyols by a chain-end control mechanism. The best catalysts also produce PCHC showing monomodal molecular weight distributions with narrow dispersity. Nevertheless, the catalyst activity is lower than other metal salen analogues, but is feasible without the need for any co-catalyst or high pressure. Using the phosphasalen alkoxide complex, it was possible to isolate and structurally characterise intermediates in the catalytic cycle. Such intermediates have never been isolated and are not yet established for the analogous metal salen species. The indium carbonate intermediate, **[LInO$_2$CO^{t}Bu]**, showed a stable bidentate chelation and the coordination of a Lewis base by this species was an equilibrium process involving changes to the carbonate coordination modes. The reaction order in catalyst was first order, with the activity being independent of carbon dioxide pressure over range 1-40 bar.

Thus, various pathways for the copolymerisation can be proposed with the most likely being a monometallic mechanism which is quite different to other metal salen analogues. Given the distinct findings using the indium catalysts, this study underscores the importance of the continued exploration of different metals for the catalysis and the need for further ligand development to enhance activity. Thus, an important immediate term development is to showing increased activity at 1 bar pressure.

3.8.2 Outlook

The principal target is to enhance the catalytic activity and two general strategies are suggested (Figure 3.26):

1. Ligand Modifications:
    a. Incorporation of other sterically hindered *ortho*-phenolate substituents may help to reduce further the binding site size which may accelerate *cis*-monomer mechanisms and help to destabilise the carbonate intermediate.
    b. A more flexible ligand scaffold may be achieved by varying the diamine bridge. For example, using C_3-linkers (propylene) or the addition of heteroatoms (e.g. O or N) in the backbone. This may also constrain the active site by increasing ligand coordination number.
    c. Varying the substituents on the phosphorous may be useful to control binding site and to modulate the electronic effects on the active metal centre.
2. Changing the metal centre: gallium is smaller than indium and has never been studied for CO_2/epoxide ROCOP coordinated to phosphasalen ligand may be interesting to reduce the binding pocket. Group 3 and lanthanide ions, have similar or higher ionic radii to indium and should be considered as possible metals for *cis* mononuclear mechanims.

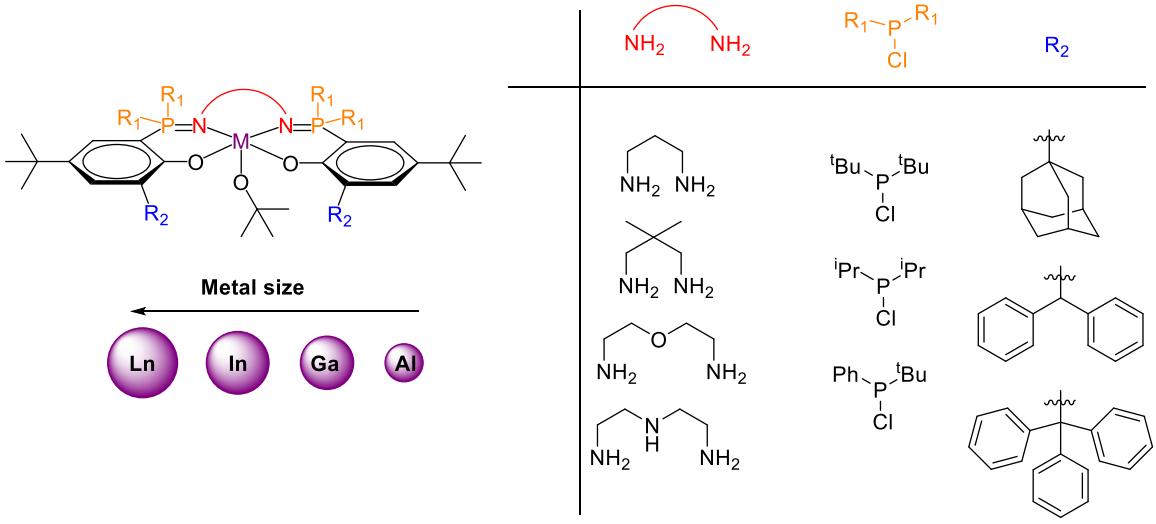

Figure 3.26. Summary of phosphasalen complexes targeted to increase activity.

These new catalysts should also be tested for ROCOP using other epoxides, especially with PO to produce PPC (polypropylene carbonate). Further increases to the ligand steric hindrance/shielding may impact the iso-selectivity and enable insight into factors controlling the stereochemistry.

In parallel, mechanistic studies must be continued to have a better understanding of:

1. Why is only PCHC afforded with phosphasalen indium complexes at 1 bar of CO_2? Could the phosphasalen ligand be implicated in CO_2 activation? The iminophosphorane (P=N) functional group is known to react with CO_2 to produce a phosphine oxide and an isocyanate under mild conditions (1 bar of CO_2).[44] Amidophosphorane frustrated Lewis pairs are also known to enable the C-O bond cleavage of CO_2.[45] An experiment to monitor the reaction between the phosphasalen ligand and CO_2 showed that CO_2 was transformed to form a phosphine oxide and an isocyanate. Further studies should be carried out to determine whether there is any such CO_2 activation by LInX (X = Cl, Br, OAc or NO_3) to investigate activation by the ligand.[46]

2. Further characterisation of the coordination of other donors (Lewis base, ions) to the metal centre, especially to the carbonate complex should be investigated. Stoichiometric reaction of LInX (X = alkoxide or carbonate) with 4-dimethylaminopyridine or bis(triphenylphosphine)iminium salt could be monitored by multinuclear NMR spectroscopy. Adducts should be isolated and crystallised to improve understanding of monomer/cocatalyst coordination modes.

3.9 References

[1] a) D. J. Darensbourg, A. D. Yeung, *Polym. Chem.* **2015**, *6*, 1103-1117; b) F. Jutz, A. Buchard, M. R. Kember, S. B. Fredriksen, C. K. Williams, *J. Am. Chem. Soc.* **2011**, *133*, 17395-17405; c) A. Buchard, F. Jutz, M. R. Kember, A. J. P. White, H. S. Rzepa, C. K. Williams, *Macromolecules* **2012**, *45*, 6781-6795.

[2] a) C. Romain, A. Thevenon, P. Saini, C. Williams, in *Carbon Dioxide and Organometallics, Vol. 53* (Ed.: X.-B. Lu), Springer International Publishing, **2016**, pp. 101-141; b) D. J. Darensbourg, *Chem. Rev.* **2007**, *107*, 2388-2410.

[3] a) Z. Q. Qin, C. M. Thomas, S. Lee, G. W. Coates, *Angew. Chem. Int. Ed.* **2003**, *42*, 5484-5487; b) C. T. Cohen, T. Chu, G. W. Coates, *J. Am. Chem. Soc.* **2005**, *127*, 10869-10878; c) C. T. Cohen, G. W. Coates, *J. Polym. Sci. Part A Polym. Chem.* **2006**, *44*, 5182-5191; d) C. T. Cohen, C. M. Thomas, K. L. Peretti, E. B. Lobkovsky, G. W. Coates, *Dalton Trans.* **2006**, 237-249; e) E. K. Noh, S. J. Na, S. Sujith, S. W. Kim, B. Y. Lee, *J. Am. Chem. Soc.* **2007**, *129*, 8082-8083; f) J. Y. Jeon, J. J. Lee, J. K. Varghese, S. J. Na, S. Sujith, M. J. Go, J. Lee, M. A. Ok, B. Y. Lee, *Dalton Trans.* **2013**, *42*, 9245-9254; g) M. Hatazawa, K. Nakabayashi, S. Ohkoshi, K. Nozaki, *Chem. Eur. J.* **2016**, *22*, 13677-13681; h) K. Nakano, M. Nakamura, K. Nozaki, *Macromolecules* **2009**, *42*, 6972-6980; i) K. Nakano, S. Hashimoto, K. Nozaki, *Chem. Sci.* **2010**, *1*, 369-373; j) X. B. Lu, L. Shi, Y. M. Wang, R. Zhang, Y. J. Zhang, X. J. Peng, Z. C. Zhang, B. Li, *J. Am. Chem. Soc.* **2006**, *128*, 1664-1674; k) Y. Liu, W. M. Ren, C. Liu, S. Fu, M. Wang, K. K. He, R. R. Li, R. Zhang, X. B. Lu, *Macromolecules* **2014**, *47*, 7775-7788; l) Y. Liu, W.-M. Ren, K.-K. He, X.-B. Lu, *Nat. Commun.* **2014**, *5*; m) W. M. Ren, G. P. Wu, F. Lin, J. Y. Jiang, C. Liu, Y. Luo, X. B. Lu, *Chem. Sci.* **2012**, *3*, 2094-2102; n) D. J.

Darensbourg, J. C. Yarbrough, *J. Am. Chem. Soc.* **2002**, *124*, 6335-6342; o) K. Nakano, T. Kamada, K. Nozaki, *Angew. Chem. Int. Ed.* **2006**, *45*, 7274-7277.

[4] a) W. M. Ren, Z. W. Liu, Y. Q. Wen, R. Zhang, X. B. Lu, *J. Am. Chem. Soc.* **2009**, *131*, 11509-11518; b) J. Liu, W. M. Ren, Y. Liu, X. B. Lu, *Macromolecules* **2013**, *46*, 1343-1349.

[5] a) S. I. Vagin, R. Reichardt, S. Klaus, B. Rieger, *J. Am. Chem. Soc.* **2010**, *132*, 14367-14369; b) R. Eberhardt, M. Allmendinger, B. Rieger, *Macrom Rapid Commun.* **2003**, *24*, 194-196; c) D. J. Darensbourg, R. M. Mackiewicz, *J. Am. Chem. Soc.* **2005**, *127*, 14026-14038; d) D. J. Darensbourg, R. M. Mackiewicz, D. R. Billodeaux, *Organometallics* **2005**, *24*, 144-148; e) D. J. Darensbourg, A. L. Phelps, *Inorg. Chem.* **2005**, *44*, 4622-4629; f) D. J. Darensbourg, *Chem Rev.* **2007**, *107*, 2388-2410; g) D. J. Darensbourg, E. B. Frantz, *Dalton Trans.* **2008**, 5031-5036; h) D. J. Darensbourg, A. I. Moncada, *Inorg. Chem.* **2008**, *47*, 10000-10008; i) D. J. Darensbourg, A. I. Moncada, W. Choi, J. H. Reibenspies, *J. Am. Chem. Soc.* **2008**, *130*, 6523-6533; j) D. J. Darensbourg, M. Ulusoy, O. Karroonnirum, R. R. Poland, J. H. Reibenspies, B. Cetinkaya, *Macromolecules* **2009**, *42*, 6992-6998; k) D. J. Darensbourg, W. C. Chung, S. J. Wilson, *ACS Catal.* **2013**, *3*, 3050-3057; l) G. P. Wu, D. J. Darensbourg, *Macromolecules* **2016**, *49*, 807-814; m) D. J. Darensbourg, R. M. Mackiewicz, A. L. Phelps, D. R. Billodeaux, *Acc. Chem. Res.* **2004**, *37*, 836-844.

[6] D. J. Darensbourg, D. R. Billodeaux, *Inorg. Chem.* **2005**, *44*, 1433-1442.

[7] a) J. E. Seong, S. J. Na, A. Cyriac, B. W. Kim, B. Y. Lee, *Macromolecules* **2010**, *43*, 903-908; b) S. Sujith, J. K. Min, J. E. Seong, S. J. Na, B. Y. Lee, *Angew. Chem. Int. Ed.* **2008**, *47*, 7306-7309.

[8] a) E. Hosseini Nejad, C. G. W. van Melis, T. J. Vermeer, C. E. Koning, R. Duchateau, *Macromolecules* **2012**, *45*, 1770-1776; b) W. Xia, K. A. Salmeia, S. I. Vagin, B. Rieger, *Chem. Eur. J.* **2015**, *21*, 4384-4390.

[9] T. Ohkawara, K. Suzuki, K. Nakano, S. Mori, K. Nozaki, *J. Am. Chem. Soc.* **2014**, *136*, 10728-10735.

[10] a) J. M. Ready, E. N. Jacobsen, *Angew. Chem. Int.Ed.* **2002**, *41*, 1374-1377; b) S. E. Schaus, B. D. Brandes, J. F. Larrow, M. Tokunaga, K. B. Hansen, A. E. Gould, M. E. Furrow, E. N. Jacobsen, *J. Am. Chem. Soc.* **2002**, *124*, 1307-1315; c) C. Mazet, E. N. Jacobsen, *Angew. Chem. Int. Ed.* **2008**, *47*, 1762-1765; d) L. P. C. Nielsen, S. J. Zuend, D. D. Ford, E. N. Jacobsen, *J. Org. Chem.* **2012**, *77*, 2486-2495; e) D. D. Ford, L. P. C. Nielsen, S. J. Zuend, C. B. Musgrave, E. N. Jacobsen, *J. Am. Chem. Soc.* **2013**, *135*, 15595-15608.

[11] a) T.-P.-A. Cao, G. Nocton, L. Ricard, X. F. Le Goff, A. Auffrant, *Angew. Chem. Int. Ed.* **2014**, *53*, 1368-1372; b) C. Bakewell, T.-P.-A. Cao, X. F. Le Goff, N. J. Long, A. Auffrant, C. K. Williams, *Organometallics* **2013**, *32*, 1475-1483.

[12] A. Thevenon, J. A. Garden, A. J. P. White, C. K. Williams, *Inorg. Chem.* **2015**, *54*, 11906-11915.

[13] a) D. Myers, Imperial College London **2017**; b) D. Myers, A. J. P. White, C. M. Forsyth, M. Bown, C. K. Williams, *Angew. Chem. Int. Ed.* **2017**, *56*, 5277-5282; c) B. M. Chamberlain, M. Cheng, D. R. Moore, T. M. Ovitt, E. B. Lobkovsky, G. W. Coates, *J. Am. Chem. Soc.* **2001**, *123*; d) A. Amgoune, C. M. Thomas, T. Roisnel, J.-F. Carpentier, *Chem. Eur. J.* **2006**, *12*, 169-179.

[14] a) C. Bakewell, A. J. P. White, N. J. Long, C. K. Williams, *Angew. Chem. Int. Ed.* **2014**, *53*, 9226-9230; b) C. Bakewell, T.-P.-A. Cao, N. Long, X. F. Le Goff, A. Auffrant, C. K. Williams, *J. Am. Chem. Soc.* **2012**, *134*, 20577-20580; c) T.-P.-A.

Cao, A. Buchard, X. F. Le Goff, A. Auffrant, C. K. Williams, *Inorg. Chem.* **2012**, *51*, 2157-2169; d) A. M. Garcia, V. Moreno, S. X. Delgado, A. E. Ramírez, L. A. Vargas, M. Á. Vicente, A. Gil, L. A. Galeano, *J. Mol. Catal. A Chem.* **2016**, *416*, 10-19.

[15] a) N. Nomura, R. Ishii, Y. Yamamoto, T. Kondo, *Chem. Eur. J.* **2007**, *13*, 4433-4451; b) A. F. Douglas, B. O. Patrick, P. Mehrkhodavandi, *Angew. Chem. Int. Ed.* **2008**, *47*, 2290-2293; c) M. Normand, V. Dorcet, E. Kirillov, J.-F. Carpentier, *Organometallics* **2013**, *32*, 1694-1709; d) S. M. Quan, P. L. Diaconescu, *Chem. Commun.* **2015**, *51*, 9643-9646.

[16] a) I. Shibata, I. Mitani, A. Imakuni, A. Baba, *Tetrahedron Lett.* **2011**, *52*, 721-723; b) P. Cocolios, R. Guilard, D. Bayeul, C. Lecomte, *Inorg. Chem.* **1985**, *24*, 2058-2062; c) J. Weidlein, *Z. Anorg. Allg. Chem.* **1970**, *378*, 245-262.

[17] A. W. Addison, T. N. Rao, J. Reedijk, J. van Rijn, G. C. Verschoor, *J. Chem. Soc., Dalton Trans.* **1984**, 1349-1356.

[18] a) D. C. Aluthge, J. M. Ahn, P. Mehrkhodavandi, *Chem. Sci.* **2015**, *6*, 5284-5292; b) D. C. Aluthge, E. X. Yan, J. M. Ahn, P. Mehrkhodavandi, *Inorg. Chem.* **2014**, *53*, 6828-6836; c) I. Yu, A. Acosta-Ramírez, P. Mehrkhodavandi, *J. Am. Chem. Soc.* **2012**, *134*, 12758-12773.

[19] W.-M. Ren, X. Zhang, Y. Liu, J.-F. Li, H. Wang, X.-B. Lu, *Macromolecules* **2010**, *43*, 1396-1402.

[20] M. H. Chisholm, Z. Zhou, *J. Am. Chem. Soc.* **2004**, *126*, 11030-11039.

[21] S. L. Hancock, M. F. Mahon, M. D. Jones, *Chem. Cent. J.* **2013**, *7*, 135.

[22] a) A. Cyriac, J. Y. Jeon, J. K. Varghese, J. H. Park, S. Y. Choi, Y. K. Chung, B. Y. Lee, *Dalton Trans.* **2012**, *41*, 1444-1447; b) S. J. Na, S. S, A. Cyriac, B. E. Kim, J.

Yoo, Y. K. Kang, S. J. Han, C. Lee, B. Y. Lee, *Inorg. Chem.* **2009**, *48*, 10455-10465.

[23] A. Cyriac, S. H. Lee, J. K. Varghese, J. H. Park, J. Y. Jeon, S. J. Kim, B. Y. Lee, *Green Chem.* **2011**, *13*, 3469-3475.

[24] a) K. Nakano, T. Hiyama, K. Nozaki, *Chem. Commun.* **2005**, 1871-1873; b) K. Nakano, K. Nozaki, T. Hiyama, *J. Am. Chem. Soc.* **2003**, *125*, 5501-5510; c) W. C. Ellis, Y. Jung, M. Mulzer, R. Di Girolamo, E. B. Lobkovsky, G. W. Coates, *Chem. Sci.* **2014**, *5*, 4004-4011.

[25] a) C. G. Jaffredo, Y. Chapurina, S. M. Guillaume, J.-F. Carpentier, *Angew. Chem. Int. Ed.* **2014**, *53*, 2687-2691; b) F. A. Bovey, *Pure Appl. Chem.* **1967**, *15*, 349-368; c) M. Sepulchre, *Makromol. Chem.* **1988**, *189*, 1117-1131.

[26] M. R. Kember, P. D. Knight, P. T. R. Reung, C. K. Williams, *Angew. Chem. Int. Ed.* **2009**, *48*, 931-933.

[27] N. Ikpo, J. C. Flogeras, F. M. Kerton, *Dalton Trans.* **2013**, *42*, 8998-9006.

[28] a) S. Kissling, M. W. Lehenmeier, P. T. Altenbuchner, A. Kronast, M. Reiter, P. Deglmann, U. B. Seemann, B. Rieger, *Chem. Commun.* **2015**, *51*, 4579-4582; b) G. W. Coates, D. R. Moore, *Angew. Chem. Int. Ed.* **2004**, *43*, 6618-6639.

[29] a) J. A. Aguilar, R. W. Adams, M. Nilsson, G. A. Morris, *J. Magn. Reson.* **2014**, *238*, 16-19; b) C. S. Johnson, *Prog. Nucl. Magn. Reson. Spectrosc.* **1999**, *34*, 203-256.

[30] Y. Zhu, C. Romain, C. K. Williams, *J. Am. Chem. Soc.* **2015**, *137*, 12179-12182.

[31] G. B. Deacon, R. J. Phillips, *Coord. Chem. Rev.* **1980**, *33*, 227-250.

[32] N. J. Brown, J. E. Harris, X. Yin, I. Silverwood, A. J. P. White, S. G. Kazarian, K. Hellgardt, M. S. P. Shaffer, C. K. Williams, *Organometallics* **2014**, *33*, 1112-1119.

[33] a) L. P. Carrodeguas, J. Gonzalez-Fabra, F. Castro-Gomez, C. Bo, A. W. Kleij, *Chem. Eur. J.* **2015**, *21*, 6115-6122; b) X. B. Lu, D. J. Darensbourg, *Chem. Soc. Rev.* **2012**, *41*, 1462-1484; c) K. Nakano, K. Kobayashi, T. Ohkawara, H. Imoto, K. Nozaki, *J. Am. Chem. Soc.* **2013**, *135*, 8456-8459; d) K. Nakano, K. Kobayashi, K. Nozaki, *J. Am. Chem. Soc.* **2011**, *133*, 10720-10723; e) A. Decortes, R. M. Haak, C. Martin, M. M. Belmonte, E. Martin, J. Benet-Buchholz, A. W. Kleij, *Macromolecules* **2015**, *48*, 8197-8207; f) H. Sugimoto, H. Ohtsuka, S. Inoue, *J. Polym. Sci. Pol. Chem.* **2005**, *43*, 4172-4186; g) H. Sugimoto, K. Kuroda, *Macromolecules* **2008**, *41*, 312-317; h) H. Zhang, B. Liu, H. Ding, J. Chen, Z. Duan, *Polymer* **2017**, *129*, 5-11; i) M. R. Kember, C. K. Williams, *J. Am. Chem. Soc.* **2012**, *134*, 15676-15679; j) B. Y. Lee, H. Y. Kwon, S. Y. Lee, S. J. Na, S.-i. Han, H. Yun, H. Lee, Y.-W. Park, *J. Am. Chem. Soc.* **2005**, *127*, 3031-3037.

[34] O. Hauenstein, M. Reiter, S. Agarwal, B. Rieger, A. Greiner, *Green Chem.* **2016**, *18*, 760-770.

[35] a) M. R. Kember, J. Copley, A. Buchard, C. K. Williams, *Polym. Chem.* **2012**, *3*, 1196-1201; b) C.-Y. Yu, H.-J. Chuang, B.-T. Ko, *Cat. Sci. Technol.* **2016**, *6*, 1779-1791.

[36] a) T. P. A. Cao, S. Labouille, A. Auffrant, Y. Jean, X. F. Le Goff, P. Le Floch, *Dalton Trans.* **2011**, *40*, 10029-10037; b) D. Bézier, O. Daugulis, M. Brookhart, *Organometallics* **2017**, *36*, 2947-2951.

[37] a) Y. Liu, W.-M. Ren, W.-P. Zhang, R.-R. Zhao, X.-B. Lu, *Nat. Commun.* **2015**, *6*; b) Y. Liu, W.-M. Ren, J. Liu, X.-B. Lu, *Angew. Chem. Int. Ed.* **2013**, *52*, 11594-11598; c) K. Nozaki, K. Nakano, T. Hiyama, *J. Am. Chem. Soc.* **1999**, *121*, 11008-11009.

[38] a) X. B. Lu, W. M. Ren, G. P. Wu, *Acc. Chem. Res.* **2012**, *45*, 1721-1735; b) G. A. Luinstra, G. R. Haas, F. Molnar, V. Bernhart, R. Eberhardt, B. Rieger, *Chem. Eur. J.* **2005**, *11*, 6298-6314.

[39] a) Y. Liu, M. Wang, W. M. Ren, Y. C. Xu, X. B. Lu, *Angew. Chem. Int. Ed.* **2015**, *54*, 7042-7046; b) Y. Liu, W. M. Ren, W. P. Zhang, R. R. Zhao, X. B. Lu, *Nat. Commun.* **2015**, *6*, 8.

[40] a) K. B. Hansen, J. L. Leighton, E. N. Jacobsen, *J. Am. Chem. Soc.* **1996**, *118*, 10924-10925; b) E. N. Jacobsen, *Acc. Chem. Res.* **2000**, *33*, 421-431.

[41] R. Shannon, *Acta Crystallogr. A* **1976**, *32*, 751-767.

[42] a) M. W. Lehenmeier, S. Kissling, P. T. Altenbuchner, C. Bruckmeier, P. Deglmann, A. K. Brym, B. Rieger, *Angew Chem Int Ed* **2013**, *52*, 9821-9826; b) J. A. Garden, P. K. Saini, C. K. Williams, *J. Am. Chem. Soc.* **2015**, *137*, 15078-15081; c) A. M. Chapman, C. Keyworth, M. R. Kember, A. J. J. Lennox, C. K. Williams, *ACS Catal.* **2015**, *5*, 1581-1588; d) M. R. Kember, F. Jutz, A. Buchard, A. J. P. White, C. K. Williams, *Chem. Sci.* **2012**, *3*, 1245-1255; e) T. Bok, H. Yun, B. Y. Lee, *Inorg. Chem.* **2006**, *45*, 4228-4237; f) D. R. Moore, M. Cheng, E. B. Lobkovsky, G. W. Coates, *J. Am. Chem. Soc.* **2003**, *125*, 11911-11924; g) Y. L. Xiao, Z. Wang, K. L. Ding, *Chem Eur. J.* **2005**, *11*, 3668-3678; h) Y. L. Xiao, Z. Wang, K. L. Ding, *Macromolecules* **2006**, *39*, 128-137.

[43] a) J. Marbach, B. Nornberg, A. F. Rahlf, G. A. Luinstra, *Cat. Sci. Technol.* **2017**, *7*, 2897-2905; b) M. Ree, J. Y. Bae, J. H. Jung, T. J. Shin, *J. Polym Sci. Part A Polym. Chem.* **1999**, *37*, 1863-1876; c) I. Kim, M. J. Yi, K. J. Lee, D. W. Park, B. U. Kim, C. S. Ha, *Cat. Today* **2006**, *111*, 292-296.

[44] a) M. A. P. Molina, A. Arques, *Synthesis* **1982**, *7*, 596-597; b) W. S. Wadsworth, in *Organic Reactions*, John Wiley & Sons, Inc., **2004**.

[45] a) K. An, J. Zhu, *Organometallics* **2014**, *33*, 7141-7146; b) L. J. Hounjet, C. B. Caputo, D. W. Stephan, *Angew. Chem. Int. Ed.* **2012**, *51*, 4714-4717.

[46] a) T. J. Schmeier, N. Hazari, C. D. Incarvito, J. A. Raskatov, *Chem. Commun.* **2011**, *47*, 1824-1826; b) T. J. Schmeier, G. E. Dobereiner, R. H. Crabtree, N. Hazari, *J. Am. Chem. Soc.* **2011**, *133*, 9274-9277.

CHAPTER 4

Di-zinc Lactide Polymerisation Catalysts: Hyper-Activity by Control of Ligand Conformation and Metallic Cooperativity

Abstract

Understanding how to moderate and improve catalytic activity is critical to improving degradable polymer production. In this chapter, mono and di-zinc catalysts, coordinated by bis(imino)diphenylamido ligands, are described. They show high activities and allow determination of the catalyst structural features controlling performance. In most cases, the di-zinc catalysts significantly out-perform the mono-zinc analogues. Further, for the best di-zinc catalyst, the ligand conformation controls activity: the catalyst with "folded" ligand conformations show TOF values up to 60,000 h^{-1} (0.1 mol% loading, 25 ^{o}C, [LA] = 1 M), whilst that with a "planar" conformation is much slower, under similar conditions (TOF = 30 h^{-1}). Di-zinc catalysts also perform very well under immortal conditions, showing improved control, and are able to tolerate loadings as low as 0.002 mol% whilst conserving high activity (TOF = 12 500 h^{-1}).

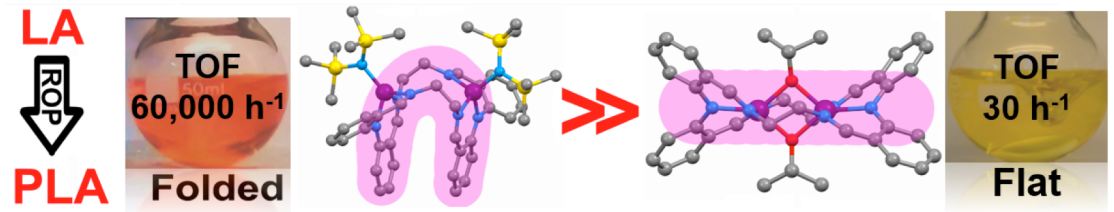

4.1 Introduction

The ring-opening polymerisation of lactide (LA) is important for production of biodegradable and renewably resourced polylactide (PLA), a material applied in both commodity and medical areas.[1] To date, the industrial production of PLA is mainly catalysed by **[Sn(II)-octanoate]** in presence of alcohol sources (Figure 4.1, **D**). Although, this tin catalyst has been approved by the food and drug administration in some countries, there remains concern about the potential hazards associated with residual tin in the resulting polymers, especially for biomedical application.[1e] In addition, there are also issues with the cost of tin waste remediation during manufacture.[1e] There is, therefore, a need to develop new robust and lower toxicity catalysts for this polymerisation. Zinc homogeneous complexes, coordinated by electron-donating ligands, such as β-diiminate (BDI) (Figure 4.1, **A**),[2] bis(amino)phenolates (Figure 4.1, **B**)[3] or pyrazolyol borates[4] are among the most active catalyst reported to date. Zinc(II) is an attractive choice of metal ion for such catalysts as it is cheap and combines high activity and selectivity with a lack of colour and redox chemistry.[5] A **[{bis(morpholinomethyl)phenoxyZnEt}$_2$]** dimer (Figure 4.1, **C**), reported by Carpentier *et al.*, showed high activity at low catalyst loading (TOF = 3200 h^{-1}, [cat] = 0.002 mol%), and is currently the most active zinc catalyst in the field.[6] One question, dominating these previous catalysts, is whether two metals in close proximity are required for high activity and low loadings.

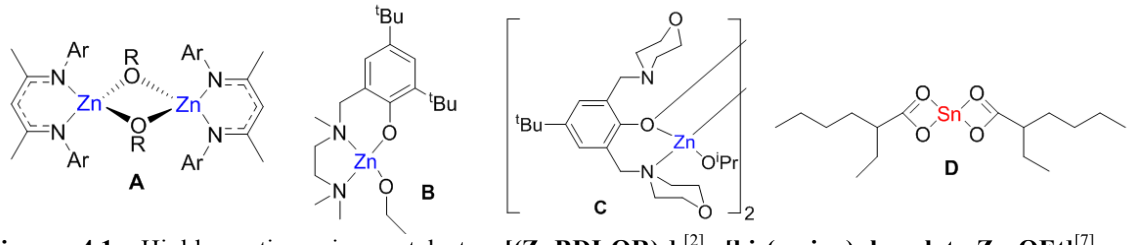

Figure 4.1. Highly active zinc catalysts: **[(ZnBDI-OR)$_2$]**,[2] **[bis(amino)phenolatesZn-OEt]**[7] and **[{bis(morpholinomethyl)phenoxyZnEt}$_2$]**[6a] denoted **A**, **B** and **C**, respectively. The activity of the series of catalyst reported in the chapter will be compared with Sn(Oct)$_2$, complex **D**.

Bimetallic homogeneous catalysts are generally interesting in catalysis as they can show higher activities and greater selectivity. Most explanations of observed enhanced performance propose a synergistic cooperation between the two metal ions.[8] This concept is also reminiscent of the mode of action of many multimetallic metalloenzymes.[9] Enzymes also moderate activity by adopting particular protein or ligand 'conformations', but the application of this concept to synthetic catalysts is less well developed.[10] Pioneering studies of bimetallic group IV catalysts for olefin polymerisations, by Marks and later others, have demonstrated much better activities, selectivities and control than for mononuclear analogues.[11] Bimetallic catalysts have also shown enhanced performances in the ring-opening polymerisation (ROP) of lactones.[12] Despite these observations, the exact nature of this cooperativity in these two fields of polymerisation catalysis is less clear. In contrast, in the area of CO_2/epoxide ROCOP the dinuclear mechanism is now widely suggested and provides a rationale for dinuclear catalyst selection.[13] There is, therefore, a need to understand the factors governing the synergic effect that two metal centers may exert in lactone ROP.

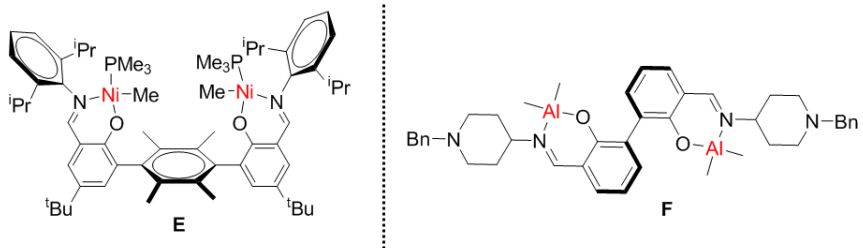

Figure 4.2. Two examples of dinuclear catalysts reported to show cooperativity. The LHS catalyst is a olefin polymerisation catalyst (**E**), reported by Agapie *et al.*[8e] and the RHS is a lactide ROP catalyst (**F**), reported by Carpentier *et al.*[12c]

Our research group recently reported a di-zinc bis(ethyl) complex coordinated by a bis(imino)diphenyl amido macrocycle, [$\mathbf{L^{Et}Zn_2Et_2}$], as a moderate *rac*-LA ROP catalyst.[14] The catalytic activity was inhibited by the low reactivity of the [Zn-Et] bonds towards alcohol, a reaction that generates the active dizinc-bis(alkoxide) initiator, [$\mathbf{L^{Et}Zn_2(O^iPr)_2}$] (Scheme 4.1). In attempts to overcome this limitation, the amido

derivative was targeted. [Zn-amido] complexes are known to react quickly with alcohol sources to generate [Zn-alkoxides].[15]

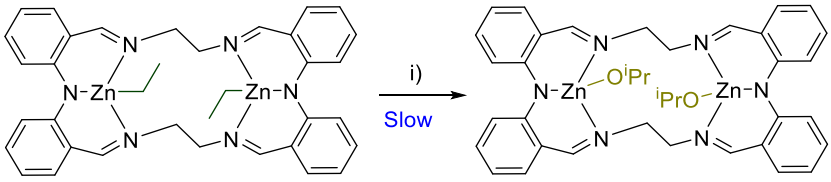

[L^{Et}Zn$_2$Et$_2$] **[L^{Et}Zn$_2$(O^{i}Pr)$_2$]**

Scheme 4.1. Illustration of the reactivity of the previously reported **[L^{Et}Zn$_2$Et$_2$]** with isopropanol to form **[L^{Et}Zn$_2$(O^{i}Pr)$_2$]**. i) 2 equiv HO^{i}Pr, THF, 25 ^{o}C.

4.2 Zinc Amido Catalysts

The previously reported $\mathbf{H_2L^{Et}}$ and $\mathbf{H_2L^{Pr}}$ macrocycles* are used as ligand for the synthesis of dinuclear zinc complexes (Scheme 2.2, a).[16] The macrocycles differ in size which allows the investigation of the influence of intermetallic separation on catalytic activity. An "open" ligand $\mathbf{HL^{Open}}$ (Scheme 1, b) was also synthesised, via the amination of diphenylamine-2,2'-dicarboxaldehyde with two equivalents of isobutylamine. The "open" ligand was necessary to prepare a mono-zinc complex with a similar coordination mode to the dinuclear catalysts. The mono-zinc complex will be useful to investigate the influence (if any) of the macrocyle coordination environment and the difference between one or two metal centres on catalytic performance.

4.2.1 Synthesis of $[L^yZn_2\{N(SiMe_3)_2\}_2]$ (y = Et, Pr) and $[L^{Open}ZnN(SiMe_3)_2]$

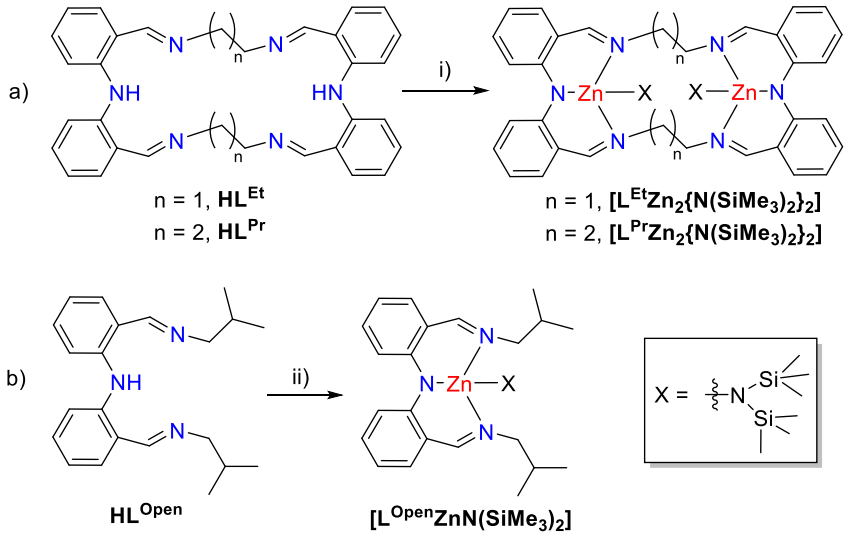

Scheme 2.2. Synthetic route to: a) $\mathbf{[L^yZn_2\{N(SiMe_3)_2\}_2]}$ (y = Et, Pr); b) $\mathbf{[L^{Open}ZnN(SiMe_3)_2]}$. Reagents and conditions: i) $\mathbf{[Zn\{N(SiMe_3)_2\}_2]}$ (2 equiv.), THF, 25 °C, for 48 h and 50 °C, for 4 h (86 % and 78 %, respectively); ii) $\mathbf{[Zn\{N(SiMe_3)_2\}_2]}$ (1 equiv.), THF, 25 °C, for 48 h, and 50 °C, for 4h (72 %).

$\mathbf{[L^yZn_2\{N(SiMe_3)_2\}_2]}$ (y = Et, Pr) and $\mathbf{[L^{Open}ZnN(SiMe_3)_2]}$ were synthesised by the reaction of $[Zn\{N(SiMe_3)_2\}_2]$ with the corresponding ligands (Scheme 2.2). Complexation reactions were monitored by ^{1}H NMR spectroscopy, in d_8-THF at 298 K, by following the

* All ligands were synthesised, isolated and purified by Hannah Davidson and Michael Bennington working with Prof Sally Brooker at the University of Otago (New Zealand).

disappearance of the NH signal at ~ 11.5 ppm of the protonated ligand and the appearance of resonances corresponding to amido ligand between -0.1 ppm and -0.2 ppm (one resonance for the mononuclear complex and two resonances for the dinuclear complexes). The three complexes were isolated as red/orange powders in high yields (< 70 %) and fully characterised by X-ray diffraction and multinuclear NMR experiments.

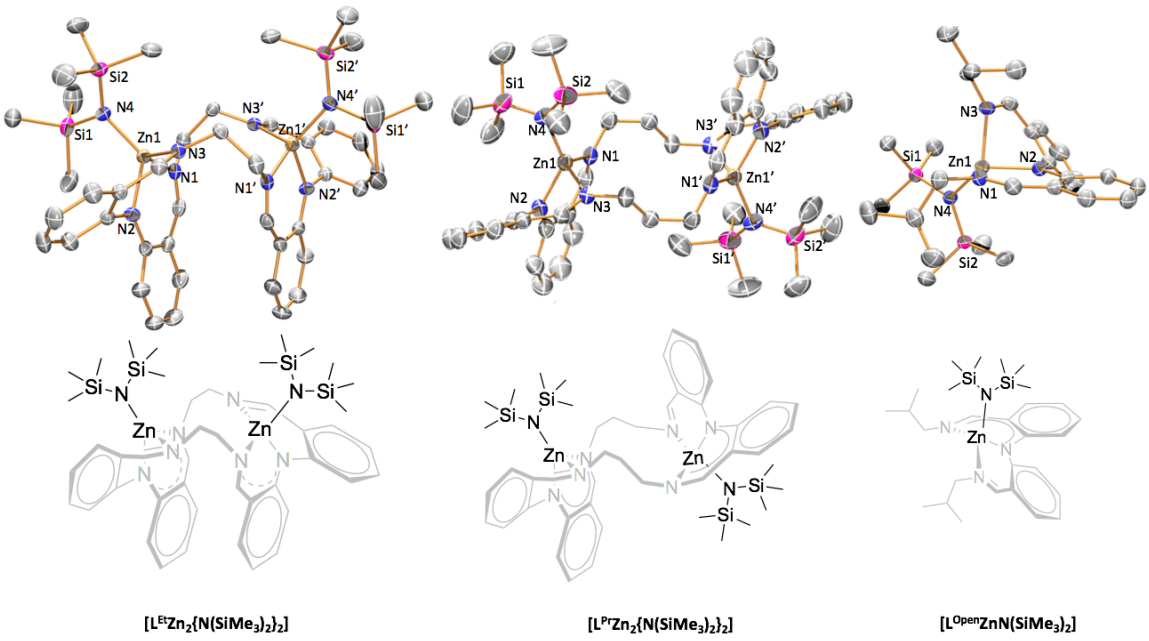

Figure 4.3. Molecular structures of **[L^{y}Zn$_2${N(SiMe$_3$)$_2$}$_2$]** (y = Et, Pr)[†] and **[L^{Open}ZnN(SiMe$_3$)$_2$]** with thermal ellipsoids at the 50 % probability level. A THF molecule for **[L^{Et}Zn$_2${N(SiMe$_3$)$_2$}$_2$]**, a hexane molecule and a second crystallographically independent molecule of **[L^{Pr}Zn$_2${N(SiMe$_3$)$_2$}$_2$]** and hydrogen atoms omitted for clarity (refer to the appendix for complete data set).

Table 4.1. Selected bond lengths (Å) for **[L^{y}Zn$_2${N(SiMe$_3$)$_2$}$_2$]** (y = Et, Pr), **[L^{Open}ZnN(SiMe$_3$)$_2$]**, and compared with the previously reported **[L^{Et}Zn$_2$Et$_2$]**[14].

Bond \ Complex	**[L^{Et}Zn$_2${N(SiMe$_3$)$_2$}$_2$]**	**[L^{Pr}Zn$_2${N(SiMe$_3$)$_2$}$_2$]**	**[L^{Open}ZnN(SiMe$_3$)$_2$]**	**[L^{Et}Zn$_2$Et$_2$]**[14]
Zn1-N1	2.018(2) Å	2.020(2) Å	2.009(1) Å	2.022(2) Å
Zn1-N2	**1.979(2) Å**	**1.983(2) Å**	**1.983(1) Å**	**2.005(2) Å**
Zn1-N3	2.102(2) Å	2.092(2) Å	2.124(1) Å	2.119(2) Å
Zn1-N4	1.941(2) Å	1.933(3) Å	1.941(1) Å	-
Zn1-Zn2	4.870(5) Å	6.217(6) Å	-	5.027(4) Å

In all cases, the zinc metal centre has a tetrahedral geometry (τ_4' = 0.79 for **1** and τ_4' = 0.84 for **2** and **3**).[17] **[L^{Et}Zn$_2${N(SiMe$_3$)$_2$}$_2$]** has C_2 symmetry and **[L^{Pr}Zn$_2${N(SiMe$_3$)$_2$}$_2$]** has C_i symmetry. The four Zn-N bond lengths are similar in the three structures. Compared

[†] Both structures were obtained by Dr Charles Romain

to the corresponding **[L^{Et}Zn$_2$Et$_2$]**, previously reported, the series have shorted Zn-N2 bond distances.[14] The distance between the two zinc centres is 4.870(5) Å in **[L^{Et}Zn$_2${N(SiMe$_3$)$_2$}$_2$]** which is smaller than in **[L^{Et}Zn$_2$Et$_2$]** [5.027(4) Å] and in **[L^{Pr}Zn$_2${N(SiMe$_3$)$_2$}$_2$]** [6.217(6) Å]. ^{1}H NMR spectra of the three complexes show that ligand resonances are shifted upfield compared to free ligand. Diasterotopic signals, assigned to the ethylene or the propylene backbone protons and the 2-dimethyl groups, are consistent with metal coordination. Whilst the ^{1}H NMR spectrum of **[L^{Pr}Zn$_2${N(SiMe$_3$)$_2$}$_2$]** (in d_8-THF) and **[L^{Open}ZnN(SiMe$_3$)$_2$]** (in C_6D_6), show sharp signals, at 298 K, the spectrum of **[L^{Et}Zn$_2${N(SiMe$_3$)$_2$}$_2$]** (in d_8-THF) shows much broader resonances. Variable temperature NMR spectroscopy of **[L^{Et}Zn$_2${N(SiMe$_3$)$_2$}$_2$]** showed the appearance of sharp signals at 193 K, indicating that several conformers are likely in equilibrium at room temperature (further described in the section 4.5.2). ^{1}H NMR spectra of **[L^{Et}Zn$_2${N(SiMe$_3$)$_2$}$_2$]** and **[L^{Pr}Zn$_2${N(SiMe$_3$)$_2$}$_2$]** also suggest that their solid state symmetry are retained in solution (i.e. C_2 and C_i respectively). On the other hand, the ^{1}H NMR spectrum of **[L^{Open}ZnN(SiMe$_3$)$_2$]** (in C_6D_6) indicates C_2 symmetry.

4.2.2 Polymerisation Studies with Zinc Amido Catalysts

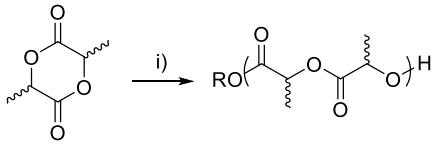

Scheme 4.3. Polymerisation of *rac*-lactide (*rac*-LA). i) **[L^{Et}Zn$_2${N(SiMe$_3$)$_2$}$_2$]** or **[L^{Pr}Zn$_2${N(SiMe$_3$)$_2$}$_2$]** or **[L^{Open}Zn N(SiMe$_3$)$_2$]** = 0.1 mol%, [*rac*-LA] = 1M, in THF, 25 ^{o}C.

The three zinc amido complexes (**[L^{Et}Zn$_2${N(SiMe$_3$)$_2$}$_2$]**, **[L^{Pr}Zn$_2${N(SiMe$_3$)$_2$}$_2$]** and **[L^{Open}ZnN(SiMe$_3$)$_2$]**) were applied as catalyst for the ROP of *rac*-LA. All of them are efficient catalysts showing high activities but **[L^{Et}Zn$_2${N(SiMe$_3$)$_2$}$_2$]** and **[L^{Pr}Zn$_2${N(SiMe$_3$)$_2$}$_2$]** are particularly notable. The di-zinc complexes polymerise 1000 equiv. of monomer within one minute, at 25 ^{o}C, without any addition of alcohol (Table

4.2). It is notable that catalyst **[$L^{Et}Zn_2\{N(SiMe_3)_2\}_2$]** is 600 times more active than the zinc-bis(ethyl) homologue, **[$L^{Et}Zn_2Et_2$]**.[14] The two di-zinc catalysts show the highest activities yet reported in the literature.[1d] The activity per zinc centre (i.e. corrected for the differing complex nuclearity) of di-zinc **2** is three times greater than that of mono-zinc **3**, providing some evidence for dinuclear cooperativity.

Table 4.2. *Rac*-LA polymerisation using zinc amido catalysts and compared to the previously reported zinc ethyl catalyst (**[$L^{Et}Zn_2Et_2$]**)

Catalyst (mol %)	**Time** (sec)	**Conv.**[a] (%)	$M_{n(cld)}$[b] (Kg/mol)	$M_{n(exp)}$ (Kg/mol)[c]	**Đ**[c]	**TOF**[d] (h^{-1})
[$L^{Et}Zn_2\{N(SiMe_3)_2\}_2$] (0.1)	53	60	43	316	1.40	20,300
[$L^{Pr}Zn_2\{N(SiMe_3)_2\}_2$] (0.1)	30	73	57	135	1.03	45,000
[$L^{Open}ZnN(SiMe_3)_2$] (0.1)	140	56	40	144	1.03	14,300
[$L^{Et}Zn_2Et_2$] (0.5)[14]	4800	78	11	9.6	1.10	120

Polymerisation conditions: [*rac*-LA] = 1 M in THF, at 25 °C. [a]Determined by integration of the methine region of the ^{1}H NMR spectrum, in $CDCl_3$, at 298 K (*rac*-LA, 4.96 – 5.04 ppm; PLA, 5.10 – 5.22 ppm). [b]Molecular weight calculated using $M_{n(cld)}$ = conversion × $[rac\text{-LA}]_0$ / [number of metal centre] × M_{LA}. [c]Experimental molecular weight and Đ determined by SEC vs polystyrene standards and corrected by a factor of 0.58, at 40 °C.[18] [b]TOF = (number of moles of epoxide consumed per mole of catalyst)/time (h).

The PLA had molecular masses that increased linearly with conversion and dispersities remained narrow throughout the reaction. Nonetheless, the molar mass values were higher than expected (Figure 4.4, RHS). MALDI-ToF analyses of the PLA shows two series of peaks: linear (end-capped by amide) and cyclic PLA, with evidence of transesterification occurring. Other metal amido catalysts have been shown to exhibit reduced control and related behaviours.[19] This is typically attributed to relatively slow initiation compared to propagation leading to PLA with higher than expected molecular weight. It is also worth noting that all PLA sample were atactic.

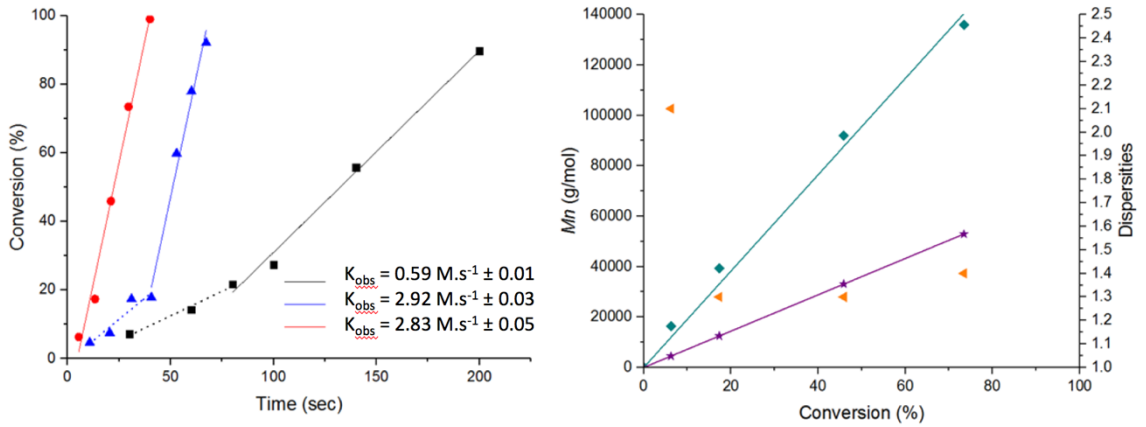

Figure 4.4. LHS: plot of *rac*-LA conversion (%) vs time (sec), using **[L^{Et}Zn$_2${N(SiMe$_3$)$_2$}$_2$]** (▲), **[L^{Pr}Zn$_2${N(SiMe$_3$)$_2$}$_2$]** (●) and **[L^{Open}ZnN(SiMe$_3$)$_2$]** (■) (1000 equivalents of *rac*-LA in THF, 25 °C, [*rac*-LA] = 1 M). Dots line represents the induction periods. RHS: plot of $M_{n(cld)}$ (g/mol) vs conversion (%) (★), $M_{n(exp)}$ (g/mol) vs conversion (%) (◆) and dispersities vs conversion (◄) for **[L^{Open}ZnN(SiMe$_3$)$_2$]** under similar conditions.

To have a better understanding of the system, kinetics studies were performed on the three catalysts (Figure 4.4, LHS). They revealed an unexpected zero-order rate dependence on *rac*-LA (monomer) concentration. An induction period, typical of metal amido initiators, was also observed for complexes **[L^{Et}Zn$_2${N(SiMe$_3$)$_2$}$_2$]** and **[L^{Open}ZnN(SiMe$_3$)$_2$]** until 15-20 % of conversion.[20] After the initiation period, however, both catalysts showed clear linear fits to conversion vs. time plots. Such rate independence in monomer concentration is very unusual in ROP,[20] however Tolman and co-workers did observe the same behaviour using Al-catalysts.[20c] They invoked a Michaelis-Menten model whereby the zeroth order arises to the pre-equilibrium constant for reversible lactone binding to the metal (Scheme 4.4). Monomer saturation kinetics are obtained if K_M << [monomer] (where K_M is the Michaelis constant related to this fast pre-equilibrium; refer to the methodology chapter for more details). The model does not imply a different operative mechanism to the well-known coordination-insertion process, but rather reflects a different rate determining step. In the present case, the relatively slow monomer saturation kinetics are rationalised by the steric hindrance of the amido ligand and by the very high absolute rates of propagation exhibited subsequently (Scheme 4.4). Indeed, it is notable that within a minute complete monomer conversion occurs.

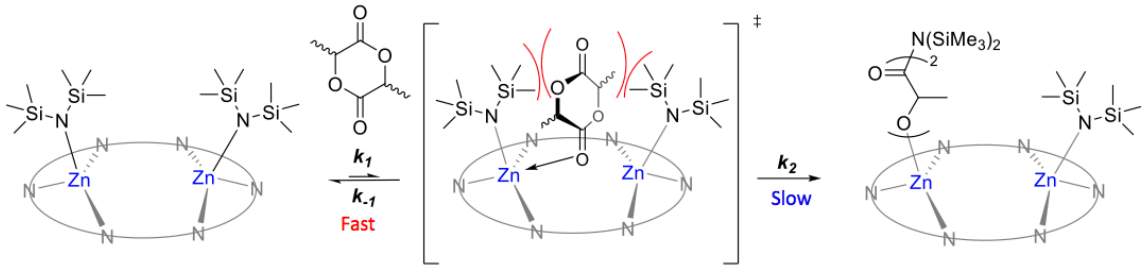

Scheme 4.4. Illustration of the Michaelis-Menton mechanistic model representing the slow pre-equilibrium of the monomer coordination, due to the amido steric hindrance (r.d.s), followed by fast initiation/propagation steps. The equation correspond to the rate of the polymerisation and highlight the special case where the overall rate is independent of the monomer concentration.

The high molecular weight obtained is therefore rationalised by only partial activation of the catalyst, due to relatively slower monomer coordination and the fast propagation. The true amount of active catalyst can be determined by comparing the experimental and calculated values of molecular weight (Equation 1-3):

Step 1: From the $M_{n(\text{exp})}$ obtained by SEC, the degree of polymerisation ($\overline{DP}$) is determined from:

$$M_{n(exp)} = \frac{Conversion \times MW_{(LA)} \times \overline{DP}}{N} \rightarrow \overline{DP} = \frac{N \times M_{n(\text{exp})}}{Conversion \times MW_{(LA)}}$$

With $M_{n(exp)}$: absolute M_n of the polymer determined by SEC with correction factor; conversion = $\frac{[LA]_t}{[LA]_o}$, determined by ^1H NMR spectroscopy; $MW_{(LA)}$ = 144.1 g/mol; N = number of initiating groups; $\overline{DP}$ = degree of polymerisation.

$\overline{DP}$ for **[L^{Et}Zn$_2${N(SiMe$_3$)$_2$}$_2$]** = 7315

$\overline{DP}$ for **[L^{Pr}Zn$_2${N(SiMe$_3$)$_2$}$_2$]** = 2568

$\overline{DP}$ for **[L^{Open}ZnN(SiMe$_3$)$_2$]** = 1736

Step 2: The amount of active catalyst is then determined from:

$$n_{LA} = n_{cat} \times \overline{DP} \rightarrow n_{cat} = \frac{n_{LA}}{\overline{DP}}$$

n_{LA} = mmol of rac-LA used; n_{cat} = mmol of active catalyst; $\overline{DP}$ = degree of polymerisation calculated previously.

$$n_{cat} = 7.2 \times 10^{-4}\ mmol\ \textbf{[L}^{\textbf{Et}}\textbf{Zn}_2\textbf{\{N(SiMe}_3\textbf{)}_2\textbf{\}}_2\textbf{]}$$

$$n_{cat} = 2.0 \times 10^{-3}\ mmol\ \textbf{[L}^{\textbf{Pr}}\textbf{Zn}_2\textbf{\{N(SiMe}_3\textbf{)}_2\textbf{\}}_2\textbf{]}$$

$$n_{cat} = 5.1 \times 10^{-4}\ mmol\ \textbf{[L}^{\textbf{Open}}\textbf{ZnN(SiMe}_3\textbf{)}_2\textbf{]}$$

Step 3: The percentage of active catalyst is determined from:

$$\%_{active\ cat} = \frac{n_{cat}}{n_{cat0}}$$

$\%_{active\ cat}$ = *percentage of active catalyst;* n_{cat} = *mmol of active catalyst;* n_{cat0} = *mmol of catalyst added.*

$\%_{active\ cat}$ **= 14 %** for **[L^{Et}Zn$_2${N(SiMe$_3$)$_2$}$_2$]**

$\%_{active\ cat}$ **= 40 %** for **[L^{Pr}Zn$_2${N(SiMe$_3$)$_2$}$_2$]**

$\%_{active\ cat}$ **= 64 %** for **[L^{Open}ZnN(SiMe$_3$)$_2$]**

Taking into account the true quantity of active catalyst, **[L^{Et}Zn$_2${N(SiMe$_3$)$_2$}$_2$]** is 1.5 times faster than **[L^{Pr}Zn$_2${N(SiMe$_3$)$_2$}$_2$]** and 6 times more active than mono-zinc **[L^{Open}ZnN(SiMe$_3$)$_2$]**. The zinc centres are closer together in **[L^{Et}Zn$_2${N(SiMe$_3$)$_2$}$_2$]** than in **[L^{Pr}Zn$_2${N(SiMe$_3$)$_2$}$_2$]** suggesting that more efficient intermetallic cooperation may contribute to its higher activity (*vide infra*). The real nature of the cooperativity is still unclear but these results suggest that there is dependence between the metal-metal distance and the cooperativity effect.

4.3 Zinc Alkoxide Catalysts

4.3.1 Synthesis of $[L^{y}Zn_2(O^{i}Pr)_2]$ (y = Et, Pr) and $[L^{Open}Zn(O^{i}Pr)]$

The amido catalysts gave high activities but suffered from a lack of control so the alkoxide derivatives were investigated to overcome these problems. In this study, the alkoxide catalysts were not isolated but generated *in-situ* before polymerisation (Scheme 4.5). Zinc amido complexes were allowed to react with isopropanol (one equiv. for $[L^{Open}ZnN(SiMe_3)_2]$ and two equiv. for $[L^{Et}Zn_2\{N(SiMe_3)_2\}_2]$ and $[L^{Pr}Zn_2\{N(SiMe_3)_2\}_2]$) for 30 minutes before the start of the polymerisation. To ensure that the alkoxide complexes were cleanly formed within this time, NMR scale experiments were also performed, in d_8-THF, at 25 °C.

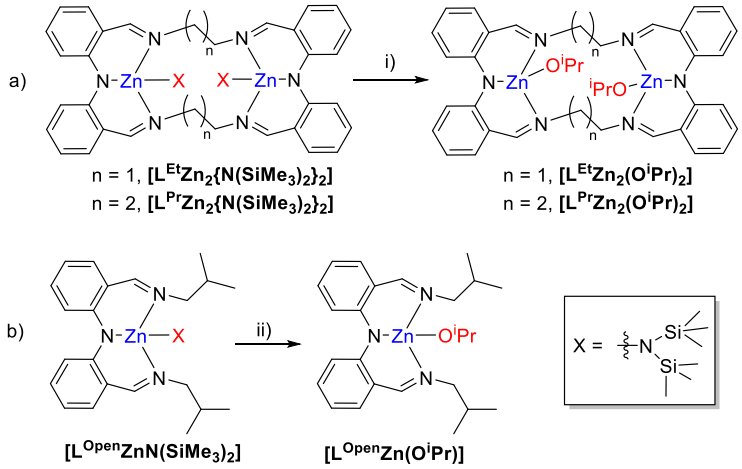

Scheme 4.5. Synthetic route to a) $[L^{y}Zn_2(O^{i}Pr)_2]$ (y = Et, Pr); b) $[L^{Open}Zn(O^{i}Pr)]$. Reagents and conditions: i) $HO^{i}Pr$ (2 equiv.), d_8-THF, 25 °C, 5 min; ii) $HO^{i}Pr$ (1 equiv.), THF, 25 °C, 5 min.

Addition of one equivalent of isopropanol (IPA) per metal centre to $[L^{Et}Zn_2\{N(SiMe_3)_2\}_2]$, $[L^{Pr}Zn_2\{N(SiMe_3)_2\}_2]$ or $[L^{Open}ZnN(SiMe_3)_2]$, in THF, changed the complexes' colour from red/orange to yellow within five minutes. The ^{1}H NMR spectra (d_8-THF) after the addition of IPA, show no remaining amido group resonances and confirmed the instantaneous formation of the corresponding alkoxides (3.85-3.78 ppm and 0.61 ppm for $[L^{Et}Zn_2(O^{i}Pr)_2]$, 3.82-3.62 ppm and 0.63 ppm for $[L^{Pr}Zn_2(O^{i}Pr)_2]$ and 3.83 ppm and 0.93 ppm for $[L^{Open}Zn(O^{i}Pr)]$) (Figure 4.5). $[L^{Et}Zn_2(O^{i}Pr)_2]$ has previously been isolated and

fully characterised.[14] Its molecular structure shows a D_2 symmetry with two trigonal-bipyramidal zinc centres and two bridging isopropoxide group (refer to the section 4.5.2). Generally, zinc-alkoxide complexes can show a tendency to aggregate,[3] so DOSY NMR analysis of **[L^{Open}Zn(O^{i}Pr)]** was performed (in d_8-THF, at 298 K) and it confirmed that **[L^{Open}Zn(O^{i}Pr)]** was monomeric under conditions related to those used in catalysis. All the alkoxide complexes were stable over the time period of polymerisation (~ 1 h).

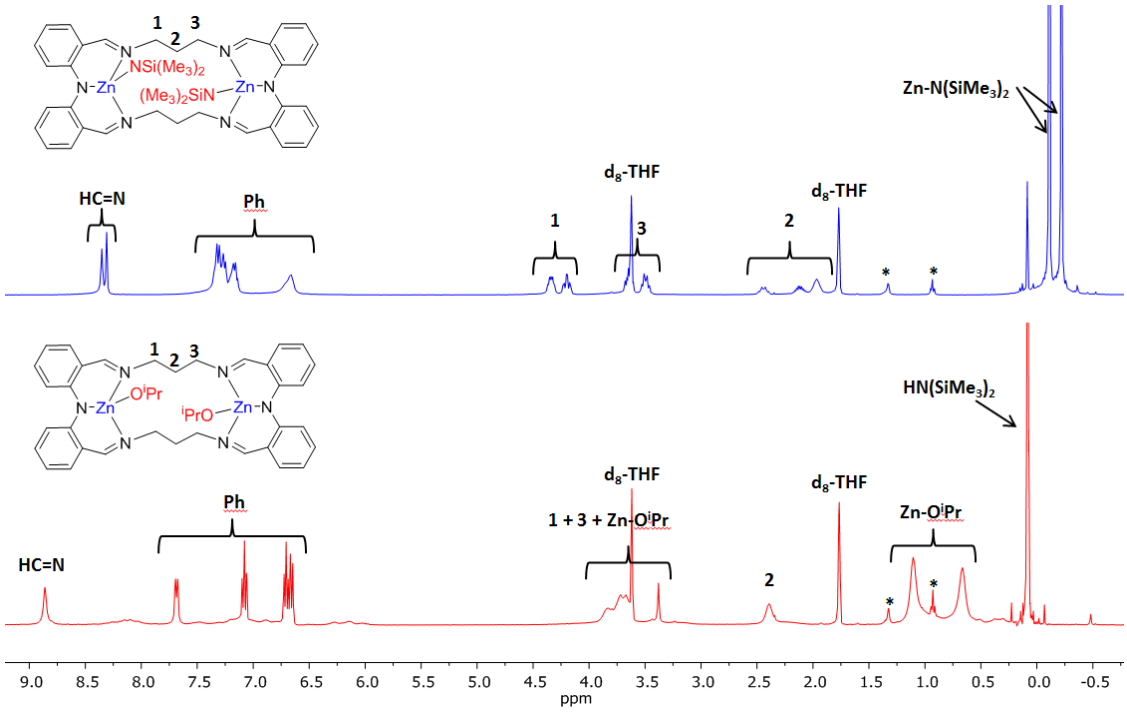

Figure 4.5. ^{1}H NMR spectra, in d_8-THF, at 298 K, of **[L^{Pr}Zn$_2${N(SiMe$_3$)$_2$}$_2$]** (top) before and after the addition of 2 equiv. of isopropanol (bottom) showing the clean formation of **[L^{Pr}Zn$_2$(O^{i}Pr)$_2$]**; *trace of hexane.

4.3.2 Polymerisation Studies with Zinc Alkoxide Catalysts

The alkoxide complexes were tested under similar conditions as for the corresponding amido complexes in catalysis. **[L^{Pr}Zn$_2$(O^{i}Pr)$_2$]** and **[L^{Open}Zn(O^{i}Pr)]** remained very active and were able to polymerise 1000 equiv. of *rac*-LA in less than two minutes (Table 4.3). **[L^{Pr}Zn$_2$(O^{i}Pr)$_2$]** and **[L^{Open}Zn(O^{i}Pr)]** are also more active than other known zinc catalysts, and shows k_{obs} almost an order of magnitude higher than the best zinc catalyst reported in the literature (Table 4.3, catalyst **A** and **B**) under similar reaction conditions.[3] Surprisingly, **[L^{Et}Zn$_2$(O^{i}Pr)$_2$]** is more than 5000 times slower than **[L^{Et}Zn$_2${N(SiMe$_3$)$_2$}$_2$]**

and only 50 % conversion was achieved after 8 h. The activity of **[L^{Et}Zn$_2$(O^{i}Pr)$_2$]** is in the same order of magnitude as **[L^{Et}Zn$_2$Et$_2$]** (in presence of alcohol) which is consistent with previous work.[14] Nonetheless, the question arises as to why the analogous amido complex is apparently so much more active?

Table 4.3. *Rac*-LA polymerisation using zinc alkoxide catalysts and compared to the previously reported **[BDIZn(O^{i}Pr)]** (**A**) and **[bis(amino)phenolatesZnEt]** (**B**).

Catalyst (mol%)	**Conv**[a] (%)	$M_{n(cld)}$[b] (Kg/mol)	$M_{n(exp)}$[c] (Kg/mol)	**Đ**[c]	**TOF**[d] (h^1)	k_{obs}[e] (s^{-1})
[L^{Et}Zn$_2$(O^{i}Pr)$_2$] (0.1)	48	35	29	1.10	30	2.4 x 10^{-5}
[L^{Pr}Zn$_2$(O^{i}Pr)$_2$] (0.1)	93	67	53	1.04	13,000	1.8 x 10^{-2}
[L^{Open}Zn(O^{i}Pr)] (0.1)	97	70	49	1.09	14,000	2.9 x 10^{-2}
A[f] (0.2)	97	28	39	1.10	600	9 x 10^{-4}
B[g] (0.1)	99	142	100	1.02	4430	1 x 10^{-3}

Polymerisation conditions: [*rac*-LA] = 1 M in THF, isopropanol (1 equiv per metal centre) at 25 °C. [a]Determined by integration of the methine region of the ^{1}H NMR spectrum, in $CDCl_3$, at 298 K (*rac*-LA, 4.96 – 5.04 ppm; PLA, 5.10 – 5.22 ppm); [b]Molecular weight calculated using: $M_{n(cld)}$ = conversion × [*rac*-LA]$_0$ / [number of metal centre] × M_{LA}; [c]Experimental molecular weight and Đ determined by SEC vs polystyrene standards, at 40 °C, and corrected by a factor of 0.58;[18] [d]TOF = (number of moles of epoxide consumed per mole of catalyst)/time (h); [e]Determined from the slope of the linear plot of ln([*rac*-LA]$_0$/[*rac*-LA]$_t$) vs time; [f]**A** = **[BDIZn(O^{i}Pr)]**, [*rac*-LA] = 0.4 M, T = 20 °C in DCM;[2] [g]**B** = **[bis(amino)phenolatesZnEt]**, DCM.[7]

In direct contrast to the amido catalysts, kinetics studies of polymerisation involving the alokides complexes show, in each case, a linear semi-logarithmic plot of ln([*rac*-LA]$_0$/[*rac*-LA]$_t$) *versus* time, which is consistent with a first order in monomer concentration (Figure 4.6, LHS). This rate difference between the amido and the alkoxide initiating groups emphasises the dependency and the influence of the steric hindrance of the co-ligand on the Michaelis constant. Carpentier and co-workers also reported that the order in [*rac*-LA] could depend upon the steric hindrance of various Schiff base complexes.[20a]

The alkoxide catalysts afforded high degree of polymerisation control and produced PLA with molecular weights close to the expected values and narrow dispersities (< 1.1) (Figure 4.6, RHS). MALDI-TOF analyses exhibit a single series of peaks, separated by 144 amu, which indicated that transesterification side reactions were minimal. Further, the polymer end-groups were only esters (arriving from alkoxide groups).

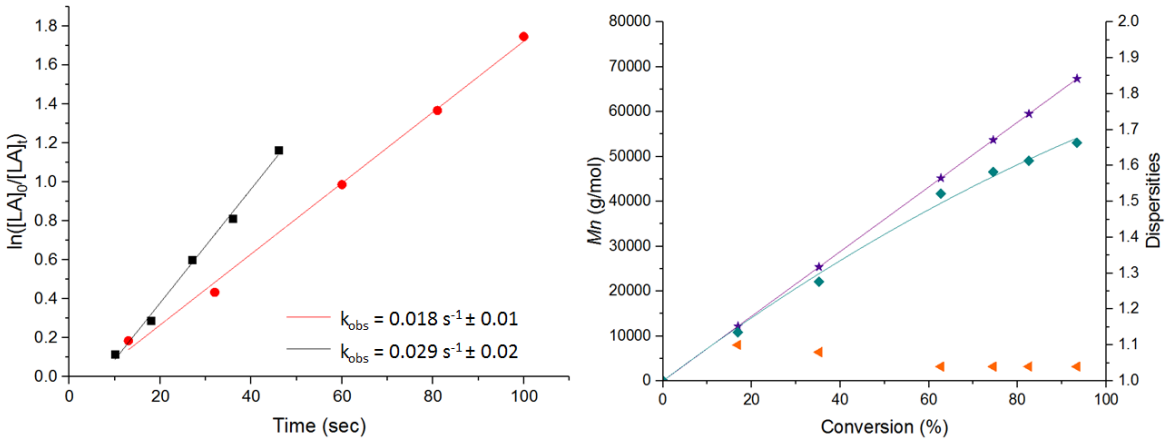

Figure 4.6. LHS: plot of ln([*rac*-LA]$_0$/[*rac*-LA]$_t$) vs time (sec), using **[L^{Pr}Zn$_2$(O^{i}Pr)$_2$]** (●) and **[L^{Open}Zn(O^{i}Pr)]** (■) (1000 equivalents of *rac*-LA in THF, 25 °C, [*rac*-LA] = 1 M).‡ RHS: plot of $M_{n(cld)}$ (g/mol) vs conversion (%) (★), $M_{n(exp)}$ (g/mol) vs conversion (%) (◆) and dispersities vs conversion (%) (◀) for **[L^{Pr}Zn$_2$(O^{i}Pr)$_2$]** under similar conditions.

‡ The rate of **L^{Et}Zn$_2$(O^{i}Pr)$_2$** is too slow, and so is not include in the same graph. The kinetic data for this catalyst can be found in the appendix.

4.4 Polymerisation under Immortal Conditions

4.4.1 Polymerisation Studies at a Catalyst Loading of 0.1 mol%

So far, the di-zinc amido catalysts showed the best rates, whereas the best control was exerted by the alkoxide analogues. In order to try to combine these beneficial properties, the catalysts were also tested under immortal conditions. An immortal polymerisation corresponds to a polymerisation process where an excess of protic reagent is added into the reaction mixture.[21] These protic compounds act as chain transfer agents by rapidly shuttling alkoxide and alcohol groups. Chain transfer reactions generally occur faster than the propagation step and so the molecular weight of the polymer is controlled by the overall amount of alcohol groups.

Table 4.4. *Rac*-LA polymerisation using zinc amido catalysts under immortal conditions and compared to the previously reported **[bis(morpholinomethyl)phenoxyZnEt]** catalyst (**C**).

Catalyst	Conv.[a] (%)	$M_{n(cld)}$[b] (Kg/mol)	$M_{n(exp)}$ (Kg/mol)[c]	Đ[c]	TOF[d] (h^{-1})	k_{obs}[e] (s^{-1})
[$L^{Et}Zn_2\{N(SiMe_3)_2\}_2$] (0.1)	97	14	14	1.07	60 000	1.4 x 10^{-1}
[$L^{Pr}Zn_2\{N(SiMe_3)_2\}_2$] (0.1)	91	13	13	1.03	50 000	7 x 10^{-2}
[$L^{Open}ZnN(SiMe_3)_2$] (0.1)	92	13	13	1.08	35 000	3.2 x 10^{-2}
C (0.1)[f]	63	13	13	1.11	18 900	-

Polymerisation conditions: [*rac*-LA] = 1 M in THF, isopropanol (10 equiv. per mol of catalyst), at 25 °C. [a]Monomer conversion determined by ^{1}H NMR spectroscopy ($CDCl_3$, 298 K). [b]Molecular weight calculated using $M_{n(cld)}$ = conversion × [*rac*-LA]$_0$ / [number of metal centre] × M_{LA}. [c]Experimental molecular weight and Đ determined by SEC vs polystyrene standards, at 40 °C, and corrected by a factor of 0.58.[18] [d]TOF calculated using: (conversion / 100) x loading / (time x number of metal centre). [e]Determined from the slope of the linear plot of ln([*rac*-LA$_0$]/[*rac*-LA$_t$]) vs time. [f]**C** = **[{bis(morpholinomethyl)phenoxyZnEt}$_2$]**, 10 equiv. of IPA / mol of catalyst, T = 60 °C in toluene.[6a]

Polymerisation reactions were carried out with 10 equivalents of isopropanol (per mol of catalyst) added to a 1 M solution of *rac*-LA in THF. This solution was directly added to a solution of the amido precursor. Under these conditions, **[$L^{Et}Zn_2\{N(SiMe_3)_2\}_2$]** and **[$L^{Pr}Zn_2\{N(SiMe_3)_2\}_2$]** remained very active: full conversion was achieved in 30 seconds (Table 4.4). It is also worth noting that **[$L^{Et}Zn_2\{N(SiMe_3)_2\}_2$]** is again 5500 times more active than **[$L^{Et}Zn_2(O^iPr)_2$]**. The k_{obs} obtained under these conditions were again around an order of magnitude higher than the best zinc catalysts reported previously in the

literature (Table 4.4).[3] Furthermore, the specific activities (per Zn) of **[L^{Et}Zn$_2${N(SiMe$_3$)$_2$}$_2$]** and **[L^{Pr}Zn$_2${N(SiMe$_3$)$_2$}$_2$]** are significantly greater than **[L^{Open}ZnN(SiMe$_3$)$_2$]**, again highlighting the potential for the zinc-zinc cooperative effect.

Kinetic studies, under immortal conditions showed a first order in monomer concentration (Figure 4.7, LHS). In all cases, polymerisation control was good with the PLA molecular weight in agreement with the expected values (Figure 4.7, RHS). MALDI-TOF analyses showed two series separated by 72 amu. The series are assigned to transesterified chains with ester and amide as end-groups. These observations suggest that both amido and alkoxide groups can initiate.

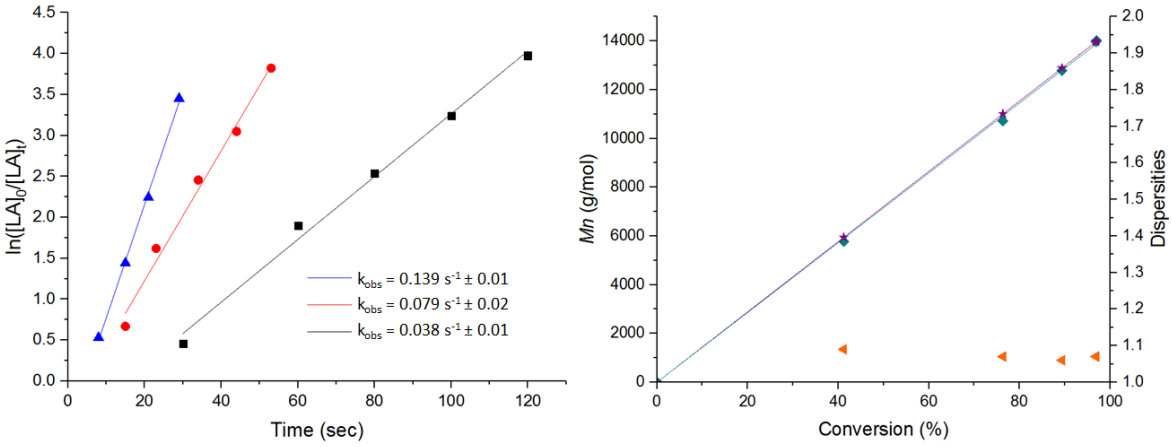

Figure 4.7. LHS: plot of ln([*rac*-LA]$_0$/[*rac*-LA]$_t$) vs time (sec), using **[L^{Et}Zn$_2${N(SiMe$_3$)$_2$}$_2$]** (▲), **[L^{Pr}Zn$_2${N(SiMe$_3$)$_2$}$_2$]** (●) and **[L^{Open}ZnN(SiMe$_3$)$_2$]** (■) (1000 equivalents of *rac*-LA in THF, 25 °C, [*rac*-LA] = 1 M). RHS: plot of $M_{n(cld)}$ (g/mol) vs conversion (%) (★), $M_{n(exp)}$ (g/mol) vs conversion (%) (◆) and dispersities vs conversion (%) (◄) for **[L^{Pr}Zn$_2$(O^{i}Pr)$_2$]** under similar conditions.

4.4.2 Catalyst Loading Limits

The ability to apply the complexes under immortal conditions (i.e. high activities and good control) prompted the investigation of catalyst loading (Table 4.5). The series of catalysts were each tried at a catalyst loading of 0.02 mol% in the presence of 10 equivalents of isopropanol. Under these conditions, **[L^{Et}Zn$_2${N(SiMe$_3$)$_2$}$_2$]** was able to reach complete conversion in only 2 min. **[L^{Et}Zn$_2${N(SiMe$_3$)$_2$}$_2$]** (k_{obs} = 0.025 s^{-1}) was an order of magnitude faster than **[L^{Pr}Zn$_2${N(SiMe$_3$)$_2$}$_2$]** (k_{obs} = 0.0029 s^{-1}). These findings are in line with the hypothesis that a close metal-metal distance improves activity.

[$L^{Et}Zn_2\{N(SiMe_3)_2\}_2$] and **[$L^{Pr}Zn_2\{N(SiMe_3)_2\}_2$]** remained effective even at a catalyst loading of 0.002 mol%. In all cases the polymerisations progressed rapidly showing linear evolution of molecular weight and narrow dispersities. Their activities are also higher than the most commonly used industrial catalyst **[$Sn(Oct)_2$]** at equivalent low loading.[22] On the other hand, under such industrially relevant catalyst loadings (Industrial scale polymerisations with **[$Sn(Oct)_2$]** are typically performed using loadings between 0.02 and 0.002 mol%),[23] the mono-zinc catalyst **[$L^{Open}ZnN(SiMe_3)_2$]** decomposed, highlighting an issue for many coordination complexes whereby the ligands are subject to protonolysis when used under immortal conditions.[24]

Table 4.5. *Rac*-LA polymerisation using zinc amido catalysts under immortal conditions and compared to the industrially relevant tin octanoate catalyst (**D**).

Catalyst (mol %)	**Conv.**[a] (%)	$M_{n(cld)}$[b] (Kg/mol)	$M_{n(exp)}$[c] (Kg/mol)	**Đ**	**TOF**[d] (h^{-1})	k_{obs}[e] (s^{-1})
[$L^{Et}Zn_2\{N(SiMe_3)_2\}_2$] (0.02)	85	61	58	1.07	165 000	1.4×10^{-1}
[$L^{Pr}Zn_2\{N(SiMe_3)_2\}_2$] (0.02)	84	67	47	1.03	51 000	7×10^{-2}
[$L^{Open}ZnN(SiMe_3)_2$] (0.02)	0	-	-	-	-	-
[$L^{Pr}Zn_2\{N(SiMe_3)_2\}_2$] (0.002)[f]	43	61	48	1.02	2655	2×10^{-5}
D (0.009)[g]	83	1340	900	2.00	1200	

Polymerisation conditions: [*rac*-LA] = 1 M in THF, isopropanol (10 equiv. per mol of catalyst), at 25 °C; [a]Monomer conversion determined by ^{1}H NMR spectroscopy ($CDCl_3$, 298 K); [b]Molecular weight calculated using $M_{n(cld)}$ = conversion × [*rac*-LA]$_0$ / [number of metal centre] × M_{LA}. [c]Experimental molecular weight and Đ determined by SEC vs polystyrene standards and corrected by a factor of 0.58. [d]TOF calculated using: (conversion / 100) x loading / (time x number of metal centre). [e]Determined from the slope of the linear plot of ln([*rac*-LA]$_0$/[*rac*-LA]$_t$) vs time; [f]50 equiv. of isopropanol per mol of catalyst; [g] **D** = tin octanoate, at 110 °C, neat, without isopropanol.[23]

4.5 Discussion

4.5.1 Rationalisation of the Hyperactivity

Given the outstanding activities (hyperactivities) observed for some of these complexes, and the dramatic differences in performance, particularly between **[L^{Et}Zn$_2${N(SiMe$_3$)$_2$}$_2$]** and **[L^{Et}Zn$_2$(O^{i}Pr)$_2$]**, it was interesting to correlate activity with structural data for the complexes.

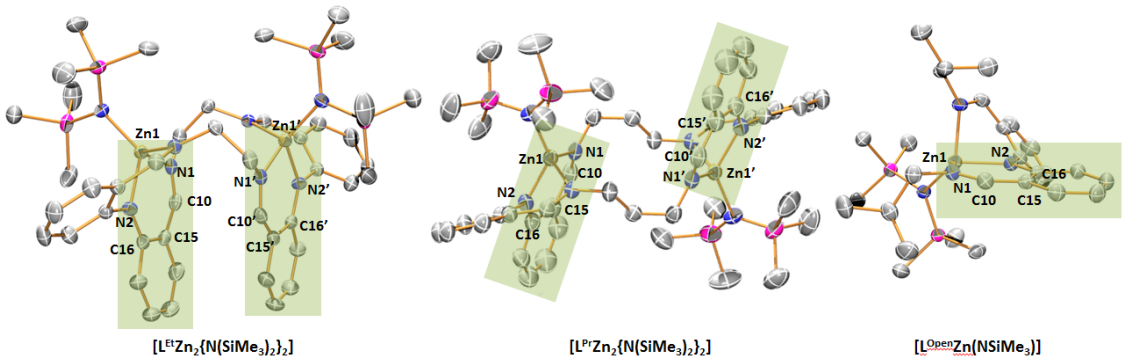

Figure 4.8. Molecular structures of **[L^{y}Zn$_2${N(SiMe$_3$)$_2$}$_2$]** (y = Et, Pr)† and **[L^{Open}ZnN(SiMe$_3$)$_2$]** with thermal ellipsoids at the 50 % probability level. The highlighting is for the zinc-BDI chelate. A THF molecule (**[L^{Et}Zn$_2${N(SiMe$_3$)$_2$}$_2$]**), a hexane molecule and a second independent molecule (**[L^{Pr}Zn$_2${N(SiMe$_3$)$_2$}$_2$]**) and hydrogen atoms are omitted for clarity (refer to the appendix for complete data set).

The molecular structures of amido complexes present a "BDI-like" zinc chelate where the zinc is coordinated in the same plane as the delocalised ligand chelate {N1-C10-C15-C16-N2}.[25] Overall, ligand coordination involved the formation of a Zn-BDI chelate with coordination of an additional imine donor.

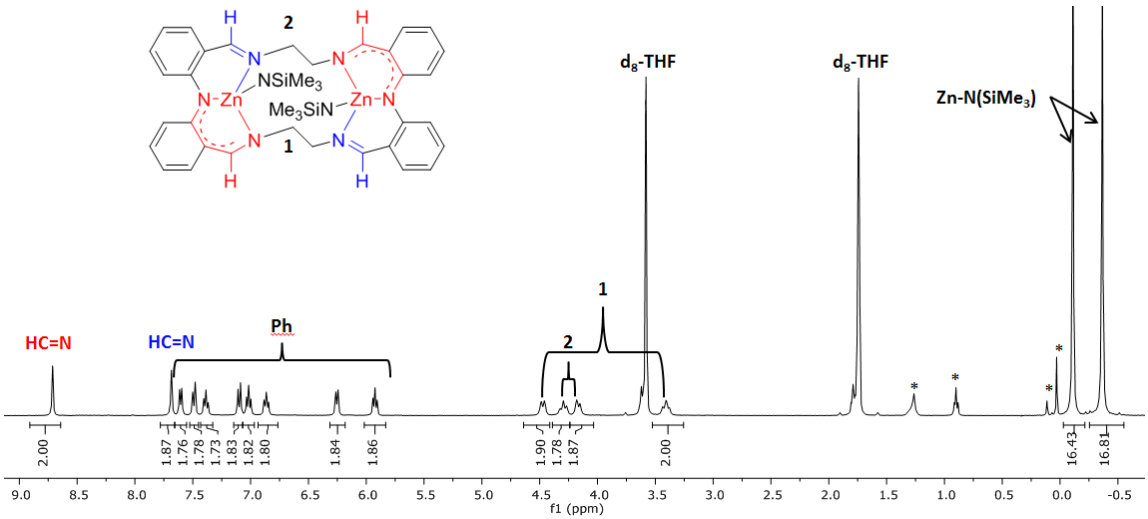

Figure 4.9. ^{1}H NMR spectrum, in d_8-THF, at 193 K, of **[L^{Et}Zn$_2${N(SiMe$_3$)$_2$}$_2$]** showing two imine resonances assigned to the "Zn-BDI" chelate (at 8.71 ppm) and the pendant imine (at 7.69 ppm); *traces of hexane and HN(SiMe)$_3$.

The solution states of the amido complexes are similar to the solid state structure. The ^{1}H NMR spectrum of **[L^{Et}Zn$_2${N(SiMe$_3$)$_2$}$_2$]**, at 193 K, and **[L^{Pr}Zn$_2${N(SiMe$_3$)$_2$}$_2$]**, at 298 K, in d_8-THF, each show two asymmetric imine resonances, at 8.71 ppm and 7.69 ppm, and 8.30 ppm and 8.26 ppm, respectively. The appearance of 2 peaks is expected with one imine being part of the "Zn-BDI" chelate and the second peak due to the pendant imine group (Figure 4.9). ^{1}H NMR spectrum of **[L^{Open}ZnN(SiMe$_3$)$_2$]**, in C_6D_6, at 298 K, presents only one imine signal, perhaps due to higher flexibility of the ligand enabling a fast equilibrium between two imine environments. Upon cooling the NMR sample to 193 K, the equilibrium is slowed and two imine signals are observed. These observations suggest that all the complexes retained the "BDI" chelate and the extra donation coordination modes for the imine groups under polymerisation conditions.

Zinc BDI complexes, originally pioneered by Coates and co-workers and subsequently investigated by many others,[2, 26] are some of the most highly active ROP catalysts (Table 4.3, catalyst **A**). In the present case, the ligands combine a "BDI-like" chelate with an extra imine donor, which enhances the electron donation to the metal, and which, in turn, results in faster rates. This observation suggests that increasing the electron density at the active

site (metal ion) accelerates the polymerisation, perhaps by labilisation of the zinc alkoxide bonds.[27]

4.5.2 Differences Between $[L^{Et}Zn_2\{N(SiMe_3)_2\}_2]$ and $[L^{Et}Zn_2(O^iPr)_2]$

The difference in activity between **$[L^{Et}Zn_2\{N(SiMe_3)_2\}_2]$** and **$[L^{Et}Zn_2(O^iPr)_2]$** may also be explained by structural differences between the complexes. Two distinct ligand conformations are observed in the two complexes and these are proposed to contribute to the stark differentiation in activities (Figure 4.10).

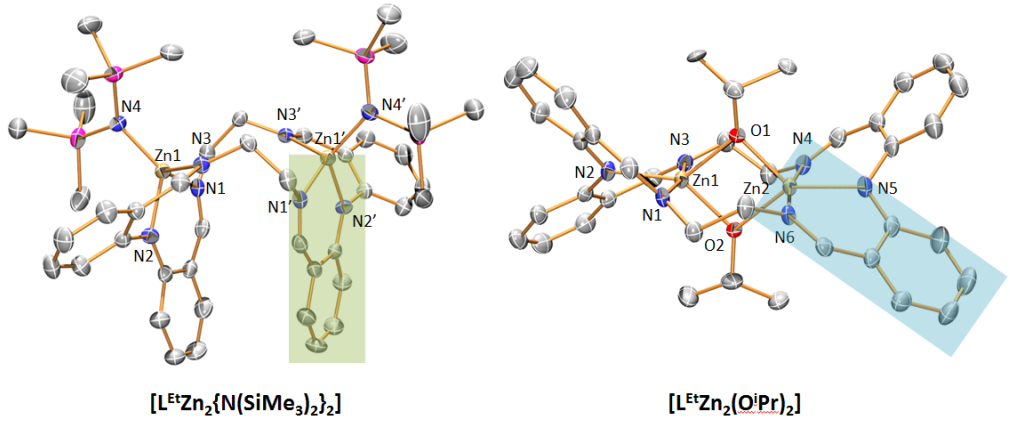

Figure 4.10. Molecular structures of **$[L^{Et}Zn_2\{N(SiMe_3)_2\}_2]$**† and **$[L^{Et}Zn_2(O^iPr)_2]$** with thermal ellipsoids at the 50 % probability level. The highlighted region shows the difference in zinc coordination mode and ligands conformation. A THF molecule (**$[L^{Et}Zn_2\{N(SiMe_3)_2\}_2]$**) and hydrogen atoms are omitted for clarity (refer to the appendix for complete data set).

It is worth noting that the complexes also feature different initiating groups, but that initiation effects are not controlling rate because the catalysts show well defined kinetic profiles (albeit quite different ones), exhibit reasonable control and yield polymers with narrow dispersities. Rather, the radically different performances seem more likely to be mediated by distinct ligand conformations. In the solid state, **$[L^{Et}Zn_2\{N(SiMe_3)_2\}_2]$** adopts a "folded" C_2 symmetric structure, with the $N(SiMe_3)_2$ groups occupying the same, convex, face of the complex. As previously described, its solution state at 193 K is similar to its solid state. The ^{1}H NMR spectrum consists of a series of well-defined resonances consistent with C_2 symmetry. ROESY NMR experiment, in d_8-THF, at 193 K, was also used to confirm that **$[L^{Et}Zn_2\{N(SiMe_3)_2\}_2]$** adopts a "folded" ligand structure. The

ROESY showed the cross peaks at 7.60 ppm/6.25 ppm and 7.49 ppm/7.02 ppm which were assigned to resonances protons *m*-Ph/*m*-Ph and *o*-Ph/*p*-Ph which are only close in space if the "folded" structure is retained.

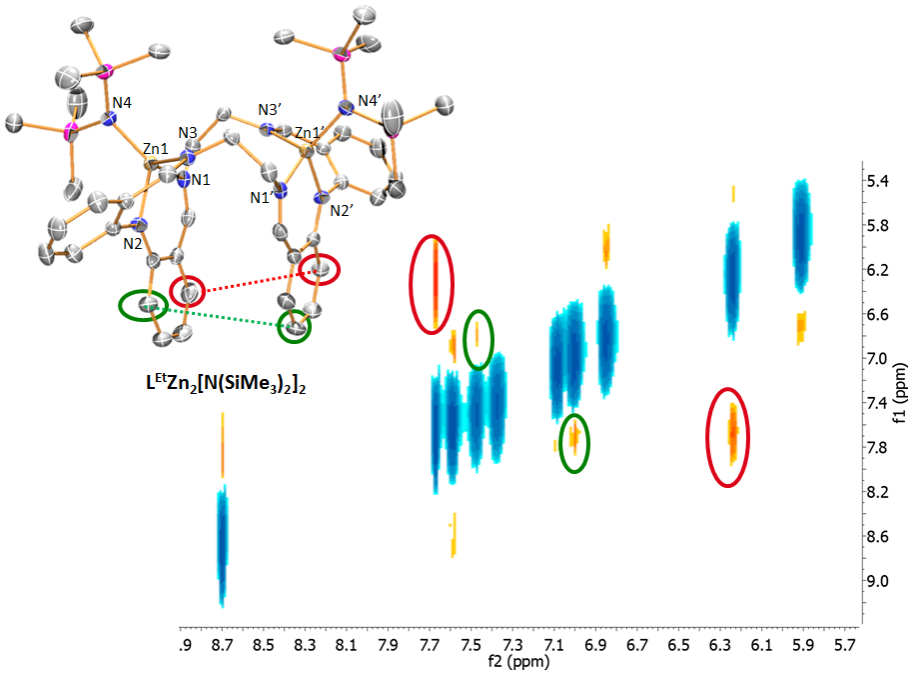

Figure 4.11. ROSESY NMR spectrum of **[L^{Et}Zn$_2${NSi(Me$_3$)$_2$}$_2$]**, d$_8$-THF, 193 K, expended in the phenyl region illustrating four cross peaks corresponding to four protons that are close in space.

VT ^{1}H NMR analysis of **[L^{Et}Zn$_2${N(SiMe$_3$)$_2$}$_2$]** indicated that the "folded" structure was retained at 253 K. Between 263 K and 293 K, signal coalescence occurs suggesting that several conformers are in equilibrium. The equilibrium is relatively slow in accordance with the steric hindrance of the N(SiMe$_3$)$_2$ group and the short ethyl linker. The dynamic process is tentatively attributed to be the rotation of the two phenyl rings around the central nitrogen atom. During this process, the zinc-BDI chelate flips from one side of the molecule to the other side. Importantly, it also retains a "folded" structure throughout this change in conformation (Figure 4.12, LHS).

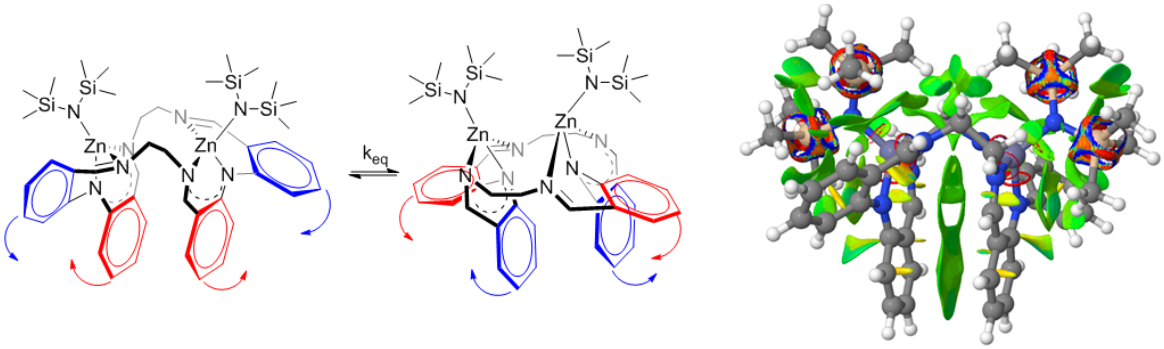

Figure 4.12. LHS: Illustration of the two proposed conformers of **[L^{Et}Zn$_2${N(SiMe$_3$)$_2$}$_2$]** which are in equilibrium; RHS: representation from DFT calculation revealing non-covalent interaction surface in **[L^{Et}Zn$_2${N(SiMe$_3$)$_2$}$_2$]** (green represents attractive interaction and red repulsive interactions). The representation shows the π-π interaction between the two opposite phenyl units.[28]

At 303 K and higher temperatures, only a single average environment is observed as expected under fast exchange conditions. A line shape analysis of the data enable the determination of the thermodynamic parameters ($\Delta G^{\neq}$ = 13 kcal/mol). The calculated value was in close agreement with value obtained from DFT calculations for the same process ($\Delta G^{\neq}$ = 17 kcal/mol).[§] As polymerisation occurs at 25 °C, the "folded" structure is proposed to be retained under reaction conditions – it is perhaps stabilised by π-π interactions between each phenyl rings (Figure 4.12, RHS, refer to the appendix for more details).

In contrast, the molecular structure of **[L^{Et}Zn$_2$(O^{i}Pr)$_2$]** shows a different, "planar", ligand conformation (Figure 4.10, RHS).[14] The solid state structure of **[L^{Et}Zn$_2$(O^{i}Pr)$_2$]** has D_2 symmetry and features two κ^2 alkoxide groups, bridging between the zinc centres (Figure 4.10).[14] Thus, the "BDI-like" zinc chelate seen in **[L^{Et}Zn$_2${N(SiMe$_3$)$_2$}$_2$]** is not present in **[L^{Et}Zn$_2$(O^{i}Pr)$_2$]**, and bridging alkoxides clearly reduce the conformational flexibility of the macrocycle. The loss of this BDI-chelate may also explain for the change in colour between the amido (red/orange) and the alkoxide complex (yellow). This change of colour is also observed during catalysis and is a useful way to quickly probe the activity of the catalyst (i.e red/orange solution = highly activity catalyst and yellow solution = low activiy

[§] DFT calculations were performed by Dr Charles Romain at Imperial College London

catalyst). The ^{1}H NMR spectrum of **[L^{Et}Zn$_2$(O^{i}Pr)$_2$]**, in d$_8$-THF, at 298 K, shows resonances in accordance with the complex retaining D_2 symmetry in solution (i.e, only one imine signal is observed), and confirms the proposed ligand coordination modes.

It is proposed that the higher activity of **[L^{Et}Zn$_2${N(SiMe$_3$)$_2$}$_2$]** results from its "folded" ligand confromation whereby the zinc active sites are pointing out on the convex face of the complex, facilitating both monomer insertion and coordination, the latter of which becomes limiting under monomer saturation conditions.

4.5.3 Immortal Polymerisation

The precise nature of the active site structure(s) when using **[L^{Et}Zn$_2${N(SiMe$_3$)$_2$}$_2$]** under immortal conditions, is a more complex problem. MALDI-ToF analysis of the polymers afforded showed that the polymerisation was initiated by both isopropoxide and amido groups (N.B. the ester groups do not form under the mass spectrometry conditions and are real products of the catalysis) (Figure 4.13). It seems unlikely that a mixture of **[L^{Et}Zn$_2${N(SiMe$_3$)$_2$}$_2$]** and **[L^{Et}Zn$_2$(O^{i}Pr)$_2$]** is present during catalysis, as the relative polymerisation rate of **[L^{Et}Zn$_2$(O^{i}Pr)$_2$]** is so much lower than **[L^{Et}Zn$_2${N(SiMe$_3$)$_2$}$_2$]** (**[L^{Et}Zn$_2${N(SiMe$_3$)$_2$}$_2$]** is 5833 times faster). Given that complete conversion occurs in only 29 seconds, under immortal conditions, there would not be sufficient time for **[L^{Et}Zn$_2$(O^{i}Pr)$_2$]** to function independently (c.f **[L^{Et}Zn$_2$(O^{i}Pr)$_2$]** takes 8 h to reach just 50 % conversion under the same conditions).

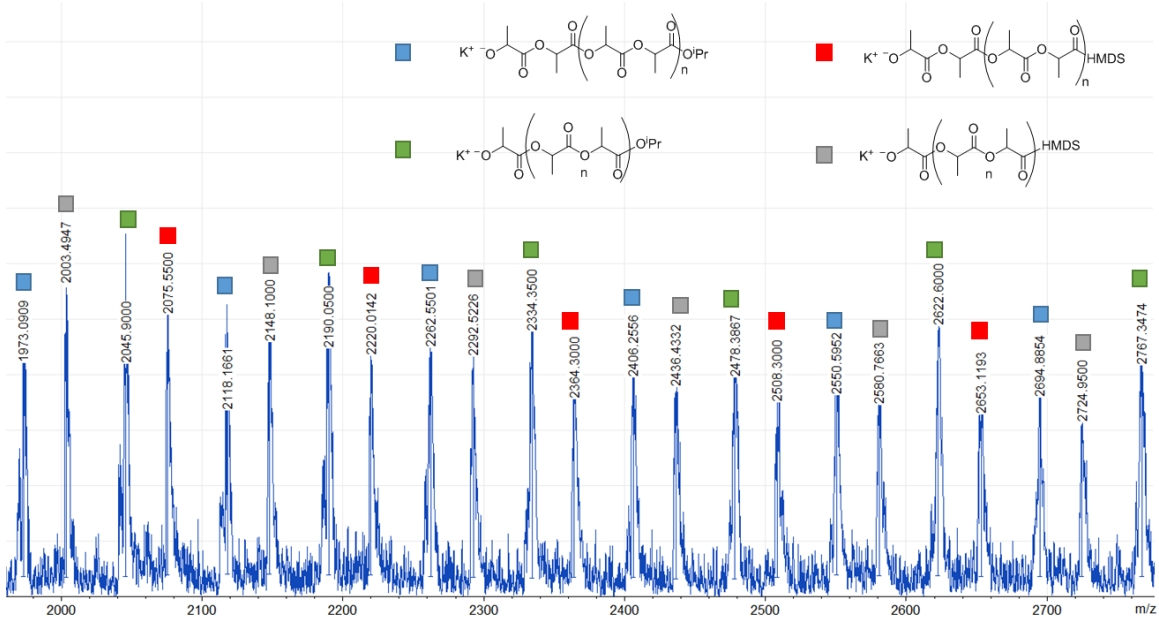

Figure 4.13. MALDI-ToF spectrum of PLA afforded under immortal conditions.

The data could be rationalised if the rate of initiation from **[L^{Et}Zn$_2${N(SiMe$_3$)$_2$}$_2$]** is approximately equal to the rate of chain exchange with alcohol and if an intermediate alkoxide complex forms which matches the activity of **[L^{Et}Zn$_2${N(SiMe$_3$)$_2$}$_2$]**, but is orders of magnitude faster than **[L^{Et}Zn$_2$(O^{i}Pr)$_2$]**. There is preliminary evidence for such a putative dizinc alkoxide species from LT-NMR data (183 K), which show unassigned low intensity intermediate alkoxide signals during alcoholysis of **[L^{Et}Zn$_2${N(SiMe$_3$)$_2$}$_2$]** to form **[L^{Et}Zn$_2$(O^{i}Pr)$_2$]**. It is also possible to observe the formation of bridging alkoxide complex **[L^{Et}Zn$_2$(O^{i}Pr)$_2$]** at the end of polymerisations run under immortal conditions as the addition of a second portion of monomer at this stage results in extremely slow rates of polymerisation, consistent with its much lower activity. It is tentatively proposed that a highly active alkoxide complex, featuring a "folded" ligand conformation, is partly responsible for the outstanding activity under immortal conditions (Scheme 4.6). The intermediate alkoxide rearranges to the thermodynamically more stable bridging species, **[L^{Et}Zn$_2$(O^{i}Pr)$_2$]**, within one minute under the reaction conditions, but in many cases polymerisation is already complete by this time. Accordingly, the rate of the initiation (k_i)

and the rate of the co-ligand exchange (k_{ex}) are proposed to be of the same magnitude but are greater than the isomerisation rate ($k_{ex} \approx k_i > k_{iso}$). Unfortunately, the lifetime of the intermediate is still too transient for more detailed analysis using common spectroscopic techniques.

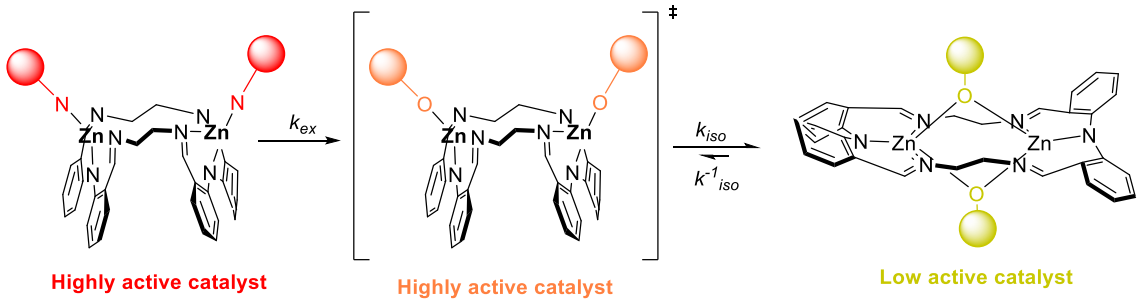

Scheme 4.6. Proposed mechanism for the reaction of two equivalents of IPA on **[L^{Et}Zn$_2${N(SiMe$_3$)$_2$}$_2$]**.

4.6 Conclusions and Outlook

4.6.1 Conclusions

In conclusion, the zinc complexes showed good activities and control for *rac*-LA ROP. There is evidence that di-zinc catalysts out-perform mono-zinc catalysts (per zinc atom present) which indicates intermetallic cooperativity is likely important in this field of catalysis. The di-zinc catalyst, showing the shortest Zn-Zn separation, shows the highest activity. Further, the macrocycle ligand conformation is implicated in controlling activity – the most active catalyst adopts a "folded" ligand conformation which is significantly (~ 6000 times) more active than when a "flat" ligand conformation is adopted. Indeed, the best catalyst shows very high rates which are at least an order of magnitude greater than the previously more active zinc catalysts. Further, the macrocycle catalysts are more stable to protonolysis (*vs.* mono zinc analogue) and can be applied under immortal conditions at low catalyst loading.

4.6.2 Outlooks

4.6.2.1 Conformational Switch Catalysis for Block Copolymer Synthesis

The stark differentiation in activity between **[$L^{Et}Zn_2[N(SiMe_3)_2]_2$]** and **[$L^{Et}Zn_2(O^iPr)_2$]**, i.e. the correlation with the pre-catalyst structure, is unexpected but may reveal a new possibility to control activity. In terms of future directions, it could be interesting to consider reversible changes to ligand conformation (perhaps thermally activated) as a means to control activity.[10] A further development could be to explore the potential for orthogonal activities dependent upon ligand conformer; such process is typically referred to as a "switch" in catalysis.[1a, 29] The goal would be that a single conformer would be active for a specific reaction and the other conformer would be active for a different chemical reaction. In polymer chemistry the use of the switch concept is very appealing as block copolymers can be prepared in one pot from a mixture of monomers.[30]

Preliminary studies have shown that **[$L^{Et}Zn_2\{N(SiMe_3)_2\}_2$]** is much less active when using other cyclic esters/carbonates in ROP [so far, only ε-caprolactone (ε-CL) and trimethylene carbonate (TMC) were tested] compared to lactide ROP [k_{obs}(*rac*-LA) = 0.139 s^{-1} vs. k_{obs}(ε-CL) = 3 x 10^{-5} s^{-1}]. It was also noted that in *rac*-LA ROP a red/orange colour was observed during polymerisation whereas a yellow colour was observed during ε-CL or TMC ROP. The colour may correlate with ligand conformation: "flat" **[$L^{Et}Zn_2(O^iPr)_2$]** yellow; "folded" **[$L^{Et}Zn_2\{N(SiMe_3)_2\}_2$]** red. This suggests that the folded complex rearranges more rapidly to the "flat" ligand conformation upon reaction with ε-CL or TMC, perhaps explaining the overall low activity using these monomers.

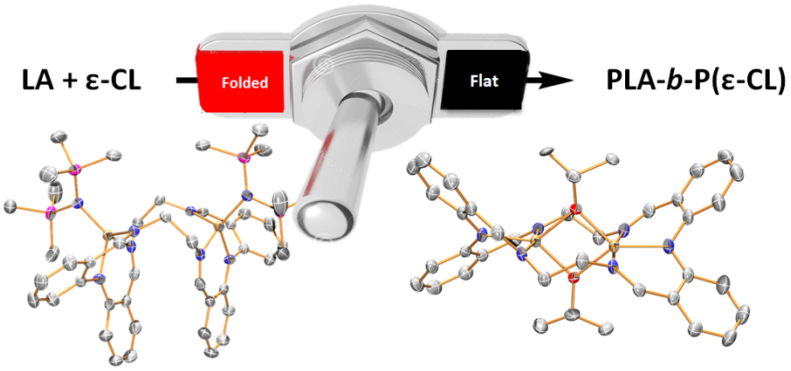

Figure 4.14. Illustration of the proposed switch process to target block copolymers.

Block copolymers could therefore be targeted starting from the "folded" **[L^{Et}Zn$_2${N(SiMe$_3$)$_2$}$_2$]** catalyst and using a mixture of *rac*-LA and ε-CL. The catalyst would be expected to initiate *rac*-LA ROP rapidly to form a PLA block. After complete conversion of the *rac*-LA, the "flat" conformer should form and the slower polymerisation of ε-CL could occur to form a second block. Initial experiments to test this hypothesis confirmed that *rac*-LA was indeed quickly polymerised during the first stage of the reaction. The ligand conformation rearrangement was also indicated by a change in the solution colour (red to yellow). During the second stage, ε-CL ROP occurred. Nevertheless, more experiments need to be done to monitor accurately the reaction kinetics and to fully confirm block copolymer formation. Overall, there is scope to explore the use of these catalysts in switchable catalysis. In future, as well as using *rac*-LA and ε-CL, other lactones (e.g. δ-decalactone, β-butyrolactone, γ-valerolactone), cyclic carbonates (e.g. trimethylene carbonate) and epoxides (e.g. CHO, PO, LO) should be explored.

4.6.2.2 Dinuclear catalysts for CO_2/epoxide ROCOP

The best di-zinc catalysts could also be used for the more demanding CO_2/epoxide ROCOP catalysis. Preliminary results, performed at 80 °C, in CHO at 1 bar of CO_2 pressure, showed no activity when using **[L^{Et}Zn$_2${N(SiMe$_3$)$_2$}$_2$]** and **[L^{Et}Zn$_2$(O^{i}Pr)$_2$]**. This is may be due to the formation of the stable "flat" alkoxide which might inhibit CO_2

insertion. On the other hand, **[$L^{Et}Zn_2\{N(SiMe_3)_2\}_2$]** and **[$L^{Open}ZnN(SiMe_3)_2$]** showed low activities (at 1 bar of CO_2) and formed mostly polyether. Therefore, the complexes should be tested at higher CO_2 pressures to establish whether selectivity (carbonate) can be improved. Other epoxides and epoxide/anhydride copolymerisation should also be tested using these catalysts.

4.7 References

[1] a) X. Wang, A. Thevenon, J. L. Brosmer, I. Yu, S. I. Khan, P. Mehrkhodavandi, P. L. Diaconescu, *J. Am. Chem. Soc.* **2014**, *136*, 11264-11267; b) C. Bakewell, A. J. P. White, N. J. Long, C. K. Williams, *Angew. Chem. Int. Ed.* **2014**, *53*, 9226-9230; c) C. A. Wheaton, P. G. Hayes, B. J. Ireland, *Dalton Trans.* **2009**, 4832-4846; d) R. H. Platel, L. M. Hodgson, C. K. Williams, *Polym. Rev.* **2008**, *48*, 11-63; e) O. Dechy-Cabaret, B. Martin-Vaca, D. Bourissou, *Chem. Rev.* **2004**, *104*, 6147-6176.

[2] B. M. Chamberlain, M. Cheng, D. R. Moore, T. M. Ovitt, E. B. Lobkovsky, G. W. Coates, *J. Am. Chem. Soc.* **2001**, *123*, 3229-3238.

[3] C. K. Williams, L. E. Breyfogle, S. K. Choi, W. Nam, V. G. Young, M. A. Hillmyer, W. B. Tolman, *J. Am. Chem. Soc.* **2003**, *125*, 11350-11359.

[4] M. H. Chisholm, N. W. Eilerts, J. C. Huffman, S. S. Iyer, M. Pacold, K. Phomphrai, *J. Am. Chem. Soc.* **2000**, *122*, 11845-11854.

[5] S. Inkinen, M. Hakkarainen, A.-C. Albertsson, A. Södergård, *Biomacromolecules* **2011**, *12*, 523-532.

[6] a) V. Poirier, T. Roisnel, J.-F. Carpentier, Y. Sarazin, *Dalton Trans.* **2009**, 9820-9827; b) M. J. Stanford, A. P. Dove, *Chem. Soc. Rev.* **2010**, *39*, 486-494.

[7] C. K. Williams, L. E. Breyfogle, S. K. Choi, W. Nam, V. G. Young, M. A. Hillmyer, W. B. Tolman, *J. Am. Chem. Soc.* **2003**, *125*.

[8] a) S. Matsunaga, M. Shibasaki, *Chem. Commun.* **2014**, *50*, 1044-1057; b) Y. Liu, W.-M. Ren, K.-K. He, X.-B. Lu, *Nat. Commun.* **2014**, *5*; c) I. Bratko, M. Gomez, *Dalton Trans.* **2013**, *42*, 10664-10681; d) D. R. Armstrong, J. A. Garden, A. R. Kennedy, R. E. Mulvey, S. D. Robertson, *Angew. Chem. Int. Ed.* **2013**, *52*, 7190-7193; e) M. R. Radlauer, A. K. Buckley, L. M. Henling, T. Agapie, *J. Am. Chem.*

Soc. **2013**, *135*, 3784-3787; f) J. Park, S. Hong, *Chem. Soc. Rev.* **2012**, *41*, 6931-6943; g) K. Nakano, S. Hashimoto, K. Nozaki, *Chem. Sci.* **2010**, *1*, 369-373.

[9] a) N. Mitić, S. J. Smith, A. Neves, L. W. Guddat, L. R. Gahan, G. Schenk, *Chem. Rev.* **2006**, *106*, 3338-3363; b) M. J. Jedrzejas, P. Setlow, *Chem. Rev.* **2001**, *101*, 607-618.

[10] a) A. Arbaoui, C. Redshaw, D. L. Hughes, *Chem. Commun.* **2008**, 4717-4719; b) B. F. Straub, *Adv. Synth. Catal.* **2007**, *349*, 204-214; c) J. Ackermann, F. Meyer, E. Kaifer, H. Pritzkow, *Chem. Eur. J.* **2002**, *8*, 247-258.

[11] a) C. Boulho, H. S. Zijlstra, S. Harder, *Eur. J. Inorg. Chem.* **2015**, *2015*, 2132-2138; b) M. R. Radlauer, M. W. Day, T. Agapie, *J. Am. Chem. Soc.* **2012**, *134*, 1478-1481; c) M. Delferro, T. J. Marks, *Chem. Rev.* **2011**, *111*, 2450-2485; d) H. Li, T. J. Marks, *Proc. Nat. Acad. Sci.* **2006**, *103*, 15295-15302; e) L. Li, M. V. Metz, H. Li, M.-C. Chen, T. J. Marks, L. Liable-Sands, A. L. Rheingold, *J. Am. Chem. Soc.* **2002**, *124*, 12725-12741.

[12] a) H.-C. Tseng, H.-Y. Chen, Y.-T. Huang, W.-Y. Lu, Y.-L. Chang, M. Y. Chiang, Y.-C. Lai, H.-Y. Chen, *Inorg. Chem.* **2016**, *55*, 1642-1650; b) L. Chen, W. Li, D. Yuan, Y. Zhang, Q. Shen, Y. Yao, *Inorg. Chem.* **2015**, *54*, 4699-4708; c) M. Normand, T. Roisnel, J. F. Carpentier, E. Kirillov, *Chem. Commun.* **2013**, *49*, 11692-11694; d) H.-Y. Chen, M.-Y. Liu, A. K. Sutar, C.-C. Lin, *Inorg. Chem.* **2010**, *49*, 665-674; e) Y. Sarazin, R. H. Howard, D. L. Hughes, S. M. Humphrey, M. Bochmann, *Dalton Trans.* **2006**, 340-350; f) E. Bukhaltsev, L. Frish, Y. Cohen, A. Vigalok, *Org. Lett.* **2005**, *7*, 5123-5126.

[13] a) S. Kissling, M. W. Lehenmeier, P. T. Altenbuchner, A. Kronast, M. Reiter, P. Deglmann, U. B. Seemann, B. Rieger, *Chem. Commun.* **2015**, *51*, 4579-4582; b) J. A. Garden, P. K. Saini, C. K. Williams, *J. Am. Chem. Soc.* **2015**, *137*, 15078-

15081; c) A. Thevenon, J. A. Garden, A. J. P. White, C. K. Williams, *Inorg. Chem.* **2015**, *54*, 11906-11915.

[14] C. Romain, M. S. Bennington, A. J. P. White, C. K. Williams, S. Brooker, *Inorg. Chem.* **2015**, 11842-11851.

[15] a) M. Helou, O. Miserque, J.-M. Brusson, J.-F. Carpentier, S. M. Guillaume, *Chem. Eur. J.* **2008**, *14*, 8772-8775; b) I. D'Auria, M. Lamberti, M. Mazzeo, S. Milione, G. Roviello, C. Pellecchia, *Chem. Eur. J.* **2012**, *18*, 2349-2360.

[16] a) S. A. Cameron, S. Brooker, *Inorg. Chem.* **2011**, *50*, 3697-3706; b) D. Black, N. Rothnie, *Aust. J. Chem.* **1983**, *36*, 2395-2406; c) D. S. C. Black, N. E. Rothnie, *Tetrahedron Lett.* **1978**, *19*, 2835-2836.

[17] A. Okuniewski, D. Rosiak, J. Chojnacki, B. Becker, *Polyhedron* **2015**, *90*, 47-57.

[18] a) A. Kowalski, A. Duda, S. Penczek, *Macromolecules* **1998**, *31*, 2114-2122; b) M. Save, M. Schappacher, A. Soum, *Macromol. Chem. Phys.* **2002**, *203*, 889-899.

[19] a) N. Ajellal, J.-F. Carpentier, C. Guillaume, S. M. Guillaume, M. Helou, V. Poirier, Y. Sarazin, A. Trifonov, *Dalton Trans.* **2010**, *39*, 8363-8376; b) A. P. Dove, V. C. Gibson, E. L. Marshall, A. J. P. White, D. J. Williams, *Dalton Trans.* **2004**, 570-578.

[20] a) M. Normand, V. Dorcet, E. Kirillov, J.-F. Carpentier, *Organometallics* **2013**, *32*, 1694-1709; b) Y. Huang, W. Wang, C.-C. Lin, M. P. Blake, L. Clark, A. D. Schwarz, P. Mountford, *Dalton Trans.* **2013**, *42*, 9313-9324; c) K. Ding, M. O. Miranda, B. Moscato-Goodpaster, N. Ajellal, L. E. Breyfogle, E. D. Hermes, C. P. Schaller, S. E. Roe, C. J. Cramer, M. A. Hillmyer, W. B. Tolman, *Macromolecules* **2012**, *45*, 5387-5396.

[21] S. Inoue, *J. Polym. Sci., Part A: Polym. Chem.* **2000**, *38*, 2861-2871.

[22] a) R. E. Drumright, P. R. Gruber, D. E. Henton, *Adv. Mater.* **2000**, *12*, 1841-1846; b) M. H. Hartmann, in *Biopolymers from Renewable Resources* (Ed.: D. L. Kaplan), Springer Berlin Heidelberg, Berlin, Heidelberg, **1998**, pp. 367-411.

[23] A. J. Nijenhuis, D. W. Grijpma, A. J. Pennings, *Macromolecules* **1992**, *25*, 6419-6424.

[24] V. Poirier, T. Roisnel, S. Sinbandhit, M. Bochmann, J.-F. Carpentier, Y. Sarazin, *Chem. Eur. J.* **2012**, *18*, 2998-3013.

[25] M. Cheng, D. R. Moore, J. J. Reczek, B. M. Chamberlain, E. B. Lobkovsky, G. W. Coates, *J. Am. Chem. Soc.* **2001**, *123*, 8738-8749.

[26] a) T. J. J. Whitehorne, B. Vabre, F. Schaper, *Dalton Trans.* **2014**, *43*, 6339-6352; b) S. Abbina, G. Du, *ACS Macro Lett.* **2014**, *3*, 689-692; c) G. Du, Y. Wei, W. Zhang, Y. Dong, Z. Lin, H. He, S. Zhang, X. Li, *Dalton Trans.* **2013**, *42*, 1278-1286; d) F. Drouin, P. O. Oguadinma, T. J. J. Whitehorne, R. E. Prud'homme, F. Schaper, *Organometallics* **2010**, *29*, 2139-2147; e) M. H. Chisholm, J. C. Gallucci, K. Phomphrai, *Inorg. Chem.* **2005**, *44*, 8004-8010; f) H.-Y. Chen, B.-H. Huang, C.-C. Lin, *Macromolecules* **2005**, *38*, 5400-5405; g) M. H. Chisholm, J. Gallucci, K. Phomphrai, *Inorg. Chem.* **2002**, *41*, 2785-2794; h) M. H. Chisholm, J. C. Huffman, K. Phomphrai, *J. Chem. Soc., Dalton Trans.* **2001**, 222-224.

[27] a) X. Wang, J. L. Brosmer, A. Thevenon, P. L. Diaconescu, *Organometallics* **2015**, *34*, 4700-4706; b) C. Bakewell, T.-P.-A. Cao, N. Long, X. F. Le Goff, A. Auffrant, C. K. Williams, *J. Am. Chem. Soc.* **2012**, *134*, 20577-20580.

[28] E. R. Johnson, S. Keinan, P. Mori-Sánchez, J. Contreras-García, A. J. Cohen, W. Yang, *J. Am. Chem. Soc.* **2010**, *132*, 6498-6506.

[29] a) A. B. Biernesser, K. R. Delle Chiaie, J. B. Curley, J. A. Byers, *Angew. Chem. Int. Ed.* **2016**, *55*, 5251-5254; b) A. J. Teator, D. N. Lastovickova, C. W. Bielawski, *Chem. Rev.* **2016**, *116*, 1969-1992.

[30] a) C. Romain, C. K. Williams, *Angew. Chem. Int. Ed.* **2014**, *53*, 1607-1610; b) C. Romain, Y. Zhu, P. Dingwall, S. Paul, H. S. Rzepa, A. Buchard, C. K. Williams, *J. Am. Chem. Soc.* **2016**, *138*, 4120-4131.

CHAPTER 5

Dinuclear Zinc Salen Catalysts for Copolymerisation of Epoxides and Carbon Dioxide or Anhydrides

Abstract

A series of four di-zinc complexes coordinated by salen ligands, derived from *ortho*-vanillin and bearing (±)-*trans*-1,2-diaminocyclohexane (L_1) or 2,2-dimethyl-1,3-propanediamine backbones (L_2), are reported. The complexes are characterised using X-ray crystallography, multinuclear NMR, DOSY and MALDI-ToF spectroscopy, and by elemental analysis. The stability of the dinuclear complexes depends on the ligand structure, with the most stable complexes having imine substituents. The complexes are tested as catalysts for ROCOP of CO_2/CHO and PA/CHO. All complexes are active and the structure/activity relationships reveal that the complex having both L_2 and imine substituents displays the highest activity. In CO_2/CHO ROCOP, its activity is equivalent to other metal salen catalysts (TOF = 44 h^{-1} at [cat] = 0.1 mol%, 30 bar of CO_2 and 80 ^oC) whilst for PA/CHO ROCOP, its activity is higher than other metal salen catalysts (TOF = 198 h^{-1} at [cat] = 1 mol% and 100 ^oC). Poly(ester-*b*-carbonate)s are also afforded using the most active catalyst by terpolymerisation of PA/CHO/CO_2.

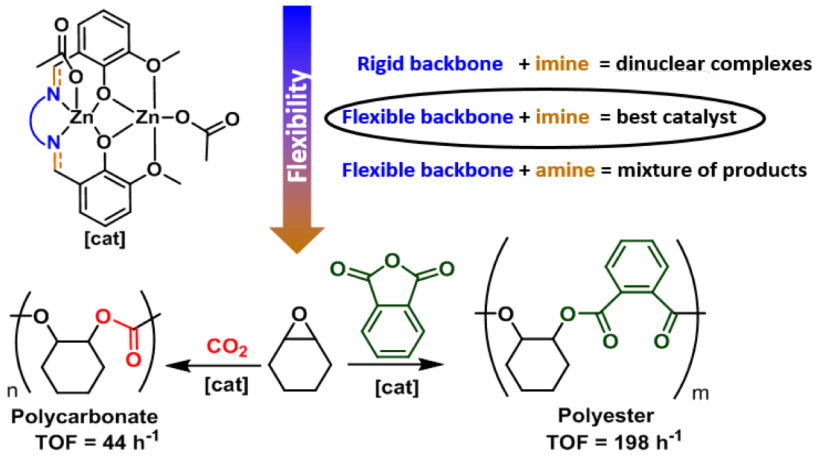

5.1 Introduction

Salen ligands are of fundamental importance in coordination chemistry and catalysis. They have been extensively studied since the pioneering work of Jacobsen[1] and Katsuki[2] using a chiral [Mn(salen)] complex for the enantioselective epoxidation of alkenes. Since then, a range of other transition metal catalysts have been reported for reactions as distinct as oxidations,[3] polymerisations[4] and epoxidations.[5] More recently, a novel class of salen ligands has been developed incorporating a Lewis donor functional group in the *ortho* position of the salicylaldehyde unit, enabling the coordination of a second metal centre within the ligand scaffold.[6] Dinuclear salen complexes, where two different metals (usually a transition metal and a lanthanide) are incorporated into the ligand, have been studied for their magnetic properties[7] and are even proposed as single-molecule magnets.[8] Such complexes are also attractive catalysts for asymmetric organic reactions, where it is proposed that they show better performances due to cooperative interactions between the two metal centres (Scheme 5.1, LHS).[9] Exactly this type of metal cooperation has also been proposed to be an important criterion in the preparation of highly active catalysts for the ring-opening copolymerisation (ROCOP) of CO_2 and epoxides (Scheme 5.1, RHS).[10]

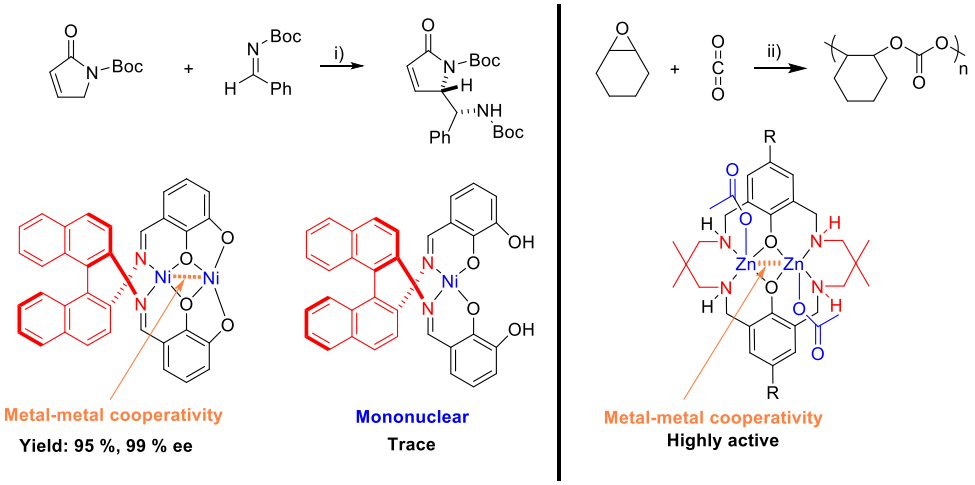

Scheme 5.1. Importance of the cooperative metal-metal interactions in dinuclear complexes used for an asymmetric Mannich-type reaction[9] and CO_2/epoxide ROCOP.[10a]

As discussed in the introduction chapter, many highly active dinuclear catalysts have been developed for CO_2/epoxide ROCOP, including those based on macrocyclic,[11] BDI,[10d, 12] Trost type 'pro-phenolate',[4d, 13] porphyrin[14] and anilido-aldimine ligand scaffolds,[15] typically coordinated to zinc, although other transition metal systems have also been investigated.[16] Mechanistic studies and DFT calculations have highlighted that the catalyst activity seems to be highly dependent on the flexibility of the ligand and the distance between the two metal centres.[10a, 10c, 11c, 17] To date, one of the most active catalyst systems for the synthesis of poly(cyclohexene carbonate) (PCHC), reported by Rieger and co-workers;[18] is based on a flexible di-zinc complex, coordinated by two β-diiminate moieties which are linked through the phenyl rings (TOF = 155 000 h^{-1} at a catalyst loading of 0.0125 mol% 100 ^{o}C, 30 bar of CO_2).

Mononuclear salen ligands coordinated to either Co(III) or Cr(III) centres and combined with a Lewis base/ionic co-catalyst have also been widely employed as catalysts for CO_2/epoxide ROCOP.[4i, 4j, 19] In this case, the interaction (ion pair formation) between the metal and co-catalyst is key of importance for the high activity.[20] Nozaki and co-workers pioneered a new generation of 'co-catalyst tethered' salen complexes, these show a significant improvement in the catalyst activity.[20] The combination of tethering the salen catalyst and co-catalyst was subsequently successfully applied by various researchers,[21] including Lu and Lee, to prepare highly active ROCOP catalysts (TOF > 20 000 h^{-1}).[22] A further benefit is that some of these tethered catalysts can be recycled from the polymer without significant loss in performance.[22g]

Another successful strategy, also initially developed by Nozaki and co-workers, has been to join together two metal salen complexes and to apply them with added co-catalyst.[23] Such dinuclear catalysts are formed using two salen ancillary ligands which have been

covalently linked to one another;[24] the catalysts show higher activity than mononuclear counterparts, particularly at low catalyst loadings.[23, 24b] Given the precedence for salen ligands and the promise of dinuclear catalysts, it is perhaps surprising that there is, so far, only a single report of ROCOP catalysts where a single salen ancillary ligand coordinates two metals.[25] The catalyst comprises a multidendate bis(benzotriazole iminophenol) ligand coordinated to two Zn(II), Ni(II) or Co(II) metal centres. The best activities were achieved with the di-Ni(II) catalyst, which for the ROCOP of cyclohexene oxide (CHO)/CO_2 shows a TOF of 53 h^{-1}, at 120 ^oC, 20 bar of CO_2.[25] These encouraging results using dinuclear salen catalysts inspired the current development of new dinuclear salen ligands and the investigation of their coordination chemistry and catalytic applications for CO_2/CHO and phthalic anhydride (PA)/CHO ROCOP. When developing new polymerisation catalysts, it is attractive to target low-cost ligands, which can be coordinated to earth-abundant metal centres.[26] *Ortho*-vanillin is an interesting candidate as it is relatively abundant and straightforward to extract from a range of plants. In addition, *ortho*-vanillin salen ligands have good precedent for the formation of dinuclear complexes, although these have not yet been applied in this area of polymerisation catalysis.[27] Zinc was also selected as the most desirable metal centre as it is abundant, non-toxic and usually results in colorless complexes.

5.2 Ligands synthesis

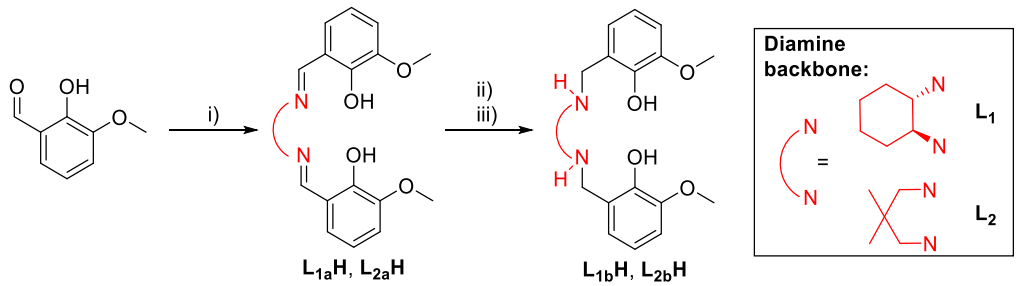

Scheme 5.2. Ligand synthesis. i) 2 equiv. *o*-vanillin, 1 equiv. corresponding diamine, MeOH, 22 °C, 4 h, (yield: > 99 %); ii) 3.5 equiv. $NaBH_4$, MeOH, 22 °C, 2 h; iii) H_2O, 22 °C, 16 h (97 % yield).

Ortho-vanillin (*o*-vanillin) was used as a starting point for the synthesis of four potential dinuclear ligands. Amination of the cheap and commercially available, *o*-vanillin, was carried out in methanol by reaction with either [(±)-*trans*-1,2-diaminocyclohexane (L_1) or 2,2-dimethyl-1,3-propanediamine (L_2)]. The reaction formed, in quantitative yield, the first two salen ligands $\mathbf{L_{1a}H}$ and $\mathbf{L_{2a}H}$ (Scheme 5.2). The ligands differ according to the diamine 'linker' group and were selected on the basis that such C_2 and C_3 linkers are common components of successful ROCOP catalysts.[11b, 11f, 20, 22a] The amination reaction was followed by ^{1}H NMR spectroscopy ($CDCl_3$) by the disappearance of the aldehyde singlet resonance at 9.82 ppm and the appearance of the imine singlet resonance at 8.24 ppm for $\mathbf{L_{1a}H}$ and 8.31 ppm for $\mathbf{L_{2a}H}$. Both ligands were fully characterised by ^{1}H and ^{13}C NMR, LC-MS and elemental analysis.

Subsequently, *in-situ* reduction using $NaBH_4$, followed by an aqueous work-up, was performed to isolate, in high yield, the two amine salan ligands $\mathbf{L_{1b}H}$ and $\mathbf{L_{2b}H}$ (Scheme 5.2). The reduction reaction was followed by ^{1}H NMR spectroscopy ($CDCl_3$) by the disappearance of the imine singlet resonance at 8.24 ppm (for $\mathbf{L_{1a}H}$) or 8.31 ppm (for $\mathbf{L_{2a}H}$) and the appearance of the benzylic resonances at 3.94 ppm for $\mathbf{L_{1b}H}$ (singlet) and 3.98 ppm for $\mathbf{L_{2b}H}$ (example illustrated in Figure 5.1). Interestingly, the benzylic resonance in $\mathbf{L_{1b}H}$ is not a singlet. Instead, the two benzylic protons at 3.88 ppm and 4.01

ppm showed an AB pattern with a $\Delta\upsilon_{AB}$ = 52.48 Hz and J_{AB} = 13.86 Hz (Figure 5.1). This phenomenon was rationalised by the rigidity of the ligand backbone and the strong hydrogen bonding between the phenol and the amine, observed with a broad signal at 5 ppm, which stabilises a single conformation. Due to this lack of rotational freedom, diasterotopic resonances were observed for the benzylic protons. This splitting is also commonly observed in other salan ligands bearing the (±)-*trans*-1,2-diaminocyclohexane backbone.[28] The two ligands were fully characterised by ^{1}H and ^{13}C NMR, LC-MS and elemental analysis. Using this one pot synthetic method in multi gram scale, large quantities of ligand with high purity were afforded in only one day.

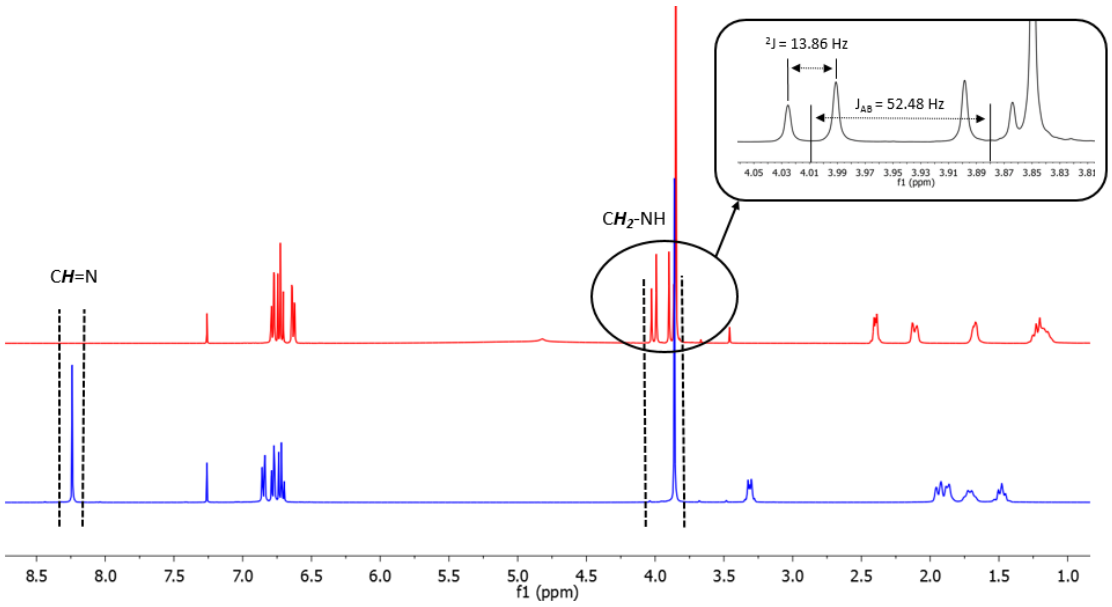

Figure 5.1. Stack of ^{1}H NMR spectra of $\mathbf{L_{1b}H}$ (lower spectrum) and $\mathbf{L_{2b}H}$ (higher spectrum) with a zoom on the benzylic region to show the large doublet of doublet ($CDCl_3$, 298 K).

5.3 Zinc Complexes

5.3.1 Zinc Complexes of $L_{1a}H$, $L_{1b}H$ and $L_{2a}H$

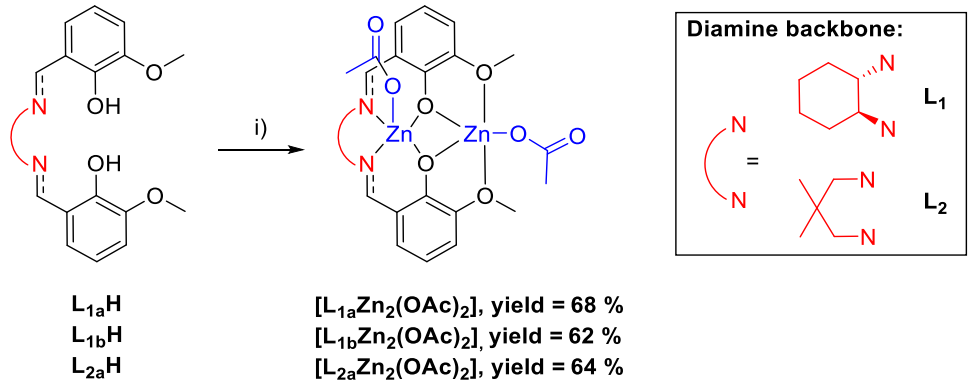

$L_{1a}H$
$L_{1b}H$
$L_{2a}H$

$[L_{1a}Zn_2(OAc)_2]$, yield = 68 %
$[L_{1b}Zn_2(OAc)_2]$, yield = 62 %
$[L_{2a}Zn_2(OAc)_2]$, yield = 64 %

Scheme 5.3. Complexation reactions with zinc acetate. i) 2 equiv. $[Zn(OAc)_2.2(H_2O)]$, MeOH, 22 °C, 16 h.

The complexation reactions of **$L_{1a}H$**, **$L_{1b}H$** and **$L_{2a}H$** were conducted in air with two equivalents of $[Zn(OAc)_2.2(H_2O)]$ in wet MeOH (Scheme 5.3). **$[L_{1a}Zn_2(OAc)_2]$**, which was insoluble in MeOH, was isolated by filtration in moderate yield, without any additional purification steps. The two other bis-zinc acetate complexes, **$[L_{1b}Zn_2(OAc)_2]$** and **$[L_{2a}Zn_2(OAc)_2]$**, were also isolated in moderate yields as white solids, after the removal of volatiles and several washings with pentane to remove the acetic acid produced during the complexation reaction. All the products were fully characterised by multinuclear NMR spectroscopy, elemental analysis and X-ray crystallography {**$[L_{1a}Zn_2(OAc)_2]$**}.

Crystals suitable for X-ray diffraction studies were obtained for **$[L_{1a}Zn_2(OAc)_2]$** by slow diffusion of pentane into a concentrated dichloromethane solution. The molecular structure of **$[L_{1a}Zn_2(OAc)_2]$** shows that both zinc centres are penta-coordinate: one within the "enclosed" phenolic site (also called "small" site), and the other in the "open" site (Figure 5.2). A κ^2-coordinated acetate ligand provides stabilisation for the dinuclear complex by bridging the two [Zn(II)] centres. The zinc centre enclosed in the "small" site is coordinated via an NNOO chelate, with similar Zn-O and Zn-N distances to previous reports (Table 5.1).[29] An acetate oxygen also coordinates to the zinc centre, which

exhibits a distorted square pyramidal geometry (τ = 0.16).[30] In contrast, the zinc occupying the "open" site has a distorted trigonal bipyramidal geometry (τ = 0.34) and is coordinated by two phenolic oxygen atoms, the bridging acetate and a terminal κ^2 acetate group. In the solid state, the two methoxy groups on the salen ligand do not coordinate to zinc [Zn2-O25, 2.764(2) Å; Zn2-O27, 2.592(2) Å]. The distance between the two zinc centres is 2.9539(5) Å, which is smaller than for reported dinuclear catalysts (~ 3.1 Å) (Table 5.1).[10a, 10b, 18b] A similar molecular structure has already been reported for the closely related hydrate complex, **[$L_{1a}Zn_2(OAc)_2 \cdot H_2O$]**, where the two zinc centres adopt distorted square pyramidal geometries (Figure 5.2).[28] The zinc centre occupying the "enclosed" site has a similar coordination mode to that of **[$L_{1a}Zn_2(OAc)_2$]** with similar bond lengths and angles. However, the zinc centre in the "open" site is coordinated to a phenolic oxygen, a methoxy group, a water molecule and two acetate ligands (one bridging and one terminal) completing the coordination sphere of the second zinc. As a result, the Zn···Zn distance is longer [3.358(1) Å] (Table 5.1). It is relevant to consider that the coordination of water by **[$L_{1a}Zn_2(OAc)_2 \cdot H_2O$]** because it indicates that the zinc coordination geometry within **[$L_{1a}Zn_2(OAc)_2$]** is likely to be altered in the presence of a Lewis donor. By analogy, under the polymerisation conditions, the epoxide (CHO) could be considered likely to coordinate to the zinc centre in the "open" site. Furthermore, the different coordination geometries of the zinc in the two structures suggest that the methoxy groups may play a role in stabilising the active sites during polymerisation.

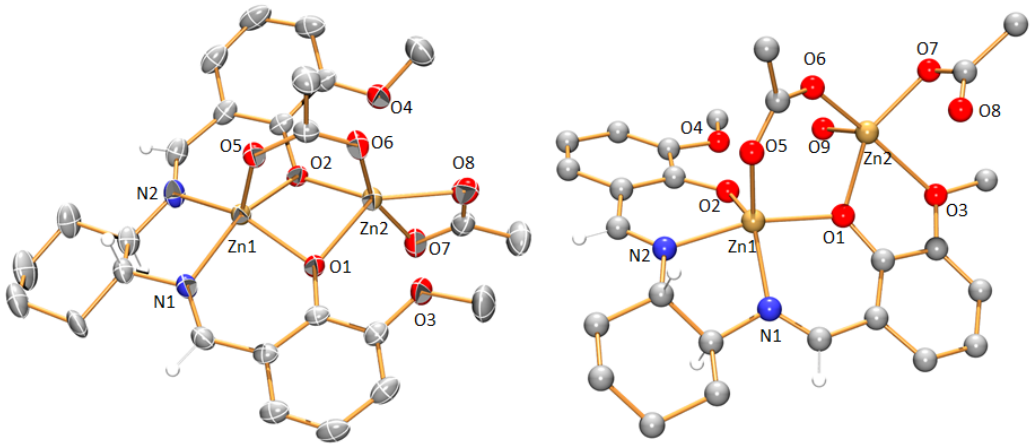

$[L_{1a}Zn_2OAc_2]$ **$[L_{1a}Zn_2OAc_2{\cdot}H_2O]$**[28]

Figure 5.2. Molecular structures of **$[L_{1a}Zn_2(OAc)_2]$** (LHS) with thermal ellipsoids at the 50 % probability level and **$[L_{1a}Zn_2(OAc)_2{\cdot}H_2O]$**[28] (RHS) with ball and stick representation. Most hydrogen atoms, a dichloromethane, a water and an ethanol molecule are omitted for clarity (refer to appendix for complete data set).

Table 5.1. Selected bond lengths (Å) and angles (°) for **$[L_{1a}Zn_2(OAc)_2]$** and **$[L_{1a}Zn_2(OAc)_2{\cdot}H_2O]$**.[28]

Bonds/angles \ Complex	**$[L_{1a}Zn_2(OAc)_2]$**	**$[L_{1a}Zn_2(OAc)_2{\cdot}H_2O]$**[28]
Zn(1)-O(1)	2.004(2)	2.046(4)
Zn(1)-O(2)	2.023(2)	1.969(5)
Zn(1)-N(1)	2.027(3)	2.090(5)
Zn(1)-N(2)	2.036(2)	2.058(4)
Zn(1)···Zn(2)	2.9539(4)	3.358(1)
O(1)-Zn(1)-N(1)	90.03(9)	88.51(2)
O(5)-Zn(1)-N(2)	115.57(10)	93.71(2)

In solution, the ^{1}H NMR spectra, in $CDCl_3$, at 298 K, of imine complexes **$[L_{1a}Zn_2(OAc)_2]$** and **$[L_{2a}Zn_2(OAc)_2]$** confirmed the two metals were coordinated, with all the resonances experiencing upfield shifts in comparison to the free ligands. Up-field shifts were observed for the imine signals (8.24 ppm in **$L_{1a}H$**, to 8.23 ppm for **$[L_{1a}Zn_2(OAc)_2]$** and from 8.31 ppm in **$L_{2a}H$**, to 8.08 ppm for **$[L_{2a}Zn_2(OAc)_2]$**) (Figure 5.3). The broadening of the methylene resonances and the loss of the phenolic proton resonance (at 13.84 ppm and 14.14 ppm) also confirmed the coordination to zinc. A new singlet resonances, at 2.00 ppm for **$[L_{1a}Zn_2(OAc)_2]$** and 1.97 ppm for **$[L_{2a}Zn_2(OAc)_2]$**, was assigned to the acetate co-ligands. Similarly, the ^{1}H NMR spectrum of the amine complex **$[L_{1b}Zn_2(OAc)_2]$** exhibited upfield resonances in comparison to those of the free ligand. In d_5-pyridine, the N-H resonances were broad (4.28 ppm) with a significant shift of the benzylic resonance (from

4.01 to 4.19 ppm), indicating that the zinc centre was coordinated in the "small" site. The acetate resonance at 2.11 ppm is assigned to both the zinc-coordinated acetate ligands.

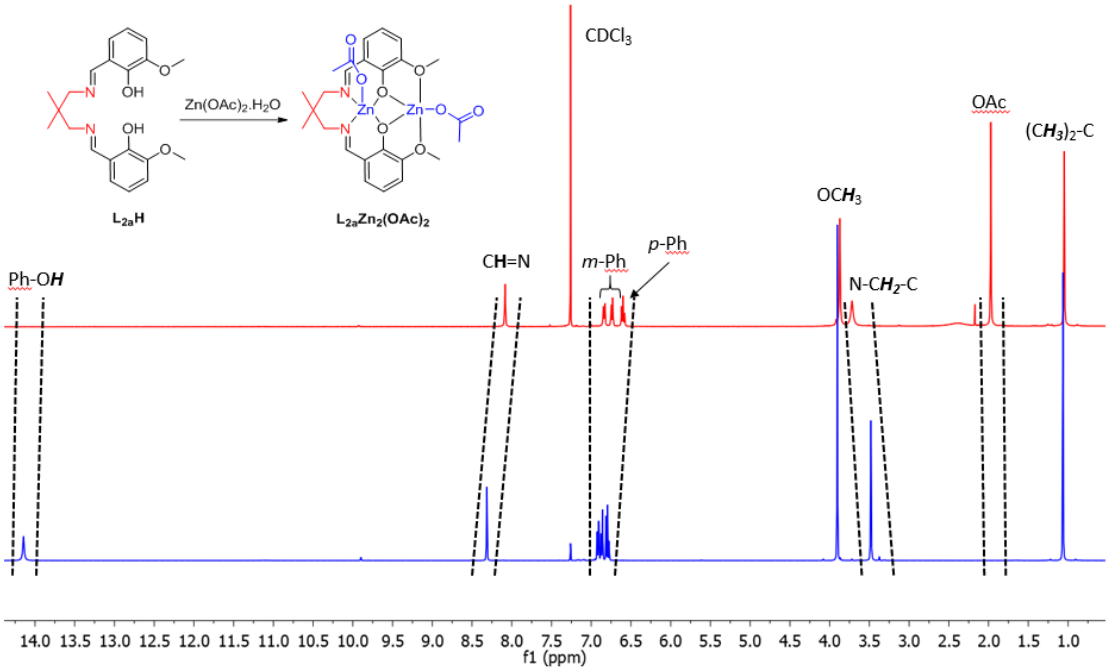

Figure 5.3. Stack of ^{1}H NMR spectra ($CDCl_3$, 298 K) of $\mathbf{L_{2a}H}$ (bottom spectrum) and $\mathbf{[L_{2a}Zn_2(OAc)_2]}$ (top spectrum).

DOSY NMR analysis of $\mathbf{[L_{2a}Zn_2(OAc)_2]}$, ($CDCl_3$, 298 K), and of $\mathbf{[L_{1b}Zn_2(OAc)_2]}$ (d_5-pyridine, 298 K) showed that in each case, all the ^{1}H NMR resonances possessed the same diffusion coefficients. The calculated molecular weights from DOSY spectra were close to the theoretical values, providing further confirmation that the dinuclear complex structures were maintained in solution. To confirm the stability of $\mathbf{[L_{2a}Zn_2(OAc)_2]}$ under typical polymerisation conditions, $\mathbf{[L_{2a}Zn_2(OAc)_2]}$ was heated to reflux for 16 h in d_8-THF. The ^{1}H NMR spectra remained constant over time, indicating that this species is thermally stable under the polymerisation conditions. Unfortunately, this test could not be performed on $\mathbf{[L_{1a}Zn_2(OAc)_2]}$ and $\mathbf{[L_{1b}Zn_2(OAc)_2]}$ as they were not soluble even in hot THF.

5.3.2 Zinc Coordination Chemistry Using $L_{2b}H$

5.3.2.1 One Pot Synthesis of $[L_{2b}Zn_2(OAc)_2]$

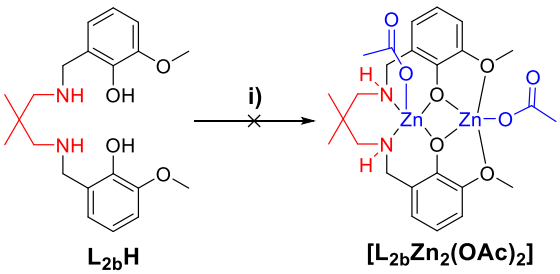

Scheme 5.4. Complexation reaction of $\mathbf{L_{2b}H}$ with zinc acetate. i) 2 equiv. $[Zn(OAc)_2.2(H_2O)]$, MeOH, 22 °C, 16 h or 2 equiv. $[Zn(OAc)_2]$, MeOH, 22 °C, 16 h.

In contrast to the other ligands, the direct reaction of $\mathbf{L_{2b}H}$ with $[Zn(OAc)_2.2(H_2O)]$ in air and with bench quality methanol was not successful (Scheme 5.4). The ^{1}H NMR spectrum of the crude product in any solvent was convoluted, no signals corresponding to the free ligand were observed. Similar results were obtained when the complexation reaction was performed under an inert atmosphere using anhydrous $[Zn(OAc)_2]$. Variation of the reaction conditions (temperature, concentration, time) did not change the composition of the final mixture.

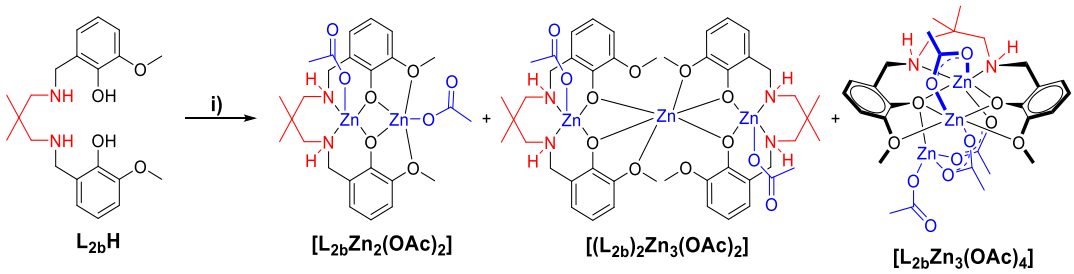

Scheme 5.5. Reactivity of $\mathbf{L_{2b}H}$ with zinc acetate giving rise to a mixture of products containing $\mathbf{[L_{2b}Zn_2(OAc)_2]}$, $\mathbf{[L_{2b}Zn_3(OAc)_4]}$ and $\mathbf{[(L_{2b})_2Zn_3(OAc)_2]}$. i) 2 equiv. $[Zn(OAc)_2.2H_2O]$, MeOH, 22 °C, 16 h. or 2 equiv. $[Zn(OAc)_2]$, MeOH, 22 °C, 16 h.

MALDI-ToF analysis of the mixture revealed the presence of the desired dinuclear complex $\mathbf{[L_{2b}Zn_2(OAc)_2]}$ {MS (MALDI-ToF): *m/z* = 563 g/mol, $\mathbf{[L_{2b}Zn_2OAc]^+}$} along with two higher molecular weight species. A a trinuclear species $\mathbf{[L_{2b}Zn_3(OAc)_4]}$ {MS (MALDI-ToF): *m/z* = 745 g/mol, $\mathbf{[L_{2b}Zn_3(OAc)_3]^+}$} and a dimeric trinuclear species $\mathbf{[(L_{2b})_2Zn_3(OAc)_2]}$ {MS (MALDI-ToF): *m/z* = 999 g/mol $\mathbf{[(L_{2b})_2Zn_3OAc]^+}$} (Scheme 5.5, Figure 5.4). DOSY NMR analysis of the product mixture, in C_6D_6, showed a range of

diffusion coefficients [-9.1 x 10^{-10} log(m^2/s) to -9.3 x 10^{-10} log(m^2/s)] confirming the presence of a mixture of product in the solution state. The predicted MW range was 496 g/mol to 977 g/mol, which is consistent with a mixture of **[$L_{2b}Zn_2(OAc)_2$]** (621 g/mol), **[$L_{2b}Zn_3(OAc)_4$]** (802 g/mol) and **[$(L_{2b})_2Zn_3(OAc)_2$]** (1061 g/mol).

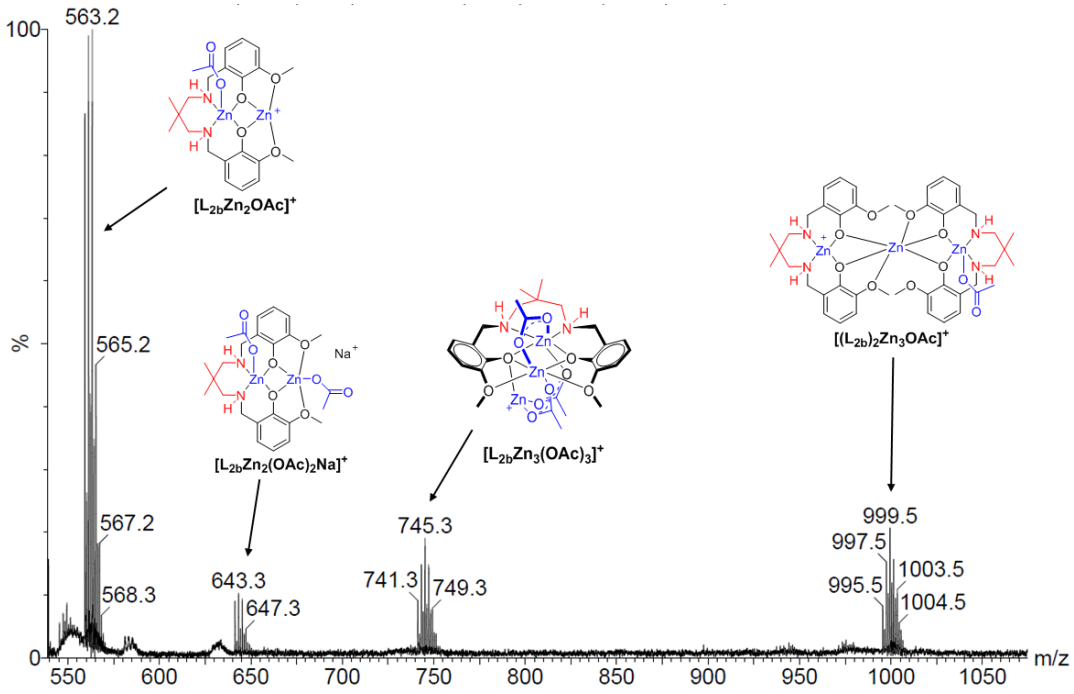

Figure 5.4. MALDI-ToF spectrum of the mixture obtained from the reaction of **$L_{2b}H$** with 2 equiv. of [$Zn(OAc)_2$].

5.3.2.2 A Stepwise Procedure to Target [$L_{2b}Zn_2OAc_2$]

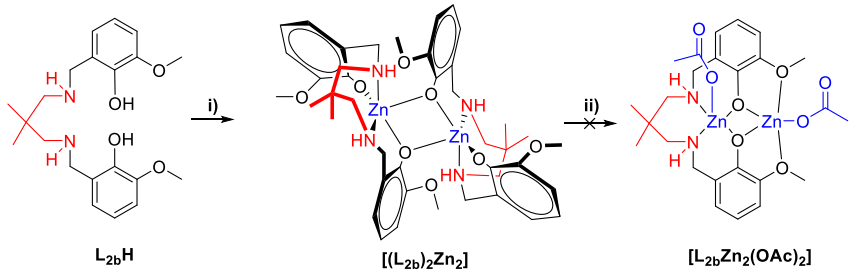

Scheme 5.6. Synthetic strategy to isolate the dinuclear **[$L_{2b}Zn_2(OAc)_2$]** complex. i) 1 equiv. [$ZnEt_2$] or 1 equiv. [$Zn(OAc)_2$], THF ii) 1 equiv. [$Zn(OAc)_2$], THF (yield: ~ 60 %).

An alternative stepwise procedure was explored as a route to pure **[$L_{2b}Zn_2(OAc)_2$]** (Scheme 5.6). Accordingly, **$L_{2b}H$** was deprotonated, using either [$Zn(OAc)_2$] or [$ZnEt_2$], in dry MeOH or dry THF, under an inert atmosphere, and a white precipitate was formed.

The product was isolated, via anaerobic filtration, and was fully characterised by X-ray crystallography, multinuclear NMR spectroscopy and elemental analysis.

The solid state structure of **[$(L_{2b})_2Zn_2$]** has been determined as both the THF and methanol solvates. Although the two solvates are very distinct crystallographically (with the structure of the THF solvate containing one independent C_i-symmetric complex, whereas that of the methanol solvate contains two independent C_i-symmetric complexes), the conformations of all three complexes are very similar. For simplicity, only the THF solvate (Figure 5.5) will be discussed here with full crystallographic details are available in the Appendix. **[$(L_{2b})_2Zn_2$-THF]** has a dimeric structure with C_i symmetry, with Zn_2O_2 core where one phenolic oxygen from each ligand bridges between the two zinc metal centres. The complex has similar bond lengths to **[$L_{1a}Zn_2(OAc)_2$]**. The zinc centres each adopt a distorted trigonal bipyramidal geometry (τ = 0.70) and the methoxy groups do not coordinate.

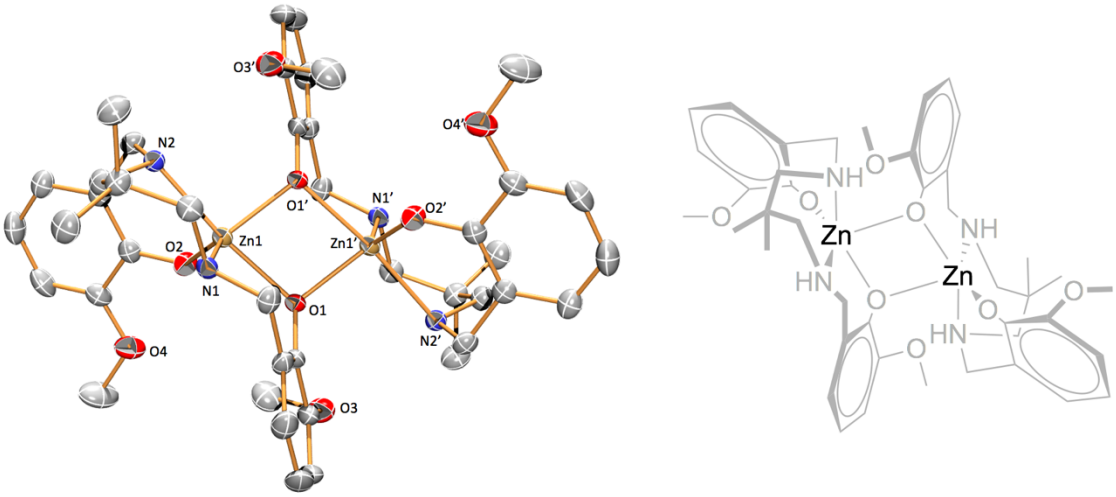

Figure 5.5. Molecular structure of **[$(L_{2b})_2Zn_2$-THF]** (LHS) with thermal ellipsoids at the 50 % probability level. Hydrogen atoms, as well as three THF molecules, are omitted for clarity (refer to appendix for complete data set). Schematic representation of **[$(L_{2b})_2Zn_2$-THF]** (RHS).

In solution, the aggregation was retained as the ^{1}H NMR spectrum, in d_8-THF at 298 K, shows 20 different proton environments: as expected for a dimeric structure with C_i symmetry containing two asymmetric **[$L_{2b}Zn$]** substructures (Figure 5.6). Each benzylic

proton was diastereotopic and could be differentiated as only one environment couples with the NH group. The same phenomenon was observed for the methylene protons. This coupling is characteristic of metal coordination.[11a] The absence of any Zn-Et resonances also suggested that only one metal is coordinated to the dianionic ligand. Two separate methoxy resonances were observable, showing that the ether groups were in different environments and providing further evidence for the formation of the dimer in solution. DOSY NMR also led to a predicted molecular weight of 753.69 g/mol, which is in reasonable agreement with that of the dimeric species (875.7 g/mol).

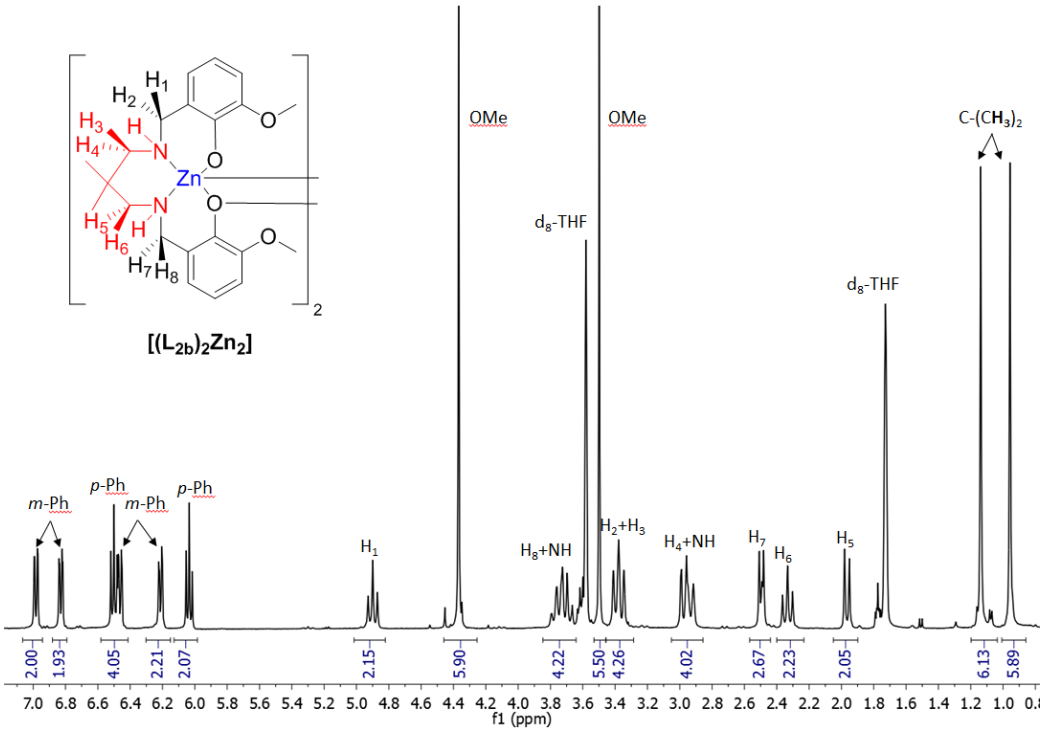

Figure 5.6. ^{1}H NMR spectrum of **[(L$_{2b}$)$_2$Zn$_2$]** (d_8-THF, 298 K).

When the dimer **[(L$_{2b}$)$_2$Zn$_2$]** was reacted with one equivalent of [Zn(OAc)$_2$], at room temperature, the same product mixture was obtained as when the ligand was reacted with two equivalents of [Zn(OAc)$_2$] (Scheme 8). Once again, changing the reaction conditions (temperature, dilution, and reaction time) did not have any influence on the composition of the final mixture.

5.3.2.3 Synthesis of $[L_{2b}Zn_2Et_2]$ and Subsequent Reaction to a Zinc Carbonate

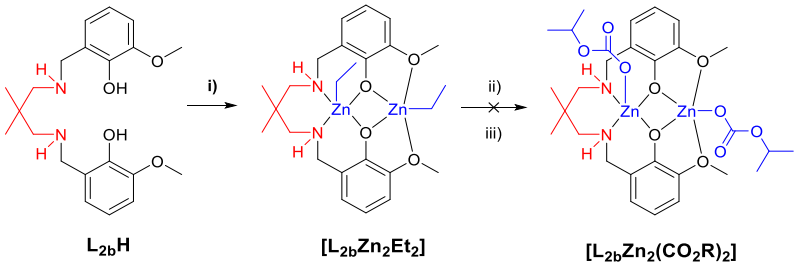

Scheme 5.7. Stepwise strategy to synthesis of **$[L_{2b}Zn_2(CO_2R)_2]$**. i) 2 equiv. [$ZnEt_2$] (yield: 75 %), THF ii) 2 equiv. HO^iPr, THF iii) CO_2, THF.

An alternate pathway to isolate a dinuclear zinc carbonate complex is illustrated in Scheme 5.7. When the dimer **$[(L_{2b})_2Zn_2]$** was reacted with [$ZnEt_2$], in THF at 22 °C, a new product was cleanly formed. The product was isolated as a white powder in quantitative yield (Scheme 5.8). The same product was also afforded by a stepwise addition of [$ZnEt_2$] to **$L_{2b}H$** by addition of an equivalent of [$ZnEt_2$] to form **$[(L_{2b})_2Zn_2]$** which was further reacted, *in-situ,* with a second equivalent of [$ZnEt_2$] (Scheme 5.8).

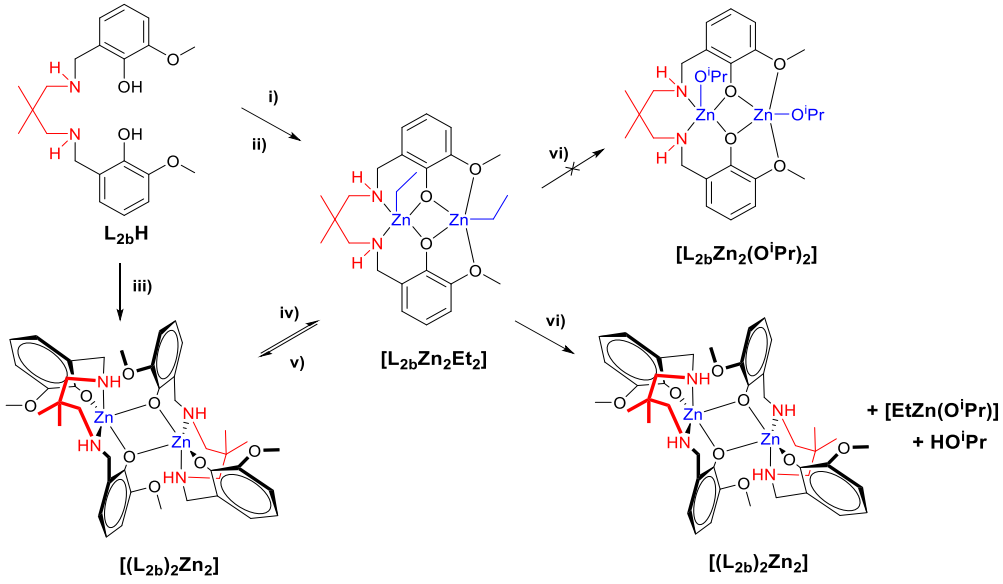

Scheme 5.8. Proposed synthetic route to **$[L_{2b}Zn_2(O^iPr)_2]$**. i) 1 equiv. [$ZnEt_2$], THF, 1 h, 22 °C, ii) 1 equiv. [$ZnEt_2$], THF, 16 h, 22 °C, iii) 1 equiv. [$ZnEt_2$], THF, 16 h, 22 °C, iv) 1 equiv. [$ZnEt_2$], THF, 16 h, 22 °C, v) 1 equiv. **$L_{2b}H$**, C_6D_6. 1 h, 22 °C, vi) 2 equiv. HO^iPr, C_6D_6, 1 h, 22 °C.

The ^1H NMR spectrum of the product, in C_6D_6 at 298 K, showed no trace of the ligand or the dimer and all resonances were shifted upfield, consistent with the coordination of a second zinc centre (Figure 5.7). Two sets of diastereotopic resonances with large coupling

constants were observed for the benzylic protons, consistent with zinc coordination. Two different sets of characteristic Zn-ethyl resonances were observed, with two triplets at 2.05 ppm and 1.79 ppm and the corresponding quartets at 0.94 ppm and 0.61 ppm. These chemical shifts were significantly different to those of diethylzinc [1.11 ppm (t) and 0.12 ppm (q) in C_6D_6],[31] confirming the coordination of the second zinc centre by the ligand. The dinuclearity of the complex was also confirmed by DOSY NMR spectroscopy (C_6D_6 at 298 K). All the resonances of **[$L_{2b}Zn_2Et_2$]** possessed the same diffusion coefficient. The ^{1}H NMR spectrum of **[$L_{2b}Zn_2Et_2$]** suggested a higher symmetry, perhaps with a C_2 symmetry compared to **[$(L_{2b})_2Zn_2$]**. It also suggested that the addition of the extra zinc cleaves the dimer to form a monomeric **[$L_{2b}Zn_2Et_2$]**. This hypothesis was confirmed by DOSY NMR where the estimated molecular weight was 503 g/mol, consistent with the value calculated for **[$L_{2b}Zn_2Et_2$]** product (561 g/mol).

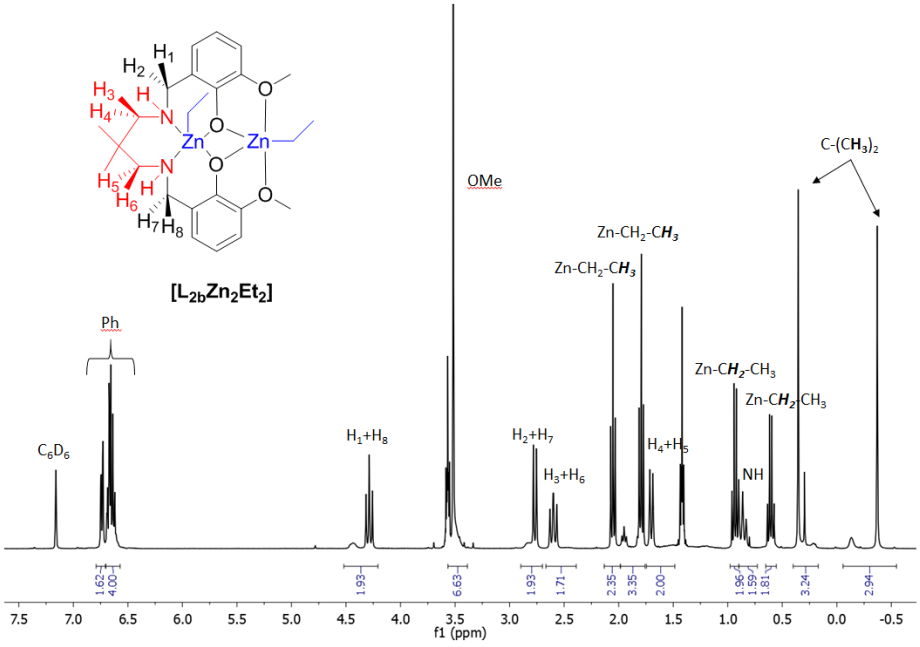

Figure 5.7. ^{1}H NMR spectrum of **[$L_{2b}Zn_2Et_2$]** (C_6D_6, 298 K).

The protonolysis reaction of **[$L_{2b}Zn_2Et_2$]** with isopropanol to form **[$L_{2b}Zn_2(O^iPr)_2$]** was then investigated (Scheme 5.8). When two equivalents of isopropanol were added to a solution of **[$L_{2b}Zn_2Et_2$]**, in C_6D_6, at 298 K, the alkoxide complex **[$L_{2b}Zn_2(O^iPr)_2$]** was not

afforded. Instead, the dimeric compound **[(L$_{2b}$)$_2$Zn$_2$]** was formed again. The ^{1}H NMR spectrum showed release of ethane, with a characteristic resonance at 0.80 ppm in C_6D_6 solvent. Nevertheless, an ethyl group was still coordinated to zinc. In addition, characteristic resonances were also observed for coordinated isopropanol (4.00 ppm). Integration of these resonances indicated a ratio Et:^{i}OPr of 1:1 suggesting the formation of a heteroleptic ethyl zinc isopropoxide species as a side product. The combination of high ligand flexibility and the open coordination site are proposed to complicate the formation of stable dinuclear complexes. To emphasise the lability of the metal centres within this ligand system, one equivalent of free ligand was added to a solution of **[L$_{2b}$Zn$_2$Et$_2$]**, in C_6D_6 at 298 K (Scheme 8). The instantaneous formation of a precipitate was observed, with concomitant release of ethane. The white precipitate was isolated, dissolved in d_8-THF and the resultant spectrum corresponded to the dimer **[(L$_{2b}$)$_2$Zn$_2$]**.

5.3.2.4 Quantification of the by-Products

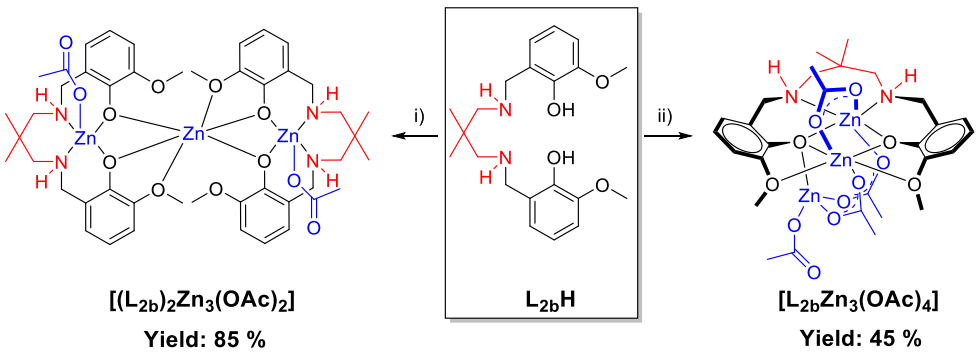

Scheme 5.9. Synthetic procedure to isolate **[L$_{2b}$Zn$_3$(OAc)$_4$]** and **[(L$_{2b}$)$_2$Zn$_3$(OAc)$_2$]**. i) 1.5 equiv. [Zn(OAc)$_2$], MeOH, 22 °C, 16 h. ii) 3 equiv. [Zn(OAc)$_2$], MeOH, 22 °C, 16 h.

Further investigations were carried out to quantify the ratio of the reaction products **[L$_{2b}$Zn$_2$(OAc)$_2$]**, **[L$_{2b}$Zn$_3$(OAc)$_4$]** and **[(L$_{2b}$)$_2$Zn$_3$(OAc)$_2$]**. Complexes **[L$_{2b}$Zn$_3$(OAc)$_4$]** and **[(L$_{2b}$)$_2$Zn$_3$(OAc)$_2$]** were independently synthesised by the reaction of **L$_{2b}$H** with 3 equivalents or 1.5 equivalents of [Zn(OAc)$_2$], in THF, respectively (Scheme 5.9). Both complexes were isolated as white powders in moderate yields.

Colourless block crystals of **[$L_{2b}Zn_3(OAc)_4$]** suitable for X-ray diffraction were obtained by slow diffusion of pentane into a saturated dichloromethane solution (Figure 5.8). The molecular structure reveals that Zn1 and Zn2 are both octahedral, while Zn3 is tetrahedral. Zn1 is coordinated at phenolate site and by two bridging acetate ligands. The Zn-O1 (2.241 Å) distance is slightly longer than for other structures {1.925 Å for **[$(L_{2b})_2Zn_2$-THF]** and 2.003 Å for **[$L_{1a}Zn_2(OAc)_2$]**} due to the coordination of Zn3 by O1. The other Zn-O and Zn-N distances are similar to previous structures. Zn2 is coordinated at the open phenolic site by both methoxy groups, although the bond distance is rather long [Zn2-O24, 2.330(4) Å and Zn2-O20, 2.576(4) Å], with two bridging acetate ligands providing further stabilisation. Zn3 is only coordinated to one phenolic oxygen and is coordinated to the other zinc centres via two κ^2-bridging acetate ligands, with coordination by an additional, terminal acetate ligand. The ligand adopts a bowl shape and has a very similar structure to the related tri-zinc complex coordinated by a bis(phenolate) tetra(amine) macrocycle.[11f]

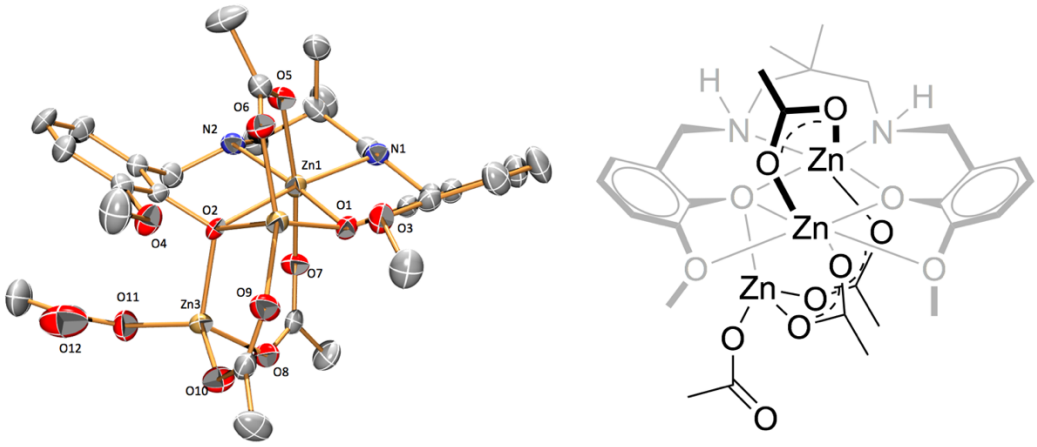

Figure 5.8. Molecular structure of **[$L_{2b}Zn_3(OAc)_4$]** (LHS) with thermal ellipsoids at the 50 % probability level. Hydrogen atoms are omitted for clarity (refer to appendix for complete data set). Schematic representation of **[$L_{2b}Zn_3(OAc)_4$]** (RHS).

The ^{1}H NMR spectrum of **[$L_{2b}Zn_3(OAc)_4$]**, in C_6D_6 at 298 K, showed two sets of resonances for the benzylic protons (4.69 ppm and 2.99 ppm) and for the methylene protons (2.83 ppm and 1.94 ppm) as expected upon zinc coordination (Figure 5.9).

Although the acetate resonance overlapped with the NH and methylene ligand resonances, its integration was in reasonable agreement with the presence of four acetate co-ligands. In addition, the DOSY NMR spectrum shows that all the resonances possess the same diffusion coefficient, and gave a calculated molecular weight of 725 g/mol, which is in reasonable agreement with the calculated value (802 g/mol).

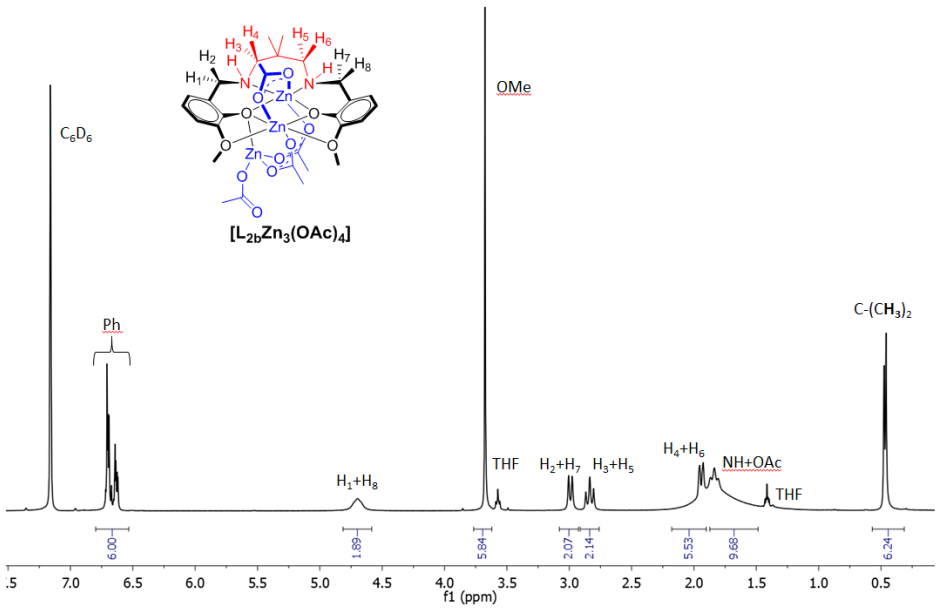

Figure 5.9. ^{1}H NMR spectrum of **[$L_{2b}Zn_3(OAc)_4$]** (C_6D_6, 298 K).

The reaction of 1.5 equivalents of [$Zn(OAc)_2$] with **$L_{2b}H$** gave a convoluted ^{1}H NMR spectrum in C_6D_6. No signals from the unreacted ligand, dimeric **[$(L_{2b})_2Zn_2$]** or the trimetallic species **[$L_{2b}Zn_3(OAc)_4$]** were observed, suggesting a new product. DOSY NMR spectroscopy reveals that the new resonances all possessed the same diffusion coefficient, corresponding to a molecular weight of 978 g/mol which is in close agreement with the value for **[$(L_{2b})_2Zn_3(OAc)_2$]** (1063 g/mol). Although crystals of **[$(L_{2b})_2Zn_3(OAc)_2$]** suitable for X-ray diffraction experiments were not obtained, it was possible to grow crystals for the closely related trizinc bis(chloride) complex, **[$(L_{2b})_2Zn_3Cl_2$]**, providing further support for the formation of a trizinc dimeric complex coordinated by the ancillary ligands (Figure 5.10).[32] The structure of **[$(L_{2b})Zn_3Cl_2$]** showed the complex has a C_2 axis. Zn1 is coordinated to the two phenolic oxygen atom and to one of the methoxy groups

from each ligand in a distorted octahedral geometry. As for the other structures, Zn2 in coordinated by the NNOO chelate with similar Zn-O and Zn-N distances. A chloride ligand is also coordinated to Zn2 to form a square pyramidal geometry.

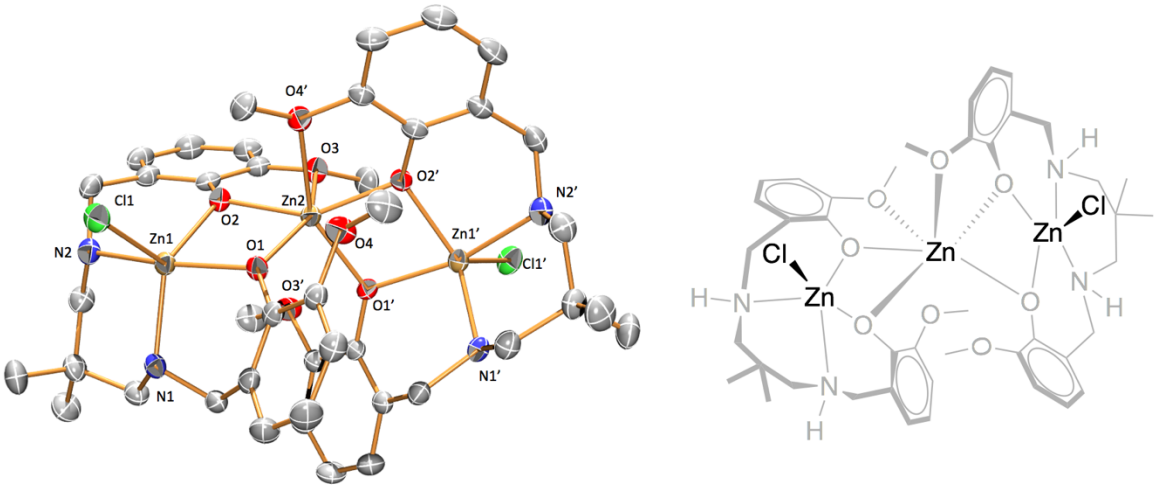

Figure 5.10. Molecular structure of **[$(L_{2b})_2Zn_3Cl_2$]** with thermal ellipsoids at the 50 % probability level. Hydrogen atoms and two THF molecules are omitted for clarity (refer to appendix for complete data set).

Comparison of the ^{1}H NMR spectra of **[$L_{2b}Zn_3(OAc)_4$]** and **[$(L_{2b})_2Zn_3(OAc)_2$]** with the products obtained from the reaction of **$L_{2b}H$** with two equivalents of [$Zn(OAc)_2$] suggested that **[$L_{2b}Zn_3(OAc)_4$]** and **[$(L_{2b})_2Zn_3(OAc)_2$]** were the two major components. DOSY NMR spectroscopy of the mixture provided further support for this observation, as two major species were observed with diffusion coefficients that correspond exactly to the values obtained for the independently prepared complexes **[$L_{2b}Zn_3(OAc)_4$]** and **[$(L_{2b})_2Zn_3(OAc)_2$]**. A third product was also present, albeit in very low concentration, which was likely to be the desired dinuclear complex [$L_{2b}Zn_2(OAc)_2$]. These findings suggested that using this ligand, the formation of the dinuclear complex was not favorable and that metal rearrangement occured to form **[$L_{2b}Zn_3(OAc)_4$]** and **[$(L_{2b})_2Zn_3(OAc)_2$]**. This was further supported by **[$L_{2b}Zn_3(OAc)_2$]** being isolated as a white precipitate from the reaction of **$L_{2b}H$** and two equivalents of [$Zn(OAc)_2$] at -78 ^{o}C. As the dinuclear complex was not isolated, the **[$L_{2b}Zn_2(OAc)_2$]** mixture, **[$L_{2b}Zn_3(OAc)_4$]** and

[$(L_{2b})_2Zn_3(OAc)_2$] were each tested within polymerisation studies. Overall, **$L_{2b}H$** did not form a dinuclear zinc complex probably due to the ligand flexibility. Formation of aggregates is, therefore, thermodynamically favored. On the plus side, **[$(L_{2b})_2Zn_2$]** could be used as a platform to target heterodinuclear complexes.

5.4 CO_2/CHO and PA/CHO Copolymerisation Catalysis

5.4.1 CO_2/CHO Copolymerisation Studies

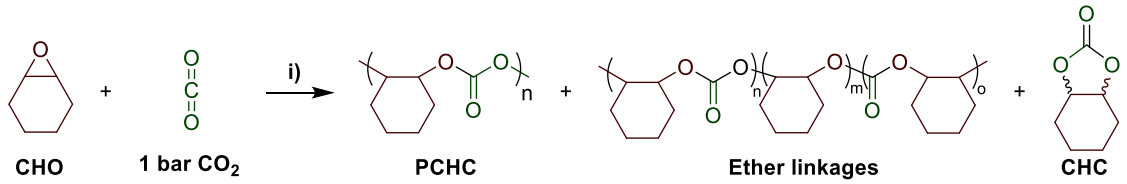

Scheme 5.10. Copolymerisation of CHO and CO_2 i) [cat], 1 mol% loading, 1 bar CO_2, 80 ^oC or [cat], 0.1 mol% loading, 30 bar CO_2, 80 ^oC.

The series of di-zinc complexes were tested as ROCOP catalysts, at 1 bar pressure of CO_2 and 80 ^oC (Scheme 5.10). As other dizinc catalysts are active under these conditions, direct comparison could be drawn.[11g, 13a, 18a] All catalysts displayed low activity, therefore, high catalyst loadings were required (Table 5.2). In particular, complexes containing the L_1 ligand backbone {**[$L_{1a}Zn_2(OAc)_2$]**, and **[$L_{1b}Zn_2(OAc)_2$]**} showed negligable TOF values (~ 0.1 h^{-1}) at a catalyst loading of 1 mol% vs. CHO. These low activities are attributed to the poor solubility of the catalyst in CHO. With the L_2 backbone, the **[$L_{2b}Zn_2(OAc)_2$]** mixture displayed improved solubility in hot CHO and showed slightly higher TOF values of 2 h^{-1}. However, after the first four and half hours of reaction, a white precipitate formed and the TOF decreased to 0.3 h^{-1}. Similarly, **[$L_{2b}Zn_3(OAc)_4$]** was active during the first six hours of polymerisation (TOF = 3 h^{-1}) with similar activity to a trizinc macrocycle catalyst reported previously,[11f] however the polymers had only low carbonate linkage content, with 45 % of ether linkages. Again, formation of a white precipitate was observed after six hours and the activity of the catalyst decreased (TOF = 1 h^{-1} after 24 hours). The white solid was isolated and its ^1H NMR spectrum ($CDCl_3$) showed catalyst decomposition. This observation suggests that the trizinc complex decomposes during polymerisation, most likely to form **[$(L_{2b})_2Zn_2$]** and [$Zn(OAc)_2$]. Under these conditions, the catalysts produced only oligomers with low molecular weights. However, slightly higher activities (TOF = 2 h^{-1} and 1 h^{-1}) were obtained with the more stable **[$L_{2a}Zn_2(OAc)_2$]** and **[$(L_{2b})_2Zn_3(OAc)_2$]**.

The imine complex **[$L_{2a}Zn_2(OAc)_2$]** also showed an improved CO_2 uptake compared to the rest of the series, producing almost perfectly alternating copolymers of low molecular weight (1500 g/mol). Despite the low activities recorded for all the catalysts, the observations from this set of experiments suggested that complexes containing the L_1 backbone tend to have lower activity compared to those with the L_2 backbone, probably due to their lack of solubility in neat CHO at high loadings.

Table 5.2. Copolymerisation of CO_2 and CHO at 1 bar pressure of CO_2 and 80 °C

Catalyst	TON[a]	TOF[b] (h^{-1})	% Carbonate linkages[c]	% Polymer selectivity[c]	M_n[d] (g/mol)	Đ[d]	Time
[$L_{1a}Zn_2(OAc)_2$]	15	0.2	71	84	400	1.09	4d
[$L_{1b}Zn_2(OAc)_2$]	14	0.1	77	83	400	1.10	4d
[$L_{2a}Zn_2(OAc)_2$]	45	2	> 99	87	1500	1.3	1d
[$L_{2b}Zn_2(OAc)_2$] mix	9	2	> 99	80	-	-	4.5h
[$L_{2b}Zn_2(OAc)_2$] mix	30	0.3	88	82	1000	1.17	4d
[$L_{2b}Zn_3(OAc)_4$][e]	19	3	45	92	-	-	6h
[$L_{2b}Zn_3(OAc)_4$][e]	24	1	52	93	-	-	24h
[$(L_{2b})_2Zn_3(OAc)_2$]	23	1	52	77	400	1.17	1d
di-zinc macrocycle catalyst[11f], f	99	17	> 99	> 99	1300	1.23	6h
tri-zinc macrocycle catalyst[11f], f	96	4	> 99	97	3400	1.21	1d

Copolymerisation conditions: catalyst/CHO = 1 mol%, 80 °C, 1 bar of CO_2. [a]TON = number of moles of epoxide consumed per mole of catalyst; [b]TOF = TON/h; [c]Determined by comparison of the integrals of signals arising from the methylene protons in the ^{1}H NMR spectra due to copolymer carbonate linkages (δ = 4.65 pmm), copolymer ether linkages (δ = 3.45 ppm) and the signals due to the cyclic carbonate byproduct (δ = 4.00 ppm);[11g] [d]Determined by SEC, at 40 °C in THF calibrated using polystyrene standards; [e]Catalyst/CHO = 0.5 mol%; [f]Catalyst/CHO = 0.1 mol%.

Previously, some di-zinc complexes showed activities dependent on CO_2 pressure; indeed this was observed for complexes coordinated by flexible ligands.[17] Therefore, the catalysts were also tested at 30 bar of CO_2 pressure. In all cases, an improvement in the catalytic activity was observed, as all the complexes produced PCHC at much lower catalyst loading (0.1 mol% catalyst vs. CHO) (Table 5.3). Nevertheless, the activity of **[$L_{1a}Zn_2(OAc)_2$]**, **[$L_{1b}Zn_2(OAc)_2$]**, the **[$L_{2b}Zn_2(OAc)_2$]** mixture and **[$(L_{2b})_2Zn_3(OAc)_2$]** were still very low. On the other hand, **[$L_{2a}Zn_2(OAc)_2$]** and **[$L_{2b}Zn_3(OAc)_4$]** showed a significant enhancement in their catalytic activities (TOF = 44 h^{-1} and 9 h^{-1} respectively) and polymer selectivities. The best catalyst, **[$L_{2a}Zn_2(OAc)_2$]** has comparable activity to other metal salen catalysts[4g, 19e] and to the di-nickel salen complex (TOF = 56 h^{-1}).[25] At

80 °C, **[$L_{2a}Zn_2(OAc)_2$]** formed PCHC with a high carbonate linkage content and polymer selectivities (M_n = 18, 800 g/mol, Đ = 1.6). These results suggest that the more flexible L_2 backbone gave catalysts with higher activity than those with the L_1 backbone.

Table 5.3. Copolymerisation of CO_2 and CHO at 30 bar pressure of CO_2 and 80 °C

Catalyst	TON[a]	TOF[b] (h^{-1})	% Carbonate linkages[c]	% Polymer selectivity[c]
[$L_{1a}Zn_2(OAc)_2$]	34	2	> 99	98
[$L_{1b}Zn_2(OAc)_2$]	16	1	> 99	89
[$L_{2a}Zn_2(OAc)_2$]	706	44	> 99	94
[$L_{2b}Zn_2(OAc)_2$] mix	29	2	> 99	94
[$L_{2b}Zn_3(OAc)_4$]	147	9	75	87
[$(L_{2b})_2Zn_3(OAc)_2$]	28	2	> 99	89

Copolymerisation conditions: catalyst/CHO = 0.1 mol%, 80 °C, 30 bar of CO_2, 16 h; [a]TON = number consumed per mole of catalyst; [b]TOF = TON/h; [c]Determined by comparison of the integrals of signals arising from the methylene protons in the ^{1}H NMR spectra due to copolymer carbonate linkages (δ = 4.65 pmm), copolymer ether linkages of moles of epoxide(δ = 3.45 ppm) and the signals due to the cyclic carbonate byproduct (δ = 4.00 ppm).[11g]

5.4.2 PA/CHO Copolymerisation Studies

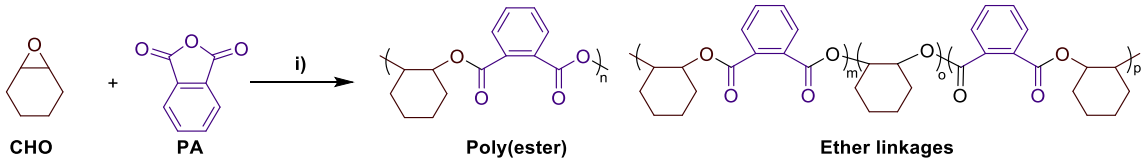

Scheme 5.11. Copolymerisation of CHO and PA i) catalyst/PA/CHO = 1/100/800, 100 °C.

The series of catalysts were also tested for the ROCOP of PA and CHO (Scheme 5.11). In 2014, Lu et al. reported that **[$L_{1a}Zn_2(OAc)_2{\cdot}H_2O$]** could polymerise maleic anhydride and CHO when an equivalent of DMAP was present.[28] In this case, all catalysts fully polymerised PA, in 16 hours, without the need for a co-catalyst (Table 5.4). While the imine complexes afforded the corresponding polyesters with high selectivity and no ether linkages, the amine complexes provided the polymers with a greater proportion of ether linkages. A possible explanation for this trend is that the more electron donating imine decreases the Lewis acidity of the metal centre, thereby decreasing the likelihood of successive ring opening two CHO molecules. Comparing the catalyst activities, **[$L_{1a}Zn_2(OAc)_2$]** gave similar activities (TOF = 70 h^{-1}) to some of the best catalysts based on chromium, cobalt or aluminium salen/salophen complexes,[16a] all of which require the use of a co-catalyst. On the other hand, **[$L_{2a}Zn_2(OAc)_2$]** was significantly more active

(TOF = 198 h^{-1}) than the majority of other known catalysts for this reaction, under similar conditions.[11a, 33] Both **[$L_{1a}Zn_2(OAc)_2$]** and **[$L_{2a}Zn_2(OAc)_2$]** afforded polymers with high ester linkages and with narrow dispersities.

Table 5.4. Copolymerisation data for ROCOP using phthalic anhydride and cyclohexene oxide, at 100 °C.

Catalyst	Time	Conv.[a] (%)	TON[b]	TOF (h^{-1})[c]	% Ester linkages[d]	M_n[e] (kDa)	Đ[e]
[$L_{1a}Zn_2(OAc)_2$]	1 h	70	70	70	> 99	4400	1.15
[$L_{1b}Zn_2(OAc)_2$]	6 h	64	64	11	27	6400	2.18
[$L_{2a}Zn_2(OAc)_2$]	30 min	99	99	198	> 99	5300	1.23
[$L_{2b}Zn_2(OAc)_2$] mix	6 h	59	59	10	21	8200	2.17
[$L_{2b}Zn_3(OAc)_4$]	1 h	28	28	28	13	7400	2.75
[$(L_{2b})_2Zn_3(OAc)_2$]	6 h	61	61	10	26	7700	2.24

Copolymerisation conditions: catalyst/PA/CHO = 1/100/800, 100 °C; [a]Determined by ^{1}H NMR spectroscopy (d_6-DMSO) by integrating the normalised resonances for PA (7.97 ppm) and the phenylene signals polyester (7.30–7.83 ppm); [b]TON = number of moles of epoxide consumed per mole of catalyst; [c]TOF = TON/h; [d]Determined by ^{1}H NMR spectroscopy (d_6-DMSO) by integrating the normalised resonances for ester linkages (4.80–5.26 ppm) and ether linkages (3.22–3.64 ppm);[33] [e]Determined by SEC, in THF at 40 °C, calibrated using polystyrene standards.

5.4.3 Terpolymerisation of PA/CHO/CO_2

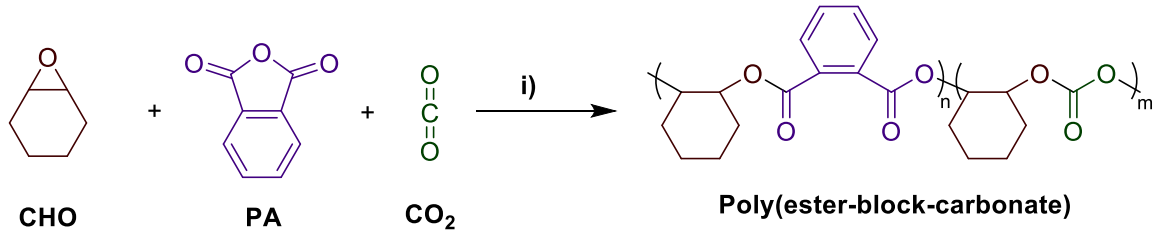

Scheme 5.12. Terpolymerisation of PA/CHO/CO_2. i) **[$L_{2a}Zn_2(OAc)_2$]**, catalyst/PA/CHO: 1/100/1000, 30 bar CO_2, 100 °C, 18 h.

The promising performance of **[$L_{2a}Zn_2(OAc)_2$]** for both CHO/CO_2 and PA/CHO ROCOP prompted the investigation of the terpolymerisation (PA/CHO/CO_2, Scheme 5.12). The reaction was carried out at 100 °C, and 30 bar of CO_2 and with a 100/1000 mixture of PA/CHO. The reaction was monitored by taking aliquots after 2 h and 18 h. After 2 h, ^{1}H NMR analysis showed selective polyester formation, with the appearance of a distinctive resonance at 5.06 ppm (74 % conversion) and with no traces of PCHC (Figure 5.11). ^{1}H NMR analysis after 18 h showed full conversion of PA (complete disappearance of the resonances at 7.84 and 7.95 ppm) and the formation of PCHC (increase of intensity of the resonance at 4.64 ppm). Between 2 h and 18 h, a clear increase in the molecular weight

was observed, from 3600 g/mol to 7100 g/mol, whilst dispersity remained narrow (Đ = 1.20). DOSY and ^{13}C NMR analysis of the crude polymer suggest that the polyester and PCHC blocks were connected, as both sets of resonances have the same diffusion coefficient of -9.81 x 10^{-10} log(m^2/s) and only two carbon signal were observed in the carbonyl region (162.7 ppm and 166.6 ppm). This evidence suggests that **[$L_{2a}Zn_2(OAc)_2$]** is successful in the synthesis of poly(ester-*block*-carbonates) from a one pot reaction with PA/CHO/CO_2.

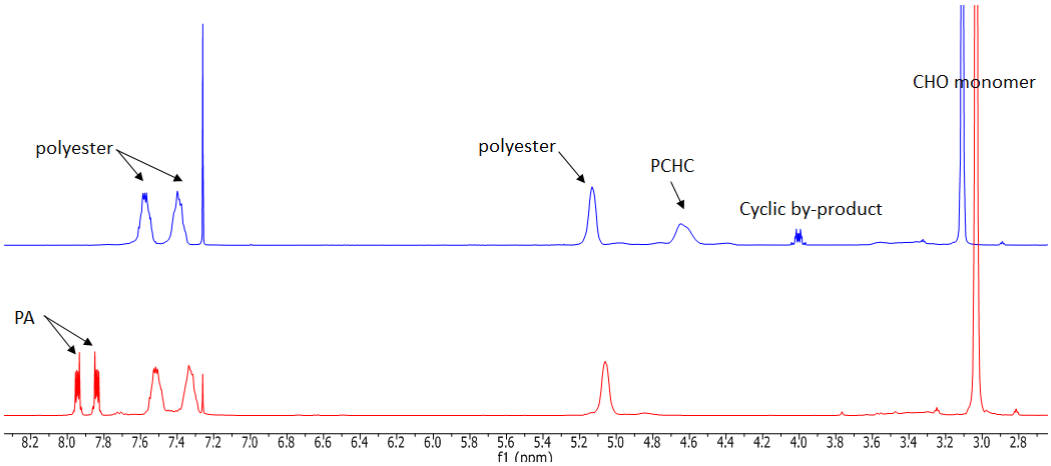

Figure 5.11. Overlaid ^1H NMR spectra of the terpolymerisation of PA/CHO/CO_2 using **[$L_{2a}Zn_2(OAC)_2$]** after 2 h of reaction (bottom) and 18 h of reaction (top) ($CDCl_3$, 298 K).

5.5 Conclusions and Outlook

5.5.1 Conclusions

A series of four dinuclear zinc salen complexes which were active catalysts for carbon dioxide/cyclohexene oxide and phthalic anhydride/cyclohexene oxide ROCOP were investigated. These studies highlighted the influence of the ligand structures on the catalytic activity and the stability of the dinuclear complexes. Ligands containing imine moieties resulted in complexes which were more stable than the amine analogues. Consequently, a mixture of products deriving from metal rearrangement was obtained with the more flexible amine $\mathbf{L_{2b}H}$ ligand, highlighting its complex solution coordination chemistry. The catalytic studies indicated that complexes with the more flexible 2,2-dimethyl propylene backbones were more active than those with the *trans*-1,2-cyclohexylene backbones. Further, the complexes with imine substituents showed much better selectivities, affording perfectly alternating copolymers, whereas complexes with amine substitutents gave higher ether-linkage contents. The best catalyst, $\mathbf{[L_{2a}Zn_2(OAc)_2]}$, combined imine donors with a flexible 2,2-dimethyl propylene backbone. It showed higher activity than other di-zinc salen catalysts for carbon dioxide/cyclohexene oxide copolymerisations and higher activities than other reported catalysts for phthalic anhydride/cyclohexene oxide copolymerisations. $\mathbf{[L_{2a}Zn_2(OAc)_2]}$ was also used to successfully afford poly(ester-*block*-carbonate) from the one pot terpolymerisation of PA/CO_2/CHO, providing further evidence that this simple system was selective and was able to synthesis polymers with more complicated structures.

5.5.2 Outlook

5.5.2.1 Heterodinuclear catalysts

Previous studies from our group using [Zn(II)]/[Mg(II)] heterodinuclear macrocycle catalyst have demonstrated greater activities compared to either of the homodiunclear analogues or any combinations of them.[11a, 11b] It is proposed that each metal centre has a specific role during the polymerisation (refer to the introduction chapter). This synergic effect is suggested to derive from the Lewis acidity difference between the two metal centres. Due to the symmetry of the macrocyclic ligand and the lability character of main group metals, the synthesis of these heterodinuclear complexes is rather challenging.

Ligands developed in this study have two binding pockets differing in size. They are therefore of interest to prepare heterodinuclear complexes. For example, complexes to target would have zinc or magnesium coordinated in the phenolate binding site and a larger metal, such as: [Ca(II)], [Cr(III)], [Sn(II)], [Mn(II)], [Fe(II)], [Co(III)], [Ni(II)], [Cu(II)], [Cd(II)], [In(III)] in the methoxy binding site. Preliminary studies have shown that heterodinuclear complexes could be prepared and three complexes (**[L_{2b}ZnMgBr_2]**, **[L_{2b}ZnSnCl_2]** and **[L_{2b}ZnCo$(OAc)_2$]**) were isolated and fully characterised. These heterodinuclear complexes showed slightly higher activities for CO_2/epoxide ROCOP compared to the dizinc complexes under un-optimised reaction conditions. Nevertheless, more work needs to be done to quantify any activity/selectivity enhancement and to optimise the conditions.

5.5.2.2 Switch Catalysis

The ability of [$L_{2a}Zn_2OAc_2$] to produce block copolymers from a mixture of CO_2/epoxide/anhydride may enable further exploration using the "switch approach" (see chapter 4). Of relevance to this notion, some preliminary tests for cyclic ester (*rac*-lactide, ε-caprolactone and β-butyrolactone) ring opening polymerisation showed that

[$L_{2a}Zn_2OAc_2$] is also a good ROP catalyst. The next step is to test **[$L_{2a}Zn_2OAc_2$]** as a catalyst in a mixture of cyclic ester, epoxide, CO_2 and anhydride to investigate whether it is able to selectively polymerise each monomer to form multiblock copolymers. To date, very few catalysts have been reported to perform such catalysis, with the first example being from our group.[34]

5.6 References

[1] W. Zhang, J. L. Loebach, S. R. Wilson, E. N. Jacobsen, *J. Am. Chem. Soc.* **1990**, *112*, 2801-2803.

[2] R. Irie, K. Noda, Y. Ito, N. Matsumoto, T. Katsuki, *Tetrahedron Lett.* **1990**, *31*, 7345-7348.

[3] a) K. C. Gupta, A. K. Sutar, *Coord. Chem. Rev.* **2008**, *252*, 1420-1450; b) N. S. Venkataramanan, G. Kuppuraj, S. Rajagopal, *Coord. Chem. Rev.* **2005**, *249*, 1249-1268.

[4] a) Y. Liu, W.-M. Ren, K.-K. He, X.-B. Lu, *Nat. Commun.* **2014**, *5*; b) X. Wang, A. Thevenon, J. L. Brosmer, I. Yu, S. I. Khan, P. Mehrkhodavandi, P. L. Diaconescu, *J. Am. Chem. Soc.* **2014**, *136*, 11264-11267; c) C. Bakewell, A. J. P. White, N. J. Long, C. K. Williams, *Angew. Chem. Int. Ed.* **2014**, *53*, 9226-9230; d) M. I. Childers, J. M. Longo, N. J. Van Zee, A. M. LaPointe, G. W. Coates, *Chem. Rev.* **2014**, *114*, 8129-8152; e) C. Bakewell, T.-P.-A. Cao, N. Long, X. F. Le Goff, A. Auffrant, C. K. Williams, *J. Am. Chem. Soc.* **2012**, *134*, 20577-20580; f) P. J. Dijkstra, H. Du, J. Feijen, *Polym. Chem.* **2011**, *2*, 520-527; g) D. J. Darensbourg, *Chem. Rev.* **2007**, *107*, 2388-2410; h) P. Hormnirun, E. L. Marshall, V. C. Gibson, R. I. Pugh, A. J. P. White, *Proc. Nat. Acad. Sci.* **2006**, *103*, 15343-15348; i) C. T. Cohen, T. Chu, G. W. Coates, *J. Am. Chem. Soc.* **2005**, *127*, 10869-10878; j) Z. Qin, C. M. Thomas, S. Lee, G. W. Coates, *Angew. Chem. Int. Ed.* **2003**, *42*, 5484-5487; k) Z. Zhong, P. J. Dijkstra, J. Feijen, *J. Am. Chem. Soc.* **2003**, *125*, 11291-11298; l) T. M. Ovitt, G. W. Coates, *J. Am. Chem. Soc.* **2002**, *124*, 1316-1326; m) D. Jhurry, A. Bhaw-Luximon, N. Spassky, *Macromol. Symp.* **2001**, *175*, 67-80.

[5] a) C. Baleizão, H. Garcia, *Chem. Rev.* **2006**, *106*, 3987-4043; b) E. M. McGarrigle, D. G. Gilheany, *Chem. Rev.* **2005**, *105*, 1563-1602.

[6] a) M. Mechler, K. Latendorf, W. Frey, R. Peters, *Organometallics* **2013**, *32*, 112-130; b) H. Golchoubian, H. R. Mardani, G. Bruno, H. A. Rudbari, *Polyhedron* **2012**, *44*, 44-51; c) J. H. Thurston, C. G. Z. Tang, D. W. Trahan, K. H. Whitmire, *Inorg. Chem.* **2004**, *43*, 2708-2713; d) L. M. Liable-Sands, C. Incarvito, A. L. Rheingold, C. J. Qin, A. L. Gavrilova, B. Bosnich, *Inorg. Chem.* **2001**, *40*, 2147-2155.

[7] a) Q.-W. Xie, S.-Q. Wu, C.-M. Liu, A.-L. Cui, H.-Z. Kou, *Dalton Trans.* **2013**, *42*, 11227-11233; b) K. Binnemans, K. Lodewyckx, B. Donnio, D. Guillon, *Chem. Eur. J.* **2002**, *8*, 1101-1105; c) M. L. Kahn, T. M. Rajendiran, Y. Jeannin, C. Mathonière, O. Kahn, *C. R. Acad. Sci. Ser. II C - Chem.* **2000**, *3*, 131-137; d) I. Ramade, O. Kahn, Y. Jeannin, F. Robert, *Inorg. Chem.* **1997**, *36*, 930-936.

[8] Q.-W. Xie, S.-Q. Wu, W.-B. Shi, C.-M. Liu, A.-L. Cui, H.-Z. Kou, *Dalton Trans.* **2014**, *43*, 11309-11316.

[9] S. Matsunaga, M. Shibasaki, *Chem. Commun.* **2014**, *50*, 1044-1057.

[10] a) A. Buchard, F. Jutz, M. R. Kember, A. J. P. White, H. S. Rzepa, C. K. Williams, *Macromolecules* **2012**, *45*, 6781-6795; b) S. Klaus, M. W. Lehenmeier, E. Herdtweck, P. Deglmann, A. K. Ott, B. Rieger, *J. Am. Chem. Soc.* **2011**, *133*, 13151-13161; c) F. Jutz, A. Buchard, M. R. Kember, S. B. Fredriksen, C. K. Williams, *J. Am. Chem. Soc.* **2011**, *133*, 17395-17405; d) M. Cheng, D. R. Moore, J. J. Reczek, B. M. Chamberlain, E. B. Lobkovsky, G. W. Coates, *J. Am. Chem. Soc.* **2001**, *123*, 8738-8749.

[11] a) J. A. Garden, P. K. Saini, C. K. Williams, *J. Am. Chem. Soc.* **2015**, *137*, 15078-15081; b) P. K. Saini, C. Romain, C. K. Williams, *Chem. Commun.* **2014**, *50*, 4164-4167; c) M. R. Kember, F. Jutz, A. Buchard, A. J. P. White, C. K. Williams, *Chem. Sci.* **2012**, *3*, 1245-1255; d) A. Buchard, M. R. Kember, K. G. Sandeman, C.

K. Williams, *Chem. Commun.* **2011**, *47*, 212-214; e) M. R. Kember, A. J. P. White, C. K. Williams, *Macromolecules* **2010**, *43*, 2291-2298; f) M. R. Kember, A. J. P. White, C. K. Williams, *Inorg. Chem.* **2009**, *48*, 9535-9542; g) M. R. Kember, P. D. Knight, P. T. R. Reung, C. K. Williams, *Angew. Chem. Int. Ed.* **2009**, *48*, 931-933.

[12] a) W. C. Ellis, Y. Jung, M. Mulzer, R. Di Girolamo, E. B. Lobkovsky, G. W. Coates, *Chem. Sci.* **2014**, *5*, 4004-4011; b) D. R. Moore, M. Cheng, E. B. Lobkovsky, G. W. Coates, *J. Am. Chem. Soc.* **2003**, *125*, 11911-11924; c) S. D. Allen, D. R. Moore, E. B. Lobkovsky, G. W. Coates, *J. Am. Chem. Soc.* **2002**, *124*, 14284-14285; d) D. R. Moore, M. Cheng, E. B. Lobkovsky, G. W. Coates, *Angew. Chem. Int. Ed.* **2002**, *41*, 2599-2602.

[13] a) Y. Xiao, Z. Wang, K. Ding, *Macromolecules* **2006**, *39*, 128-137; b) Y. Xiao, Z. Wang, K. Ding, *Chem. Eur. J.* **2005**, *11*, 3668-3678.

[14] a) C. Chatterjee, M. H. Chisholm, A. El-Khaldy, R. D. McIntosh, J. T. Miller, T. Wu, *Inorg. Chem.* **2013**, *52*, 4547-4553; b) N. D. Harrold, Y. Li, M. H. Chisholm, *Macromolecules* **2013**, *46*, 692-698; c) C. Chatterjee, M. H. Chisholm, *Inorg. Chem.* **2012**, *51*, 12041-12052; d) C. Chatterjee, M. H. Chisholm, *Inorg. Chem.* **2011**, *50*, 4481-4492; e) H. Sugimoto, H. Ohshima, S. Inoue, *J. Polym. Sci., Part A Polym. Chem.* **2003**, *41*, 3549-3555; f) S. Mang, A. I. Cooper, M. E. Colclough, N. Chauhan, A. B. Holmes, *Macromolecules* **2000**, *33*, 303-308; g) N. Takeda, S. Inoue, *Makromol. Chem.* **1978**, *179*, 1377-1381.

[15] a) T. Bok, H. Yun, B. Y. Lee, *Inorg. Chem.* **2006**, *45*, 4228-4237; b) B. Y. Lee, H. Y. Kwon, S. Y. Lee, S. J. Na, S.-i. Han, H. Yun, H. Lee, Y.-W. Park, *J. Am. Chem. Soc.* **2005**, *127*, 3031-3037.

[16] a) S. Paul, Y. Zhu, C. Romain, R. Brooks, P. K. Saini, C. K. Williams, *Chem. Commun.* **2015**, *51*, 6459-6479; b) C. Romain, A. Thevenon, P. Saini, C. Williams,

in *Carbon Dioxide and Organometallics, Vol. 53* (Ed.: X.-B. Lu), Springer International Publishing, **2016**, pp. 101-141.

[17] M. W. Lehenmeier, S. Kissling, P. T. Altenbuchner, C. Bruckmeier, P. Deglmann, A.-K. Brym, B. Rieger, *Angew. Chem. Int. Ed.* **2013**, *52*, 9821-9826.

[18] a) S. Kissling, M. W. Lehenmeier, P. T. Altenbuchner, A. Kronast, M. Reiter, P. Deglmann, U. B. Seemann, B. Rieger, *Chem. Commun.* **2015**, *51*, 4579-4582; b) S. Kissling, P. T. Altenbuchner, M. W. Lehenmeier, E. Herdtweck, P. Deglmann, U. B. Seemann, B. Rieger, *Chem. Eur. J.* **2015**, *21*, 8148-8157.

[19] a) X.-B. Lu, D. J. Darensbourg, *Chem. Soc. Rev.* **2012**, *41*, 1462-1484; b) X.-B. Lu, Y. Wang, *Angew. Chem. Int. Ed.* **2004**, *43*, 3574-3577; c) D. J. Darensbourg, R. M. Mackiewicz, A. L. Phelps, D. R. Billodeaux, *Acc. Chem. Res.* **2004**, *37*, 836-844; d) R. Eberhardt, M. Allmendinger, B. Rieger, *Macromol. Rapid Commun.* **2003**, *24*, 194-196; e) D. J. Darensbourg, J. C. Yarbrough, *J. Am. Chem. Soc.* **2002**, *124*, 6335-6342.

[20] K. Nakano, T. Kamada, K. Nozaki, *Angew. Chem. Int. Ed.* **2006**, *45*, 7274-7277.

[21] a) D. J. Darensbourg, W.-C. Chung, S. J. Wilson, *ACS Catal.* **2013**, *3*, 3050-3057; b) H. Li, Y. Niu, *Polym. J.* **2011**, *43*, 121-125.

[22] a) A. Cyriac, J. Y. Jeon, J. K. Varghese, J. H. Park, S. Y. Choi, Y. K. Chung, B. Y. Lee, *Dalton Trans.* **2012**, *41*, 1444-1447; b) W.-M. Ren, Y. Liu, G.-P. Wu, J. Liu, X.-B. Lu, *J. Polym. Sci., Part A Polym. Chem.* **2011**, *49*, 4894-4901; c) J. Yoo, S. J. Na, H. C. Park, A. Cyriac, B. Y. Lee, *Dalton Trans.* **2010**, *39*, 2622-2630; d) W.-M. Ren, X. Zhang, Y. Liu, J.-F. Li, H. Wang, X.-B. Lu, *Macromolecules* **2010**, *43*, 1396-1402; e) S. J. Na, S. S, A. Cyriac, B. E. Kim, J. Yoo, Y. K. Kang, S. J. Han, C. Lee, B. Y. Lee, *Inorg. Chem.* **2009**, *48*, 10455-10465; f) W.-M. Ren, Z.-W. Liu, Y.-Q. Wen, R. Zhang, X.-B. Lu, *J. Am. Chem. Soc.* **2009**, *131*, 11509-11518; g) S.

S, J. K. Min, J. E. Seong, S. J. Na, B. Y. Lee, *Angew. Chem. Int. Ed.* **2008**, *47*, 7306-7309; h) E. K. Noh, S. J. Na, S. S, S.-W. Kim, B. Y. Lee, *J. Am. Chem. Soc.* **2007**, *129*, 8082-8083.

[23] K. Nakano, S. Hashimoto, K. Nozaki, *Chem. Sci.* **2010**, *1*, 369-373.

[24] a) Y. Liu, W.-M. Ren, J. Liu, X.-B. Lu, *Angew. Chem. Int. Ed.* **2013**, *52*, 11594-11598; b) S. I. Vagin, R. Reichardt, S. Klaus, B. Rieger, *J. Am. Chem. Soc.* **2010**, *132*, 14367-14369; c) R. M. Thomas, P. C. B. Widger, S. M. Ahmed, R. C. Jeske, W. Hirahata, E. B. Lobkovsky, G. W. Coates, *J. Am. Chem. Soc.* **2010**, *132*, 16520-16525; d) W. Hirahata, R. M. Thomas, E. B. Lobkovsky, G. W. Coates, *J. Am. Chem. Soc.* **2008**, *130*, 17658-17659; e) J. M. Ready, E. N. Jacobsen, *Angew. Chem. Int. Ed.* **2002**, *41*, 1374-1377.

[25] C.-H. Li, H.-J. Chuang, C.-Y. Li, B.-T. Ko, C.-H. Lin, *Polym. Chem.* **2014**, *5*, 4875-4878.

[26] C. Bakewell, G. Fateh-Iravani, D. W. Beh, D. Myers, S. Tabthong, P. Hormnirun, A. J. P. White, N. Long, C. K. Williams, *Dalton Trans.* **2015**, *44*, 12326-12337.

[27] a) M. Andruh, *Dalton Trans.* **2015**, *44*, 16633-16653; b) X.-Q. Lü, W.-X. Feng, Y.-N. Hui, T. Wei, J.-R. Song, S.-S. Zhao, W.-Y. Wong, W.-K. Wong, R. A. Jones, *Eur. J. Inorg. Chem.* **2010**, *2010*, 2714-2722; c) H. Mihara, Y. Xu, N. E. Shepherd, S. Matsunaga, M. Shibasaki, *J. Am. Chem. Soc.* **2009**, *131*, 8384-8385; d) W.-Y. Bi, X.-Q. Lü, W.-L. Chai, J.-R. Song, W.-Y. Wong, W.-K. Wong, R. A. Jones, *J. Mol. Struct.* **2008**, *891*, 450-455.

[28] L. Wu, X. Lu and R. Lu, *Chin. J. Polym. Sci.* **2014**, *32*, 768-777.

[29] a) R. M. Haak, A. M. Castilla, M. Martinez Belmonte, E. C. Escudero-Adan, J. Benet-Buchholz, A. W. Kleij, *Dalton Trans.* **2011**, *40*, 3352-3364; b) C. Yu, Z. Zhang, L. Liu, H. Li, Y. He, X. Lu, W.-K. Wong, R. A. Jones, *New J. Chem.* **2015**,

39, 3698-3707; c) G. A. Morris, H. Zhou, C. L. Stern, S. T. Nguyen, *Inorg. Chem.* **2001**, *40*, 3222-3227.

[30] A. W. Addison, T. N. Rao, J. Reedijk, J. van Rijn, G. C. Verschoor, *J. Chem. Soc., Dalton Trans.* **1984**, 1349-1356.

[31] D. R. Armstrong, J. A. Garden, A. R. Kennedy, S. M. Leenhouts, R. E. Mulvey, P. O'Keefe, C. T. O'Hara, A. Steven, *Chem. Eur. J.* **2013**, *19*, 13492-13503.

[32] R. Shakya, Z. Wang, D. R. Powell, R. P. Houser, *Inorg. Chem.* **2011**, *50*, 11581-11591.

[33] P. K. Saini, C. Romain, Y. Zhu, C. K. Williams, *Polym. Chem.* **2014**, *5*, 6068-6075.

[34] a) C. Romain, C. K. Williams, *Angew. Chem. Int. Ed.* **2014**, *53*, 1607-1610; b) S. Kernbichl, M. Reiter, F. Adams, S. Vagin, B. Rieger, *J. Am. Chem. Soc.* **2017**, *139*, 6787-6790.

CHAPTER 6

Conclusion

6.1 General Conclusion

This thesis presented three families of homogenous mono and dinuclear catalysts, applied to the ring opening copolymerisation of carbon dioxide and epoxide and the ring opening polymerisation of *rac*-lactide. Overall, the results should be seen as enabling further research and helping to describe the requirements for more efficient ROP/ROCOP catalysts. The thesis also adds to the understanding of mechanisms using spectroscopy and kinetic methods (Figure 6.1). It revealed some of the subtleties of "catalyst design" and the importance of developing suitable ligands, choosing metal centres and initiating groups to achieve high activities and selectivity.

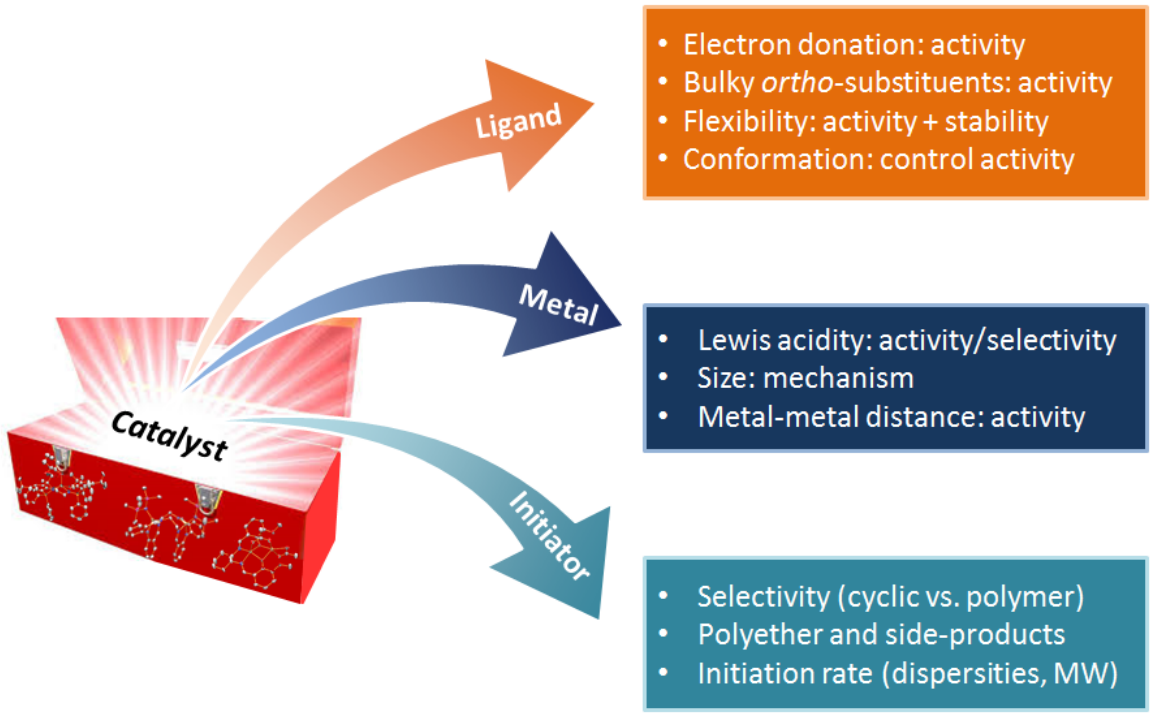

Figure 6.1. Summary of the key findings presented in this thesis.

6.1.1 Conclusions: Ligands

The electron donation of the ligand plays a pivotal role in the selectivity and the activity of CO_2/epoxide ROCOP catalysts. In Chapter 3, more electron donating phosphasalen ligands (bearing two iminophosphorane moieties) coordinated to [In(III)] enabled the formation of polycarbonate, at only 1 bar of CO_2. In contrast, analogous salen complex only formed

polyether. In Chapter 5, di-zinc complexes bearing more electron donating imine substituents showed improve performances and selectivity compared to complexes having amine substituents. Thus, metal centres where ligands reduce Lewis acidity appear to be beneficial for this catalysis, perhaps by increasing the lability of the metal-alkoxide bond to CO_2 insertion reactions (either through destabilisation of the ground state or by stabilisation of the transition state).

The *ortho*-phenol substituents also appear to play an important role in the activity of indium phosphasalen catalysts and in the stereoselectivity of the polymerisation. It is proposed that increasing steric hindrance at the metal centre may destabilise the hexacoordinate indium carbonate intermediate and favour the formation of the pentacoordinate alkoxide complex (formed by epoxide ring-opening). It seems likely that phosphasalen indium catalysts owe the stereoselectivity, in part, to steric shielding by the two ortho-phenolate substituents, which control over epoxide enchainment and/or coordination of the growing polymer chain.

Another important factor in controling catalyst activity is ligand flexibility. Chapter 5 highlighted the activity enhancement observed for catalysts bearing a more flexible 2,2-dimethyl-1.3-propanediamine backbone. Furthermore, the flexibility of the ligand played an important role in the stability of its corresponding dinuclear complex. In Chapter 4, the difference in flexibility and catalyst conformation resulting in a “folded” di-zinc compmlex or a “flat” di-zinc alkoxide was very important to high activity (the “folded” catalyst is ~ 6000 times more active than the “flat” catalyst). It is proposed that more flexible catalysts may stabilise the transition state implicated in the rate determining step.

6.1.2 Conclusions: the Metal Centre

As mentioned in the previous section, the Lewis acidity of the metal centre appear to be involved in controlling catalytic selectivity and activity. Results from Chapter 3 and 5 demonstrated that a more Lewis acidic metal centre led to catalysts with lower activities and selectivity (polycarbonate vs. polyether). The control of the Lewis acidity of the active site can either be achieved by increasing the electron donation of the ligand (*vide supra*) or by changing the metal centre to one with similar ionic radius but different Lewis acidity (e.g. changing [Zn(II)] or [In(III)] for a transition metal centre).

The size of the metal centre seems to also play a role in the mechanism of the polymerisation. In Chapter 3, the indium phosphasalen catalysts are proposed to operate via a rare *cis* mononuclear pathway for the CO_2/epoxide ROCOP. The larger size of [In(III)] (80 pm) compared to [Cr(III)] (61 pm) and [Co(III)] (60 pm) may be responsible for enabling the *cis* mononuclear mechanism.

Finally, the distance between the two metal centres in dinuclear catalysts seems to be important for intermetallic cooperativity. Chapter 5 described di-zinc catalysts that out-perform mono-zinc analogues (up to 7 times more active per metal centre). In addition, there was a correlation between activity and the Zn-Zn distance.

6.1.3 Conclusions: Initiating Group

Theoretically, the initiator has only an effect on the initiation step in a controlled polymerisation. Initiation is expected to be faster than propagation in order to fulfilll the criteria that all the catalyst is active during the polymerisation. The polymerisations in Chapter 3 and 4 showed that inefficient initiation lead to polymers with molecular weights higher than expected and broad dispersities (e.g. [Zn-amido] in Chapter 4) or with multi modal molecular weight distributions (e.g. [In-Cl] in Chapter 3). Changing the initiating

group to an alkoxide led to the formation of polymers with predictable molecular weight and narrow dispersities.

Therefore, the initiating group selection is important and several factors need to be taken into account. Firstly, the initiating group should be labile and sufficiently nucleophilic to initiate (e.g. the [In-OAc] catalyst in Chapter 3 was inactive). A second parameter is the metal-initiator covalent bond character. In Chapter 3, the polymerisation initiated by [In-NO_3] gave a bimodal distribution which was tentatively proposed to arise from free nitrate anion resulting from metal-nitrate bond dissociation. A third parameter is the capacity of the initiator to act as a good leaving group, favouring the backbiting side reactions and forming side products (e.g. [In-Br] catalyst in Chapter 3 only gave cyclic carbonate). Finally, the steric bulk of the initiating group seems to be crucial for efficient monomer coordination to the metal centre. In Chapter 4, the results suggest that sterically hindered amido initiators was responsible for monomer coordination being sufficiently slow to be relevant in the rate determining step and resulting in polymers with molecular weights higher than expected.

6.2 Outlook

Each chapter defined the near-term next steps in the development of new CO_2/epoxide ROCOP and *rac*-lactide ROP catalysts, including:

1. Ligand structure-activity relationships
2. Other metals to target for catalysis
3. Developing "switchable" catalysts (control of metal-chain end group)

This outlook focuses more on the remaining big challenges and the future directions for the overall field of catalysts to make oxygenated polymers.

Catalytic activity is a key parameter in CO_2/epoxide ring opening copolymerisation. There are still very few highly active catalysts (TOF > 1000 h^{-1}), particularly when using propylene oxide (PO) and other alkylene oxides.[1] These commodity epoxides are annually produced on a multi-ton scale (production of PO in 1999: ~ 6 Mt with an annual growth of ~ 4-5 %).[2] In addition, polycarbonates produced from PO have desirable mechanical properties (see the introduction chapter).[3] There is, therefore, a clear need to develop more ROCOP catalysts active.

Producing polycarbonate from PO is still very challenging as the thermodynamic barrier to form cyclic carbonate is very low.[4] As a consequence, the catalyst should be highly active at low temperature (typically < 60 ^oC) or have a big difference in relative barriers. There is still a lack of understanding on how to prepare low activation barrier catalysts for PO copolymerisation and future research needs to concentrate on this area. A long term target would be an air stable robust catalyst highly active for PO/CO_2 ROCOP, at ~ 100 ^oC, working at low CO_2 pressure (< 10 bar), under neat conditions, to facilitate its implementation in existing plant.

In addition, investigating ROCOP with bio-derived monomers [e.g. limonene oxide (LO) or cyclohexyl diene oxide (CHD)] are also of interest, currently mostly in academic laboratories.[5] One aspect preventing commercialisation of these polycarbonates is that there are not yet any catalysts capable of polymerising all isomers of LO.[5] This means the products are too expensive since a portion of monomer always remains unreacted. Nevertheless recent papers showing scratch resistant coatings, resins and rigid plastics made from poly(limonene carbonate) demonstrate very encouraging properties and spur on efforts to develop these materials.[6] There is, therefore, an increasing interest in developing suitable catalysts able to incorporate all the isomers of LO in a controlled fashion.

Cyclohexene oxide (CHO) is made by industry but not currently at the same scale as PO. PCHC properties are interesting but may need modifications for example by plastisation, or to improve toughness [T_g of isotactic poly(cyclohexene carbonate) (PCHC) is close to poly(bisphenol A carbonate)].[7] Thus, producing block copolymers from PCHC with other epoxides or even lactones is of high interest.[8] There is still a limited number of these so called “switch catalysts”, able to form block copolymers in one pot from a mixture of monomers.[9] Future research effort has to focus on the development of more examples of such catalysts.

6.3. References

[1] a) S. S, J. K. Min, J. E. Seong, S. J. Na, B. Y. Lee, *Angew. Chem. Int. Ed.* **2008**, *47*, 7306-7309; b) C. Romain, A. Thevenon, P. Saini, C. Williams, in *Carbon Dioxide and Organometallics, Vol. 53* (Ed.: X.-B. Lu), Springer International Publishing, **2016**, pp. 101-141.

[2] T. A. Nijhuis, M. Makkee, J. A. Moulijn, B. M. Weckhuysen, *Ind. Eng. Chem. Res.* **2006**, *45*, 3447-3459.

[3] G. A. Luinstra, *Polym. Rev.* **2008**, *48*, 192-219.

[4] D. J. Darensbourg, A. D. Yeung, *Macromolecules* **2013**, *46*, 83-95.

[5] a) C. M. Byrne, S. D. Allen, E. B. Lobkovsky, G. W. Coates, *J. Am. Chem. Soc.* **2004**, *126*, 11404-11405; b) C. J. Whiteoak, N. Kielland, V. Laserna, F. Castro-Gómez, E. Martin, E. C. Escudero-Adán, C. Bo, A. W. Kleij, *Chem. Eur. J.* **2014**, *20*, 2264-2275.

[6] a) Sto, C. Li, J. Unruangsri, P. K. Saini, R. J. Sablong, M. A. R. Meier, C. K. Williams, C. Koning, *Polym. Chem.* **2017**, *8*, 6099-6105; b) O. Hauenstein, M. Reiter, S. Agarwal, B. Rieger, A. Greiner, *Green Chem.* **2016**, *18*, 760-770; c) S. J. Poland, D. J. Darensbourg, *Green Chem.* **2017**.

[7] C. Koning, J. Wildeson, R. Parton, B. Plum, P. Steeman, D. J. Darensbourg, *Polymer* **2001**, *42*, 3995-4004.

[8] a) Y. Zhu, C. Romain, C. K. Williams, *J. Am. Chem. Soc.* **2015**, *137*, 12179-12182; b) S. Paul, Y. Zhu, C. Romain, R. Brooks, P. K. Saini, C. K. Williams, *Chem. Commun.* **2015**, *51*, 6459-6479.

[9] a) X. Wang, A. Thevenon, J. L. Brosmer, I. Yu, S. I. Khan, P. Mehrkhodavandi, P. L. Diaconescu, *J. Am. Chem. Soc.* **2014**, *136*, 11264-11267; b) S. Kernbichl, M. Reiter, F. Adams, S. Vagin, B. Rieger, *J. Am. Chem. Soc.* **2017**, *139*, 6787-6790; c)

M. Reiter, S. Vagin, A. Kronast, C. Jandl, B. Rieger, *Chem. Sci.* **2017**, *8*, 1876-1882; d) C. Romain, C. K. Williams, *Angew. Chem. Int. Ed.* **2014**, *53*, 1607-1610.

CHAPTER 7

Experimental Procedures and Data

7.1 General Comments

7.1.1 Materials and methods

All solvents and reagents were obtained from commercial sources (Aldrich and Merck) and used as received, unless stated otherwise. THF, toluene, and hexane were pre-dried, over activated molecular sieves (THF) or potassium hydroxide (toluene and hexane), then refluxed, over sodium/benzophenone ([H_2O] < 5 ppm). All dry solvents were degassed, by several freeze-pump-thaw cycles, and stored, under nitrogen and activated molecular sieves. Dichloromethane and diethyl ether, used for ligands syntheses, were taken directly from an Innovative Technology.inc solvent purification system. MeCN was dried using a Pure Solv MD-6 Solvent Purification System. Isopropanol was dried over calcium hydride, distilled and stored over molecular sieves, under an inert atmosphere. Anhydrous complexation reactions were conducted under nitrogen, using either a double-manifold Schlenk vacuum line, under a nitrogen atmosphere, or in a nitrogen-filled glovebox. Cyclohexene oxide (CHO) was dried over calcium hydride, filtered, purified by fractional distillation prior to use and stored under an inert nitrogen atmosphere. Phthalic anhydride (PA) was purified by dissolving it in benzene, filtering, crystallization from chloroform and then sublimation. Research grade carbon dioxide (99.9995 %) was used for copolymerization studies. Rac-LA was recrystallized (two times) from toluene, under inert atmosphere, followed by sublimation, at 80 ^{o}C under reduced pressure. ε-Caprolactone was dried over CaH_2, distilled under inert atmosphere and stored under inert atmosphere. Trimethylene carbonate (TMC) was dissolved in THF (at a concentration of 0.7 g/mL), stirred over CaH_2 for 2 days, before being filtered, recrystallized twice from cold THF, dried under reduced pressure and stored, under inert atmosphere. KO^{t}Bu was sublimed prior to use.[1] Zinc bis[bis(trimethylsilyl)amide] [$Zn\{N(SiMe_3)_2\}_2$] was prepared as described previously.[2]

7.1.2 Measurement

NMR: Imperial College London (ICL): ^{1}H (400.2 MHz), $^{13}C\{^{1}H\}$ (101.0 MHz), $^{31}P\{^{1}H\}$ (162.0 MHz) and 2D NMR (COSY, HMQC, HMBC) spectra were recorded using a Bruker AV 400 MHz spectrometer at 298 K (unless otherwise stated). DOSY analysis was performed using a Bruker AV 500 MHz spectrometer at 298 K (see the DOSY NMR section for more details). University of Oxford (UniOx): ^{1}H (400.2 MHz) and $^{31}P\{^{1}H\}$ (162.0 MHz) NMR spectra were collected using a Bruker Advance III HD nanobay NMR equipped with a 9.4T magnet. $^{13}C\{^{1}H\}$ NMR, COSY, HMBC and HSQC NMR spectra were collected with a Bruker Avance NMR equipped with an 11.75T magnet and a $^{13}C\{^{1}H\}$ (125.8 MHz) detect cryoprobe. NMR spectra were processed and analysed using MestReNova and Bruker TopSpin software packages.

$^{1}H\{^{1}H\}$ (homonuclear decoupled) NMR spectra: $^{1}H\{^{1}H\}$ experiments were performed on either a Bruker Av500 spectrometer, or a DRX 400 spectrometer. Peak deconvolution, using MestReNova software package, was used to improve accuracy in the determination of tetrad integrals.

MALDI-ToF MS (ICL and UniOX): MALDI ToF analysis was carried out on Micromass MALDI micro MX spectrometer. Catalyst characterization: The matrix used was *trans*-2-[3-(4-tert-butylphenyl)-2-methyl-2-propenylidene]malononitrile (DCTB). Sodium acetate was used as an additive, when necessary. The samples were prepared as followed: 10 mg/mL THF solutions of the complex, matrix and additive were separately prepared. Then, 20 μL of the complex and 20 μL of the matrix solution were mixed, along with 10 μL of the additive solution, if required. This mixture (2 μL) was then spotted on the MALDI plate and allowed to dry. Polymer characterization: The matrix used was the dithranol. Potassium trifluoroacetate was used as an additive, as required. The samples were prepared in the following manner: 10 mg/mL THF solutions of the polymer, matrix

and additive were separately prepared. Then, 20 μL of the polymer and 20 μL of the matrix solution were mixed, along with 10 μL of the additive solution, if required. This mixture (2 μL) was then spotted on the MALDI plate and allowed to dry.

X-ray diffraction: ICL: All X-ray crystallography was carried out by Dr Andrew J. P. White. Data were collected using an Agilent Xcalibur PX 3E diffractometer, and the structures were refined using the SHELXTL and SHELX-2013 program systems.[11] **UniOx:** Crystal structures were either carried out by me (with the supervision from Dr Amber Thompson) or by Dr Christopher Durr. Samples were isolated in a glovebox, under a pool of fluorinated oil, and mounted on MiTeGen MicroMounts. The crystal was then cooled to 150 K, with an Oxford Cryosystems Cryostream nitrogen cooling device. Data collection was carried out with an Oxford Diffraction Supernova diffractometer using, Cu Kα (λ = 1.5417 Å) radiation. The resulting raw data was processed using CrysAlisPro.[12] Structures were solved by SHELXT and Full-matrix least-squares refinements, based on F_2, were performed in SHELXL-14,[13] as incorporated in the WinGX package.[14] For each methyl group, the hydrogen atoms were added at calculated positions using a riding model, with U(H) = 1.5 Ueq (bonded carbon atom). The rest of the hydrogen atoms were included in the model, at calculated positions, using a riding model with U(H) = 1.2 Ueq (bonded atom). Neutral atom scattering factors were used and include terms for anomalous dispersion.[15]

Elemental analysis: Elemental analysis was determined by Stephen Boyer at London Metropolitan University.

SEC: Two Mixed Bed PSS SDV linear S columns were used in series, with THF as the eluent, at a flow rate of 1 mL/min, on a Shimadzu LC-20AD instrument at 40 °C. The polymer samples were dissolved in SEC grade THF and filtered prior to analysis. Polymer

molecular weight (M_n) was determined by comparison against polystyrene standards and where appropriate correction factors were applied as reported in the literature.

$$Mn_{corrected} = x \,.\, Mn_{sec}$$

Table 1. Correction factors for various polymers used in this thesis.

Polymer	x	Ref
PLA	x = **0.58** ± 0.05	[3]
PCL	x = **0.56** ± 0.05	[3b]
PTMC	$M_{n(sec)}$ < 5'000; x = **0.57** $M_{n(sec)}$ > 10'000; x = **0.88** 5'000 < $M_{n(sec)}$ < 10'000 x = **0.76** (average value) or x = **7.10^{-5}.[$M_{n(sec)}$] + 0.18**	[4]

DOSY NMR Spectroscopy: Diffusion-Ordered Spectroscopy (DOSY) NMR experiments were performed at 298 K on a Bruker 500 AVANCE III HD NMR spectrometer operating at a frequency of 500.13 MHz for proton resonance under TopSpin (version 3.2, Bruker Biospin, Karlsruhe) and equipped with a z-gradient bbfo/5 mm tuneable "SmartProbe"^{TM} probe and a GRASP II gradient spectroscopy accessory providing a maximum gradient output of 53.5 G/cm (5.35 G/cmA). Diffusion ordered NMR data was acquired using the Bruker pulse program ledbpgp2s with a spectral width of 5500 Hz (centred on 4.5 ppm) and 32768 data points. A relaxation delay of 12 s was employed along with a diffusion time (large delta) of 100 ms and a longitudinal eddy current delay (LED) of 5 ms. Bipolar gradient pulses (little delta/2) of 2.2 ms and homospoil gradient pulses of 0.6 ms were used. The gradient strengths of the 2 homospoil pulses were -17.13 % and -13.17 %. 32 experiments were collected with the bipolar gradient strength, initially at 5 % (1st experiment), linearly increased to 95 % (32nd experiment). All gradient pulses were smooth-square shaped (SMSQ10.100) and after each application a recovery delay of 200 μs used. The experiment was run with 24 scans per

increment, employing one stimulated echo with two spoiling gradients. DOSY plots were generated by using the DOSY processing module of TopSpin. Parameters were optimized empirically to find the best quality of data for presentation purposes. Diffusion coefficients were calculated by fitting intensity data to the Stejskal-Tanner expression.[5]

Calibration plots for DOSY analysis:[6] A calibration plot used for DOSY analysis was determined using a range of standards spanning the molecular weight range of 161.4 to 643.4 g mol^{-1} [hexamethyldisilazane ($HN(SiMe_3)_2$), 161.4; $Zn\{[N(SiMe_3)_2]_2\}_2$, 386.2; β-diketiminate ligand $HC(C(Me)N\text{-}2,6\text{-}^iPr_2C_6H_3)_2$, (BDIH), 418.7; $(BDI)Zn([N(SiMe_3)_2]_2)$, 643.4 g mol^{-1}, Table 1]. From the diffusion coefficients of the external standards, linear calibration plots were obtained from logD vs logMW (Graph 7.1). Following DOSY analysis of the product, the diffusion coefficient obtained for the signals corresponding to the product allowed an estimate of the MW of the species present in solution.

Table 7.2. Diffusion coefficients of standards in d_8-THF solution compared to their molecular weight.

Compound	LogD	MW (g mol^{-1})	LogMW
d_8-THF	-8.568	80.2	1.9040
$HN(SiMe_3)_2$	-8.763	161.4	2.2079
$Zn\{[N(SiMe_3)_2]_2\}_2$	-8.943	386.2	2.5868
BDIH	-8.990	418.7	2.6219

Graph 7.1. LogD vs LogMW representation from the ^{1}H DOSY NMR data obtained for the standards $HN(SiMe_3)_2$, $Zn\{[N(SiMe_3)_2]_2\}_2$ and BDIH in d_8-THF solvent.

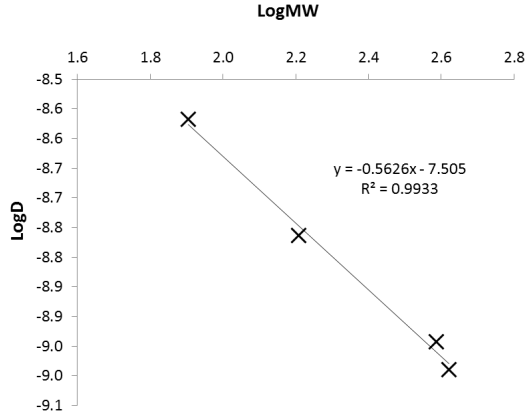

Low pressure CO_2 line: Low pressure copolymerization studies were performed using a triple manifold Young tap CO_2/N_2/vacuum Schlenk line. Research grade carbon dioxide was used and dried by one drierite column and two low pressure drying columns MC1 (Micro Torr) connected in series.

Figure 7.1. Pictures of the drying columns (L.H.S.) and the triple manifold Young tap CO_2/N_2/vacuum Schlenk line used for the low CO_2 pressure polymerization.

High pressure CO_2 line: High pressure copolymerization studies were performed in a 25 mL Parr 5500 HP Compact Reactor using research grade carbon dioxide dried by two high pressure drying columns (in series) VICI (Thames Restek).

Figure 7.2. Pictures of the drying columns (L.H.S. picture), the high pressure reactor disassembled (upper middle picture), the high pressure reactor assembled (R.H.S picture) and the controller unit (lower middle picture) used for high CO_2 pressure polymerization.

***In situ* ATR-IR measurements**: In situ ATR-IR measurements were performed on a Mettler-Toledo ReactIR ic.10 spectrometer equipped with a MCT detector and a silver halide DiComp probe.

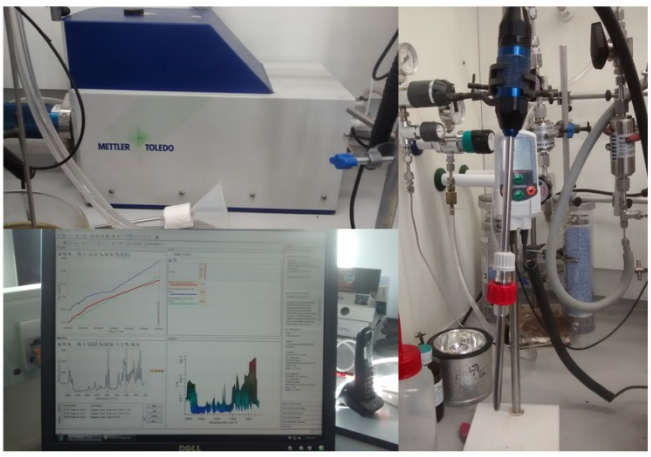

Figure 7.3. Pictures of the *in-situ* ATR-IR probe set up. The upper left picture is the principal unit of the system containing a liquid nitrogen tank. It is connected to the probe (right picture) via an optic fibre cable and to a computer to a iC IR software (lower left picture).

Computational Details:[*] All calculations were performed using the Gaussian 09 suite of codes (revision C.01). Calculations were carried out at the DFT level of theory, using hybrid functional ωB97XD. All atoms, including zinc, have been described with a 6-31G(d,p) basis set. Geometry optimizations were carried out without any symmetry restrictions. Conductor-like polarizable continuum model (CPCM) was used with THF as the solvent to model solvation. The nature of the extrema was verified with analytical frequency calculations: the stationary points (minima) do not feature imaginary modes, and all transition states reveal precisely one imaginary mode corresponding to the intended reaction. For IITS, an IRC calculation was performed which also confirmed the identity of the transition state. Data available at https://doi.org/10.14469/hpc/430.

[*] All the calculations were performed by Dr Charles Romain at Imperial College London.

7.2 Typical Phosphasalen and Salen Ligands Synthesis Procedures[8]

7.2.1 Typical Procedure to Synthesis ^{R}S1

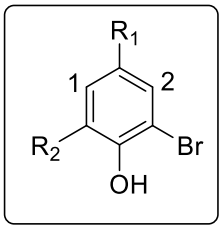

At 0 ^{o}C, N-bromosuccinimide (1 equiv.) was added to a solution of the phenol (5.0 g) in acetonitrile (~ 200 mL) under continuous stirring. The mixture was allowed to warm to 25 ^{o}C and left stirring for 12 h. After which, a saturated solution of sodium sulphite (~ 100 mL) was added and the reaction mixture left to stir for 15 mins. The solid from the afforded white suspension was then filtered and the product extracted into petroleum ether (3 x 50 mL). The organic layer was then dried ($MgSO_4$), filtered, and the solvent removed under reduced pressure. The crude was used in the next step without any purification.

S1 (R_1 = R_2 = ^{t}Bu) (6.2 g, 22 mmol, 92 %)

1H NMR (400 MHz, $CDCl_3$, 298 K) δ (ppm): 7.31 (d, $^{4}J_{H,H}$ = 2.5 Hz, 1H, *1*), 7.23 (d, $^{4}J_{H,H}$ = 2.5 Hz, 1H, *2*), 5.65 (s, 1H, O*H*), 1.40 (s, 9H, C(CH_3)$_3$), 1.28 (s, 9H, C(CH_3)$_3$). Elemental Analysis calculated for $C_{14}H_{21}BrO$ (285.23 g/mol): C, 58.95; H, 7.42 Found: C, 58.95; H, 7.41.

^{Amyl}S1 (R_1 = R_2 = Amyl) (5.9 g, 18 mmol, 90 %)

^{1}H NMR (400 MHz, $CDCl_3$, 298 K) δ (ppm): 7.28 (d, $^{4}J_{H,H}$ = 3.0 Hz, 1H, *1*), 7.13 (d, $^{4}J_{H,H}$ = 2.2 Hz, 1H, *2*), 5.63 (s, 1H, O*H*), 1.88 (q, *J* = 7.5 Hz, 2H, CH_2CH_3), 1.61 (q, *J* = 7.4 Hz, 2H, CH_2CH_3), 1.38 (s, 6H, C(CH_3)$_2$), 1.27 (s, 6H, C(CH_3)$_2$), 0.70 (t, $^{3}J_{H,H}$ = 7.4 Hz, 3H, CH_2) 0.67 (t, $^{3}J_{H,H}$ = 7.4 Hz, 3H, CH_2). Elemental Analysis calculated for $C_{16}H_{25}BrO$ (313.28 g/mol): C, 61.34; H, 8.04 %; Found: C, 61.24; H, 8.17 %.

^{Cumyl}S1 (R_1 = R_2 = Cumyl) (6.3 g, 12 mmol, 80 %)

^{1}H NMR (400 MHz, $CDCl_3$, 298 K) δ (ppm): 7.34-7.17 (m, 12H, Ph), 5.17 (s, 1H, O*H*), 1.70 (s, 6H, $C^{IV}(CH_3))_2$Ph), 1.62 (s, 6H, $C^{IV}(CH_3))_2$Ph). Elemental Analysis calculated for $C_{24}H_{25}BrO$ (409.37 g/mol): C, 70.42; H, 6.16 %; Found: C, 70.36; H, 6.24 %.

^{OMe}S1 (R_1 = OMe, R_2 = ^{t}Bu) (5.5 g, 21 mmol, 78 %)

^{1}H NMR (400 MHz, $CDCl_3$, 298 K) δ (ppm): 7.88 (d, $^4J_{H\text{-}H}$ = 3.0 Hz, 1H, *1*), 6.84 (d, $^4J_{H,H}$ = 3.0 Hz, 1H, *2*), 5.42 (s, 1H, O*H*), 3.74 (s, 3H, O-CH_3), 1.38 (s, 9H, $C^{IV}(CH_3)_3$).

7.2.2 Typical Procedure to Synthesis ^{R}S2

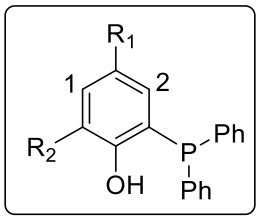

Under a dry atmosphere of N_2, a solution of the selected bromo-phenol (3.0 g), in Et_2O (60 mL), was cooled, to -78 ^{o}C, before addition of a solution of *n*-BuLi (1.6 M in hexanes, 2 equiv.), dropwise. The reaction mixture was allowed to warm, to 25 ^{o}C, under continuous stirring. The mixture was left stirring, at 25 ^{o}C, for 30 mins, after which, the solution was cooled again, to -78 ^{o}C. Chlorodiphenylphosphine (1 equiv.) was added to the solution and the mixture allowed to warm, to 25 ^{o}C. The solution formed a white suspension on warming and was left stirring, at 25 ^{o}C, for 15 h. The solution was extracted with aqueous solutions of $Na_2H_2PO_4$ (0.1 M, 2 x 100 mL) and the organic layer filtered to remove inorganic salts. The solution was then dried ($MgSO_4$), filtered, and concentrated to ~ 10 mL. MeOH (5 mL) was then added and left until crystallization of the phosphine product.

S2 ($R_1 = R_2 = {}^tBu$) (3.2 g, 8.2 mmol, 78 %)

^{1}H NMR (400 MHz, $CDCl_3$, 298 K) δ (ppm): 7.31-7.36 (m, 2H, *Ph*), 7.30 (d, $^4J_{H,H}$ = 2.8 Hz, 1H, C_bH), 6.85-6.91 (m, 6H, *Ph*), 6.82 (dd, $^3J_{P,H}$ = 6.4 Hz, $^4J_{H,H}$ = 2.4 Hz, 1H, C_dH), 6.78 (d, *J* = 2.8 Hz, 1H, O*H*), 3.70 (s, 6H, O*Me*), 1.42 (s, 9H, C-CH_3)$_3$), 1.13 (s, 9H, C-CH_3)$_3$); ^{13}C{^{1}H} NMR (75 MHz, $CDCl_3$, 298 K) δ (ppm): 156.3 (d, $^2J_{P,C}$ = 19.2 Hz, OC^{IV}), 142.5 (d, $^3J_{P,C}$ = 3.0 Hz, *o*-PhC^{IV}-*o*-^{t}Bu), 135.6 (d, $^2J_{P,C}$ = 3.0 Hz, C^{IV}(PPh$_2$)), 135.5 (d, $^3J_{P,C}$ = 1.0 Hz, , *p*-PhC^{IV}-*p*-^{t}Bu), 133.6 (d, $^{2/3}J_{P,C}$ = 18.5 Hz, *o*-or *m*-*C*H(PPh$_2$)), 129.5 (d, $^2J_{P,C}$ = 3.5 Hz, *1*), 129.1 (s, *p*-*C*H(PPh$_2$)), 128.8 (d, $^{2/3}J_{P,C}$ = 7.5 Hz, *o*-or *m*-*C*H(PPh$_2$)), 126.6 (s, *2*), 120.1 (s, C^{IV}-PPh$_2$), 35.4 (d, $^4J_{P,C}$ = 2.0 Hz, C-*C*(CH$_3$)$_3$), 34.7 (s, C-*C*(CH$_3$)$_3$), 31.7 (s, C-C(*C*H$_3$)$_3$), 29.2 (s, C-C(*C*H$_3$)$_3$); ^{31}P{^{1}H} NMR (160 MHz, $CDCl_3$, 298 K) δ (ppm): -50.7 (s, *P*). Elemental Analysis calculated for $C_{26}H_{31}PO$ (390.21 g/mol): C, 79.96; H, 8.00 Found: C, 79.89; H, 8.03.

^{Amyl}S2 ($R_1 = R_2$ = Amyl) (2.5 g, 6.0 mmol, 66 %)

^{1}H NMR (400 MHz, $CDCl_3$, 298 K) δ (ppm): 7.37-7.29 (m, 10H, P*Ph*$_2$), 7.22 (d, $^4J_{H,H}$ = 2.4 Hz, 1H, *1*), 6.79 (dd, $^3J_{P,H}$ = 5.8 Hz, $^4J_{H,H}$ = 2.4 Hz, 1H, *2*), 6.59 (d, *J* = 10.0 Hz, 1H, O*H*), 1.87 (q, $^3J_{H,H}$ = 7.4 Hz, 2H, C(CH$_3$)$_2$C*H*$_2$CH$_3$), 1.46 (q, $^3J_{H,H}$ = 7.4 Hz, 2H, C(CH$_3$)$_2$C*H*$_2$CH$_3$), 1.38 (s, 6H, C(C*H*$_3$)$_2$), 1.11 (s, 6H, C(C*H*$_3$)$_2$), 0.65 (t, $^3J_{H,H}$ = 7.4 Hz, 3H, CH$_2$C*H*$_3$), 0.58 (t, $^3J_{H,H}$ = 7.4 Hz, 3H, CH$_2$C*H*$_3$); ^{13}C{^{1}H} NMR (100 MHz, $CDCl_3$, 298 K) δ (ppm): 155.8 (d, $^2J_{P,C}$ = 18.4 Hz, C^{IV}-OH), 140.3 (d, $^3J_{P,C}$ = 2.7 Hz, *o*-PhC^{IV}-*o*-^{t}Bu), 135.6 (d, $^3J_{P,C}$ = 3.4 Hz, *p*-PhC^{IV}-*p*-^{t}Bu), 133.5 (s, *Ph*), 133.3 (d, $J_{P,C}$ = 20.5 Hz, *Ph*), 130.0 (d, $^2J_{P,C}$ = 3.6 Hz, *1*), 128.8 (s, *Ph*), 128.6 (d, $J_{P,C}$ = 6.9 Hz, *Ph*), 128.3 (s, *2*), 119.5 (s, C^{IV}-P), 38.6 (s, C^{IV}(CH$_3$)$_2$), 37.5 (s, C^{IV}(CH$_3$)$_2$), 37.0 (s, *C*H$_2$), 33.0 (s, *C*H$_2$), 28.4 (s, C^{IV}(*C*H$_3$)$_2$), 27.7 (s, C^{IV}(*C*H$_3$)$_2$), 9.5 (s, CH$_2$*C*H$_3$), 9.0 (s, CH$_2$*C*H$_3$); ^{31}P{^{1}H} NMR (160 MHz, CDCl3, 298 K) δ (ppm): -30.0 (s, *P*). Elemental Analysis calculated for $C_{28}H_{35}OP$ (418.24 g/mol): C, 80.35; H, 8.43 %; Found: C, 80.52; H, 8.56 %.

^{Cumyl}S2 (R_1 = R_2 = Cumyl) (2.1 g, 3.9 mmol, 53 %)

^{1}H NMR (400 MHz, $CDCl_3$, 298 K) δ (ppm): 7.31 (d, $^4J_{H,H}$ = 2.3 Hz, 1H, *1*), 7.30-7.12 (m, 20H, $C^{IV}(CH_3)_2Ph$ + PPh_2), 6.54 (dd, $^3J_{P,H}$ = 5.3 Hz, $^4J_{H,H}$ = 2.3 Hz, 1H, *2*), 5.11 (d, ^4J = 1.9 Hz, 1H, O*H*), 1.61 (s, 6H, $C^{IV}(CH_3)_2$), 1.53 (s, 6H, $C^{IV}(CH_3)_2$); $^{13}C\{^1H\}$ NMR (100 MHz, $CDCl_3$, 298 K) δ (ppm): 154.1 (d, $^2J_{P,C}$ = 18.8 Hz, C^{IV}-OH) 150.8 (s, *o*-cumyl-C^{IV}), 149.0 (s, *p*-cumyl-C^{IV}), 142.6 (s, *o*-PhC^{IV}-*o*-^{t}Bu), 136.3 (d, $J_{P,C}$ = 7.1 Hz, *Ph*), 134.7 (s, *p*-PhC^{IV}-*p*-^{t}Bu), 133.7 (d, $J_{P,C}$ = 18.9 Hz, *Ph*), 131.1 (s, *1*), 128.9 (s, *Ph*), 128.7 (s, *Ph*), 128.5 (d, $J_{P,C}$ = 7.5 Hz, *Ph*), 128.0 (s, *Ph*), 126.8 (s, *Ph*), 126.7 (s, *2*), 126.0 (d,$^2J_{P,C}$ = 101.7 Hz, C^{IV}-P), 42.6 (s, *o*-$C^{IV}(CH_3)_2$), 42.2 (s, *p*-$C^{IV}(CH_3)_2$), 30.9 (s, *o*-$C^{IV}(CH_3)_2$), 29.7 (s, *p*-$C^{IV}(CH_3)_2$); $^{31}P\{^1H\}$ NMR (160 MHz, $CDCl_3$, 298 K) δ (ppm): -20.5 (s, *P*). Elemental Analysis calculated for $C_{36}H_{35}OP$ (514.24): C, 84.02; H, 6.86 %; Found: C, 83.86; H, 6.76 %.

^{OMe}S2 (R_1 = OMe, R_2 = ^{t}Bu) (2.8 g, 7.7 mmol, 70 %)

^{1}H NMR (400 MHz, $CDCl_3$, 298 K) δ (ppm): 7.36 (m, 10H, C*H*(PPH_2)), 6.94 (d, $^4J_{H,H}$ = 3.0 Hz, 1H. *1*), 6.49 (d, $^2J_{P,H}$ = 10 Hz, 1H, O*H*), 6.35 (dd, $^3J_{H,H}$ = 5.0 Hz, $^4J_{H,H}$ = 3.0 Hz 1H, *2*), 3.58 (s, 3H, O-CH_3) 1.41 (s, 9H, $C^{IV}(CH_3)_3$); $^{13}C\{^1H\}$ NMR (100 MHz, $CDCl_3$, 298 K) δ (ppm): 152.9 (d, $^2J_{P,C}$ = 3.0 Hz, C^{IV}-OH) 152.6 d, ($^2J_{P,C}$ = 1.5 Hz, C^{IV}-OMe) 137.9 (d, $J_{P,C}$ = 1.5 Hz, *o*-PhC^{IV}-*o*-^{t}Bu), 135.0 (d, PhC^{IV}-PPh_2), 133.5 (d, $^{2/3}J_{P,C}$ = 18.9 Hz, *m* or *o*-*C*H(PPH_2)), 129.1 (s, *p*-CH$(PPh)_2$), 128.8 (d, $^{2/3}J_{P,C}$ = 7.5 Hz, *m* or *o*-*C*H(PPH_2)), 121.3 (d, $J_{P,C}$ = 1.0 Hz, C^{IV}-PPh_2), 116.7 (s, *1*), 115.2 (d,$^2J_{P,C}$ = 3.0 Hz, 2), 55.5 (s, O-*C*H_3), 35.2 (s, *o*-C^{IV} ^{t}Bu), 29.6 (s, *o*-^{t}Bu); $^{31}P\{^1H\}$ NMR (160 MHz, $CDCl_3$, 298 K) δ (ppm): -28.3 (s, *P*). HRMS (EI+) ($C_{23}H_{25}O_2P$): calculated m/z: 364.1592, found 364.1603.

7.2.3 Typical Synthesis of the Phosphasalen Ligands

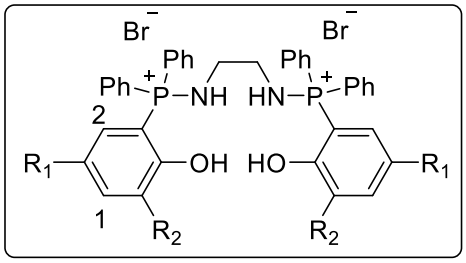

At -78 °C, bromine (2 equiv.) was slowly added to a solution of 2-(diphenylphosphino)-4,6-substituted-phenol (2.0 g) in dichloromethane (~ 50 mL). The cold bath was then removed and the solution was left to stir, for 2 h, at 25 °C. The solution was then cooled again, to –78 °C. Once cool, tributylamine (2 equiv.) was added, followed by 2,2'ethyl-amine (1 equiv.). The cold bath was then removed and the solution left stirring, for 16 h, at 25 °C. After 16 h, the solvent was removed *in vacuo* leaving a gelatinous glue. THF (5 mL) was then added causing precipitation of the product as a white solid which was left stirring for 30 mins, after which, the white solid was isolated by filtration and washed five times with a cold solution of THF and then dried.

LH_2 (2.0 g, 2.0 mmol, 40 %)

^{1}H NMR (400 MHz, $CDCl_3$, 298 K): δ (ppm): 8.14 (s, 2H, *1*), 7.72−7.50 (m, 20H, *PPh*$_2$), 6.93 (bs, 2H, N*H*), 6.43 (dd, $^4J_{H,H}$ = 2.1 Hz, $^3J_{P,H}$ = 15.2 Hz, 2*H*, 2), 3.70 (bs, 4H, NH-C*H*$_2$), 1.50 (s, 18H, *o*-^{t}Bu), 1.06 (s, 18H, *p*-^{t}Bu); ^{13}C{^{1}H} NMR (126 MHz, $CDCl_3$, 298 K) δ (ppm): 155.8 (s, *C*^{IV}-OH), 146.3 (d, $J_{P,C}$ = 12.3 Hz, *o*-Ph*C*^{IV}-*o*-^{t}Bu), 142.8 (d, $J_{P,C}$ = 10.0 Hz, *p*-Ph*C*^{IV}-*p*-P(Ph)$_2$), 134.4 (d, $J_{P,C}$ = 4.2 Hz, *p*-Ph*C*^{IV}), 133.8 (d, $J_{P,C}$ = 12.9 Hz, 1), 131.8 (s, *p*-*C*HP(Ph)$_2$), 129.8 (d, $J_{P,C}$ = 14.7 Hz, *2*), 128.6 (d, $J_{P,C}$ = 14.7 Hz, *i*-PPh*C*^{IV}), 123.0 (s, *o*-PPh), 122.1 (s, *o*-PPh), 115.1 (s, *m*-PPh), 114.3 (s, *m*-PPh), 44.2 (dd, $J_{P,C}$ = 2.2 Hz, $J_{P,C}$ = 7.8 Hz, NH-*C*H$_2$), 35.3 (s, *o*-*C*^{IV}(CH$_3$)$_3$), 34.7 (s, *p*-*C*^{IV}(CH$_3$)$_3$), 32.2 (s, *o*-^{t}Bu), 30.8 (s, *p*-^{t}Bu); ^{31}P{^{1}H} NMR (160 MHz, $CDCl_3$, 298 K) δ (ppm): 40.3 (s, P). Elemental

Analysis calculated for $C_{54}H_{68}Br_2N_2O_2P_2$ (998.21 g/mol): C, 66.03; H, 7.26; N, 2.66 %; Found: C, 65.94; H, 7.26; N, 2.62 %.

^{Amyl}**LH$_2$** (1.7 g, 1.6 mmol, 34 %)

^{1}H NMR (400 MHz, $CDCl_3$, 298 K) δ (ppm): 8.11 (s, 2H, OH), 7.72-7.51 (m, 22H, PPh_2 + *1*), 6.90 (m, 2H, NH), 6.36 (dd, $^3J_{P,H}$ = 16.0 Hz, $^4J_{H,H}$ = 2.3 Hz, 2H, *2*), 3.80-3.67 (m, 4H, NH-CH_2), 1.95 (q, $^3J_{H,H}$ = 7.4 Hz, 4H, *o*-CH_2CH$_3$(CH$_3$)$_2$), 1.45 (s, 12H, *o*-CH$_2$CH$_3$(CH_3)$_2$), 1.38 (q, $^3J_{H,H}$ = 7.4 Hz, 4H, *p*-CH_2CH$_3$(CH$_3$)$_2$), 1.00 (s, 12H, *p*-CH$_2$CH$_3$(CH_3)$_2$), 0.67 (t, $^3J_{H,H}$ = 7.4 Hz, 6H, *o*-CH$_2$CH_3(CH_3)$_2$), 0.55 (t, $^3J_{H,H}$ = 7.4 Hz, 6H, *p*-CH$_2$CH$_3$(CH_3)$_2$); ^{13}C{^{1}H} NMR (126 MHz, $CDCl_3$, 298 K) δ (ppm): 155.7 (s, C^{IV}-OH), 143.6 (d, $J_{P,C}$ = 13.5 Hz, *o*-PhC^{IV}-*o*-Amyl), 141.2 (d, $J_{P,C}$ = 10.0 Hz, *p*-PhC^{IV}-*p*-Amyl), 134.4 (s, *p*-PPh), 133.8 (d, $J_{P,C}$ = 7.2 Hz, 2), 133.8 (d, $J_{P,C}$ = 10.0 Hz, *o*-PhC^{IV}-*o*-PPh), 129.9 (d, $J_{P,C}$ = 13.6 Hz, 1), 129.3 (s, *i*-PPh_2), 123.2 (s, *o*-Ph), 122.1 (s, *o*-Ph), 115.3 (s, *m*-Ph), 114.20 (s, *m*-Ph), 44.2 (dd, $J_{P,C}$ = 6.8 Hz, $J_{P,C}$ = 13.2 Hz, NH-*C*H$_2$), 39.0 (s, *o*-*C^{IV}*CH$_2$(CH$_3$)$_2$), 37.8 (s, *p*-*C^{IV}*CH$_2$(CH$_3$)$_2$), 36.7 (s, *o*-CH$_2$*C*H$_3$(CH$_3$)$_2$), 34.2 (s, *p*-CH$_2$*C*H$_3$(CH$_3$)$_2$), 28.8 (s, *o*-CH$_2$CH$_3$(*CH$_3$*)$_2$), 28.2 (s, *p*-CH$_2$CH$_3$(*CH$_3$*)$_2$), 9.7 (s, *o*-CH$_2$*C*H$_3$(CH$_3$)$_2$), 9.1 (s, *p*-CH$_2$*C*H$_3$(CH$_3$)$_2$); ^{31}P{^{1}H} NMR (160 MHz, $CDCl_3$, 298 K) δ (ppm): 39.9 (s, *P*). Elemental Analysis calculated for $C_{58}H_{76}Br_2N_2O_2P_2$ (1054.37 g/mol): C, 66.03; H, 7.26; N, 2.66 %; Found: C, 65.94; H, 7.26; N, 2.62 %

^{Cumyl}**LH$_2$** (1.5 g, 3.1 mmol, 31 %)

^{1}H NMR (400 MHz, $CDCl_3$, 298 K) δ (ppm): 7.58 ($^4J_{H,H}$= 2.1 Hz, 2H, 1), 7.57-7.53 (m, 4H, PPh), 7.53-7.45 (m, 8H, PPh), 7.42-7.37 (m, 8H, PPH_2), 7.29-7.07 (m, 20H, C-Ph), 6.96 (m, 2H, NH), 6.77 (dd, $^3J_{P,H}$= 15.5 Hz, $^4J_{H,H}$= 2.1 Hz, 2H, 2), 6.12 (m, 2H, OH), 3.19 (s, 4H, NH$_2$CH_2), 1.63 (s, 12H, *o*-Ph(CH_3)$_2$) 1.57 (s, 12H, *p*-Ph(CH_3)$_2$); ^{13}C{^{1}H} NMR (126 MHz, $CDCl_3$, 298 K) δ (ppm): 154.8 (*C^{IV}*-OH), 149.3 (*o*-PhC^{IV}-*o*-Cumyl), 147.8 (*o*-

Ph*C*^{IV}-*o*-Cumyl), 145.5 (*o*-*C*^{IV}Cumyl), 139.8 (*p*-*C*^{IV}Cumyl), 134.2 (*o*-Ph*C*^{IV}-PPh_2), 133.4 (2), 133.1 (*p*-PPh_2), 131.1 (*i*-PPh_2), 129.6 (1), 129.1 (*o*-*o*-Cumyl), 128.3 (*m*-*o*-Cumyl), 126.9 (*o*-*p*-Cumyl), 126.8 (*m*-*p*-Cumyl), 126.0 (*p*-*o*-Cumyl), 126.0 (*p*-*p*-Cumyl), 122.1 (*o*-PPh_2), 121.3 (*o*-PPh_2), 112.2 (*m*-PPh_2), 111.4 (*m*-PPh_2), 43.7 (NH_2CH_3), 43.0 (*o*-*C*^{IV}Cumyl), 42.2 (*p*-*C*^{IV}Cumyl), 30.8 (*o*-$CH_2Ph(CH_3)_2$), 29.9 (*p*-$CH_2Ph(CH_3)_2$); $^{31}P\{^1H\}$ NMR (202 MHz, $CDCl_3$, 298 K) δ (ppm): 39.4 (s, *P*). Elemental Analysis calculated for $C_{74}H_{76}Br_2N_2O_4P_2$ (1247.29 g/mol): C, 71.27; H, 6.14; N, 2.25 %; Found: C, 70.88; H, 6.21; N, 2.26 %.

$^{OMe}LH_2$ (1.4 g, 1.5 mmol, 27 %)

^1H NMR (400 MHz, $CDCl_3$, 298 K) δ (ppm): 8.02 (t, $^3J_{H,H}$= 8.0 Hz, 2H, *1*), 7.72-7.63 (m, 12H, *PPh*), 7.63-7.50 (m, 8H, *PPh*), 7.20 (m, 2H, *OH*), 6.97 (m, 2H, N*H*), 5.97 (dd, $^3J_{P,H}$= 15.5 Hz, $^4J_{H,H}$= 2.1 Hz, 2H, *2*), 3.70 (bs, 4H, NHC*H*$_2$), 3.51 (s, 6H, OC*H*$_3$) 1.47 (s, 18H, *p*-^{t}*Bu*); $^{13}C\{^1H\}$ NMR (126 MHz, $CDCl_3$, 298 K) δ (ppm): 154.7 (s, *C*^{IV}-OH), 151.9 (s, *C*^{IV}-OMe), 145.8 (d, $J_{P,C}$ = 12.3 Hz, *o*-Ph*C*^{IV}-*o*-^{t}Bu), 134.4 (s, *p*-PPh), 133.7 (s, *o*-PPh), 129.8 (s, *m*-PPh), 122.2 (s, *i*-PPh), 121.3 (d, $J_{P,C}$ = 6.8 Hz, 2), 116.2 (s, C^{IV}-PPh_2), 115.2 (d, $J_{P,C}$ = 15.1 Hz, *1*), 55.6 (s, O-*C*H_3), 44.2 (dd, $J_{P,C}$ = 5.3 Hz, $J_{P,C}$ = 14.3 Hz, NH_2CH_3), 35.4 (s, *o*-^{t}Bu), 30.4 (s, *m*-^{t}Bu); $^{31}P\{^1H\}$ NMR (202 MHz, $CDCl_3$, 298 K) δ (ppm): 39.4 (s, *P*). Elemental Analysis calculated for $C_{48}H_{56}Br_2N_2O_4P_2$ (946.74 g/mol): C, 60.90; H, 5.96; N, 2.96 %; Found: C, 60.71; H, 6.02; N, 3.02 %.

7.2.4 Typical Synthesis Salen Ligand

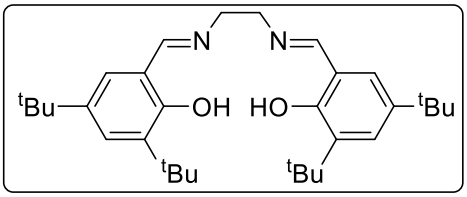

A solution of 1,2-ethylene diamine (260 mg, 4.27 mmol, 1 equiv.) in MeOH (3 mL) was added, dropwise, into a solution of 1-hydroxo-2,4-di-*tert*-butyl benzaldehyde (2.0 g, 8.54 mmols, 2 equiv.), at 25 ^{o}C. The reaction was monitored by ^{1}H NMR spectroscopy and the solution was stirred until completion (for 4 h). **L'H$_2$** was isolated, after removing the solvent in vaccuo, as a yellow powder (2.1 g, 4.26 mmol, 100 %,).

^{1}H NMR (400 MHz, $CDCl_3$, 298 K) δ (ppm): 13.64 (s, 2H, OH), 8.39 (s, 2H, *H*C=N), 7.36 (s, 1H, 1), 7.07 (s, 1H, 2), 3.92 (s, 4H, HC=NC*H$_2$*) 1.43 (s, 18H, *o*-^{t}Bu), 1.28 (s, 17H, *p*-^{t}Bu); ^{13}C{^{1}H} NMR (126 MHz, $CDCl_3$, 298 K) δ (ppm): 167.7 (s, H*C*=N), 158.2 (s, C^{IV}-OH), 140.2 (s, *C^{IV}*-HC=N), 136.7 (s, *o*-*C^{IV}*(CH_3)$_2$), 127.2 (s, 2), 126.2 (s, 1), 117.9 (s, *p*-*C^{IV}*(CH_3)$_2$), 59.8 (s, NH_2CH_2), 36.2 (s, *o*-*C*^{IV}^{t}Bu), 34.3 (s, *p*-*C*^{IV}^{t}Bu), 31.6 (s, *o*-^{t}Bu), 29.6 (s, *p*-^{t}Bu). Elemental Analysis calculated for $C_{32}H_{48}N_2O_4$ (492.75 g/mol): C, 78.00; H, 9.82; N, 5.69 %; Found: C, 78.26; H, 9.84; N, 5.72 %.

7.3 Synthesis of Indium Initiators

7.3.1 [L'InCl]

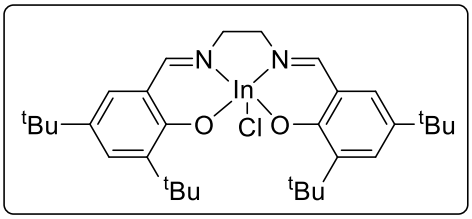

$K[N(SiMe_3)_2]$ (160 mg, 0.80 mmol) was added into a solution of **L'H₂** (200 mg, 0.40 mmol), in THF (10 mL), at 25 °C. The mixture was stirred for 16 h before removing the insoluble potassium salt. $[InCl_3]$ (90 mg, 0.40 mmol) was added. The mixture was stirred, for 16 h, at 25 °C. The potassium chloride salt was removed by filtration and the solvent was evaporated, under reduce pressure, to afford **[L'InCl]** (223 mg, 0.36 mmol, 86 %). The product was recrystallized by the slow diffusion of hexane (2 mL) into a concentrated solution of **[L'InCl]** in toluene (0.1 mL), at -40 °C (0.128 mg, 0.2 mmol 50 %).

^{1}H NMR (400 MHz, $CDCl_3$, 298 K) δ (ppm): 8.38 (s, 2H, *H*C=N), 7.51 (d, $^2J_{H\text{-}H}$ = 2.56 Hz, 2H, 1), 6.95 (d, $^2J_{H\text{-}H}$ = 2.46 Hz, 2H 2), 4.08 (m, 2H, N-C*H*H), 3.77 (m, 2H, N-CH*H*), 1.49 (s, 18H, *o*-^{t}Bu), 1.30 (s, 18H, *p*-^{t}Bu); $^{13}C\{^1H\}$ NMR (126 MHz, $CDCl_3$, 298 K) δ (ppm): 167.7 (s, H*C*=N), 158.2 (s, C^{IV}-O-In), 140.2 (s, C^{IV}-HC=N), 136.7 (s, *o*-$C^{IV}(CH_3)_2$), 127.2 (s, 2), 126.2(s, 1), 117.9 (s, *p*-$C^{IV}(CH_3)_2$), 59.8 (s, N-*C*H_2), 35.2 (s, *o*-C^{IVt}Bu), 34.3 (s, *p*-C^{IVt}Bu), 31.6 (s, *o*-^{t}Bu), 29.6 (s, *p*-^{t}Bu). Elemental Analysis calculated for $C_{32}H_{46}ClInN_2O_2$ (641.00): C, 59.96; H, 7.23; N 4.37 %. Found: C, 60.23; H, 7.35; N, 4.56 %.

7.3.2 [LInCl]

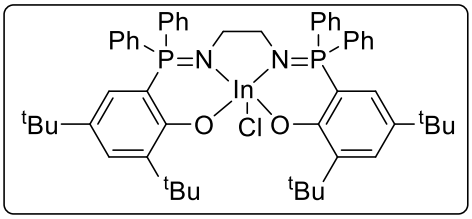

$K[N(SiMe_3)_2]$ (160 mg, 0.80 mmol) was added into a slurry of **LH_2** (200 mg, 0.20 mmol), in THF (10 mL), at 25 °C. The deprotonation reaction was monitored, by $^{31}P\{^1H\}$ NMR spectroscopy in C_6D_6, by a resonance shift from 40.0 ppm corresponding to **LH_2** to 25.4 ppm corresponding to **[LK_2]**. The insoluble potassium bromide salt was removed. $[InCl_3]$ (44 mg, 0.20 mmol) was added to the solution and was stirred, for 16 h, at 25 °C. **[LInCl]** precipitated from THF as a white solid. The $^{31}P\{^1H\}$ NMR spectrum, in C_6D_6, showed formation of **[LInCl]** (a singlet at 42.1 ppm). The solvent was removed under reduced pressure. **[LInCl]** was extracted from the potassium chloride salt with dichloromethane (2 x 10 mL). **[LInCl]** was isolated by solvent evaporation, under reduced pressure and was crystallized by the slow diffusion of hexane (2 mL) into a concentrated solution of **[LInCl]** in chloroform (0.1 mL), at -40 °C (166 mg, 0.17 mmol, 84 %).

^1H NMR (400 MHz, $CDCl_3$, 298 K) δ (ppm): 7.75 (d, J = 2.5 Hz, 2H, 1), 7.74 – 7.64 (m, 4H, *o*-PPh_2), 7.42 (dd, J = 11.7, 7.6 Hz, 4H, *o*-PPh_2), 7.11 – 6.93 (m, 8H, *m*- or *p*-PPh_2), 6.93 – 6.82 (m, 4H, *m*- or *p*-PPh_2), 6.63 (dd, J = 17.6, 2.5 Hz, 2H, 2), 3.23 – 2.91 (m, 2H, N-C*H*H), 2.80 (t, J = 10.4 Hz, 2H, N-CH*H*), 1.94 (s, 18H, *m*-^{t}Bu), 1.12 (s, 18H, *p*-^{t}Bu); $^{13}C\{^1H\}$ NMR (126 MHz, $CDCl_3$, 298 K) δ (ppm): 169.2 (d, $J_{P,C}$ = 14.9 Hz, C^{IV}-O-In), 142.5 (d, $J_{P,C}$ = 10.3 Hz, *o*-PhC^{IV}-*o*-^{t}Bu), 136.2 (d, $J_{P,C}$ = 14.8 Hz, *p*-PhC^{IV}-*p*-^{t}Bu), 133.9 (d, $J_{P,C}$ = 9.5 Hz,*o*-PPh_2), 132.8 (d, $J_{P,C}$ = 9.2 Hz, *o*-PPh_2), 132.5 (s, *p*-PPh_2), 132.0 (s, *p*-PPh_2), 129.7 (s, C^{IV}-PPh_2), 129.0 (s, *m*-PPh_2), 128.9 (d, $J_{P,C}$ = 4.3 Hz, 1), 128.3 (s, *m*-PPh_2), 126.74 (d, $J_{P,C}$ = 15.3 Hz, 2) 107.7 (s, *i*-PPh_2), 106.8 (s, *i*-PPh_2), 46.3 (dd $J_{P,C}$ = 5.2

Hz, $J_{P,C}$ = 13.8 Hz, N-*C*H_2), 36.1 (s, *o*-*C*$^{IV}(CH_3)_2$), 34.0 (s, *p*-*C*$^{IV}(CH_3)_2$), 31.4 (s, *o*-^{t}Bu), 30.3 (s, *p*-^{t}Bu); $^{31}P\{^1H\}$ NMR (161 MHz, $CDCl_3$, 298 K): δ (ppm): 42.1 (s, P). Elemental Analysis calculated for $C_{54}H_{64}ClInN_2O_2P_2$ (998.29): C, 63.69; H, 6.37; N 2.73 %. Found: C, 63.56; H, 6.65; N, 2.73 %.

7.3.3 [LInBr]

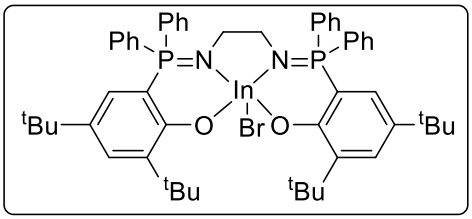

K[$N(SiMe_3)_2$] (160 mg, 0.80 mmol) was added into a slurry of **LH_2** (200 mg, 0.20 mmol), in THF (10 mL), at 25 ^{o}C. The deprotonation reaction was monitored, by $^{31}P\{^1H\}$ NMR spectroscopy, in C_6D_6, by a resonance shift from 40.0 ppm corresponding to **LH_2** to 25.4 ppm corresponding to **[LK_2]**. The insoluble potassium bromide salt was removed by filtration. [$InBr_3$] (71 mg, 0.20 mmol) was added to the solution and was stirred, for 16 h, at 25 ^{o}C. The $^{31}P\{^1H\}$ NMR spectrum showed the formation of **[LInBr]** (a singlet at 41.9 ppm). The potassium bromide salt was removed and the solvent was evaporated, under reduced pressure, to afford **[LInBr]**. **[LInBr]** was recrystallized by the slow diffusion of hexane (2 mL) into a concentrated solution of **[LInBr]** in toluene (0.1 mL), at -40 ^{o}C (183 mg, 0.18 mmol, 89 %).

^1H NMR (400 MHz, $CDCl_3$, 298 K) δ (ppm): 7.68-7.71 (m, 4H, *o*-Ph), 7.60 (t, $^2J_{H-H}$ = 7.36 Hz, 2H, *p*-Ph), 7.53-7.50 (m, 6H, *p*+*m*-Ph), 7.47 – 7.43 (m, 4H, *o*-Ph), 7.40 (d, $^2J_{H-H}$ = 2.69 Hz, 2H, 1), 7.39-7.36 (m, 4H, *o*-Ph), 6.31 (dd, $^2J_{H-H}$ = 2.52 Hz, $^3J_{H-P}$ = 17.67 Hz, 2H, 2), 3.11-3.05 (m, 2H, 3), 2.92 – 2.86 (m, 2H, 4), 1.53 (s, 9H, *o*-^{t}Bu), 1.02 (s, 18H, *p*- ^{t}Bu); $^{13}C\{^1H\}$ NMR (126 MHz, $CDCl_3$, 298 K) δ (ppm): 169.1 (d, $J_{P,C}$ = 14.9 Hz, C^{IV}-O-In), 142.3 (d, $J_{P,C}$ = 10.5 Hz, *o*-PhC^{IV}-*o*-^{t}Bu), 136.0 (d, $J_{P,C}$ = 15.3 Hz,*p*-PhC^{IV}-*p*-^{t}Bu), 133.8 (d,

$J_{P,C}$ = 9.4 Hz, *o*-PPh_2), 132.6 (d, $J_{P,C}$ = 12.4 Hz, *o*-PPh_2), 132.4 (s, *p*-PPh_2), 131.8 (s, *p*-PPh_2), 129.7 (s, C^{IV}-PPh_2), 129.1 (s, *m*-PPh_2), 129.0 (s, *m*-PPh_2), 128.7 (d, $J_{P,C}$ = 12.4 Hz, 1), 126.6 (d, $J_{P,C}$ = 13.6 Hz, 2), 107.2 (s, *i*-PPh_2), 106.3 (s, *i*-PPh_2), 45.9 (dd, d, $J_{P,C}$ = 5.6 Hz, $J_{P,C}$ = 13.1 Hz, N-CH_2), 36.0 (s, *o*-$C^{IV}(CH_3)_2$), 33.9 (s, *p*-$C^{IV}(CH_3)_2$), 31.3 (s, *o*-^{t}Bu), 30.2 (s, *p*-^{t}Bu); $^{31}P\{^1H\}$ NMR (161 MHz, $CDCl_3$, 298 K) δ (ppm): 41.9 (s, P). Elemental analysis calculated for $C_{54}H_{64}BrInN_2O_2P_2$ (1028.27 g/mol): C, 62.98; H, 6.26; N 2.72 %. Found: C, 62.80; H, 6.38; N, 2.83 %.

7.3.4 [LInO^{t}Bu][8e]

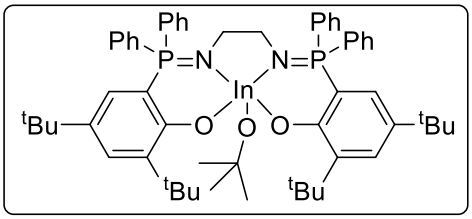

$K[N(SiMe_3)_2]$ (160 mg, 0.80 mmol) was added into a slurry of ligand **LH_2** (200 mg, 0.20 mmol), in THF (10 mL), at 25 ^{o}C. The deprotonation reaction was monitored, by $^{31}P\{^1H\}$ NMR in C_6D_6. After 16 h, the deprotonation product was obtained with a characteristic resonance at 25.4 ppm in the $^{31}P\{^1H\}$ NMR spectrum, in C_6D_6. A cloudy solution was yielded and the insoluble potassium bromide salt was removed. [$InCl_3$] (71 mg, 0.20 mmol) was added and the solution was stirred, for 16 h, at 25 ^{o}C. The $^{31}P\{^1H\}$ NMR spectrum, in C_6D_6, showed the formation of the **[LInCl]** complex (a singlet at 42.0 ppm). KO^{t}Bu (23 mg, 0.20 mmol) and was added and the solution was stirred, for 4 h, at 25 ^{o}C. The $^{31}P\{^1H\}$ NMR spectrum, in C_6D_6, showed the formation of a complex with one singlet at 40.3 ppm. The potassium chloride salt was removed; the solvent was evaporated, under reduced pressure. **[LInO^{t}Bu]** was isolated as a white powder, after crystallization by the slow diffusion of hexane (2 mL) into a concentrated solution of **[LInO^{t}Bu]** in THF (0.1 mL), at -40 ^{o}C (130 mg, 0.13 mmol, 63 %).

^{1}H NMR (400 MHz, C_6D_6, 298 K) δ (ppm): 7.78-7.75 (m, 4H,*o*-Ph) , 7.74 (d, $^{2}J_{H-H}$ = 2.4 Hz, 2H, 1), 7.50-7.42 (m, 4H, *o*-Ph), 7.11-7.05 (m, 6H, *m*-Ph or *p*-Ph), 7.00-6.85 (m, 6H, *m*-Ph or *p*-Ph), 6.59 (dd, $^{4}J_{H-H}$ = 2.3 Hz, $^{3}J_{H-P}$ = 17.00 Hz, 2H, 2), 3.11 (m, br, 2H, 3), 2.82 (m, br, 2H, 2H, 4), 1.97 (s, 18H, *o*-^{t}Bu) , 1.44 (s, 9H, O^{t}Bu), 1.12 (s, 18H, *p*-^{t}Bu); ^{13}C{^{1}H} NMR (126 MHz, C_6D_6, 298 K) δ (ppm): 171.1 (d, $J_{P,C}$ = 15.1 Hz, C^{IV}-O-In), 142.9 (d, $J_{P,C}$ = 12.4 Hz, *o*-PhC^{IV}-*o*-^{t}Bu), 135.7 (d, $J_{P,C}$ = 14.9 Hz, *p*-PhC^{IV}-*p*-^{t}Bu), 134.3 (d, $J_{P,C}$ = 9.4 Hz, *o*-PPh), 132.9 (d, $J_{P,C}$ = 9.5 Hz, *o*-PPh), 132.2 (d, $J_{P,C}$ = 13.5 Hz, C^{IV}-PPh), 131.4 (s, *p*-PPh), 130.9 (s, *p*-PPh), 129.2 (s, *m*-PPh_2), 128.8 (d, $J_{P,C}$ = 4.2 Hz, 1), 128.6 (s, *m*-PPh_2), 126.8 (d, $J_{P,C}$ = 15.3 Hz, 2), 108.2 (s, *i*-PPh_2), 107.2 (s, *i*-PPh_2), 69.2 (dd, $J_{P,C}$ = 10.4 Hz, $J_{P,C}$ = 14.3 Hz, N-CH_2), 46.6 (s, In-C^{IV}-O^{t}Bu), 36.6 (s, *o*-$C^{IV}(CH_3)_2$), 35.0 (s, O-(CH_3)$_3$), 34.2 (s, *p*-$C^{IV}(CH_3)_2$), 31.6 (s, *o*-^{t}Bu), 31.0 (s, *p*-^{t}Bu); ^{31}P{^{1}H} NMR (161 MHz, C_6D_6, 298 K) δ (ppm): 40.3 (s, P). Elemental analysis calculated for $C_{58}H_{73}InN_2O_3P_2$ (1022.41 g/mol): C, 68.10; H, 7.19; N 2.74 %. Found: C, 67.87; H, 7.32; N, 2.82 %.

7.3.5 [LInOAc]

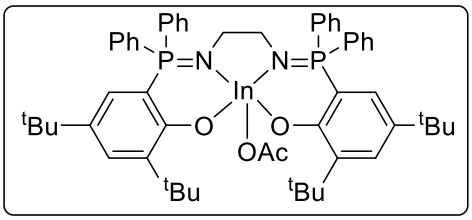

$K[N(SiMe_3)_2]$ (160 mg, 0.80 mmol) was added into a slurry of **LH_2** (200 mg, 0.20 mmol), in THF (10 mL), at 25 ^{o}C. The deprotonation reaction was monitored, by ^{31}P{^{1}H} NMR spectroscopy, in C_6D_6, by a resonance shift from 40.0 ppm corresponding to **LH_2** to 25.4 ppm corresponding to **[LK_2]**. The insoluble potassium bromide salt was removed by filtration. [$InBr_3$] (71 mg, 0.20 mmol) was added to the solution and was stirred, for 16 h, at 25 ^{o}C. The ^{31}P{^{1}H} NMR spectrum, in C_6D_6, showed formation of **[LInBr]** (a singlet at 41.9 ppm). The potassium bromide salt was removed and KOAc (25 mg, 0.25 mmol) was added. The mixture was stirred, for 16 h, at 25 ^{o}C. The ^{31}P{^{1}H} NMR spectrum, in C_6D_6,

showed the formation of **[LInOAc]** (a singlet at 38.7 ppm). The potassium bromide salt was removed and the solvent was evaporated under reduced pressure. **[LInOAc]** was isolated as a white powder, after crystallization by the slow diffusion of hexane (2 mL) into a concentrated solution of **[LInOAc]** in THF (0.1 mL), at -40 °C (165 mg, 0.16 mmol, 72 %).

^{1}H NMR (400 MHz, C_6D_6, 298 K) δ (ppm): 7.76 (d, $^{2}J_{H-H}$ = 2.54 Hz, 2H, 1), 7.64 (bs, 8H, *o*-Ph), 6.95-7.10 (m, 12H, *m*+*p*-Ph), 6.71 (dd, $^{2}J_{H-H}$ = 2.58 Hz, $^{3}J_{H-P}$ = 17.07 Hz, 2H, 2), 3.01 (bs, 2H, N-C*H*H), 2.84 (bs, 2H, N-CHC*H*), 1.87 (s, 9H, *o*-^{t}Bu), 1.85 (s, 3H, OAc), 1.13 (s, 18H, *p*- ^{t}Bu); ^{13}C{^{1}H} NMR (126 MHz, C_6D_6, 298 K) δ (ppm): 182.7 (s, $C^{IV}O_2$Me), 171.1 (d, $J_{P,C}$ = 4.3 Hz, C^{IV}-O-In), 142.8 (d, $J_{P,C}$ = 10.3 Hz, *o*-PhC^{IV}-*o*-^{t}Bu), 135.8 (d, $J_{P,C}$ = 15.0 Hz, *p*-PhC^{IV}-*p*-^{t}Bu), 134.3 (bs, *o*-PPh), 133.0 (bs, *o*-PPh), 132.1 (bs, *m*-PPh), 131.3 (bs, *m*-PPh), 129.3 (d, $J_{P,C}$ = 2.3 Hz,1), 128.6 (s, *p*-PPh), 127.5 (s, C^{IV}-PPh), 126.8 (d, $J_{P,C}$ = 14.3 Hz, 2), 109.3 (s, *i*-PPh), 108.3 (s, *o*-PPh), 47.1 (dd, $J_{P,C}$ = 5.2 Hz, d, $J_{P,C}$ = 11.5 Hz, N-*C*H$_2$), 36.2 (s, *o*-C^{IV}(CH$_3$)$_2$), 34.0 (s, *p*-C^{IV}(CH$_3$)$_2$), 31.7 (s, *o*-^{t}Bu), 30.5 (s, *p*-^{t}Bu), 20.2 (s, $C^{IV}O_2$*Me*); ^{31}P{^{1}H} NMR (161 MHz, C_6D_6, 298 K) δ (ppm): 38.7 (s, P). Elemental analysis calculated for $C_{56}H_{67}InN_2O_4P_2$ (1008.32 g/mol): C, 63.63; H, 7.41; N 3.59 %. Found: C, 63.95; H, 7.26; N, 3.31 %.

7.3.6 [LInNO$_3$]

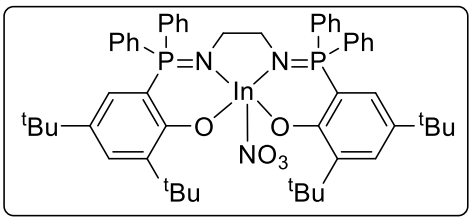

K[N(SiMe$_3$)$_2$] (160 mg, 0.80 mmol) was added into a slurry of **LH$_2$** (200 mg, 0.20 mmol), in THF (10 mL), at 25 °C. The deprotonation reaction was monitored, by ^{31}P{^{1}H} NMR spectroscopy, in C_6D_6, by a resonance shift from 40.0 ppm corresponding to **LH$_2$** to

25.4 ppm corresponding to **[LK$_2$]**. The insoluble potassium bromide salt was removed by filtration. [$InCl_3$] (71 mg, 0.20 mmol) was added to the solution and was stirred, for 16 h, at 25 ^oC. The $^{31}P\{^1H\}$ NMR spectrum in C_6D_6 showed formation of **[LInCl]** (a singlet at 41.9 ppm). $AgNO_3$ (34 mg, 0.20 mmol) was added and the mixture was stirred, for 16 h, at 25 ^oC. The $^{31}P\{^1H\}$ NMR spectrum in C_6D_6 showed the formation of [**LInNO$_3$]** (a singlet at 40.8 ppm). The silver bromide salt was removed and the solvent was evaporated under reduced pressure. **[LInNO$_3$]** was isolated as a white powder, after crystallization by the slow diffusion of hexane (2.0 mL) into a concentrated solution of **[LInNO$_3$]** in THF (0.10 mL), at -40 ^oC (143 mg, 0.14 mmol, 68 %).

^1H NMR (400 MHz, C_6D_6, 298 K) δ (ppm): 7.75 (d, $^2J_{H-H}$ = 2.62 Hz, 2H, 1), 7.54 (bs, 8H, *o*-Ph), 7.04 (bs, 4H, *p*-Ph), 6.98 (bs, 8H, *m*-Ph), 6.67 (dd, $^2J_{H-H}$ = 2.57 Hz, $^3J_{H-P}$ = 17.17 Hz, 2H, 2), 2.96 (bs, 2H, N-C*H*H), 2.76 (bs, 2H, N-CH*H*), 1.81 (s, 9H, *o*-^{t}Bu), 1.12 (s, 18H, *p*- ^{t}Bu); $^{13}C\{^1H\}$ NMR (126 MHz, C_6D_6, 298 K) δ (ppm): 169.7 (d, $J_{P,C}$ = 3.6 Hz, C^{IV}-O-In), 142.7 (d, $J_{P,C}$ = 10.3 Hz, *o*-PhC^{IV}-*o*-^{t}Bu), 136.5 (d, $J_{P,C}$ = 15.0 Hz, *p*-PhC^{IV}-*p*-^{t}Bu), 133.7 (bs, *o*-PPh), 132.8 (bs, *o*-PPh), 132.5 (bs, *m*-PPh), 131.35 (bs, *m*-PPh), 129.3 (d, $J_{P,C}$ = 2.0 Hz, 1), 128.4 (s, *p*-PPh), 127.5 (s, *p*-PPh), 126.6 (d, $J_{P,C}$ = 13.7 Hz, 2), 108.8 (s, *i*-PPh), 107.9 (s, *i*-PPh), 46.5 (dd, $J_{P,C}$ = 4.6 Hz, d, $J_{P,C}$ = 11.3 Hz N-*C*H_2), 35.9 (s, *o*-$C^{IV}(CH_3)_2$), 33.9 (s, *p*-$C^{IV}(CH_3)_2$), 31.2 (s, *o*-^{t}Bu), 29.8 (s, *p*-^{t}Bu); $^{31}P\{^1H\}$ NMR (161 MHz, C_6D_6, 298 K) δ (ppm): 40.9 (s, P). Elemental analysis calculated for $C_{54}H_{64}InN_3O_5P_2$ (1011.89 g/mol): C, 64.10; H, 6.38; N 4.15 %. Found: C, 63.96; H, 6.47; N, 4.28 %.

7.3.7 [^{Amyl}LInO^{t}Bu]

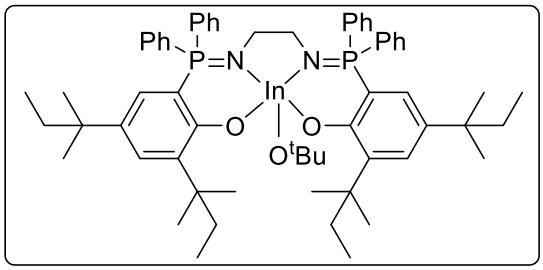

Sodium hydride (28.0 mg, 1.16 mmol) was added with continuous stirring, to a slurry of ligand ^{Amyl}**LH$_2$** (204 mg, 0.19 mmol), in THF (10 mL), at 25 ^{o}C. After 16 h, a cloudy solution was afforded, and the ^{31}P{^{1}H} NMR spectrum, in C_6D_6, showed formation of the deprotonated species (a singlet at 25.2 ppm). The insoluble sodium bromide salts were removed. [$InCl_3$] (42.8 mg, 0.19 mmol) was then added and the solution was stirred, for 16 h. The ^{31}P{^{1}H} NMR spectrum, in C_6D_6, of the afforded cloudy solution confirmed the formation of an indium chloride complex (a singlet at 41.4 ppm). Potassium *tert*-butoxide (21.7 mg, 0.19 mmol) was then added to the mixture, yielding a cloudy solution. Stirring was continued, for 24 h, and the product analysed by ^{31}P{^{1}H} NMR spectroscopy. The ^{31}P{^{1}H} NMR spectrum, in C_6D_6, showed formation of the indium alkoxide species (a singlet at 40.0 ppm). Insoluble salts were filtered and the solvent removed from the filtrate under reduced pressure. The afforded brown residue was then dissolved in a cyclohexane: hexane mixture (2.0 mL, 1:2) and the product was isolated as colourless crystals (140 mg, 0.126 mmol, 68 %).

^{1}H NMR (400 MHz, C_6D_6, 298 K) δ (ppm): 7.74 (m, 4H, P-*Ph*), 7.58 (d, $^{4}J_{H,H}$ = 2.6 Hz, 2H, 1), 7.44 (m, 4H, P-*Ph*), 7.09 (m, 4H, P-*Ph*), 6.96 (m, 6H, P-*Ph*), 6.51 (dd, $^{3}J_{P,H}$ = 17.3 Hz, $^{4}J_{H,H}$ = 2.5 Hz, 2H, 2), 3.10 (m, 2H, N-C*H*H), 2.83 (m, 2H, N-CH*H*), 2.71 (m, 2H, *o*-C^{IV}(C*H$_2$*CH$_3$)(CH$_3$)$_2$), 2.48 (m, 2H, *p*-C^{IV}(C*H$_2$*CH$_3$)(CH$_3$)$_2$), 1.90 (s, 6H, *o*-C^{IV}(CH$_2$*C*H$_3$)(C*H$_3$*)$_2$), 1.83 (s, 6H, *o*-C^{IV}(CH$_2$*C*H$_3$)(C*H$_3$*)$_2$), 1.44 (s, 9H, O^{t}Bu), 1.10 (s, 12H, *p*-C^{IV}(CH$_2$ *C*H$_3$)(C*H$_3$*)$_2$), 1.04 (t, $^{3}J_{H,H}$ = 7.4 Hz, 6H, *o*-C^{IV}(CH$_2$*CH$_3$*)(CH$_3$)$_2$), 0.64 (t, $^{3}J_{H,H}$ = 7.4 Hz,

6H, *o*-C^{IV}*(*CH$_2$*CH$_3$*)(CH$_3$)$_2$); ^{13}C{^{1}H} NMR (100 MHz, C$_6$D$_6$, 298 K) δ (ppm): 170.9 (d, J$_{P,C}$ = 4.3 Hz, C^{IV}-O-In), 148.2 (s, *o*-Ph*C*^{IV}-*o*-^{t}Bu), 146.5 (s, *p*-Ph*C*^{IV}-*p*-^{t}Bu), 134.3 (d, J$_{P,C}$ = 9.3 Hz, PPh), 133.5 (d, J$_{P,C}$ = 9.0 Hz, PPh) 132.9 (d, J$_{P,C}$ = 9.6 Hz, PPh), 132.2 (s, PPh), 131.4 (s, PPh), 131.3 (s, 1), 130.6 (s, PPh), 129.2 (s, PPh), 128.8 (d, J$_{P,C}$ = 11.8 Hz, 2), 128.7 (s, PPh), 128.6 (d, J$_{P,C}$ = 11.4 Hz, PPh), 127.6 (d, ^{2}J$_{P,C}$ = 11.5 Hz, PPh), 68.2 (O*C*^{IV}(Me)$_3$), 46.6 (s, N-*C*H$_2$), 40.1 (s, *o*-*C*^{IV}*(*CH$_2$CH$_3$)(CH$_3$)$_2$), 37.3 (s, *o*-C^{IV}*(C*H$_2$CH$_3$)(CH$_3$)$_2$), 35.2 (s, O^{t}Bu), 33.2 (s, *p*-*C*^{IV}*(*CH$_2$ CH$_3$)(CH$_3$)$_2$), 32.0 (s, *p*-C^{IV}*(C*H$_2$CH$_3$)(CH$_3$)$_2$), 28.8 (s, *o*-C^{IV}*(*CH$_2$CH$_3$)(*C*H$_3$)$_2$), 28.6 (s, *p*-C^{IV}*(*CH$_2$CH$_3$)(*C*H$_3$)$_2$), 10.5 (s, *o*-C^{IV}*(*CH$_2$*C*H$_3$)(CH$_3$)$_2$), 9.4 (s, *o*-C^{IV}*(*CH$_2$*C*H$_3$)(CH$_3$)$_2$); ^{31}P{^{1}H} NMR (162 MHz, C$_6$D$_6$, 298 K) δ (ppm): 40.0 (s, *P*). Elemental analysis calculated for C$_{62}$H$_{81}$InN$_2$O$_3$P$_2$ (1079.11 g/mol): C, 69.01; H, 7.57; N, 2.60 %; Found: C, 68.96; H, 7.72; N, 2.70 %

7.3.8 [^{cumyl}LInO^{t}Bu]

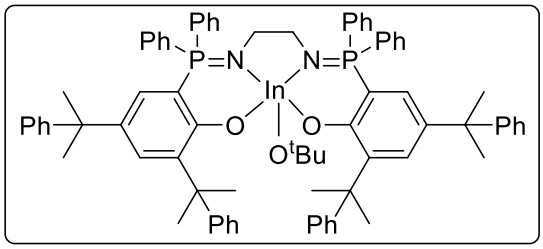

K[N(SiMe$_3$)$_2$] (130 mg, 0.64 mmol) was added into a slurry of ligand ^{Cumyl}**LH$_2$** (200 mg, 0.16 mmol), in THF (10 mL), at 25 ^{o}C. The deprotonation reaction was monitored, by ^{31}P{^{1}H} NMR spectroscopy, in C$_6$D$_6$. After 16 h, the deprotonation product was obtained showing a characteristic resonance at 20.9 ppm. A cloudy solution was yielded and the insoluble potassium bromide salt was removed. [InCl$_3$] (36 mg, 0.16 mmol) was added and the solution was stirred, for 16 h, at 25 ^{o}C. The ^{31}P{^{1}H} NMR spectrum, in C$_6$D$_6$, showed the formation of a complex (a singlet at 40.5 ppm). The potassium chloride salt was removed by filrtation. KO^{t}Bu (18 mg, 0.16 mmol) was added and the solution was stirred, for 4 h, at 25 ^{o}C. The ^{31}P{^{1}H} NMR spectrum, in C$_6$D$_6$, showed the formation of a

complex (a singlet at 41.8 ppm). The potassium chloride salt was removed by filtration; the solvent was evaporated under reduced pressure. Crystallization by the slow diffusion of hexane (2 mL) into a saturated solution of **[^{Cumyl}LInO^{t}Bu]** dissolved in THF (0.1 mL) enable isolation of the pure product as a white crystalline solid (120 mg, 0.01 mmol, 70 %).

^{1}H NMR (400 MHz, C_6D_6, 298 K) δ (ppm): 7.52-7.46 (m, 4H, *o*-PPh), 7.45 (d, $^{4}J_{H,H}$ = 2.6 Hz, 2H, 1), 7.43 (s, 2H, PPh or C-Ph), 7.38-7.30 (m, 2H, PPh or C-Ph), 7.27-7.19 (m, 4H, *o*-PPh), 7.19-7.13 (m, 8H, PPh or C-Ph), 7.13-7.00 (m, 12H, PPh or C-Ph), 7.00-6.87 (m, 10 H, PPh or C-Ph), 6.35 (dd, $^{3}J_{P,H}$ = 17.3 Hz, $^{4}J_{H,H}$ = 2.5 Hz, 2H, 2), 2.96 (m, 2H, N-C*H*H), 2.68 (m, 2H, N-CH*H*), 2.37 (s, 6H, *o*-PhC*H*$_3$CH$_3$) 2.10 (s, 6H, *o*-PhCH$_3$C*H*$_3$), 1.48 (s, 9H, O^{t}Bu), 1.39 (s, 12 H, *p*-Ph(C*H*$_3$)$_2$); ^{13}C{^{1}H} NMR (126 MHz, C_6D_6, 298 K) δ (ppm): 170.6 (d, $J_{P,C}$ = 4.3 Hz, C^{IV}-O-In), 152.2 (s, *o*-Ph*C*^{IV}-*o*-^{t}Bu), 151.3 (s, *p*-Ph*C*^{IV}-*p*-^{t}Bu), 142.6 (s, $J_{P,C}$ = 9.3 Hz, C^{IV}-PPh), 135.7 (d, 1, $J_{P,C}$ = 14.3 Hz,), 134.2 (d, $J_{P,C}$ = 9.3 Hz, PPh or C-Ph), 132.8 (s, PPh or C-Ph), 132.7 (d, $J_{P,C}$ = 9.9 Hz, PPh or C-Ph), 132.2 (s, PPh or C-Ph), 131.2 (s, PPh or C-Ph), 131.8 (s, PPh or C-Ph), 128.8 (d, $J_{P,C}$ = 4.3 Hz, 2), 127.7 (s, PPh or C-Ph), 127.0 (s, PPh or C-Ph), 125.5 (s, PPh or C-Ph), 125.0 (s, PPh or C-Ph), 110.1 (s, *i*-Ph), 109.1 (s, *i*-Ph), 69.4 (s, OC^{IV}(Me)$_3$), 54.4 (s, *o*-C^{IV}Ph(CH$_3$)$_2$), 46.7 (dd, $J_{P,C}$ = 4.6 Hz, d, $J_{P,C}$ = 11.3 Hz, N-*C*H$_2$), 44.3 (s, *p*-C^{IV}Ph(CH$_3$)$_2$), 42.4 (s, *o*-C^{IV}Ph*C*H$_3$CH$_3$), 35.1 (s, O^{t}Bu), 31.5 (s, *o*-C^{IV}Ph(*C*H$_3$)$_2$), 28.4 (s, *o*-C^{IV}PhCH$_3$*C*H$_3$); ^{31}P NMR (162 MHz, C_6D_6, 298 K) δ (ppm): 38.9 (s, P). Elemental analysis calculated for $C_{78}H_{81}InN_2O_3P_2$ (1275.88 g/mol): C, 70.60; H, 6.83; N 2.74 %. Found: C, 70.75; H, 6.48; N, 2.43 %.

7.3.9 [^{OMe}LInO^{t}Bu]

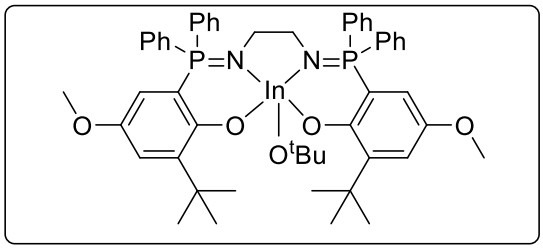

K[N(SiMe$_3$)$_2$] (52 mg, 0.40 mmol) was added into a slurry of ligand ^{OMe}**LH$_2$** (100 mg, 0.10 mmol), in THF (10 mL), at 25 ^{o}C. The deprotonation reaction was monitored, by ^{31}P{^{1}H} NMR spectroscopy, in C_6D_6. After 16 h, the deprotonated product was obtained, showing a characteristic resonance at 25.4 ppm. A cloudy solution was yielded and the insoluble potassium bromide salt was removed. [InCl$_3$] (23 mg, 0.10 mmol) was added and the reaction was stirred, for 16 h, at 25 ^{o}C. The ^{31}P{^{1}H} NMR spectrum, in C_6D_6, showed the formation of a complex (a singlet at 41.9 ppm). The potassium chloride salt was removed by filtration. KO^{t}Bu (11 mg, 0.10 mmol) and was added and the solution was stirred, for 4 h, at 25 ^{o}C. The ^{31}P{^{1}H} NMR spectrum, in C_6D_6, showed the formation of a complex (one singlet at 39.4 ppm). The potassium chloride salt was removed by filtration; the solvent was evaporated under reduced pressure. Crystallization by the slow diffusion of hexane (2 mL) into a saturated solution of **[^{OMe}LInO^{t}Bu]** dissolved in THF (0.1 mL) enable isolation of the pure product as a white crystalline solid (64 mg, 0.06 mmol, 63 %).

^{1}H NMR (400 MHz, C_6D_6, 298 K) δ (ppm): 7.71-7.62 (m, 4H, *o*-Ph), 7.48-7.41 (m, 4H, *o*-Ph), 7.40 (d, $^{2}J_{H-H}$ = 2.4 Hz, 2H, *1*), 7.11-6.96 (m, 8H, *m*-Ph or *p*-Ph), 6.95-6.85 (m, 4H, *m*-Ph or *p*-Ph), 6.14 (dd, $^{4}J_{H-H}$ = 2.3 Hz, $^{3}J_{H-P}$ = 17.00 Hz, 2H, *2*), 3.22 (s, 6H, O-C*H$_3$*) 3.07 (m, br, 2H, N-C*H$_2$*), 2.89 (m, br, 2H, 2H, 4), 1.89 (s, 18H, *o*-^{t}Bu) , 1.51 (s, 9H, *O^{t}Bu*); ^{13}C{^{1}H} NMR (126 MHz, C_6D_6, 298 K) δ (ppm): 167.9 (d, $J_{P,C}$ = 3.5 Hz, C^{IV}-O-In), 149.2 (d, $J_{P,C}$ = 19.9 Hz, *p*-PhC^{IV}-OMe), 145.1 (d, $J_{P,C}$ = 9.9 Hz, *p*-PhC^{IV}-^{t}Bu), 134.3 (d, $J_{P,C}$ = 9.9 Hz, *1*), 132.9 (d, $J_{P,C}$ = 8.9 Hz, *2*), 132.2 (s, PhC^{IV}-PPH$_2$), 131.5 (s, PPH$_2$), 130.9 (s, PPH$_2$),

130.2 (s, PPH_2), 128.8 (s, PPH_2), 128.6 (s, PPH_2), 128.4 (s, PPH_2), 120.9 (s, PPH_2), 113.4 (s, PPH_2), 108.3 (s, *i*-PPH_2), 107.3 (s, *i*-PPH_2), 67.8 (dd, $J_{P,C}$ = 4.38 Hz, $J_{P,C}$ = 12.4 Hz, N-*C*H_2), 55.3 (s, O-*C*H_3) 46.0 (s, O-$C^{IV}(CH_3)_3$), 36.5 (s, *o*-$C^{IV}Ph(CH_3)_2$), 35.2 (s, O-^{t}*Bu*), 30.7 (s, *o*-^{t}Bu); $^{31}P\{^{1}H\}$ NMR (162 MHz, C_6D_6, 298 K) δ (ppm): 39.4 (s, P). Elemental analysis calculated for $C_{52}H_{61}InN_2O_5P_2$ (970.83 g/mol): C, 64.33; H, 6.33; N 2.89 %. Found: C, 64.53; H, 6.23; N, 2.93 %.

7.4 Copolymerization of CO_2 and Epoxide with Indium Initiators

7.4.1 Low Pressure Copolymerization Reactions

In a glove box, the indium catalyst (1 equiv.) was dissolved in CHO (1 mL, 1000 equiv.) under nitrogen, and added into a Schlenk tube equipped with a magnetic stirrer bar. The Schlenk tube was sealed, removed from the glove box and connected to the vac-CO_2-N_2 line, where the reaction mixture was subjected to three cycles of vac-CO_2. The solution was then heated to the desired temperature (60 ^oC or 80 ^oC), under 1 bar of CO_2 pressure for the desired time (24 h or 48 h). The crude polymer was isolated by evaporation of the excess CHO, under reduced pressure. The polymer was dissolved in THF (1 mL) and purified by precipitation (2 times) using pentane (5 mL) to yield a white powder.

7.4.2 High pressure Copolymerization Reactions

In a glove box, the indium catalyst (1 equiv.) was dissolved in CHO or PO (6 mL, 1000 equiv.), under nitrogen, and added into a 25 mL Paar reactor (equipped with a mechanical stirrer). The reactor was sealed, removed from the glove box and connected to the high pressure CO_2 line. The reactor was heated to 80 ^oC and pressurized with CO_2. Polymerizations were stirred for 24 h, at 80 ^oC, at 10-40 bar of CO_2. Once the reaction time had elapsed, the reactor was cooled to ambient temperature, over 5 min, and the pressure was released. The crude polymer was isolated by evaporation of the excess CHO, under reduced pressure. The crude polymer was dissolved in THF (5 mL) and purified by precipitation (2 times) from pentane (20 mL) to yield a white powder.

7.4.3 *In-situ* ATR-IR Monitoring of CO_2/CHO ROCOP (1 bar of CO_2)

The ATR-IR probe was dried, overnight, under reduced pressure, prior any polymerization reactions. In a glove box, the indium catalyst (1 equiv.) was dissolved in CHO (1.5 mL, 500-1200 equiv.) and added into a Schlenk tube equipped with a magnetic stirrer bar. The Schlenk tube was sealed, removed from the glove box and connected to the vac-CO_2-N_2

line, where the reaction mixture was subjected to three cycles of vac-N_2 fill. The IR probe was quickly connected to the Schlenck tube under a N_2 atmosphere. The probe was plunged into the solution. CO_2 was added at the same time at the start of the acquisition (1 scan/15 min). The solution was heated to 80 ^oC under 1 bar of CO_2 pressure for the desired time (24 h or 48 h). The final conversion of the polymer was determined by ^1H NMR spectroscopy using an aliquot taken when the reaction was stopped. The crude polymer was isolated by evaporation of the excess CHO, under reduced pressure. The polymers was dissolved in THF (1 mL) and purified by precipitation (2 times) using pentane (5 mL) to yield a white powder.

7.4.4 *In-situ* Monitoring of CO_2 Insertion into [LInO^{t}Bu]

The ATR-IR probe was dried overnight, under reduced, pressure prior to the reaction. In a glove box, **[LInO^{t}Bu]** (100 mg, 0.1 mmol) was dissolved in THF (1.0 mL) and added into a two neck Schlenk tube equipped with a magnetic stirrer bar. The Schlenk tube was sealed, removed from the glove box and connected to the vac-CO_2- N_2 line, where the reaction mixture was subjected to three cycles of vac-N_2 fill. The IR probe was connected to the Schlenck tube under nitrogen but not immersed in the solution. The solution was degassed (to remove N_2) by freezing it (liquid N_2) and applying vacuum. The solution was warmed to 25 ^oC. The probe was immersed into the reaction solution. The data acquisition was started (1 scan/15 sec) and after 5 minutes, CO_2 was added at 1 bar of pressure. The reaction was monitored for 15 min, after which, a THF (0.5 mL) solution of DMAP (24 mg, 0.2 mmol, 2 equiv.) was injected into the reaction mixture. The reaction was monitored for 1 h, at 25 ^oC. The final product was isolated, in air by removing the THF, and was analyzed by ^1H NMR and $^{31}P\{^1H\}$ NMR spectroscopy, in C_6D_6.

7.5 Bis(imino)diphenylamido Ligands Synthesis[†][9]

7.5.1 Synthesis of $L^{Et}H_2$

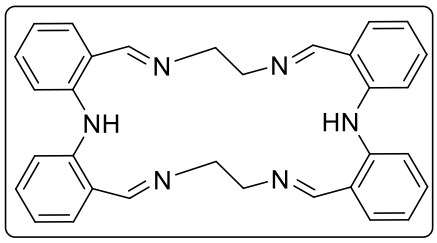

To a refluxing solution of 2,2'-iminobisbenzaldehyde (1.30 g, 6.0 mmol, 1 equiv.), in MeOH (120 mL), was added a solution, in MeOH (100 mL), of 1,2-ethylenediamine (360 mg, 6.0 mmol, 1 equiv.). Within 20 min a bright yellow precipitate formed. The solution was refluxed for a further 2 h. The precipitate was filtered, washed with ice-cold MeOH (20 mL), and dried under vacuum (2.40 g, 4.8 mmol, 80 %).

^{1}H NMR (300 MHz, $CDCl_3$, 298 K) δ (ppm): 11.54 (s, 2H, N*H*), 8.49 (s, 4H, C*H*N), 7.58 (d, $^2J_{H,H}$ = 7.5 Hz, *o*-Ph, 4H), 7.27 (d, $^2J_{H-H}$ = 7.4 Hz, 4H, *m*-Ph), 7.21 (t, $^2J_{H-H}$ = 7.6, 4H, *p*-Ph), 6.88 (t, $^2J_{H-H}$ = 7.1, 4H, *m*-Ph), 3.96 (s, 8H, NCH_2). ^{13}C{^{1}H} NMR (75 MHz, $CDCl_3$, 298 K) δ (ppm): 163.14 (s, *C*HN), 143.44 (s, 1-Ph), 131.30 (s, 5-Ph), 131.07 (s, 3-Ph), 123.38 (s, 2-Ph), 120.36 (s, 4-Ph), 117.51 (s, 6-Ph), 62.22 (s, N*C*H_2). IR (KBr): (cm^{-1}) = 3010 (w), 2836 (w), 1630 (s), 1587 (s), 1534 (m), 1384 (m), 1456 (s), 1384 (m), 1316 (m), 1208 (w), 1150 (w), 1015 (w), 982 (w), 745 (s), 486 (w). ESI(+)-MS (*m/z*): 499.26; $[C_{32}H_{30}N_6]^+$. Elemental Analysis calculated for $C_{32}H_{30}N_6$: C, 77.08; H, 6.06; N, 16.85. Found: C, 77.19; H, 6.00; N, 16.67.

[†] Ligands were prepared by Hannah Davidson and Michael Bennington at the University of Otago (New Zealand) as part of a collaboration with Prof. Sally Brooker.

7.5.2 Synthesis of $L^{Pr}H_2$

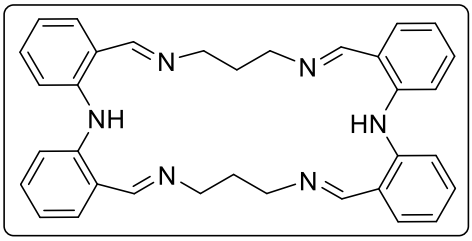

To a refluxing solution of 2,2'-iminobisbenzaldehyde (1.30 g, 6.0 mmol, 1 equiv.), in MeOH (120 mL), was added a solution in MeOH (100 mL) of 1,3-propylenediamine (390 mg, 6.0 mmol, 1 equiv.). Within 20 min a bright yellow precipitate formed. The solution was refluxed for a further 2 h. The precipitate was filtered, washed with ice-cold MeOH (20 mL), and dried under vacuum (2.50 g, 4.8 mmol, 80 %).

^{1}H NMR (300 MHz, $CDCl_3$, 298 K) δ (ppm): 11.33 (s, 2H, N*H*), 8.52 (s, 4H, C*H*N), 7.59 (dd, $^{2}J_{H,H}$ = 7.8 Hz, $^{3}J_{H,H}$ = 1.8 Hz, *o*-Ph, 4H), 7.41 (dd, $^{2}J_{H\text{-}H}$ = 8.4 Hz, $^{3}J_{H\text{-}H}$ = 0.9 Hz, 4H, *m*-Ph), 7.27 (dt, $^{2}J_{H\text{-}H}$ = 7.2, $^{2}J_{H\text{-}H}$ = 1.8 Hz, 4H, *p*-Ph), 6.94 (dt, $^{2}J_{H\text{-}H}$ = 7.5, $^{3}J_{H\text{-}H}$ = 0.9 Hz, 4H, *m*-Ph), 3.73 (t, $^{2}J_{H\text{-}H}$ = 7.2 Hz, 8H, NCH_2) 2.06 (quin, $^{2}J_{H\text{-}H}$ = 7.2 Hz, 4H, NCH_2CH_2). $^{13}C\{^{1}H\}$ NMR (75 MHz, $CDCl_3$, 298 K) δ (ppm): 161.56 (s, *C*HN), 143.48 (s, 1-Ph), 131.43 (s, 3-Ph), 130.94 (s, 5-Ph), 124.20 (s, 2-Ph), 120.55 (s, 4-Ph), 118.22 (s, 6-Ph), 60.24 (s, NCH_2), 33.20 (NCH_2CH_2). IR (KBr): (cm^{-1}) = 2920 (w), 2818 (m), 1641 (s), 1515 (s), 1451 (s), 1385 (m), 1310 (s), 1197 (w), 1156 (m), 1015 (w), 971 (w), 744 (s), 607 (w), 463 (w). ESI(+)-MS (*m/z*): 527.29; $[C_{34}H_{34}N_6]^{+}$. Elemental Analysis calculated for $C_{34}H_{34}N_6$: C, 77.54; H, 6.51; N, 15.96. Found: C, 77.30; H, 6.81; N, 16.08.

7.5.3 Synthesis of $L^{Open}H_2$

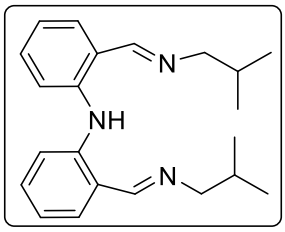

To a MeCN (20 mL) solution of 2,2′-iminobisbenzaldehyde (500 mg, 2.2 mmol) at reflux, was added a dry MeCN (25 mL) solution of isobutylamine (0.8 mL, 8 mmol). The resulting pale yellow solution was refluxed for a further 150 minutes, before cooling to 25 ^{o}C and evaporation to to dryness under reduced pressure, giving an orange oil. Analysis of the ^{1}H NMR spectrum, in $CDCl_3$, indicated some free aldehyde was still present, so the oil was taken up in dry MeCN (25 mL) and the orange solution brought to reflux before adding a dry MeCN (20mL) solution of isobutylamine (0.8 mL, 8mmol). After refluxing for a further hour the solution was left to cool, then evaporated to dryness, *in vacuo,* giving **HL^{Open}** as an orange-brown oil (570 mg, 1.7 mmol, 77 %).

^{1}H NMR (400 MHz, $CDCl_3$, 298 K) δ (ppm): 11.33 (br. s, 1H, N*H*), 8.44 (s, 2H, *H*C=N), 7.66 (d, J = 7.57 Hz, 2H, *o*-Ph), 7.26 (m, 4H, *p*-Ph/*m*-Ph), 6.95 (m, 2H, *m*-Ph), 3.40 (dd, J = 6.6, 1.2 Hz, 4H, N-*C*H_2-CH), 1.97 (t sep, J = 6.6, 6.7 Hz, 2H, *C*H-(CH_3)$_2$), 0.95 (d, J = 6.7 Hz, 12H, (CH_3)$_2$- CH)). ^{13}C{^{1}H} NMR (101 MHz, $CDCl_3$, 298 K) δ (ppm): 161.1 (s, H*C*=N), 143.8 (s, *o*-Ph), 131.0 (s, *m*-Ph), 130.9 (s, *o*-Ph), 124.4 (s, *i*-Ph), 120.6 (s, *p*-Ph), 118.5 (s, *o*-Ph), 69.9 (s, N-*C*H_2-CH), 29.9 (s, *C*H-(CH_3)$_2$), 20.8 (s, (*C*H_3)$_2$- CH)). ESI(+)-MS (*m/z*): 336.2405 (calc. for $[C_{22}H_{30}N_3]^+$ = 336.2434); 358.2220 (calc. for $[C_{22}H_{29}N_3Na]^+$ = 358.2254). Elemental Analysis calculated for $C_{22}H_{29}N_3$ (335.50 g mol^{-1}): C, 78.76; H, 8.71; N, 12.53 %. Found: C, 78.69; H, 8.86; N, 12.65 %..

7.6 Bis(imino)diphenylamido Zinc Initiators Synthesis

7.6.1 [$L^{Et}Zn_2\{N(SiMe_3)_2\}_2$]:

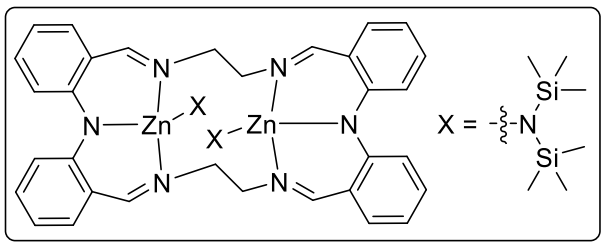

Under a nitrogen atmosphere, $\mathbf{H_2L^{Et}}$ (200 mg, 0.4 mmol, 1 equiv.) was suspended in THF (5 mL). $Zn[N(SiMe_3)_2]_2$ (310 mg, 0.8 mmol, 2 equiv) was dissolved in THF (2 mL), and was added dropwise to the ligand slurry, at 22 ^oC. Upon the addition, the solution colour changed from yellow to deep red. The solution was stirred for 24 h, at 25 ^oC, and for 2 h, at 50 ^oC, to drive the reaction to completion. The THF was removed and the crude product was dried under reduced pressure. **[$L^{Et}Zn_2\{N(SiMe_3)_2\}_2$]** was isolated as a red powder after several washing with cold hexane (350 mg, 0.37 mmol, 86 %).

^1H NMR (400 MHz, d_8-THF, 198 K) δ (ppm): 8.71 (s, 2H, *H*C=N), 7.69 (s, 2H, *H*C=N), 7.60 (d, *J* = 7.6 Hz, 2H, *m*-Ph), 7.49 (d, *J* = 8.2 Hz, 2H, *o*-Ph), 7.39 (t, *J* = 7.5 Hz, 2H, *p*-Ph), 7.10 (d, *J* = 8.8 Hz, 2H, *o*-Ph), 7.02 (t, *J* = 7.5 Hz, 2H, *p*-Ph), 6.86 (t, *J* = 7.8 Hz, 2H, *p*-Ph), 6.25 (d, *J* = 7.5 Hz, 2H, *m*-Ph), 5.92 (t, *J* = 7.3 Hz, 2H, *p*-Ph), 4.47 (d, *J* = 11.5 Hz, 2H, N-C*H*H-CH_2), 4.30 (t, *J* = 11.6 Hz, 2H, N-C*H*H-CH_2), 4.17 (d, *J* = 11.7 Hz, 2H, N-CH*H*-CH_2), 3.41 (t, *J* = 11.6 Hz, 2H, N-CH*H*-CH_2), -0.11 (s, 16H, $Si(CH_3)_2$), -0.37 (s, 17H, $Si(CH_3)_2$). $^{13}C\{^1H\}$ NMR (101 MHz, d_8-THF, 198 K) δ (ppm): 173.8 (s, H*C*=N), 171.9 (s, H*C*=N), 152.7 (s, *i*-Ph), 152.6 (s, *i*-Ph), 139.2 (s, *m*-Ph), 135.3 (s, *m*-Ph), 133.7 (s, *m*-Ph), 132.6 (s, m-Ph), 128.0 (s, *o*-Ph), 124.8 (s, o-Ph), 121.2 (s, *p*-Ph), 117.8 (s, *o*-Ph), 115.7 (s, *p*-Ph), 113.2 (s, *o*-Ph), 65.8 (s, N-*C*H_2-CH_2), 60.2 (s, N-*C*H_2-CH_2), 6.4 (s, Si(*C*H_3)$_2$), 5.5 (s, Si(*C*H_3)$_2$). Elemental analysis calculated for $C_{44}H_{64}N_8Si_4Zn_2$ (948 g/mol): C, 55.74; H, 6.80; N 11.82 %. Found: C, 55.56; H, 6.76; N, 11.67 %.

7.6.2 $[L^{Pr}Zn_2\{N(SiMe_3)_2\}_2]$

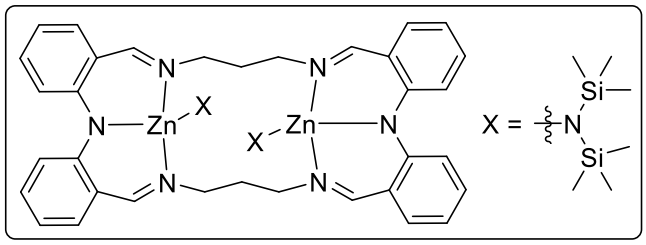

Under a nitrogen atmosphere, $\mathbf{H_2L^{Pr}}$ (200 mg, 0.38 mmol, 1 equiv.) was suspended in THF (5 mL). $Zn[N(SiMe_3)_2]_2$ (295 mg, 0.76 mmol, 2 equiv) was dissolved in THF (2 mL) and was added dropwise to the ligand slurry, at 22 °C. Upon the addition, the solution colour changed from yellow to deep red. The solution was stirred for 24 h, at 25 °C, and for 2 h, at 50 °C, to drive the reaction to completion. The THF was removed and the crude product was dried under reduced pressure. $\mathbf{[L^{Pr}Zn_2\{N(SiMe_3)_2\}_2]}$ was isolated as a red powder after several washing with cold hexane (240 mg, 0.25 mmol, 78 %).

^{1}H NMR (400 MHz, d_8-THF, 298 K) δ (ppm): 8.30 (s, 2H, *H*C=N), 8.26 (s, 2H, *H*C=N), 7.27 (d, *J* = 8.5 Hz, 4H, *m*-Ph), 7.24 – 7.18 (m, 4H, *o*-Ph), 7.12 (td, *J* = 8.6, 4.2 Hz, 4H, *p*-Ph), 6.74 – 6.50 (m, 4H, *m*-Ph), 4.30 (dt, $^2J_{H,H}$ = 12.0, $^2J_{H,H}$ = 6.5 Hz, 2H, NC*H*H), 4.16 (td, $^2J_{H,H}$ = 11.7, $^2J_{H,H}$ 3.7 Hz, 2H, NC*H*H), 3.65 – 3.53 (m, 2H, NCH*H*), 3.44 (dt, ^2J = 11.6 Hz, $^2J_{H,H}$ = 7.9 Hz, 2H, NCH*H*$_2$), 2.39 (dddd, $^2J_{H,H}$ = 15.7 Hz, $^2J_{H,H}$ = 11.5 Hz , $^2J_{H,H}$ = 7.9 Hz, $^3J_{H,H}$ = 4.2 Hz, 1H, NCH$_2$C*H*H), 2.07 (tq, $^2J_{HH}$ = 18.2 Hz, $^2J_{H,H}$ = 6.3 Hz, 1H, NCH$_2$C*H*H), 1.92 (bs, 2H, NCH$_2$C*H*$_2$), -0.15 (s, 18H, Si-(C*H*$_3$)$_2$), -0.26 (s, 18H, Si-(C*H*$_3$)$_2$). ^{13}C{^{1}H} NMR (101 MHz, d_8-THF, 298 K) δ (ppm): 170.50 (s, H*C*=N), 170.17 (s, H*C*=N), 152.48 (s, *i*-Ph), 135.51 (s, *m*-Ph), 132.32 (s, *p*-Ph), 121.59 (s, *o*-Ph), 119.13 (s, *m*-Ph), 58.32 (s, N-*C*H$_2$-CH$_2$), 57.81 (s, N-*C*H$_2$-CH$_2$), 33.94 (s, CH$_2$-*C*H$_2$-CH$_2$), 5.27 (s, Si-(*C*H$_3$)$_2$), 4.90 (s, Si-(*C*H$_3$)$_2$). Elemental Analysis calculated for $C_{46}H_{68}N_8Si_4Zn_2$ (948 g/mol): C, 56.60; H, 7.02; N 11.48 %. Found: C, 56.42; H, 6.83; N, 11.27 %.

7.6.3 [$L^{Open}ZnN(SiMe_3)_2$]

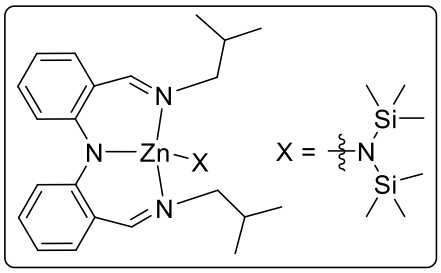

[$L^{Open}ZnN(SiMe_3)_2$] was synthesized by the reaction between **HL^{Open}** (100 mg, 0.3 mmol, 1 equiv.) and $Zn[N(SiMe_3)_2]_2$ (115 mg, 0.3 mg, 1 equiv.), in THF (5 mL), for 24 h, at 25 ^oC. After the reaction time had elapsed, the solvent was removed, under reduced pressure, yielding an orange powder. The crude product was washed with hexane (3 x 1 mL), filtered and dried under reduced pressure (91 mg, 55 %). A further quantity of product was obtained by crystallisation of the filtrate, at -40 ^oC, overnight (120 mg, 0.2 mmol, 72 %,).

^1H NMR (400 MHz, C_6D_6, 298 K) δ (ppm): 7.59 (s, 2H, C*H*=N), 7.39 (d, *J* = 8.8 Hz, 2H, *m*-Ph), 7.00 (m, 4H, *p*-Ph + *o*-Ph), 6.58 (t, *J* = 7.5, 2H, *m*-Ph), 3.54 (br. s, 2H, N-CH_2-C), 2.97 (br. s, 2H, N-CH_2-C), 2.06 (sep, *J* = 6.7 Hz, 2H), 0.72 (br. s, 12H), 0.20 (s, 18H, N(Si(CH_3)$_3$)$_2$). $^{13}C\{^1H\}$ NMR (101 MHz, C_6D_6, 298 K) δ (ppm): 168.50 (*C*H=N), 152.66 (*o*-Ph), 135.58 (*o*-Ph), 132.51 (*p*-Ph), 117.01 (*m*-Ph), 69.13 (N-*C*H_2-C), 29.06 (CH_2-*C*H-(CH_3)$_2$), 19.70 ((CH_3)$_2$), 5.64 (N(Si(*C*H_3)$_3$)$_2$). No conclusive elemental analysis was conducted for **3** due to its instability. Elemental analysis indicates product decomposition and formation of the corresponding **$L^{Open}ZnOH$** complex and $HN(SiMe_3)_2$. Elemental Analysis calculated for $C_{28}H_{47}N_3ZnO$ + 1.5 equiv. $C_6H_{19}NSi_2$: C, 56.50; H, 8.80; N 9.57 %. Found: C, 56.54; H, 8.54; N, 9.17 %.

7.6.4 $[L^{Et}Zn_2(O^iPr)_2]$[10]

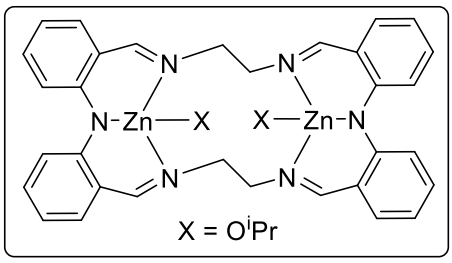

$[L^{Et}Zn_2(O^iPr)_2]$ was first synthesised by Dr Charles Romain at Imperial College of London. Here, an improved synthesis is reported by the reaction of **$[L^{Et}Zn_2\{N(SiMe_3)_2\}_2]$** and isopropanol. In this study, **$[L^{Et}Zn_2(O^iPr)_2]$** was not isolated but was generated *in-situ* during catalysis experiments (refer to section 7.7). The reaction was monitored by ^{1}H NMR spectroscopy, at 25 ^{o}C, to ensure product formation.

To a Young's tap NMR tube was added **$[L^{Et}Zn_2\{N(SiMe_3)_2\}_2]$** (20 mg, 0.02 mmol, 1 equiv) and isopropanol (0.84 mL of a 0.05 M stock solution = 0.05 M, in d_8-THF, 0.04 mmol, 2 equiv.), at 25 ^{o}C. ^{1}H and ^{13}C{^{1}H} NMR spectra were in accordance with previously reported data.[9]

^{1}H NMR (400 MHz, d_8-THF, 298 K) δ (ppm): 8.32 (s, 4 H, C*H*=N), 7.22 (dd, $^3J_{H,H}$ = 8.0 Hz, $^4J_{H,H}$ = 1.2 Hz, 4H, Ph-*H*), 6.93 (ddd, $^3J_{H,H}$ = 7.8 Hz, $^3J_{H,H}$ = 8.2 Hz, $^4J_{H,H}$ = 1.2 Hz, 4 H, Ph-*H*), 6.90 (d, $^3J_{H,H}$ = 7.6 Hz, 4 H, Ph-*H*), 6.58 (dd, $^3J_{H,H}$ = 8.1 Hz, $^3J_{H,H}$ = 8.0 Hz, 4 H, Ph-*H*), 4.13 (m, 4 H, CH_2), 3.85−3.78 (m, 6 H, CH_2+O*iPr*), 0.61 (d, $^3J_{H,H}$ = 5.5 Hz, 6 H, O*iPr*), 0.60 (d,$^3J_{H,H}$ = 5.5 Hz, 6 H, O*iPr*).^{13}C{^{1}H} NMR (100 MHz, d_8-THF) δ (ppm) 167.7 (s, *C*H=N), 157.6 (s, C^{IV}Ph), 134.5 (s, Ph), 131.1 (s, Ph), 124.3 (br s, Ph), 123.9 (s, C^{IV}Ph), 116.9 (br s, Ph), 65.0 (s, *C*H_2N*C*H_2), 63.4 (s, O*C*H(CH_3)$_2$), 28.1 (s, OCH(*C*H_3)$_2$). Elemental Analysis calculated: C, 61.22; H, 5.68; N, 11.27. Found: C, 60.96; H, 5.78; N, 11.16.

7.6.5 [$L^{Pr}Zn_2(O^iPr)_2$]

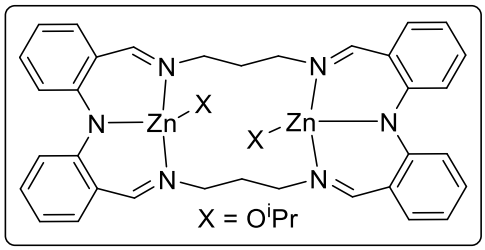

In this study, **[$L^{Pr}Zn_2(O^iPr)_2$]** was not isolated but was generated *in-situ* during catalysis experiments (refer to section 7.7). The reaction was monitored by ^{1}H NMR spectroscopy, at 25 ^{o}C, to ensure product formation.

To a Young's tap NMR tube was added **[$L^{Pr}Zn_2\{N(SiMe_3)_2\}_2$]** (20 mg, 0.02 mmol, 1 equiv) and isopropanol (0.84 mL of a 0.05 M stock solution = 0.05 M, in d_8-THF, 0.04 mmol, 2 equiv.), at 25 ^{o}C.

^{1}H NMR (400 MHz, d_8-THF, 298 K) δ (ppm): 8.82 (s, 4H, C*H*=N), 7.65 (d, $^3J_{H,H}$ = 7.6 Hz, Ph-*H*), 7.04 (ddd, $^3J_{H,H}$ = 7.8 Hz, $^3J_{H,H}$ = 8.0 Hz, $^4J_{H,H}$ = 2.0 Hz, Ph-*H*), 6.66 (dt, $^3J_{H,H}$ = 15.2 Hz, $^3J_{H,H}$ = 7.2 Hz, Ph-*H*), 3.82-3.62 (m, 10H, NC*H*$_2$CH$_2$ + O-C*H*(CH$_3$)$_2$), 2.33 (br. s, 4H, CH$_2$C*H*$_2$CH$_2$), 0.98 (s, 6H, O-CH(C*H*$_3$)$_2$), 0.63 (s, 6H, O-CH(C*H*$_3$)$_2$). ^{13}C{^{1}H} NMR (100 MHz, d_8-THF) δ (ppm): 165.8 (C^{IV}Ph), 165.0 (s, *C*H=N), 131.4 (s, Ph), 130.5 (s, Ph), 124.9 (s, Ph), 123.7 (s, C^{IV}Ph), 62.7 (s, O-*C*H(CH$_3$)$_2$), 55.8 (s, N*C*H$_2$CH$_2$), 53.2 (s, NC*H*$_2$CH$_2$), 32.3 (s, CH$_2$*C*H$_2$CH$_2$), 24.7 (s, OCH(*C*H$_3$)$_2$).

7.6.6 [$L^{Open}Zn(O^iPr)$]

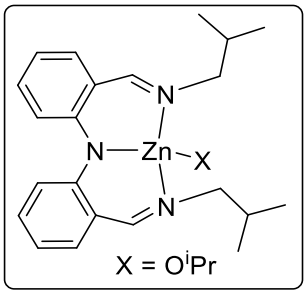

In this study, **[$L^{Open}Zn(O^iPr)$]** was not isolated but was generated *in-situ* during catalysis experiments (refer to section 7.7). The reaction was monitored by ^{1}H NMR spectroscopy, at 25 ^{o}C, to ensure product formation.

To a Young's tap NMR tube was added **[$L^{Open}ZnN(SiMe_3)_2$]** (20 mg, 0.02 mmol, 1 equiv) and isopropanol (0.42 mL of a 0.05 M stock solution = 0.05 M, in d_8-THF, 0.02 mmol, 1 equiv.), at 25 ^{o}C.

^{1}H NMR (400 MHz, d_8-THF, 298 K) δ (ppm): 8.23 (s, 2 H, C*H*=N), 7.60 (br s, 2H, Ph-*H*), 7.25 (br. s, 1 H, Ph-*H*), 7.10 (br. s, 2 H, Ph-*H*), 6.91 (br. s, 1H, Ph-*H*), 6.67 (br s., 2H, Ph-*H*) 3.83 (m, 3 H, NCH_2CH + OC*H*$(CH_3)_2$), 3.28 (m, 1 H, NC*H*HCH), 3.14 (m, 1H, NCH*H*CH) 2.08 (br. s, 1H, $NCH_2CH(CH_3)_2$), 1.98 (m, 1H, $NCH_2CH(CH_3)_2$), 0.93 (m, 18 H, $CH(CH_3)_2$ +O*iPr*).^{13}C{^{1}H} NMR (100 MHz, d_8-THF) δ (ppm) 164.21 (s, *C*H=N), 155.1 (s, C^{IV}Ph), 143.4 (C^{IV}Ph), 132.4 (s, Ph), 132.1 (s, Ph), 132.0 (s, Ph), 130.7 (s, Ph), 124.3 (C^{IV}Ph), 122.1 (s, Ph), 121.9 (s, Ph), 118.0 (s, Ph), 117.4 (s, Ph), 69.5 (s, N*C*H_2CH), 69.5 (s, O*C*H$(CH_3)_2$), 62.7 (s, N*C*H_2CH), 29.9 (s, $CH_2CH(CH_3)_2$), 29.03 (s, $CH_2CH(CH_3)_2$), 27.9 (s, OCH$(CH_3)_2$, 20.1 (s, CH$(CH_3)_2$), 19.80 (s, CH$(CH_3)_2$).

7.7 Typical Ring Opening Polymerization Procedures

7.7.1 *rac*-Lactide (*rac*-LA) Ring Opening Polymerization (ROP)

7.7.1.1. Leaving Polymerization with Amido Initiators

In a glove box, *rac*-LA (1000 equiv. unless otherwise stated) was dissolved in THF. The concentration of *rac*-LA, in THF, was kept at 1 M for all polymerization reactions. The rac-LA solution was added to a solution of the initiator (5 mg, 1 equiv.), in THF (0.2 mL), and the polymerization reaction was stirred, at 25 ^{o}C. The reaction was followed by taking aliquots and quenching the reaction mixture in hexane at different times. Aliquots were analysed by ^{1}H NMR spectroscopy, homonuclear-decoupled ^{1}H NMR, in $CDCl_3$, and by SEC, in THF.

7.7.1.2 Leaving Polymerization with Alkoxide Initiators

In a glove box, *rac*-LA (1000 equiv. unless otherwise stated) was dissolved in THF. The concentration of *rac*-LA, in THF, was kept at 1 M for all polymerization reactions. The alkoxide was generated *in-situ* by addition of two equivalents (1 equiv for **[L^{Open}Zn N(SiMe$_3$)$_2$]**) of isopropanol to the catalyst precursor. The solution was stirred, for 30 min, at 25 ^{o}C, prior the addition of *rac*-LA. The rac-LA solution was added to a solution of the initiator (5 mg, 1 equiv.), in THF (0.2 mL), and the polymerization reaction was stirred, at 25 ^{o}C. The reaction was followed by taking aliquots and quenching the reaction mixture in hexane at different times. Aliquots were analysed by ^{1}H NMR spectroscopy, homonuclear-decoupled ^{1}H NMR, in $CDCl_3$, and by SEC, in THF.

7.7.1.3 Immortal Polymerization with Amido Initiators

In a glove box, *rac*-LA (1000 equiv. unless otherwise stated) was dissolved in THF. The concentration of *rac*-LA in THF was kept at 1 M for all polymerization reactions. The required amount of isopropanol (from a stock solution of isopropanol, in THF, 0.05 M), was also added to the *rac*-LA solution. The rac-LA solution was added to a solution of the

initiator (5 mg, 1 equiv.), in THF (0.2 mL), and the polymerization reaction was stirred, at 25 ^{o}C. The reaction was followed by taking aliquots and quenching the reaction mixture in hexane at different times. Aliquots were analysed by ^{1}H NMR spectroscopy, homonuclear-decoupled ^{1}H NMR, in $CDCl_3$, and by SEC, in THF.

7.7.2 ε-Caprolactone (ε-CL) and Trimethylene Carbonate (TMC) ROP

In a glove box, the desired monomer [1000 equiv., *ε*-CL or TMC] was dissolved in THF. The concentration of monomer was kept at 1 M for all the polymerization reactions. Isopropanol (10 equiv.), from a stock solution of isopropanol, in THF [0.05 M], was added on the monomer solution. The monomer solution was added to a solution of the initiator (5 mg, 1 equiv.), in THF (0.2 mL), and the polymerization reaction was stirred, at 25 ^{o}C. The reaction was followed by taking aliquots and quenching the reaction mixture in hexane at different times. Aliquots were analysed by ^{1}H NMR spectroscopy, in $CDCl_3$, and by SEC, in THF.

7.7.3 Procedures for ε-CL/*rac*-LA Copolymerization Reactions

In a glove box, *rac*-LA (150 mg, 1.0 mmol, 200 equiv.), *ε*-CL (470 mg, 4.1 mmol, 800 equiv.) and isopropanol (1 mL of a 0.05 M stock solution, in THF, 10 equiv.) were dissolved in THF (3.6 mL). The monomers solution was injected to a solution of **[$L^{Et}Zn_2\{N(SiMe_3)_2\}_2$]** (5 mg, 0.005 mmol, 1 equiv.), in THF (0.2 mL), at 25 ^{o}C. The total monomer concentration was 1 M. The reaction progress was monitored by taking aliquots and quenching the reaction mixture in hexane at different times Aliquots were analysed by ^{1}H NMR spectroscopy, in $CDCl_3$, and by SEC, in THF.

7.8 Synthesis of *o*-Vanillin Derived Ligands.

7.8.1 Typical Procedure for *o*-Vanillin Amination Reaction

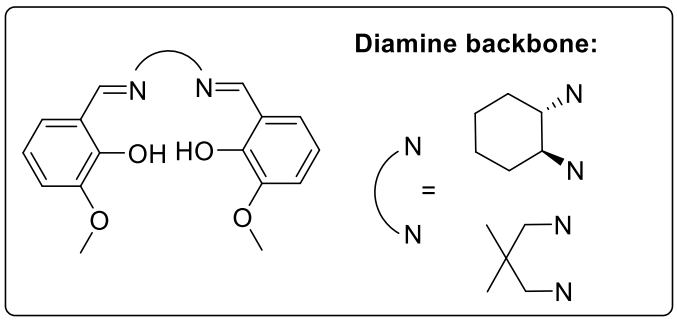

The appropriate diamine [(±)-*trans*-1,2-diaminocyclohexane (1.90 g, 16.0 mmol) or 2,2-dimethyl-1,3-propanediamine (1.67 g, 16.0 mmol)] in MeOH (5 mL) was added dropwise to a pale yellow solution of *o*-vanillin (5.0 g, 33.0 mmol) in MeOH (50 mL). Upon addition of the diamine, a deep yellow solution was obtained. The mixture was stirred for 4 h at 22 ^{o}C and the solvent was subsequently removed under vacuum to give a yellow powder. (**L_{1a}H**: 6.1 g, 16.0 mmol, 100 %, **L_{2a}H**: 5.9 g, 16.0 mmol 100 %).

L_{1a}H: ^{1}H NMR (400 MHz, $CDCl_3$, 298 K) δ (ppm): 13.84 (s, 2H, Ph-O*H*), 8.24 (s, 2H, C*H*=N), 6.85 (d, $^{3}J_{H,H}$ = 7.9 Hz, 2H, *m*-Ph), 6.78 (d, $^{3}J_{H,H}$ = 7.8 Hz, 2H, *m*-Ph), 6.72 (t, $^{3}J_{H,H}$ = 7.9 Hz, 2H, *p*-Ph), 3.86 (s, 6H, O-C*H*$_3$), 3.31 (m, 2H, chiral C*H*-cyclohexyl), 1.94 (m, 2H, C*H*$_2$-cyclohexyl), 1.87 (m, 2H, C*H*$_2$-cyclohexyl), 1.71 (m, 2H, C*H*$_2$-cyclohexyl), 1.48 (m, 2H, C*H*$_2$-cyclohexyl); ^{13}C{^{1}H} NMR (101 MHz, $CDCl_3$) δ (ppm): 164.8 (s, H*C*=N), 151.7 (s, *i*-Ph), 148.3 (s, *o*-Ph), 123.2 (s, *m*-Ph), 118.5 (s, *o*-Ph), 118.0 (s, *p*-Ph), 113.9 (s, *m*-Ph), 72.5 (s, *C*H chiral-cyclohexyl), 56.1 (s, O-*C*H$_3$), 33.1 (s, *C*H$_2$-cyclohexyl), 24.1 (s, *C*H$_2$-cyclohexyl). ESI(+)-MS (*m/z*): 383; [**L_{1a}H** + H]$^{+}$; Elemental analysis calculated for $C_{22}H_{26}N_2O_4$ (382.86 g/mol): C, 69.09; H, 6.85; N 7.32 %. Found: C, 69.21; H, 6.93; N, 7.38 %.

$L_{2a}H$: ^{1}H NMR (400 MHz, $CDCl_3$, 298 K) δ (ppm): 14.14 (s, 2H, Ph-O*H*), 8.31 (s, 2H, C*H*=N), 6.91 (d, $^{3}J_{H,H}$ = 7.9 Hz, 2H, *m*-Ph), 6.87 (d, $^{3}J_{H,H}$ = 7.9 Hz, 2H, *m*-Ph), 6.79 (t, $^{3}J_{H,H}$ = 7.8 Hz, 2H, *p*-Ph), 3.90 (s, 6H, O-CH_3), 3.48 (s, 4H, N-CH_2-C), 1.06 (s, 6H, C-(CH_3)$_2$); $^{13}C\{^{1}H\}$ NMR (101 MHz, $CDCl_3$, 298 K) δ (ppm): 165.9 (s, H*C*=N), 152.2 (s, *i*-Ph), 148.5 (s, *o*-Ph), 123.0 (s, *m*-Ph), 118.5 (s, *o*-Ph), 118.0 (s, *p*-Ph), 113.9 (s, *m*-Ph), 67.4 (s, N-*C*H$_2$-C), 56.1 (s, O-*C*H$_3$), 36.3 (s, CH$_2$-*C*-(CH$_3$)$_2$), 24.4 (s, C-(*C*H$_3$)$_2$)). ESI-MS (*m/z*): 371; ([**$L_{2a}H$** + H]$^{+}$, 100 %); Elemental analysis calculated for $C_{21}H_{26}N_2O_4$ (370.49 g/mol): C, 68.09; H, 7.07; N, 7.56. Found: C, 68.21; H, 6.99; N, 7.45 %.

7.8.2 Typical Reduction Procedure for the Synthesis of $L_{1b}H$ and $L_{2b}H$

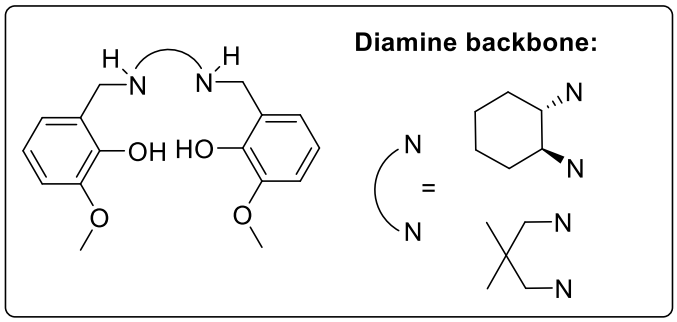

The reduction was performed *in situ* following the synthesis of **$L_{1a}H$** or **$L_{2a}H$** in methanol solution, by slow addition of 3.5 equivalents of $NaBH_4$ (Careful: exothermic!). The reaction mixture was stirred for 2 h at 22 ^{o}C. Water was then added until a white precipitate was obtained. The suspension was left to stir for 16 h before the product was isolated via filtration, as a white powder. (**$L_{1b}H$**, 6.0 g, 15.5 mmol, 97 % and **$L_{2b}H$**, 6.0 g, 16 mmol, 97 %)

$L_{1b}H$: ^{1}H NMR (400 MHz, $CDCl_3$, 298 K) δ (ppm): 6.78 (dd, 2H, $^{3}J_{H,H}$ = 8.1, 1.6 Hz, *m*-Ph), 6.72 (t, $^{3}J_{H,H}$ = 7.5 Hz, 2H, *p*-Ph), 6.63 (dd, $^{3}J_{H,H}$ = 7.5, 1.6 Hz, 2H, *m*-Ph), 4.01 (d, $^{3}J_{H,H}$ = 13.6 Hz, 2H, NH-CH_2-Ph), 3.88 (d, $^{3}J_{H,H}$ = 13.6 Hz, 2H, NH-CH_2-Ph), 3.85 (s, 6H, O-CH_3), 2.40 (m, C*H*-cyclohexyl), 2.11 (m, 2H, CH_2-cyclohexyl), 1.67 (m, 2H, CH_2-cyclohexyl), 1.20 (m, 4H, CH_2-cyclohexyl); $^{13}C\{^{1}H\}$ NMR (101 MHz, $CDCl_3$, 298 K) δ

(ppm): 147.9 (s, *i*-Ph), 146.8 (s, *o*-Ph), 124.1 (s, *o*-Ph), 120.7 (s, *m*-Ph), 118.9 (s, *p*-Ph), 110.8 (s, *m*-Ph), 60.5 (s, *C*H chiral-cyclohexyl), 56.0 (s, O-*C*H_3), 49.1 (s, C-*C*H_2-NH), 30.6 (s, *C*H_2-cyclohexyl), 24.3 (s, *C*H_2-cyclohexyl). ESI-MS (*m/z*): 387; [$\mathbf{L_{1b}H}$ + H]$^+$; Elemental calculated analysis for $C_{22}H_{30}N_2O_4$ (386.49 g/mol): C, 68.37; H, 7.82; N, 7.18 %. Found: C, 68.23; H, 7.91; N, 7.16 %.

L_{2b}H: ^{1}H NMR (400 MHz, $CDCl_3$, 298 K) δ (ppm): 6.84 (dd, $^3J_{H,H}$ = 7.5, 1.6 Hz, 2H, *m*-Ph), 6.75 (t, $^3J_{H,H}$ = 7.8 Hz, 2H, *p*-Ph), 6.65 (dd, $^3J_{H,H}$ = 7.5 Hz, 1.6 Hz, 2H, *m*-Ph), 4.79 (s, 4H, N*H* and Ph-O*H*), 3.98 (s, 4H, NH-C*H*$_2$-Ph), 3.87 (s, 6H, O-C*H*$_3$), 2.56 (s, 4H, NH-C*H*$_2$-C), 1.00 (s, 6H, C-(C*H*$_3$)); ^{13}C{^{1}H} NMR (101 MHz, $CDCl_3$, 298 K) δ (ppm): 148.1 (s, *i*-Ph), 147.2 (s, *o*-Ph), 123.1 (s, *o*-Ph), 120.6 (s, *m*-Ph), 118.8 (s, *p*-Ph), 111.0 (s, *m*-Ph), 57.7 (s, C-*C*H_2-NH), 55.9 (s, O-*C*H_3), 53.2 (s, NH-*C*H_2-Ph), 34.7 (s, $(CH_3)_2$-*C*-$(CH_2)_2$), 24.4 (s, C-(*C*H_3)$_2$). ESI-MS (*m/z*): 375; [$\mathbf{L_{2b}H}$ + H]$^+$; Elemental analysis calculated for $C_{21}H_{30}N_2O_4$ (374.48 g/mol): C, 67.35; H, 8.078; N 7.48 %. Found: C, 67.19; H, 7.90; N 7.49 %.

7.9. Synthesis of *o*-Vanillin Derived Zinc Initiators

7.9.1 $[L_{1a}Zn_2(OAc)_2]$[7a] and $[L_{1b}Zn_2(OAc)_2]$

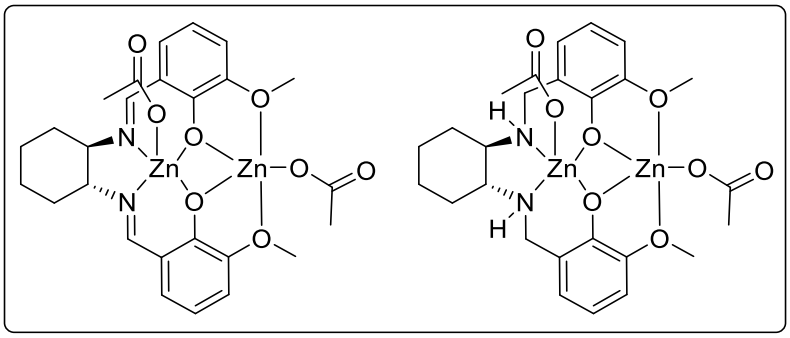

A solution of $[Zn(OAc)_2.(H_2O)_2]$ (2 equiv.) in MeOH (15 mL) was added in one portion into a solution of $\mathbf{L_{1a}H}$ or $\mathbf{L_{1b}H}$ (500 mg) in MeOH (3 mL). The reaction mixture was stirred at 22 °C for 16 h. The di-zinc complexes $\mathbf{[L_{1a}Zn_2(OAc)_2]}$ and $\mathbf{[L_{1b}Zn_2(OAc)_2]}$ were isolated as a white powder via filtration ($\mathbf{[L_{1a}Zn_2(OAc)_2]}$**:** 400 mg, 0.63 mmol, 65 %; $\mathbf{[L_{1b}Zn_2(OAc)_2]}$**:** 500 mg, 0.80 mmol, 62 %).

$\mathbf{[L_{1a}Zn_2(OAc)_2]}$**:** ^{1}H NMR (400 MHz, $CDCl_3$, 298 K) δ (ppm): 8.23 (s, 2H, C*H*=N), 6.84 (d, $^3J_{H,H}$ = 7.5 Hz, 2H, *m*-Ph), 6.79 (d, $^3J_{H,H}$ = 8.2 Hz, 2H, *m*-Ph), 6.60 (t, $^3J_{H,H}$ = 7.8 Hz, 2H, *p*-Ph), 3.88 (s, 6H, O-C*H*$_3$), 3.35 (br m, 2H, C*H* chiral cyclohexyl), 2.43 (br m, 2H, C*H*$_2$-cyclohexyl), 2.00 (br m, 6H *OAc* and 2H C*H*$_2$-cyclohexyl), 1.46 (br m, 4H, C*H*$_2$-cyclohexyl); $^{13}C\{^1H\}$ NMR (101 MHz, $CDCl_3$, 298 K) δ (ppm): 165.4 (s, H*C*=N), 150.8 (s, *i*-Ph), 126.2 (s, *m*-Ph), 119.2 (s, *o*-Ph), 115.0 (s, *p*-Ph), 113.5 (s, *m*-Ph), 110.1 (s, *o*-Ph), 65.6 (s, CH-cyclohexyl), 55.7 (s, O-*C*H$_3$), 27.9 (s, *C*H$_2$-cyclohexyl), 24.4 (s, *C*H$_2$-cyclohexyl), 22.9 (s, *OAc*). Elemental Analysis calculated for $C_{26}H_{30}N_2O_8Zn_2$ (629 g/mol): C, 49.62; H, 4.81; N, 4.45 %. Found: C, 49.50; H, 4.89; N, 4.55 %.

$\mathbf{[L_{1b}Zn_2(OAc)_2]}$**:** ^{1}H NMR (400 MHz, d_5-py, 298 K) δ (ppm): 6.75 (m, 4H, *m*-Ph), 6.61 (t, $^3J_{H,H}$ = 7.7 Hz, 2H, *p*-Ph), 4.28 (br s, 4H, NH-C*H*$_2$-Ph and NH), 4.19 (br s, 2H, NH-C*H*$_2$-Ph), 3.60 (s, 6H, O-CH$_3$), 2.63 (s, 2H, chiral C*H*-cyclohexyl), 2.32 (m, 2H, C*H*$_2$-

cyclohexyl), 2.09 (s, 11H, *OAc+HOAc*), 1.60 (s, 2H, C*H*$_2$-cyclohexyl), 1.09 (m, 4H, C*H*$_2$-cyclohexyl); ^{13}C{^{1}H} NMR (101 MHz, d_5-pyr, 298 K) δ (ppm): 176.1 (s, *i*-Ph), 153.4 (s, *o*-Ph), 150.1 (s, *o*-Ph), 122.8 (s, *m*-Ph), 115.1 (s, *p*-Ph), 110.4 (s, *m*-Ph), 59.7 (s, chiral *C*H-cyclohexyl), 54.9 (s, O-*C*H$_3$), 50.3 (s, NH-*C*H$_2$-Ph), 29.9 (s, *C*H$_2$-cyclohexyl), 24.9 (s, *C*H$_2$-cyclohexyl), 22.3 (s, *OAc*). Elemental Analysis calculated for $C_{26}H_{34}N_2O_8Zn_2$ (633 g/mol): C, 49.31; H, 5.41; N, 4.42 %. Found: C, 49.18; H, 5.34; N, 4.39 %.

7.9.2 [$L_{2a}Zn_2(OAc)_2$]

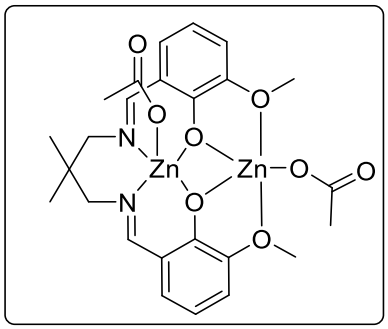

A solution of [Zn(OAc)$_2$.(H$_2$O)$_2$] (440 mg, 2.0 mmol) in MeOH (15 mL) was added to a solution of **L_{2a}H** (370 mg, 1.0 mmol) in MeOH (3 mL) and the reaction mixture was stirred at 22 ^{o}C for 16 h. After removal of all volatiles in vacuo, **[$L_{2a}Zn_2(OAc)_2$]** was isolated as a yellow powder. The pure product was obtained after washing with pentane (3 x 2 mL) followed by crystallization, from THF (0.1 mL)/pentane (1 mL) at -40 ^{o}C (420 mg, 0.68 mmol, 68 %).

^{1}H NMR (400 MHz, CDCl$_3$, 298 K) δ (ppm): 8.08 (s, 2H, C*H*=N), 6.84 (d, $^3J_{H,H}$ = 7.9 Hz, 2H, *m*-Ph), 6.74 (dd, $^3J_{H,H}$ = 8.0 Hz, 1.7 Hz, 2H, *m*-Ph), 6.60 (t, $^3J_{H,H}$ = 7.8 Hz, 2H, *p*-Ph), 3.87 (s, 6H, O-C*H*$_3$), 3.72 (s, 4H, N-C*H*$_2$-C), 1.97 (s, 6H, *OAc*), 1.05 (s, 6H, C-(C*H*$_3$)$_2$); ^{13}C{^{1}H} NMR (101 MHz, CDCl$_3$, 298 K) δ (ppm): 171.1 (s, *C*H=N), 150.4 (s, *i*-Ph), 126.4 (s, *m*-Ph), 118.1 (s, *o*-Ph), 115.1 (s, *p*-Ph), 113.8 (s, *m*-Ph), 74.7 (s, (CH$_2$)$_2$-*C*-(CH$_3$)$_2$), 55.9 (s, O-*C*H$_3$), 35.3 (s, *OAc*), 24.8 (s, C-(*C*H$_3$)$_2$), 23.0 (s, N-*C*H$_2$-C). Elemental Analysis

calculated for $C_{25}H_{30}N_2O_8Zn_2$ (617 g/mol): C, 48.64; H, 4.90; N 4.54 %. Found: C, 48.66; H, 5.03; N, 4.43 %.

7.9.3 $[(L_{2b})_2Zn_2]$

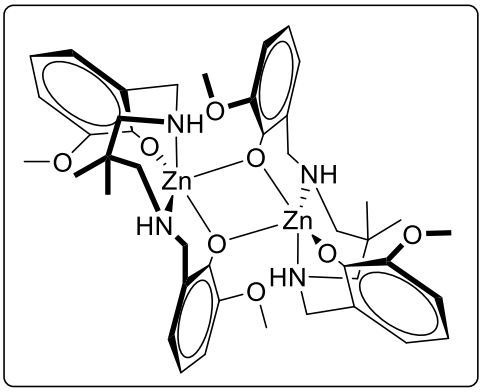

Under a nitrogen atmosphere, $\mathbf{L_{2b}H}$ (1.0 g, 2.6 mmol) was dissolved in dry THF (35 mL). Subsequently, [$ZnEt_2$] (330 mg, 2.6 mmol) was dissolved in dry THF (5 mL) and added dropwise into the ligand solution. The reaction mixture was then stirred at 22 °C for 16 h. **$[(L_{2b})_2Zn_2]$** was isolated via canular transfer of the solvent as a white powder (730 mg, 0.83 mmol, 62 %).

^{1}H NMR (400 MHz, d_8-THF, 298 K) δ (ppm): 6.98 (dd, $^3J_{H,H}$ = 7.9, 1.7 Hz, 1H, *m*-Ph), 6.83 (dd, $^3J_{H,H}$ = 7.5, 1.8 Hz, 1H- *m*-Ph), 6.50 (t, $^3J_{H,H}$ = 7.7 Hz, 1H, *p*-Ph), 6.46 (dd, $^3J_{H,H}$ = 7.8, 1.7 Hz, 1H, *m*-Ph), 6.21 (dd, $^3J_{H,H}$ = 7.5, 1.7 Hz, 1H, *m*-Ph), 6.03 (t, $^3J_{H,H}$ = 7.6 Hz, 1H, *p*-Ph), 4.90 (t, $^2J_{H,H}$ = 11.6 Hz, 1H, Ph-C*H*H-NH), 4.37 (s, 3H, O-CH_3), 3.82 – 3.65 (m, 2H, C*H*H-NH+N*H*), 3.50 (s, 3H, O-CH_3), 3.38 (t, $^2J_{H,H}$ = 14.5, 11.9, 1.9 Hz, 2H, Ph-CH*H*-NH+NH-C*H*H-C), 3.08 – 2.84 (m, 2H, NH-C*H*H-C+NH), 2.56 – 2.43 (m, 1H, Ph-CH*H*-NH), 2.33 (t, $^2J_{H,H}$ = 12.5 Hz, 1H, NH-C*H*H-C), 1.97 (d, $^2J_{H,H}$ = 11.9 Hz, 1H, NH-CH*H*-C), 1.14 (s, 3H, C(CH_3)$_2$), 0.96 (s, 3H, C(CH_3)$_2$); ^{13}C{^{1}H} NMR (101 MHz, d_8-THF, 298 K) δ (ppm): 159.4 (s, *i*-Ph), 158.0 (s, *i*-Ph), 152.5 (s, *o*-Ph), 152.0 (s, *o*-Ph), 130.9 (s, *o*-Ph), 126.7 (s, *m*-Ph), 123.9 (s, *m*-Ph), 122.7 (s, *m*-Ph), 122.4 (s, *o*-Ph), 116.9 (s, *p*-Ph), 112.9 (s, *m*-Ph), 111.8 (s, *p*-Ph), 62.9 (s, O*C*H$_3$), 60.2 (s, Ph-*C*H$_2$-NH), 56.3 (s, Ph-*C*H$_2$-

NH), 56.0 (s, Ph-*C*H_2-NH), 55.9 (s, O-*C*H_3), 54.5 (s, NH-*C*H_2-C), 33.6 (s, *C*$(CH_3)_2$), 26.9 (s, C(*C*$H_3)_2$), 26.7 (s, C(*C*$H_3)_2$). Elemental Analysis calculated for $C_{21}H_{28}N_2O_4Zn$ (875 g/mol): C, 57.61; H, 6.45; N, 6.40 %. Found: C, 57.38; H, 6.31; N, 6.34 %.

7.9.4 [$L_{2b}Zn_2(OAc)_2$] mixture

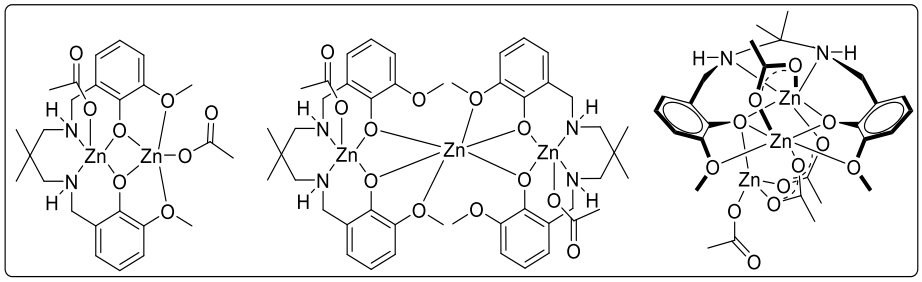

From **$L_{2b}H$**: To a solution of **$L_{2b}H$** (200 mg, 0.53 mmol) in MeOH (10 mL), a methanol solution of [$Zn(OAc)_2$] (235 mg, 1.1 mmol in 10 mL) was added. The reaction mixture was stirred at 22 ^oC for 16 h, prior to removal of all solvent, under reduced pressure. The resultant white powder was washed with pentane and dried under reduced pressure (yield: 71 %, 235 mg).

From dimer **[$(L_{2b})_2Zn_2$]**: Under a nitrogen atmosphere, the dimer **[$(L_{2b})_2Zn_2$]** (100 mg, 0.23 mmol) was suspended in dry THF (3 mL). Subsequently, a suspension of [$Zn(OAc)_2$] (41.9 mg, 0.23 mmol) in dry THF (2 mL) was added in one portion to the ligand solution. After 16 h of stirring at ambient temperature, all volatiles were removed under vacuum and the product mixture was isolated as a white powder (90 mg, 0.15 mmol, 64 %).

The ^1H and the $^{13}C\{^1H\}$ NMR spectra is convoluted and consist of the combination of the spectra of **[$(L_{2b})_2Zn_3(OAc)_4$]** and **[$L_{2b}Zn_3(OAc)_4$]** which are reported below.

Elemental Analysis calculated for $C_{25}H_{34}N_2O_8Zn_2$ (621 g/mol): C, 48.33; H, 5.52; N, 4.51 %. Found: C, 48.18; H, 5.63; N, 4.34 %.

7.9.5 $[(L_{2b})_2Zn_3(OAc)_4]$

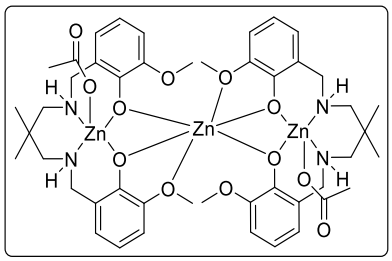

A methanol solution of $[Zn(OAc)_2.(H_2O)_2]$ (88 mg, 0.40 mmol in 3 mL) was injected into a solution of $\mathbf{L_{2b}H}$ (100 mg, 0.27 mmol) in MeOH solvent (3 mL). The reaction mixture was stirred for 16 h at 22 ^oC then all solvent was removed in vacuo. The resultant white solid was washed with pentane (3 x 2 mL) and was dried under reduced pressure (244 mg, 0.40 mmol, 85 %).

^1H NMR (400 MHz, C_6D_6, 298 K) δ (ppm): 6.75-6.69 (m, 12H, Ph), 4.76 (d, $^3J_{H,H}$ = 12.8 Hz, 2H, Ph-C*H*H-NH), 4.15 (s, 3H, O-CH_3), 3.78 (bs, 4H, Ph-C*H*H-NH and Ph-CH*H*-NH), 3.50 (br s, 2H, Ph-CH*H*-NH), 3.42 (m, 2H, NH), 3.10 (m, 2H, NH-CH*H*-C), 2.99 (s, 6H, O-CH_3), 2.81 (s, 3H, O-CH_3), 2.50 (t, 2H, $^3J_{H,H}$ = 12.4 Hz, 2H, NH-CH*H*-C), 2.05 (m, 6H, NH-CH*H*-C), 1.06 (s, 6H,OAc), 0.47 (s, 12H, C(CH_3)$_2$); Elemental Analysis calculated for $C_{46}H_{62}N_4O_{12}Zn_3$ (1034 g/mol): C, 52.16; H, 5.90; N, 5.29 %. Found: C, 52.08; H, 5.59; N, 5.19 %.

7.9.6 [$L_{2b}Zn_3(OAc)_4$]

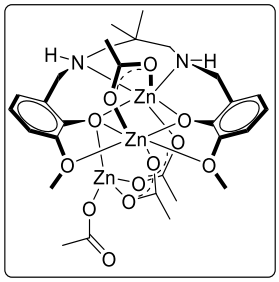

$L_{2b}H$ (400 mg, 1.1 mmol was dissolved in THF (20 mL) and [$Zn(OAc)_2$] (390 mg, 2.1 mmol) was subsequently added as a solid. After 16 h of stirring at ambient temperature, all solvent was removed under reduced pressure to give **[$L_{2b}Zn_3(OAc)_4$]** as a white powder. The pure product was obtained by washing with pentane (3 x 2 mL) (320 mg, 0.50 mmol, 47 %).

^{1}H NMR (400 MHz, C_6D_6, 298 K) δ (ppm): 6.66 (m, 6H, Ph), 4.68 (br s, 2H, Ph-C*H*H-NH), 3.67 (s, 6H, O-C*H*$_3$), 2.98 (d, $^2J_{H,H}$ = 11.6 Hz, 2H, Ph-CH*H*-NH), 2.82 (t, $^3J_{H,H}$ = 12.7, 2H, NH-C*H*H-C), 1.93 (m, 6H, NH-CH*H*-C and OAc), 1.82 (br t, $^3J_{H,H}$ = 14.0 Hz, 3H, N*H* and *OAc*), 0.45 (s, 3H, C(C*H*$_3$)$_2$), 0.46 (s, 3H, C(C*H*$_3$)$_2$); ^{13}C{^{1}H} NMR (101 MHz, C_6D_6, 298 K) δ (ppm): 150.3 (s, *i*-Ph), 150.0 (s, *o*-Ph), 126.0 (s, *o*-Ph), 123.2 (s, *m*-Ph), 118.1 (s, *p*-Ph), 111.8 (s, *m*-Ph), 61.4 (s, NH-*C*H$_2$-C), 55.9 (s, O-*C*H$_3$), 54.0 (s, Ph-*C*H$_2$-NH), 33.7 (s, *C*(CH$_3$)$_2$), 27.9 (s, C(*C*H$_3$CH$_3$)), 22.4 (s, *OAc*), 20.0 (s, C(CH$_3$*C*H$_3$)). Elemental Analysis calculated for $C_{29}H_{40}N_2O_{12}Zn_3$ (621 g/mol): C, 48.33; H, 5.52; N, 4.51 %; Found: C, 48.17; H, 5.63; N, 4.37 %.

7.9.7 [$L_{2b}Zn_2Et_2$]

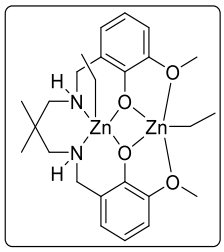

Under a nitrogen atmosphere, **[$(L_{2b})_2Zn_2$]** (200 mg, 0.46 mmol) was suspended in dry THF (5 mL). A solution of [$ZnEt_2$] (56 mg, 0.46 mmol) in dry THF (3 mL) was added dropwise into the previous solution to obtain a colorless solution. The reaction mixture was stirred at ambient temperature for 16 h then all volatiles were removed under reduced pressure to give **[$L_{2b}Zn_2Et_2$]** as a white powder (190 mg, 0.34 mmol, 75 %).

^{1}H NMR (400 MHz, C_6D_6, 298 K) δ (ppm): 6.74 (dd, $^2J_{H,H}$ = 7.1, 2.1 Hz, 2H, *m*-Ph), 6.65 (m, 4H, *m*-Ph + *p*-Ph), 4.29 (t, $^2J_{H,H}$ = 11.7 Hz, 2H, Ph-C*H*H-NH), 3.52 (s, 6H, O-*C*H_3), 2.77 (d, $^2J_{H,H}$ = 11.2 Hz, 2H, Ph-CH*H*-NH), 2.60 (t, $^2J_{H,H}$ = 13.8, 11.3 Hz, 2H, NH-C*H*H-C), 2.05 (t, $^2J_{H,H}$ = 8.1 Hz, 3H, Zn-CH_2C*H*$_3$), 1.79 (t, $^2J_{H,H}$ = 8.1 Hz, 3H, Zn-CH_2C*H*$_3$), 1.69 (d, $^2J_{H,H}$ = 11.50 Hz, 2H, NH-CH*H*-C), 0.94 (q, $^2J_{H,H}$ = 8.1 Hz, 2H, Zn-C*H*$_2$CH$_3$), 0.86 (t, $^2J_{H,H}$ = 13.3 Hz, 2H, N*H*), 0.61 (q, $^2J_{H,H}$ = 8.1 Hz, 2H, Zn-C*H*$_2$CH$_3$), 0.35 (s, 3H, C(C*H*$_3$)$_2$), -0.37 (s, 3H, C(C*H*$_3$)$_2$); ^{13}C{^{1}H} NMR (101 MHz, C_6D_6, 298 K) δ (ppm): 154.10 (s, *i*-Ph), 149.3 (s, *o*-Ph), 124.9 (s, *o*-Ph), 123.1 (s, *m*-Ph), 113.9 (s, *m*-Ph), 111.1 (s, *p*-Ph), 61.7 (s, NH-*C*H_2-C), 55.9 (s, O-*C*H_3), 54.8 (s, Ph-*C*H_2-NH), 33.6 (s, *C*(CH$_3$)$_2$), 27.8 (s, C(*C*H$_3$)(CH$_3$)), 20.5 (s, C(CH$_3$)(*C*H$_3$)), 15.0 (s, Zn-CH_2C*H*$_3$), 13.6 (s, Zn-CH_2C*H*$_3$), -1.7 (s, Zn-*C*H_2CH$_3$), -3.8 (s, Zn-*C*H_2CH$_3$). Elemental Analysis calculated for $C_{25}H_{38}N_2O_4Zn_2$ (561 g/mol): C, 53.49; H, 6.82; N, 4.99 %. Found: C, 53.35; H, 7.19; N, 4.84 %.

7.10 Copolymerization of CO_2 and CHO with Zinc Catalysts

7.10.1 CO_2/CHO Copolymerization Reactions at 1 bar of CO_2

The zinc catalyst (1 equiv.) was suspended in CHO (1.0 mL, 100 equiv.), under N_2, in a Schlenk tube charged with a stirrer bar. The Schlenk tube was connected to a CO_2 line, where the reaction mixture was degassed three times, then heated to 80 ^oC under 1 bar of CO_2 pressure for the desire time. The crude polymer was obtained by evaporation of the remaining CHO under reduced pressure. The polymer was dissolved in THF (1 mL) and was purified by precipitation from hexane (5 mL) to yield a white powder.

7.10.2 CO_2/CHO Copolymerization Reactions at 30 bar of CO_2 Pressure

The zinc catalyst (1 equiv.) was suspended in CHO (6.0 mL, 1000 equiv), under N_2, in a Schlenk tube charged with a stirrer bar. The Paar reactor was purged five times with CO_2. The reaction mixture was transferred into the reactor at 1 atm of CO_2 pressure. The pressure was then adjusted to 30 bar at 80 ^oC, unless otherwise stated. The crude polymer was obtained by evaporation of the remaining CHO under reduced pressure. The polymer was dissolved in THF (2 mL) and was purified by precipitation from hexane (10 mL) to yield a white powder.

7.10.3 PA/CHO Copolymerization Reactions

The zinc catalyst (1 equiv.) was suspended in CHO (1.0 mL, 100 equiv.), under nitrogen, in screw cap vial charged with a stirrer bar. PA (100 equiv.) was added and the vial was sealed and heated to 100 ^oC. The crude polymer was obtained by evaporation of the remaining CHO under reduced pressure. The polymer was dissolved in THF (1 mL) and was purified by precipitation from hexane (5 mL) to yield a white powder.

7.10.4 Terpolymerization of PA/CO_2/CHO

$L_{2a}Zn_2(OAc)_2$ (36 mg, 0.060 mmols, 1 equiv.) and PA (880 mg, 5.93 mmols, 100 equiv.) were suspended in CHO (6.0 mL, 59.3 mmols, 1000 equiv.), under nitrogen, in a Schlenk

tube charged with a stirrer bar. The Parr reactor was purged five times with CO_2. The reaction mixture was then transferred into the reactor at 1 atm of CO_2 pressure. The pressure was then adjusted to 30 bar at 100 ^{o}C. Aliquots were taken after 2 h and 18 h by a depressurization-repressurization procedure at 100 ^{o}C. The crude polymer was obtained by evaporation of the remaining CHO under reduced pressure. The polymer was dissolved in THF (2 mL) and was purified by precipitation from hexane (10 mL) to yield a white powder.

7.11 References

[1] B. Halton, G. M. Dixon, *Org. Biomol. Chem.* **2004**, *2*, 3139-3149.

[2] M. Bochmann, G. Bwembya, K. J. Webb, M. A. Malik, J. R. Walsh, P. O'Brien, in *Inorg. Synth.*, John Wiley & Sons, Inc., **2007**, pp. 19-24.

[3] a) A. Kowalski, A. Duda, S. Penczek, *Macromolecules* **1998**, *31*, 2114-2122; b) M. Save, M. Schappacher, A. Soum, *Macromol. Chem. Phys.* **2002**, *203*, 889-899.

[4] a) I. Palard, M. Schappacher, B. Belloncle, A. Soum, S. M. Guillaume, *Chem. Eur. J.* **2007**, *13*, 1511-1521; b) D. Delcroix, B. Martín-Vaca, D. Bourissou, C. Navarro, *Macromolecules* **2010**, *43*, 8828-8835.

[5] D. Sinnaeve, *Concepts Magn. Res. Part A* **2012**, *40A*, 39-65.

[6] a) J. A. Garden, P. K. Saini, C. K. Williams, *J. Am. Chem. Soc.* **2015**, *137*, 15078-15081; b) A. Thevenon, J. A. Garden, A. J. P. White, C. K. Williams, *Inorg. Chem.* **2015**, *54*, 11906-11915.

[7] a) D. F. Li-ying Wu, X. q. Lu and R. Lu, *Chin. J. Polym. Sci.* **2014**, *32*, 768-777; b) T. Ishida, R. Watanabe, K. Fujiwara, A. Okazawa, N. Kojima, G. Tanaka, S. Yoshii, H. Nojiri, *Dalton Trans.* **2012**, *41*, 13609-13619.

[8] a) T.-P.-A. Cao, G. Nocton, L. Ricard, X. F. Le Goff, A. Auffrant, *Angew. Chem. Int. Ed.* **2014**, *53*, 1368-1372; b) C. Bakewell, A. J. P. White, N. J. Long, C. K. Williams, *Angew. Chem. Int. Ed.* **2014**, *53*, 9226-9230; c) C. Bakewell, T.-P.-A. Cao, N. Long, X. F. Le Goff, A. Auffrant, C. K. Williams, *J. Am. Chem. Soc.* **2012**, *134*, 20577-20580; d) T.-P.-A. Cao, A. Buchard, X. F. Le Goff, A. Auffrant, C. K. Williams, *Inorg. Chem.* **2012**, *51*, 2157-2169; e) D. Myers, A. J. P. White, C. M. Forsyth, M. Bown, C. K. Williams, *Angew. Chem. Int. Ed.* **2017**, *56*, 5277-5282.

[9] a) S. A. Cameron, S. Brooker, *Inorg. Chem.* **2011**, *50*, 3697-3706; b) D. Black, N. Rothnie, *Aust. J. Chem.* **1983**, *36*, 2395-2406; c) D. S. C. Black, N. E. Rothnie, *Tetrahedron Lett.* **1978**, *19*, 2835-2836.

[10] C. Romain, M. S. Bennington, A. J. P. White, C. K. Williams, S. Brooker, *Inorg. Chem.* **2015**, 11842-11851.

[11] SHELXTL, Bruker AXS, Madison, WI; (b) SHELX-2013, http://shelx.uni-ac.gwdg.de/SHELX/index.php

[12]. *CrysAlisPro*, Oxford Diffraction/Agilent Technologies UK Ltd.: Yarnton, England.

[13]. Sheldrick, G. M., A short history of SHELX. *Acta Crystallographica Section A: Foundations of Crystallography* **2008,** *64*, 112-122.

[14]. Farrugia, L. J., WinGX and ORTEP for Windows: an update. *Journal of Applied Crystallography* **2012,** *45*, 849-854.

[15]. Wilson, A. J. C., *International Tables for Crystallography*. 1st ed.; Kluwer Academic Publishers: Dordrecht, 1992; Vol. C.

APPENDICES

Appendix A: Crystallography Data

A.1. Molecular Structures Reported in Chapter 3:

Table A.1. Summary of crystallographic refinement for complexes **[L'InCl]**, **[LInBr]** and **[LInO^{t}Bu]**.*

Data	**[L'InCl]**	**[LInBr]**	**[LInO^{t}Bu]***
Chemical formula	$C_{32}H_{46}N_2O_2ClIn$	$C_{58}H_{72}N_2O_3P_2BrIn$	$C_{62}H_{79}N_2O_3P_2In$
Solvent	-	-	$0.5(C_6H_{14})$
Fw	714.18	1101.84	1120.11
T (°C)	–123	–123	–100
Space group	*P*bca	*P*-1	*P*-1
a (Å)	19.8736(5)	12.0970(2)	11.5034(2)
b (Å)	9.6676(3)	13.7584(2)	20.4916(4)
c (Å)	34.8047(11)	17.4723(3)	26.8509(6)
α (deg)	90	93.243(1)	82.4708(17)
β (deg)	90	93.955(1)	87.2568(17)
γ (deg)	90	98.039(2)	79.8414(18)
V (Å^3)	6687.0(3)	2866.11(8)	6174.5(2)
Z	8	2	4
ρ_{calcd} (g cm^{-3})	1.273	1.277	1.205
λ (Å)	1.5406	1.5406	0.71073
μ (mm^{-1})	6.592	4.960	0.479
R_1(obs) [a]	0.0739	0.0329	0.0405
wR_2(all) [b]	0.1682	0.0844	0.1045

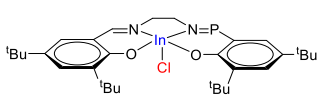

[L'InCl]

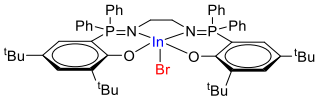

[LInBr]

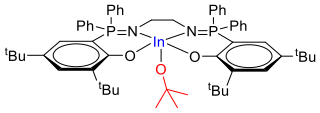

[LInO^{t}Bu]

[a] $R_1 = \Sigma||F_o| - |F_c||/\Sigma|F_o|$. [b] $wR_2 = \{\Sigma[w(F_o^2 - F_c^2)^2] / \Sigma[w(F_o^2)^2]\}^{1/2}$; $w^{-1} = \sigma^2(F_o^2) + (aP)^2 + bP$.

Table A.2. Selected bond lengths and angles for **[L'InCl]**.

Bond	Bond length (Å)	Bond	Bond angle (°)
N(1)-In(1)	2.207(6)	O(1)-In(1)-O(2)	96.0(2)
N(2)-In(1)	2.214(6)	O(1)-In(1)-N(1)	85.0(2)
O(1)-In(1)	2.043(5)	O(2)-In(1)-N(1)	149.3(2)
O(2)-In(1)	2.050(5)	O(1)-In(1)-N(2)	136.3(2)
Cl(1)-In(1)	2.370(2)	O(2)-In(1)-N(2)	83.7(2)
		N(1)-In(1)-N(2)	75.0(2)
		O(1)-In(1)-Cl(1)	112.18(18)
		O(2)-In(1)-Cl(1)	105.26(17)
		N(1)-In(1)-Cl(1)	102.63(17)
		N(2)-In(1)-Cl(1)	109.90(18)

* Molecular structure was obtained by Dr Dominic Myers at Imperial College London

Table A.3. Selected bond lengths and angles for **[LInBr]**.

Bond	Bond length (Å)	Bond	Bond angle (°)
N(1)-In(1)	2.1784(19)	O(1)-In(1)-O(2)	103.00(6)
N(2)-In(1)	2.1769(19)	O(1)-In(1)-N(2)	160.19(7)
O(1)-In(1)	2.0936(16)	O(2)-In(1)-N(2)	89.07(7)
O(2)-In(1)	2.1025(15)	O(1)-In(1)-N(1)	88.04(7)
O(3)-In(1)	2.4715(17)	O(2)-In(1)-N(1)	164.35(7)
Br(1)-In(1)	2.6110(3)	N(2)-In(1)-N(1)	77.44(7)
N(2)-In(1)	2.1769(19)	O(1)-In(1)-O(3)	77.25(6)
		O(2)-In(1)-O(3)	85.05(6)
		N(2)-In(1)-O(3)	88.39(7)
		N(1)-In(1)-O(3)	86.66(7)
		O(1)-In(1)-Br(1)	95.16(4)
		O(2)-In(1)-Br(1)	95.18(5)
		N(2)-In(1)-Br(1)	99.38(5)
		N(1)-In(1)-Br(1)	94.82(6)
		O(3)-In(1)-Br(1)	172.24(4)

Table A.4. Selected bond lengths and angles for **[LInO^{t}Bu]**.*

Bond	Bond length (Å)	Bond	Bond angle (°)
In(1)-O(3)	2.0053(17)	O(3)-In(1)-O(1)	97.23(7)
In(1)-O(1)	2.0750(15)	O(3)-In(1)-O(2)	118.77(8)
In(1)-O(2)	2.0979(15)	O(1)-In(1)-O(2)	85.53(6)
In(1)-N(2)	2.1954(18)	O(3)-In(1)-N(2)	110.06(7)
In(1)-N(1)	2.2289(18)	O(1)-In(1)-N(2)	151.59(7)
		O(2)-In(1)-N(2)	88.05(6)
		O(3)-In(1)-N(1)	108.00(8)
		O(1)-In(1)-N(1)	88.86(6)
		O(2)-In(1)-N(1)	133.23(7)
		O(3)-In(1)-O(1)	97.23(7)

Table A.5. Summary of crystallographic refinement for complexes **[LInOAc]**, **[LInNO$_3$]** and **[^{Amyl}LInO^{t}Bu]**.*

Data	**[LInOAc]**	**[LInNO$_3$]**	**[^{Amyl}LInO^{t}Bu]***
chemical formula	$C_{62}H_{81}N_2O_4P_2In$	$C_{60}H_{78}N_3O_5P_2In$	$C_{62}H_{81}N_2O_3P_2In$
Solvent	C_6C_{14}	C_6C_{14}	C_4H_8O
Fw	1095.04	1098.01	1151.15
T (°C)	–123	–123	–100
space group	$P2_1/c$	$P2_1/c$	P-1
a (Å)	19.3450(2)	19.3561(3)	12.8461(4)
b (Å)	11.16010(10)	11.2195(2)	16.1610(7)
c (Å)	28.8507(3)	28.6971(6)	16.2133(6)
α (deg)	90	90	81.366(3)
β (deg)	105.9230(10)	107.254(2)	69.926(3)
γ (deg)	90	90	82.584(3)
V (Å^3)	5989.65(11)	5951.6(2)	3114.8(2)
Z	4	4	2
ρ_{calcd} (g cm^{-3})	1.214	1.225	1.227
λ (Å)	1.5406	1.5406	0.71073

μ (mm^{-1})	4.003	4.049	0.477
R_1(obs) [a]	0.0382	0.0416	0.0516
wR_2(all) [b]	0.1089	0.1144	0.0989

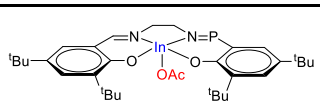

[LInOAc]

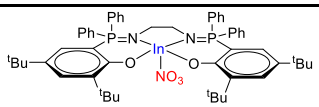

[$LInNO_3$]

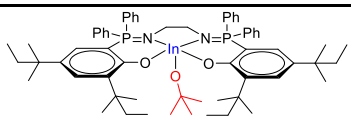

[^{Amyl}LInO^{t}Bu]

[a] $R_1 = \Sigma||F_o| - |F_c||/\Sigma|F_o|$. [b] $wR_2 = \{\Sigma[w(F_o^2 - F_c^2)^2] / \Sigma[w(F_o^2)^2]\}^{1/2}$; $w^{-1} = \sigma^2(F_o^2) + (aP)^2 + bP$.

Table A.6. Selected bond lengths and angles for **[LInOAc]**.

Bond	Bond length (Å)	Bond	Bond angle (°)
N(1)-In(1)	2.196(2)	O(2)-In(1)-O(1)	92.18(7)
N(2)-In(1)	2.1586(19)	O(2)-In(1)-N(2)	90.00(7)
O(1)-In(1)	2.1083(18)	O(1)-In(1)-N(2)	111.76(8)
O(2)-In(1)	2.1064(16)	O(2)-In(1)-N(1)	168.59(7)
O(3)-In(1)	2.231(2)	O(1)-In(1)-N(1)	88.18(7)
O(4)-In(1)	2.292(2)	N(2)-In(1)-N(1)	79.29(7)
		O(2)-In(1)-O(3)	93.25(7)
		O(1)-In(1)-O(3)	97.94(9)
		N(2)-In(1)-O(3)	149.98(9)
		N(1)-In(1)-O(3)	98.00(8)
		O(2)-In(1)-O(4)	94.19(8)
		O(1)-In(1)-O(4)	155.11(8)
		N(2)-In(1)-O(4)	92.30(9)
		N(1)-In(1)-O(4)	90.23(9)
		O(3)-In(1)-O(4)	57.72(9)
		O(2)-In(1)-C(55)	94.09(9)
		O(1)-In(1)-C(55)	126.87(11)
		N(2)-In(1)-C(55)	120.92(12)
		N(1)-In(1)-C(55)	94.82(10)
		O(3)-In(1)-C(55)	29.08(12)
		O(4)-In(1)-C(55)	28.63(12)

Table A.7. Selected bond lengths and angles for **[$LInNO_3$]**.

Bond	Bond length (Å)	Bond	Bond angle (°)
N(1)-In(01)	2.178(2)	O(2)-In(01)-O(1)	94.77(8)
N(2)-P(002)	1.602(2)	O(2)-In(01)-N(2)	90.91(8)
N(2)-In(01)	2.153(2)	O(1)-In(01)-N(2)	116.55(10)
O(1)-In(01)	2.090(2)	O(2)-In(01)-N(1)	171.06(9)
O(2)-In(01)	2.087(2)	O(1)-In(01)-N(1)	90.03(9)
O(3)-In(01)	2.257(2)	N(2)-In(01)-N(1)	80.19(9)
O(4)-In(01)	2.340(3)	O(2)-In(01)-O(3)	92.36(9)
		O(1)-In(01)-O(3)	95.18(9)
		N(2)-In(01)-O(3)	147.69(10)
		N(1)-In(01)-O(3)	94.72(9)
		O(2)-In(01)-O(4)	92.71(9)
		O(1)-In(01)-O(4)	150.66(9)
		N(2)-In(01)-O(4)	91.61(10)
		N(1)-In(01)-O(4)	86.72(10)
		O(3)-In(01)-O(4)	56.14(9)

Table A.8. Selected bond lengths and angles for **[^{Amyl}LInO^{t}Bu]**.*

Bond	Bond length (Å)	Bond	Bond angle (°)
In(1)-O(3)	2.012(6)	O(3)-In(1)-O(2)	103.0(4)
In(1)-O(2)	2.1123(17)	O(3)-In(1)-O(1)	104.8(4)
In(1)-O(1)	2.1175(18)	O(2)-In(1)-O(1)	87.54(7)
In(1)-N(1)	2.196(2)	O(3)-In(1)-N(1)	115.2(4)
In(1)-N(2)	2.200(2)	O(2)-In(1)-N(1)	141.73(8)
		O(1)-In(1)-N(1)	85.09(7)
		O(3)-In(1)-N(2)	111.6(4)
		O(2)-In(1)-N(2)	87.93(7)
		O(1)-In(1)-N(2)	143.39(8)
		N(1)-In(1)-N(2)	76.39(8)

Table A.9. Summary of crystallographic refinement for complexes **[LInCHD]** and **[(LInO$_2$C)$_2$POD]**.

Data	**[LInCHD]**	**[(LInO$_2$C)$_2$POD]**
chemical formula	$C_{66}H_{87}N_2O_6P_2In$	$C_{119}H_{146}N_4O_{12}P_4In_2$
Solvent	C_6C_{14}	C_2H_4O
Fw	1181.13	2177.91
T (°C)	–123	–123
space group	P-1	Pbcn
a (Å)	12.7684(4)	17.5120(2)
b (Å)	15.1118(5)	18.3743(2)
c (Å)	19.4416(8)	35.2302(5)
α (deg)	89.598(3)	90
β (deg)	78.609(3)	90
γ (deg)	83.967(3)	90
V (Å^3)	3656.7(2)	11336.0(2)
Z	2	4
ρ_{calcd} (g cm^{-3})	1.073	1.276
λ (Å)	1.5406	1.5406
μ (mm^{-1})	3.332	4.257
R_1(obs) [a]	0.0528	0.0561
wR_2(all) [b]	0.1461	0.1350

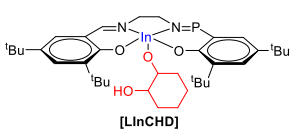

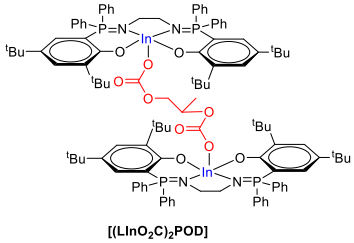

[a] $R_1 = \Sigma||F_o| - |F_c||/\Sigma|F_o|$. [b] $wR_2 = \{\Sigma[w(F_o^2 - F_c^2)^2] / \Sigma[w(F_o^2)^2]\}^{1/2}$; $w^{-1} = \sigma^2(F_o^2) + (aP)^2 + bP$.

Table A.10. Selected bond lengths and angles for **[LInCHD]**.

Bond	Bond length (Å)	Bond	Bond angle (°)
N(1)-In(1)	2.164(3)	O(3)-In(1)-O(1)	105.47(11)
N(2)-In(1)	2.198(2)	O(3)-In(1)-O(2)	112.97(10)
O(1)-In(1)	2.093(2)	O(1)-In(1)-O(2)	88.56(8)
O(2)-In(1)	2.096(2)	O(3)-In(1)-N(1)	108.57(11)
O(3)-In(1)	2.070(2)	O(1)-In(1)-N(1)	87.15(9)
		O(2)-In(1)-N(1)	137.85(10)
		O(3)-In(1)-N(2)	98.81(11)
		O(1)-In(1)-N(2)	154.67(10)
		O(2)-In(1)-N(2)	88.55(9)
		N(1)-In(1)-N(2)	78.28(10)

Table A.11. Selected bond lengths and angles for **[(LInO$_2$C)$_2$POD]**.

Bond	Bond length (Å)	Bond	Bond angle (°)
N(1)-In(01)	2.159(3)	O(2)-In(01)-O(1)	96.86(11)
N(2)-In(01)	2.180(3)	O(2)-In(01)-N(1)	108.37(13)
O(1)-In(01)	2.099(3)	O(1)-In(01)-N(1)	88.12(12)
O(2)-In(01)	2.098(3)	O(2)-In(01)-N(2)	86.96(12)
O(3)-In(01)	2.337(3)	O(1)-In(01)-N(2)	168.03(13)
O(4)-In(01)	2.223(4)	N(1)-In(01)-N(2)	79.91(14)
		O(2)-In(01)-O(4)	91.94(13)
		O(1)-In(01)-O(4)	95.38(13)
		N(1)-In(01)-O(4)	158.87(14)
		N(2)-In(01)-O(4)	95.82(14)
		O(2)-In(01)-O(3)	147.96(13)
		O(1)-In(01)-O(3)	96.13(12)
		N(1)-In(01)-O(3)	101.21(14)
		N(2)-In(01)-O(3)	86.33(13)
		O(4)-In(01)-O(3)	57.72(14)

Table A.12. Summary of crystallographic refinement for complexes **[(LIn)$_2$O$_3$C]** and **[(LInOH)$_2$]**.

Data	**[(LIn)$_2$O$_3$C]**	**[(LInOH)$_2$]**
chemical formula	$C_{109}H_{128}N_4O_7P_4In_2$	$C_{148}H_{146}N_4O_6P_4In_2$
Solvent	-	-
Fw	1958.58	2430.34
T (°C)	–123	20
space group	*P*-1	*P*-1
a (Å)	11.6130(5)	11.5354(10)
b (Å)	17.8474(7)	14.5773(10)
c (Å)	26.5788(9)	20.5227(10)
α (deg)	93.344(3)	89.658(10)
β (deg)	93.043(3)	87.435(10)
γ (deg)	100.180(4)	68.657(10)
V (Å^3)	5401.5(4)	3210.9(4)
Z	4	1
ρ_{calcd} (g cm^{-3})	1.249	1.257
λ (Å)	1.5406	0.68890

μ (mm^{-1})	4.402	0.466
R_1(obs) [a]	0.0622	0.0289
wR_2(all) [b]	0.1713	0.1018
	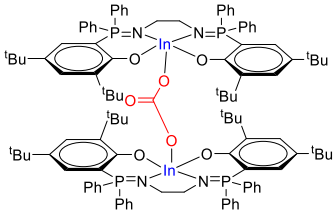 **[(LIn)$_2$O$_3$C]**	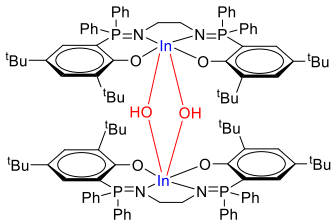 **[(LInOH)$_2$]**

[a] $R_1 = \Sigma||F_o| - |F_c||/\Sigma|F_o|$. [b] $wR_2 = \{\Sigma[w(F_o^2 - F_c^2)^2] / \Sigma[w(F_o^2)^2]\}^{1/2}$; $w^{-1} = \sigma^2(F_o^2) + (aP)^2 + bP$.

Table A.13. Selected bond lengths and angles for **[(LIn)$_2$O$_3$C]**.

Bond	Bond length (Å)	Bond	Bond angle (°)
N(1)-In(1)	2.207(4)	O(2)-In(1)-O(1)	89.67(18)
N(2)-In(1)	2.178(5)	O(2)-In(1)-O(5)	91.98(17)
N(3)-In(2)	2.175(4)	O(1)-In(1)-O(5)	90.75(16)
N(4)-In(2)	2.149(5)	O(2)-In(1)-N(2)	88.29(18)
O(1)-In(1)	2.108(4)	O(1)-In(1)-N(2)	108.1(2)
O(2)-In(1)	2.094(4)	O(5)-In(1)-N(2)	161.16(19)
O(3)-In(2)	2.121(4)	O(2)-In(1)-N(1)	165.82(17)
O(4)-In(2)	2.100(3)	O(1)-In(1)-N(1)	89.33(17)
O(5)-In(1)	2.166(4)	O(5)-In(1)-N(1)	102.17(17)
O(6)-In(1)	2.299(4)	N(2)-In(1)-N(1)	78.59(19)
O(7)-In(2)	2.064(4)	O(2)-In(1)-O(6)	97.08(17)
		O(1)-In(1)-O(6)	148.93(16)
		O(5)-In(1)-O(6)	58.84(14)
		N(2)-In(1)-O(6)	102.42(18)
		N(1)-In(1)-O(6)	91.04(16)
		O(7)-In(2)-O(4)	96.10(16)
		O(7)-In(2)-O(3)	103.67(18)
		O(4)-In(2)-O(3)	86.27(16)
		O(7)-In(2)-N(4)	122.9(2)
		O(4)-In(2)-N(4)	87.02(18)
		O(3)-In(2)-N(4)	133.4(2)
		O(7)-In(2)-N(3)	108.95(17)
		O(4)-In(2)-N(3)	154.94(18)
		O(3)-In(2)-N(3)	88.55(17)
		N(4)-In(2)-N(3)	78.84(19)

Table 14. Selected bond lengths and angles for **[(LInOH)$_2$]**.

Bond	Bond length (Å)	Bond	Bond angle (°)
N(1)-In(1)	2.199(4)	O(2)-In(1)-O(1)	96.28(18)
N(2)-In(1)	2.232(4)	O(1)-In(1)-O(3)	93.85(17)
O(1)-In(1)	2.129(5)	O(1)-In(1)-O(3')	91.96(16)
O(2)-In(1)	2.205(4)	O(2)-In(1)-N(2)	87.76(18)
O(3)-In(1)	2.112(4)	O(1)-In(1)-N(2)	166.00(2)
O(3')-In(1)	2.232(4)	O(3)-In(1)-N(2)	86.44(19)
		O(2)-In(1)-N(1)	98.62(17)
		O(1)-In(1)-N(1)	87.23(17)

N(2)-In(1)-N(1)	78.90(19)
O(2)-In(1)-O(3)	93.73(17)
O(3)-In(1)-O(3')	76.46(14)
N(2)-In(1)-O(3')	99.26(18)
N(1)-In(1)-O(3)	167.41(16)

A.2. Molecular Structures Reported in Chapter 4:

Table A.15. Summary of crystallographic refinement for complexes **[L^{Et}Zn$_2${N(SiMe$_3$)$_2$}$_2$]**[†], **[L^{Pr}Zn$_2${N(SiMe$_3$)$_2$}$_2$]**[†] and **[L^{Open}ZnN(SiMe$_3$)$_2$]**.

Data	[L^{Et}Zn$_2${N(SiMe$_3$)$_2$}$_2$]†	[L^{Pr}Zn$_2${N(SiMe$_3$)$_2$}$_2$]†	[L^{Open}ZnN(SiMe$_3$)$_2$]
Chemical formula	$C_{44}H_{64}N_8Si_4Zn_2$	$C_{46}H_{68}N_8Si_4Zn_2$	$C_{28}H_{46}N_4Si_2Zn$
Solvent	C_4H_8O	C_6H_{14}	-
Fw	1092.34	1062.35	560.24
T (°C)	–100	–100	–100
Space group	*P*ccn	*P*21/c	*P*21/n
a (Å)	15.3644(5)	21.5374(2)	9.70000(12)
b (Å)	15.7314(5)	20.73239(18)	13.84428(17)
c (Å)	23.9599(10)	13.04210(15)	23.2122(3)
α (deg)	90	90	90
β (deg)	90	96.7198(10)	98.8744(13)
γ (deg)	90	90	90
V (Å^3)	5791.2(4)	5783.59(10)	3079.85(7)
Z	4	4	4
ρ_{calcd} (g cm^{-3})	1.253	1.220	1.208
λ (Å)	0.71073	1.54184	1.54184
μ (mm^{-1})	0.955	2.114	2.009
R_1(obs) [a]	0.0422	0.0536	0.0299
wR_2(all) [b]	0.1115	0.1654	0.0815

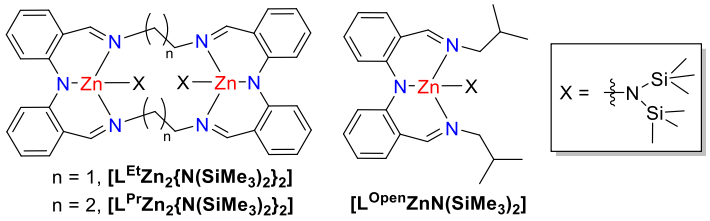

[a] $R_1 = \Sigma||F_o| - |F_c||/\Sigma|F_o|$. [b] $wR_2 = \{\Sigma[w(F_o^2 - F_c^2)^2] / \Sigma[w(F_o^2)^2]\}^{1/2}$; $w^{-1} = \sigma^2(F_o^2) + (aP)^2 + bP$.

[†] Molecular structures were obtained by Dr Charles Romain at Imperial College London

Table A.16. Selected bond lengths and angles for **[L^{Et}Zn$_2${N(SiMe$_3$)$_2$}$_2$]**.†

Bond	Bond length (Å)	Bond	Bond angle (°)
Zn(1)-N(4)	1.942(2)	N(4)-Zn(1)-N(2)	126.46(10)
Zn(1)-N(2)	1.979(2)	N(4)-Zn(1)-N(1)	112.24(9)
Zn(1)-N(1)	2.018(2)	N(2)-Zn(1)-N(1)	94.72(9)
Zn(1)-N(3)	2.102(2)	N(4)-Zn(1)-N(3)	116.06(9)
		N(2)-Zn(1)-N(3)	86.90(9)
		N(1)-Zn(1)-N(3)	117.45(8)

Table A.17. Selected bond lengths and angles for the crystallographically independent molecule A of **[L^{Pr}Zn$_2${N(SiMe$_3$)$_2$}$_2$]**.†

Bond	Bond length (Å)	Bond	Bond angle (°)
Zn(1A)-N(4A)	1.933(2)	N(4A)-Zn(1A)-N(2A)	126.86(10)
Zn(1A)-N(2A)	1.993(2)	N(4A)-Zn(1A)-N(3A)	111.87(10)
Zn(1A)-N(3A)	2.020(2)	N(2A)-Zn(1A)-N(3A)	94.40(10)
Zn(1A)-N(1A)	2.092(2)	N(4A)-Zn(1A)-N(1A)	112.25(10)
		N(2A)-Zn(1A)-N(1A)	87.15(10)
		N(3A)-Zn(1A)-N(1A)	122.59(9)

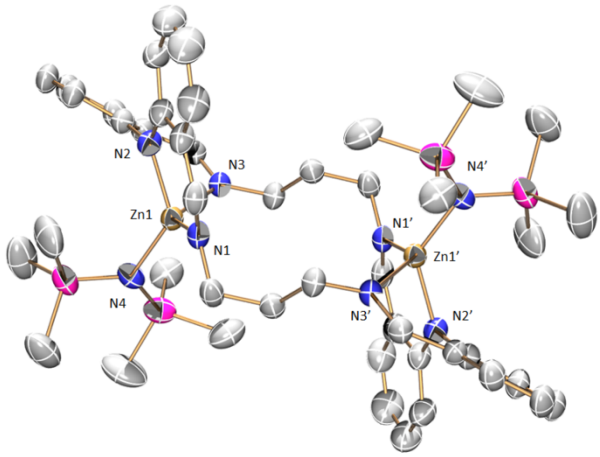

Figure A.1. Molecular structure of the second crystallographically independent molecule (B) of **[L^{Pr}Zn$_2${N(SiMe$_3$)$_2$}$_2$]**† with thermal ellipsoids at the 50 % probability level. A hexane molecule and hydrogen atoms omitted for clarity.

Table A.18. Selected bond lengths and angles for the crystallographically independent molecule B of **[L^{Pr}Zn$_2${N(SiMe$_3$)$_2$}$_2$]**.†

Bond	Bond length (Å)	Bond	Bond angle (°)
Zn(1B)-N(4B)	1.941(2)	N(4B)-Zn(1B)-N(2B)	129.63(10)
Zn(1B)-N(2B)	1.983(2)	N(4B)-Zn(1B)-N(1B)	113.02(10)
Zn(1B)-N(1B)	2.024(2)	N(2B)-Zn(1B)-N(1B)	94.17(9)
Zn(1B)-N(3B)	2.126(2)	N(4B)-Zn(1B)-N(3B)	108.92(9)
		N(2B)-Zn(1B)-N(3B)	85.85(9)
		N(1B)-Zn(1B)-N(3B)	124.22(8)

Table A.19. Selected bond lengths and angles for **[L^{Open}Zn(NSiMe$_3$)]**.

Bond	Bond length (Å)	Bond	Bond angle (°)
Zn(1)-N(4)	1.9409(14)	N(4)-Zn(1)-N(2)	122.29(6)
Zn(1)-N(2)	1.9834(14)	N(4)-Zn(1)-N(1)	116.86(6)
Zn(1)-N(1)	2.0091(14)	N(2)-Zn(1)-N(1)	95.29(6)
Zn(1)-N(3)	2.1241(15)	N(4)-Zn(1)-N(3)	116.79(5)
		N(2)-Zn(1)-N(3)	86.32(6)
		N(1)-Zn(1)-N(3)	114.10(6)

Table A.20. Summary of crystallographic refinement for complexes **[L^{Et}Zn$_2$(O^{i}Pr)$_2$]**.†

Data	**[L^{Et}Zn$_2$(O^{i}Pr)$_2$]†**
Chemical formula	$C_{39}H_{42}N_6O_4Zn_2$
Solvent	-
Fw	789.52
T (°C)	–100
Space group	*C*2/c
a (Å)	37.6404(5)
b (Å)	16.9073(2)
c (Å)	17.4493(2)
α (deg)	90
β (deg)	90.1883(12)
γ (deg)	90
V (Å^3)	11104.6(2)
Z	12
ρ_{calcd} (g cm^{-3})	1.417
λ (Å)	1.54184
μ (mm^{-1})	1.985
R_1(obs) [a]	0.0443
wR_2(all) [b]	0.1465

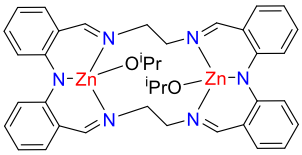

[L^{Et}Zn$_2$(O^{i}Pr)$_2$]

[a] $R_1 = \Sigma||F_o| - |F_c||/\Sigma|F_o|$. [b] $wR_2 = \{\Sigma[w(F_o^2 - F_c^2)^2] / \Sigma[w(F_o^2)^2]\}^{1/2}$; $w^{-1} = \sigma^2(F_o^2) + (aP)^2 + bP$.

Table A.21. Selected bond lengths and angles for **[$L^{Et}Zn_2(O^iPr)_2$]**.†

Bond	Bond length (Å)	Bond	Bond angle (°)
Zn(1)-O(1)	1.972(2)	O(1)-Zn(1)-N(2)	141.69(10)
Zn(1)-N(2)	1.986(2)	O(1)-Zn(1)-O(2)	108.52(10)
Zn(1)-O(2)	2.040(3)	N(9)-Zn(1)-O(2)	109.75(11)
Zn(1)-N(1)	2.166(3)	O(1)-Zn(1)-N(1)	90.23(9)
Zn(1)-N(3)	2.200(3)	N(2)-Zn(1)-N(1)	87.41(10)
Zn(2)-O(1)	1.974(2)	O(2)-Zn(1)-N(1)	91.04(12)
Zn(2)-N(5)	1.997(2)	O(1)-Zn(1)-N(3)	94.39(10)
Zn(2)-O(2)	2.056(3)	N(2)-Zn(1)-N(3)	88.32(10)
Zn(2)-N(6)	2.154(2)	O(2)-Zn(1)-N(3)	88.46(11)
Zn(2)-N(4)	2.179(2)	N(1)-Zn(1)-N(3)	175.26(10)
		O(1)-Zn(2)-N(5)	138.14(10)
		O(1)-Zn(2)-O(2)	115.03(10)
		N(5)-Zn(2)-O(2)	106.65(11)
		O(1)-Zn(2)-N(6)	92.35(9)
		N(5)-Zn(2)-N(6)	89.24(9)
		O(2)-Zn(2)-N(6)	92.77(11)
		O(1)-Zn(2)-N(4)	89.84(9)
		N(5)-Zn(2)-N(4)	86.36(10)
		O(2)-Zn(2)-N(4)	90.07(11)
		N(6)-Zn(2)-N(4)	175.30(10)

A.3. Molecular Structures Reported in Chapter 5:

Table A.22. Summary of crystallographic refinement for complexes **[$L_{1a}Zn_2(OAc)_2$]**, **[$(L_{2b})_2Zn_2$-THF]**, **[$(L_{2b})_2Zn_2$-MeOH]**.

Data	**[$L_{1a}Zn_2(OAc)_2$]**	**[$(L_{2b})_2Zn_2$-THF]**	**[$(L_{2b})_2Zn_2$-MeOH]**
chemical formula	$C_{26}H_{30}N_2O_8Zn_2$	$C_{42}H_{56}N_4O_8Zn_2$	$C_{42}H_{56}N_4O_8Zn_2$
Solvent	CH_2Cl_2	$6(C_4H_8O)$	$2(CH_4O)$
Fw	714.18	1308.27	939.73
T (°C)	–100	–100	–100
space group	P-1 (no. 2)	P-1 (no. 2)	P-1 (no. 2)
a (Å)	8.2671(3)	11.0206(4)	11.3488(4)
b (Å)	12.7351(8)	12.7927(5)	14.2169(5)
c (Å)	14.1980(6)	13.4261(6)	15.4784(4)
α (deg)	89.017(4)	108.871(4)	95.168(3)
β (deg)	87.860(3)	108.312(4)	100.165(3)
γ (deg)	79.825(4)	92.889(3)	111.371(3)
V (Å^3)	1470.18(13)	1675.87(13)	2256.46(13)
Z	2	1	2
ρ_{calcd} (g cm^{-3})	1.613	1.296	1.383
λ (Å)	0.71073	0.71073	0.71073
μ (mm^{-1})	1.864	0.780	1.123
R_1(obs) [a]	0.0379	0.0462	0.0400
wR_2(all) [b]	0.0905	0.1149	0.1053

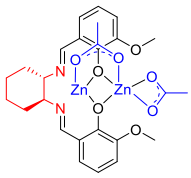

$[L_{1a}Zn_2OAc_2]$

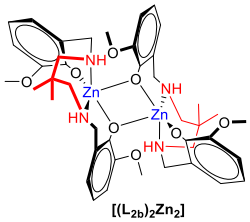

$[(L_{2b})_2Zn_2]$

[a] $R_1 = \Sigma||F_o| - |F_c||/\Sigma|F_o|$. [b] $wR_2 = \{\Sigma[w(F_o^2 - F_c^2)^2] / \Sigma[w(F_o^2)^2]\}^{1/2}$; $w^{-1} = \sigma^2(F_o^2) + (aP)^2 + bP$.

Table A.23. Selected bond lengths and angles for **$[L_{1a}Zn_2(OAc)_2]$**.

Bond	Bond length (Å)	Bond	Bond angle (°)
Zn(1)-O(5)	1.994(2)	O(5)-Zn(1)-O(1)	97.75(8)
Zn(1)-O(1)	2.0034(19)	O(5)-Zn(1)-O(2)	97.02(8)
Zn(1)-O(2)	2.023(2)	O(1)-Zn(1)-O(2)	80.27(8)
Zn(1)-N(1)	2.027(3)	O(5)-Zn(1)-N(1)	115.18(10)
Zn(1)-N(2)	2.036(2)	O(1)-Zn(1)-N(1)	90.03(9)
Zn(1)-Zn(2)	2.9539(5)	O(2)-Zn(1)-N(1)	147.40(10)
Zn(2)-O(2)	2.0205(19)	O(5)-Zn(1)-N(2)	115.57(10)
Zn(2)-O(6)	2.023(2)	O(1)-Zn(1)-N(2)	145.88(10)
Zn(2)-O(1)	2.055(2)	O(2)-Zn(1)-N(2)	88.21(9)
Zn(2)-O(8)	2.096(2)	N(1)-Zn(1)-N(2)	82.59(10)
Zn(2)-O(7)	2.191(2)	O(2)-Zn(2)-O(6)	96.14(8)
		O(2)-Zn(2)-O(1)	79.11(8)
		O(6)-Zn(2)-O(1)	93.99(9)
		O(2)-Zn(2)-O(8)	140.68(9)
		O(6)-Zn(2)-O(8)	100.11(9)
		O(1)-Zn(2)-O(8)	134.43(8)
		O(2)-Zn(2)-O(7)	98.24(8)
		O(6)-Zn(2)-O(7)	161.27(8)
		O(1)-Zn(2)-O(7)	100.45(9)
		O(8)-Zn(2)-O(7)	61.20(9)

Table A.24. Selected bond lengths and angles for **$[(L_{2b})_2Zn_2$-THF]**.

Bond	Bond length (Å)	Bond	Bond angle (°)
Zn(1)-O(2)	1.9253(17)	O(2)-Zn(1)-O(1')	116.98(8)
Zn(1)-O(1')	2.0040(17)	O(2)-Zn(1)-O(1)	91.19(7)
Zn(1)-O(1)	2.0883(16)	O(1')-Zn(1)-O(1)	79.11(7)
Zn(1)-N(1)	2.109(2)	O(2)-Zn(1)-N(1)	131.60(9)
Zn(1)-N(2)	2.160(2)	O(1')-Zn(1)-N(1)	110.83(8)
Zn(1)-Zn(1')	3.1556(6)	O(1)-Zn(1)-N(1)	90.69(8)
O(1)-Zn(1')	2.0040(17)	O(2)-Zn(1)-N(2)	92.54(8)
		O(1)-Zn(1)-N(2)	173.79(7)
		N(1)-Zn(1)-N(2)	90.54(8)
		O(1')-Zn(1)-N(2)	94.77(8)

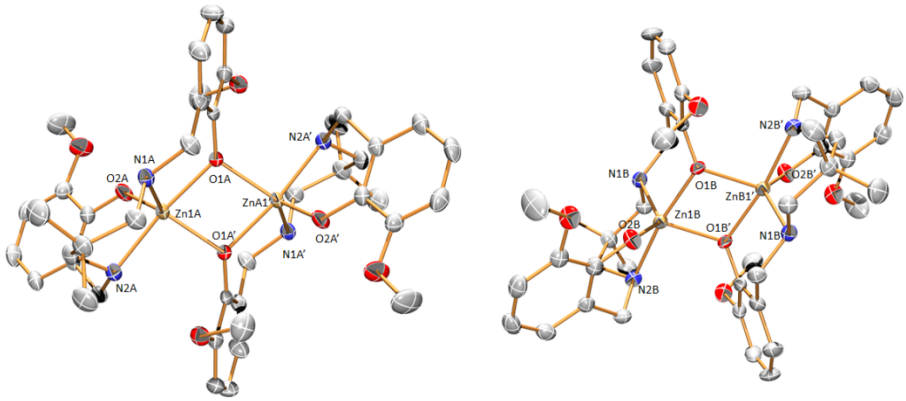

Figure A.2. Molecular structure of **[$(L_{2b})_2Zn_2$-MeOH]** representing two crystallographically independents molecules (A and B) with thermal ellipsoids at the 50 % probability level. Hydrogen atoms as well as one MeOH molecule are omitted for clarity.

Table A.25. Selected bond lengths and bond angles for the crystallographically independent molecule A of **[$(L_{2b})_2Zn_2$-MeOH]**.

Bond	Bond length (Å)	Bond	Bond angle (°)
Zn(1A)-O(2A)	1.9338(18)	O(2A)-Zn(1A)-O(1A')	127.16(8)
Zn(1A)-O(1A')	2.0119(16)	O(2A)-Zn(1A)-O(1A)	93.12(7)
Zn(1A)-O(1A)	2.0801(17)	O(1A')-Zn(1A)-O(1A)	78.09(7)
Zn(1A)-N(1A)	2.099(2)	O(2A)-Zn(1A)-N(1A)	118.05(8)
Zn(1A)-N(2A)	2.136(2)	O(1A')-Zn(1A)-N(1A)	114.15(8)
Zn(1A)-Zn(1A')	3.1785(5)	O(1A)-Zn(1A)-N(1A)	91.12(8)
O(1A)-Zn(1A')	2.0118(16)	O(2A)-Zn(1A)-N(2A)	91.69(8)
		O(1A)-Zn(1A)-N(2A)	173.03(7)
		N(1A)-Zn(1A)-N(2A)	91.06(8)
		O(1A')-Zn(1A)-N(2A)	94.98(7)

Table A.26. Selected bond lengths and bond angles for the crystallographically independent molecule B of **[$(L_{2b})_2Zn_2$-MeOH]**.

Bond	Bond length (Å)	Bond	Bond angle (°)
Zn(1B)-O(2B)	1.9242(18)	O(2B)-Zn(1B)-O(1B')	117.43(8)
Zn(1B)-O(1B')	2.0266(16)	O(2B)-Zn(1B)-O(1B)	92.98(7)
Zn(1B)-O(1B)	2.0744(17)	O(1B')-Zn(1B)-O(1B)	78.40(7)
Zn(1B)-N(1B)	2.134(2)	O(2B)-Zn(1B)-N(1B)	132.81(8)
Zn(1B)-N(2B)	2.169(2)	O(1B')-Zn(1B)-N(1B)	109.40(8)
Zn(1B)-Zn(1B')	3.1783(5)	O(1B)-Zn(1B)-N(1B)	90.78(8)
O(1B)-Zn(1B')	2.0266(16)	O(2B)-Zn(1B)-N(2B)	93.10(8)
		O(1B)-Zn(1B)-N(2B)	170.53(7)
		N(1B)-Zn(1B)-N(2B)	90.42(9)
		O(1B')-Zn(1B)-N(2B)	92.35(8)

Table A.27. Summary of crystallographic refinement for complexes **[$L_{2b}Zn_3(OAc)_4$]**, **[$L_{2b}Zn_3Cl_2$]**.

data	**[$L_{2b}Zn_3(OAc)_4$]**	**[$L_{2b}Zn_3Cl_2$]**
chemical	$C_{29}H_{40}N_2O_{12}Zn_3$	$C_{42}H_{56}Cl_2N_4O_8Zn_3$
solvent	—	$4(C_4H_8O)$
fw	804.74	1300.33
T (°C)	–70	–100
space group	*Pbca* (no. 61)	*C*2/*c* (no. 15)
a (Å)	18.7381(11)	17.2730(5)
b (Å)	18.6958(6)	20.0374(5)
c (Å)	18.9958(6)	19.2903(6)
α (deg)	90	90
β (deg)	90	114.880(4)
γ (deg)	90	90
V (Å^3)	6654.7(5)	6056.8(3)
Z	8	4
ρ_{calcd} (g cm^{-3})	1.606	1.426
λ (Å)	0.71073	0.71073
μ (mm^{-1})	2.208	1.329
R_1(obs) [a]	0.0531	0.0358
wR_2(all) [b]	0.1102	0.0852

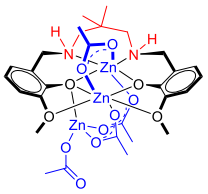

[$L_{2b}Zn_3(OAc)_4$]

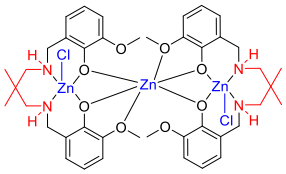

[$(L_{2b})_2Zn_3Cl_2$]

[a] $R_1 = \Sigma||F_o| - |F_c||/\Sigma|F_o|$. [b] $wR_2 = \{\Sigma[w(F_o^2 - F_c^2)^2] / \Sigma[w(F_o^2)^2]\}^{1/2}$; $w^{-1} = \sigma^2(F_o^2) + (aP)^2 + bP$.

Table 28. Selected bond lengths and angles for **[$L_{2b}Zn_3(OAc)_4$]**.

Bond	Bond length (Å)	Bond	Bond angle (°)
Zn(1)-O(1)	2.043(4)	O(1)-Zn(1)-N(2)	168.68(17)
Zn(1)-N(2)	2.087(5)	O(1)-Zn(1)-N(1)	92.93(16)
Zn(1)-N(1)	2.095(4)	N(2)-Zn(1)-N(1)	97.10(18)
Zn(1)-O(7)	2.105(4)	O(1)-Zn(1)-O(7)	96.10(15)
Zn(1)-O(5)	2.191(4)	N(2)-Zn(1)-O(7)	89.14(17)
Zn(1)-O(2)	2.241(3)	N(12)-Zn(1)-O(7)	90.14(17)
Zn(1)-Zn(2)	3.0546(9)	O(1)-Zn(1)-O(5)	89.56(15)
Zn(2)-O(9)	1.943(4)	N(2)-Zn(1)-O(5)	84.29(17)
Zn(2)-O(6)	1.950(4)	N(1)-Zn(1)-O(5)	95.46(17)
Zn(2)-O(1)	1.994(4)	O(7)-Zn(1)-O(5)	171.83(15)
Zn(2)-O(2)	2.139(4)	O(1)-Zn(1)-O(2)	77.95(13)
Zn(2)-O(3)	2.330(4)	N(2)-Zn(1)-O(2)	92.05(15)
Zn(3)-O(11)	1.947(4)	N(1)-Zn(1)-O(2)	170.85(16)
Zn(3)-O(8)	1.963(4)	O(7)-Zn(1)-O(2)	90.06(14)
Zn(3)-O(10)	1.966(4)	O(5)-Zn(1)-O(2)	85.36(14)
Zn(3)-O(2)	2.005(3)	O(9)-Zn(2)-O(6)	133.46(18)
		O(9)-Zn(2)-O(1)	113.39(16)
		O(6)-Zn(2)-O(1)	108.85(16)

O(9)-Zn(2)-O(2)	106.70(15)
O(6)-Zn(2)-O(2)	97.87(15)
O(1)-Zn(2)-O(2)	81.45(14)
O(9)-Zn(2)-O(3)	82.27(15)
O(6)-Zn(2)-O(3)	90.01(15)
O(1)-Zn(2)-O(3)	75.83(14)
O(2)-Zn(2)-O(3)	157.27(13)
O(11)-Zn(3)-O(8)	102.49(18)
O(11)-Zn(3)-O(10)	126.61(18)
O(8)-Zn(3)-O(10)	100.40(16)
O(11)-Zn(3)-O(2)	104.31(16)
O(8)-Zn(3)-O(2)	109.79(15)
O(10)-Zn(3)-O(2)	112.07(16)

Table A.29. Selected bond lengths and angles for **$[(L_{2b})_2Zn_3Cl_2]$**.

Bond	Bond length (Å)
Zn(1)-O(2)	2.0093(16)
Zn(1)-O(2')	2.0094(16)
Zn(1)-O(1')	2.0213(16)
Zn(1)-O(1)	2.0213(16)
Zn(1)-O(4')	2.3553(17)
Zn(1)-O(4)	2.3554(17)
Zn(2)-O(1)	2.0371(17)
Zn(2)-O(2)	2.0676(17)
Zn(2)-N(1)	2.093(2)
Zn(2)-N(2)	2.148(2)
Zn(2)-Cl(1)	2.3043(7)
Zn(1)-O(2)	2.0093(16)
Zn(1)-O(2')	2.0094(16)
Zn(1)-O(1')	2.0213(16)
Zn(1)-O(1)	2.0213(16)
Zn(1)-O(4')	2.3553(17)
Zn(1)-O(26)	2.3554(17)
Zn(2)-O(1)	2.0371(17)
Zn(2)-O(2)	2.0676(17)
Zn(2)-N(1)	2.093(2)
Zn(2)-N(2)	2.148(2)
Zn(2)-Cl(1)	2.3043(7)

Bond	Bond angle (°)
O(2)-Zn(1)-O(2')	147.93(10)
O(2)-Zn(1)-O(1')	125.70(7)
O(2')-Zn(1)-O(1')	77.47(7)
O(2)-Zn(1)-O(1)	77.47(7)
O(2')-Zn(1)-O(1)	125.70(7)
O(1')-Zn(1)-O(1)	96.86(10)
O(2)-Zn(1)-O(4')	86.27(6)
O(2')-Zn(1)-O(4')	73.08(6)
O(1')-Zn(1)-O(4')	148.02(6)
O(1)-Zn(1)-O(4')	90.41(7)
O(2)-Zn(1)-O(4)	73.08(6)
O(2')-Zn(1)-O(4)	86.27(6)
O(1')-Zn(1)-O(4)	90.41(7)
O(1)-Zn(1)-O(4)	148.02(6)
O(4')-Zn(1)-O(4)	99.74(9)
O(1)-Zn(2)-O(2)	75.82(6)
O(1)-Zn(2)-N(1)	92.50(8)
O(2)-Zn(2)-N(1)	133.30(8)
O(1)-Zn(2)-N(2)	162.33(8)
O(2)-Zn(2)-N(2)	88.58(8)
N(1)-Zn(2)-N(2)	92.28(9)
O(1)-Zn(2)-Cl(1)	104.01(5)
O(2)-Zn(2)-Cl(1)	116.74(5)
N(1)-Zn(2)-Cl(1)	109.95(6)
N(2)-Zn(2)-Cl(1)	90.29(6)
Zn(1)-O(1)-Zn(2)	103.05(7)

Appendix B: DOSY NMR Spectra

B.1. DOSY NMR Spectra of Complexes Reported in Chapter 3.

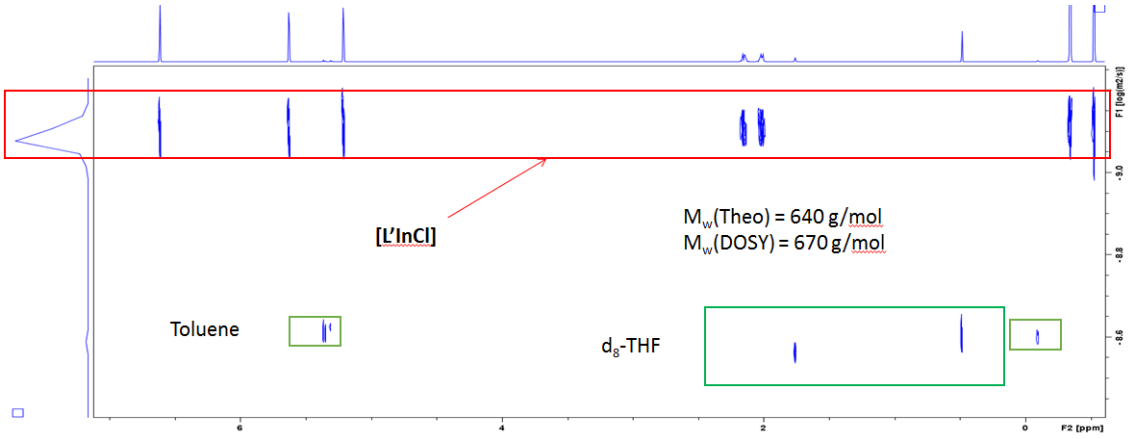

Figure B.1. DOSY NMR spectrum of **[L'InCl]** (d_8-THF, 298 K).

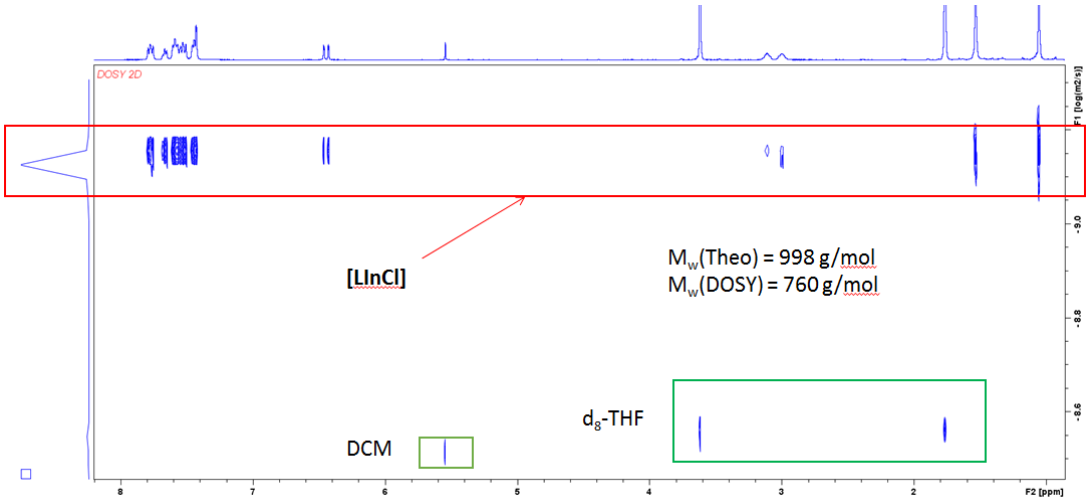

Figure B.2. DOSY NMR spectrum of **[LInCl]** (d_8-THF, 298 K).

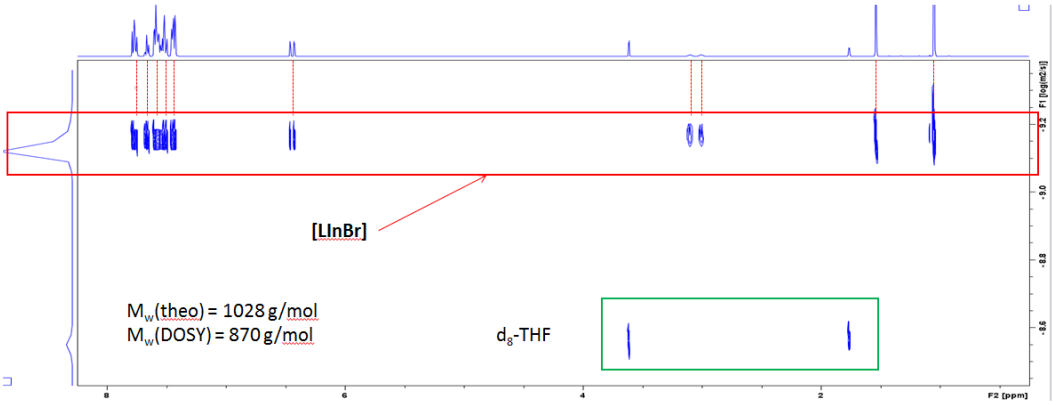

Figure B.3. DOSY NMR spectrum of **[LInBr]** (d_8-THF, 298 K). As it can be seen from the DOSY, there is no mixing of the d_8-THF and LInBr resonances indicating that THF is not coordinating to indium in solution.

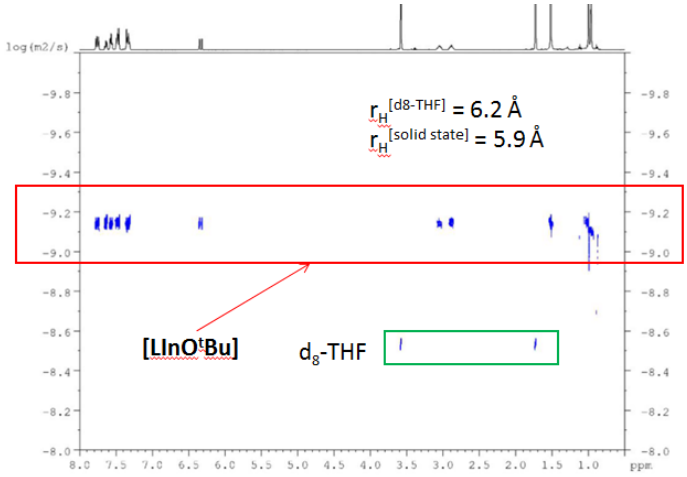

Figure B.4. DOSY NMR spectrum of **[LInO^{t}Bu]** (d_8-THF, 298 K).‡

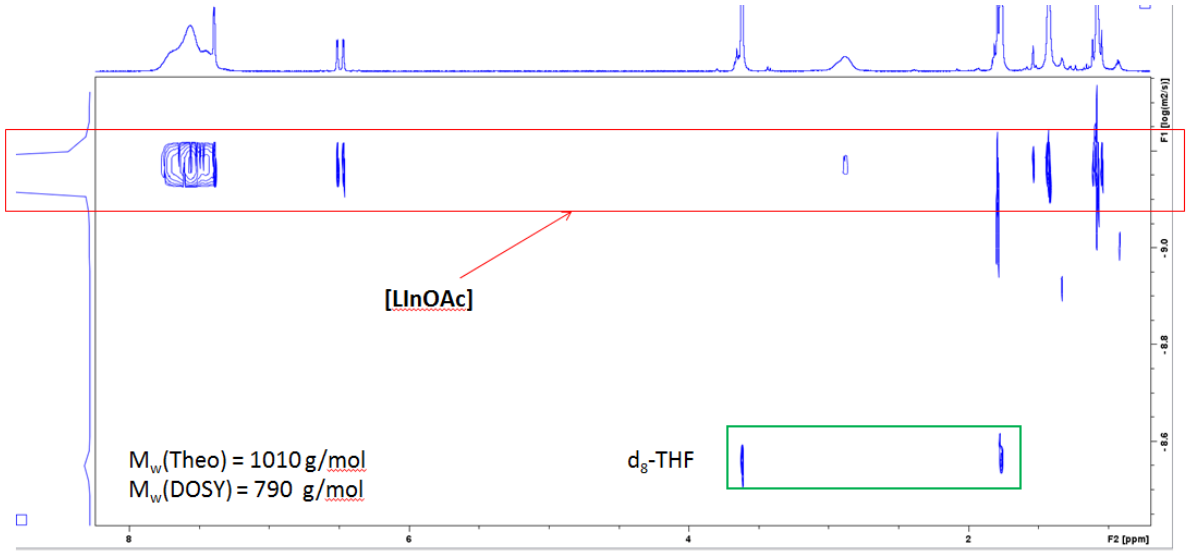

Figure B.5. DOSY NMR spectrum of **[LInOAc]** (d_8-THF, 298 K).

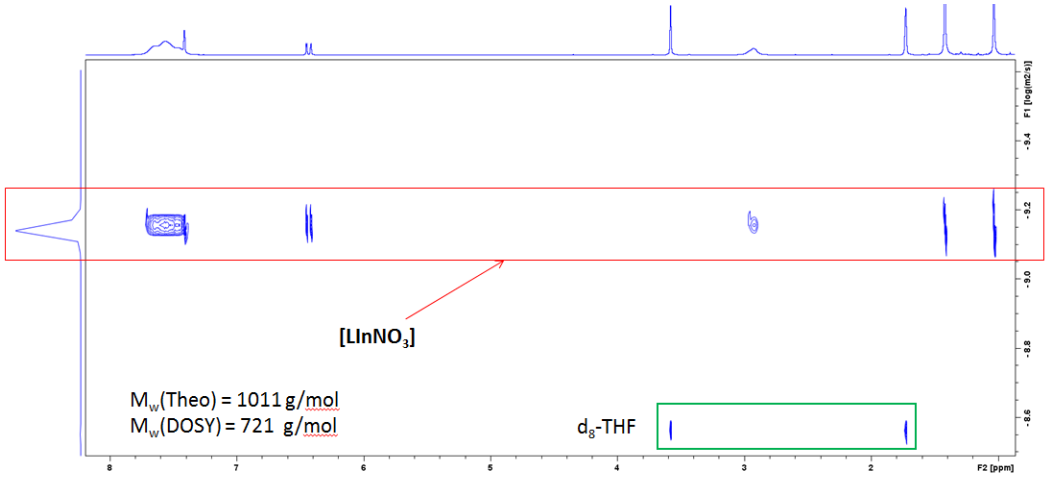

Figure B.6. DOSY NMR spectrum of **[LInNO$_3$]** (d_8-THF, 298 K).

‡ DOSY NMR performed by Dr Dominic Myers at Imperial College London.

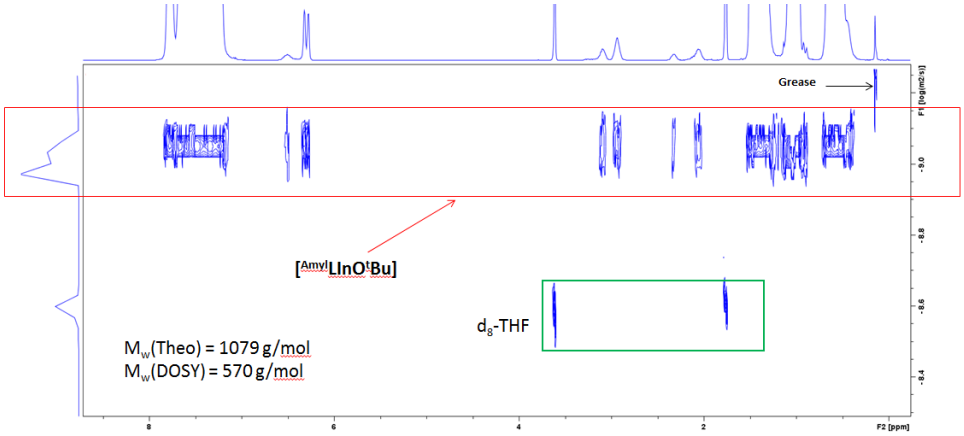

Figure B.7. DOSY NMR spectrum of **[^{Amyl}LInO^{t}Bu]** (d_8-THF, 298 K).

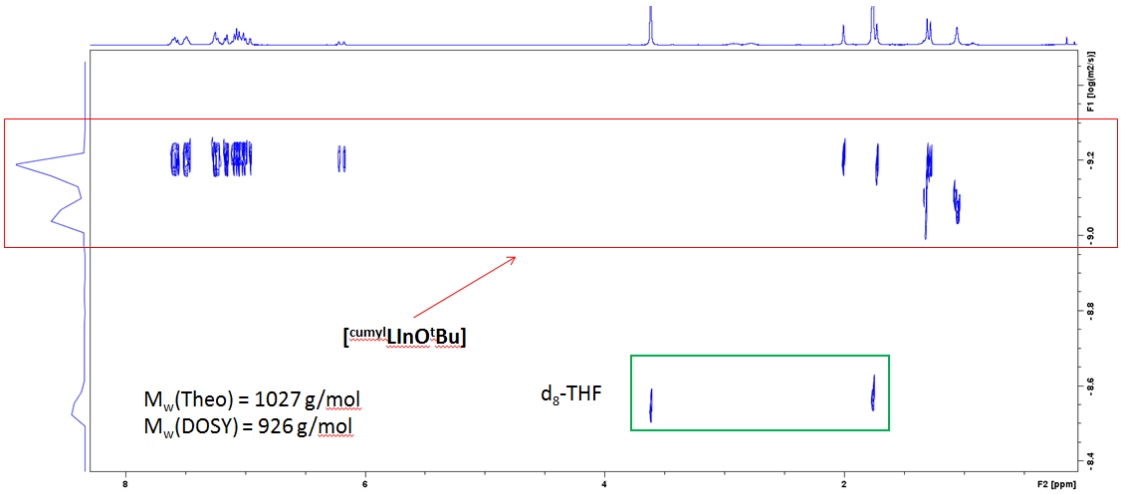

Figure B.8. DOSY NMR spectrum of **[^{Cumyl}LInO^{t}Bu]** (d_8-THF, 298 K).

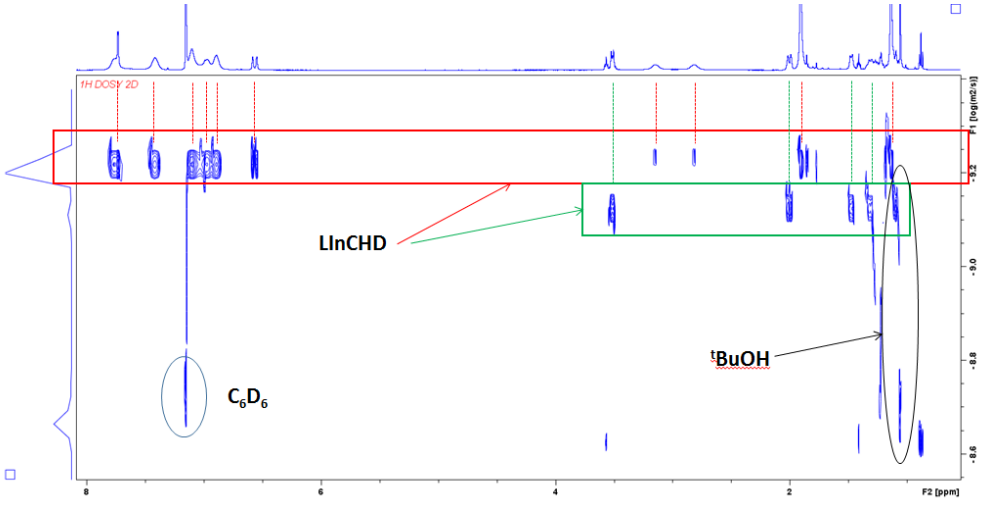

Figure 9. DOSY NMR spectrum of **[LInCHD]** (C_6D_6, 298 K).

B.2. DOSY NMR Spectra of Complexes Reported in Chapter 6.

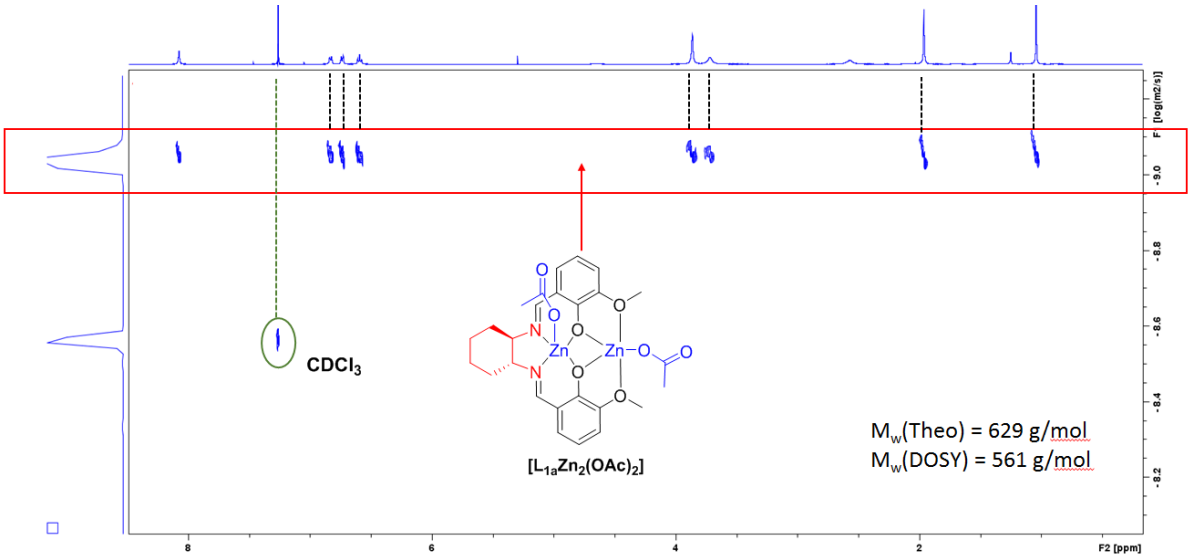

Figure B.10. DOSY spectrum of **[$L_{1a}Zn_2(OAc)_2$]** ($CDCl_3$, 298 K).

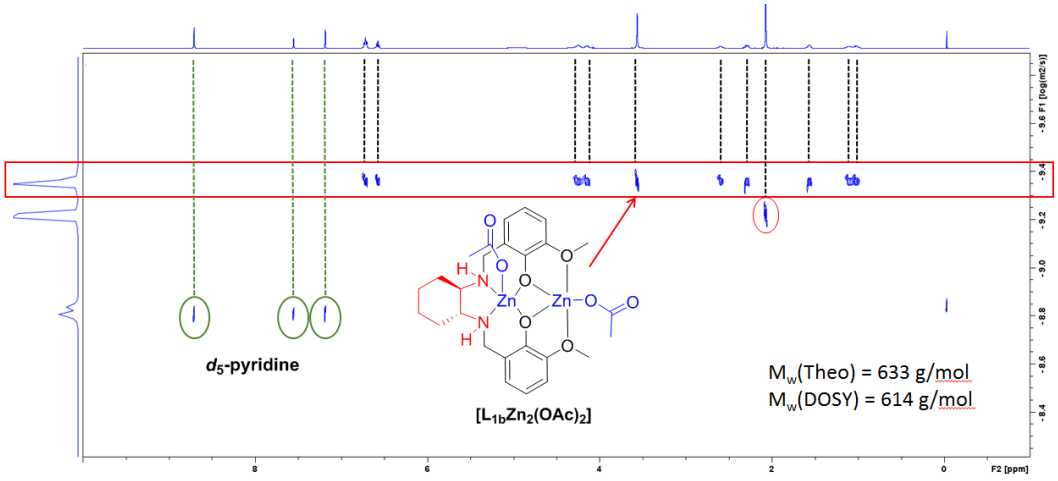

Figure B.11. DOSY spectrum of **[$L_{1b}Zn_2(OAc)_2$]** (d_5-pyr, 298 K). The acetate signal is not perfectly aligned with the rest of the product due to residual acetic acid, which is interacting with the acetate group.

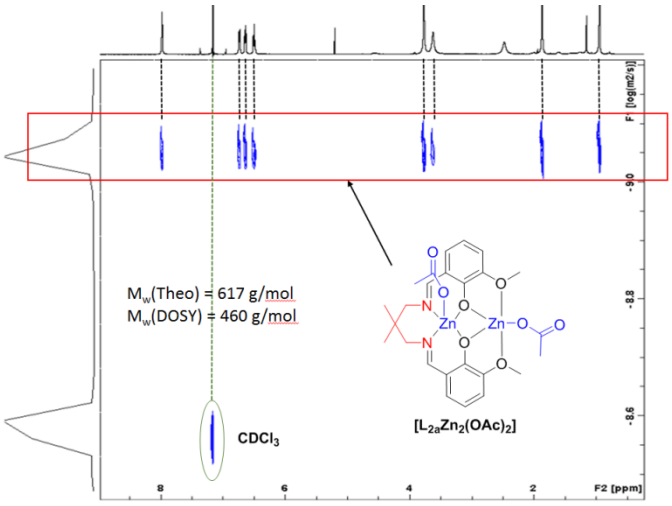

Figure B.12. DOSY spectrum of **[$L_{2a}Zn_2(OAc)_2$]** ($CDCl_3$, 298 K).

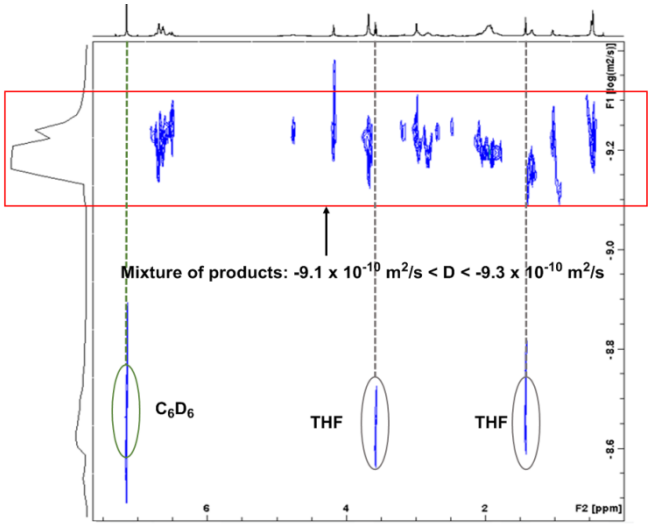

Figure B.13. DOSY spectrum of the mixture of product obtained from the reaction of $\mathbf{L_{2b}H}$ with 2 equivalents of $[Zn(OAc)_2]$ (C_6D_6, 298 K).

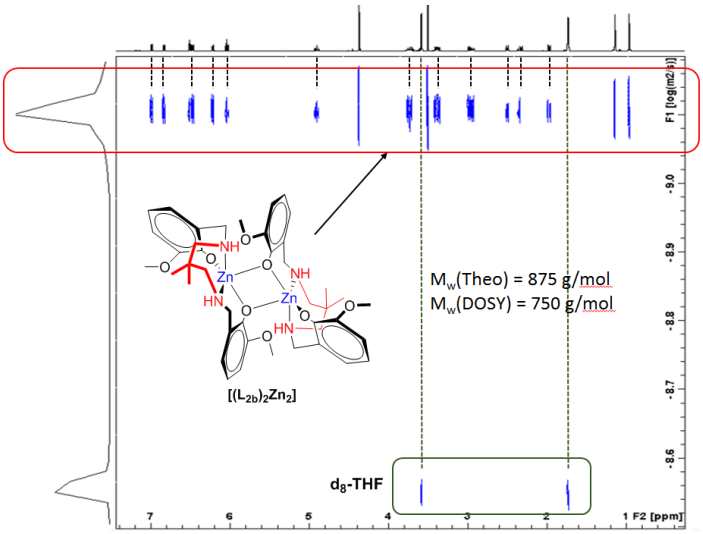

Figure B.14. DOSY spectrum of $\mathbf{[(L_{2b})_2Zn_2]}$ (d_8-THF, 298 K).

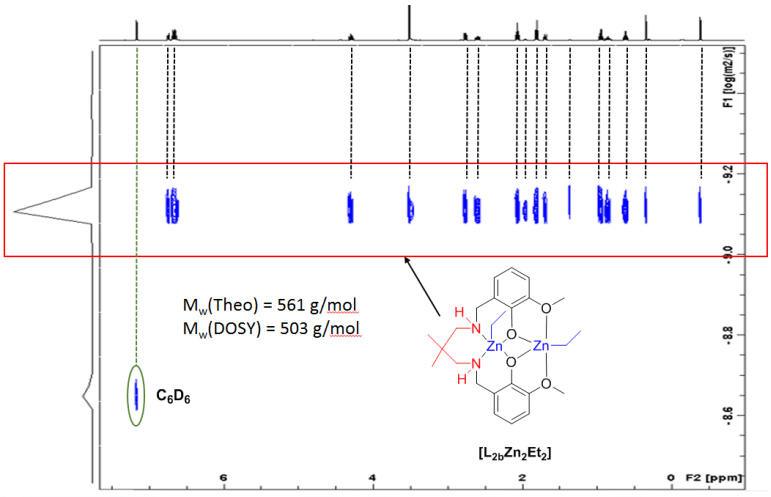

Figure B.15. DOSY spectrum of $\mathbf{[L_{2b}Zn_2Et_2]}$ (C_6D_6, 298 K).

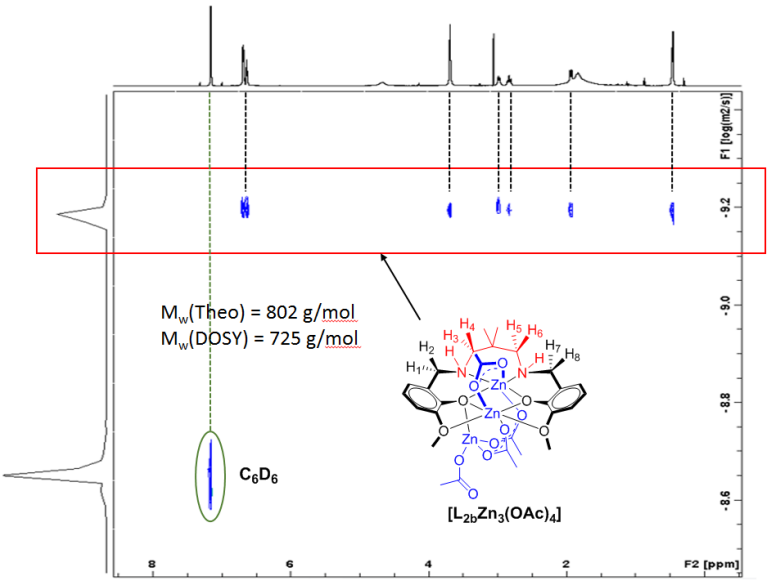

Figure B.16. DOSY spectrum in C_6D_6 of **$[L_{2b}Zn_3(OAc)_4]$** (C_6D_6, 298 K).

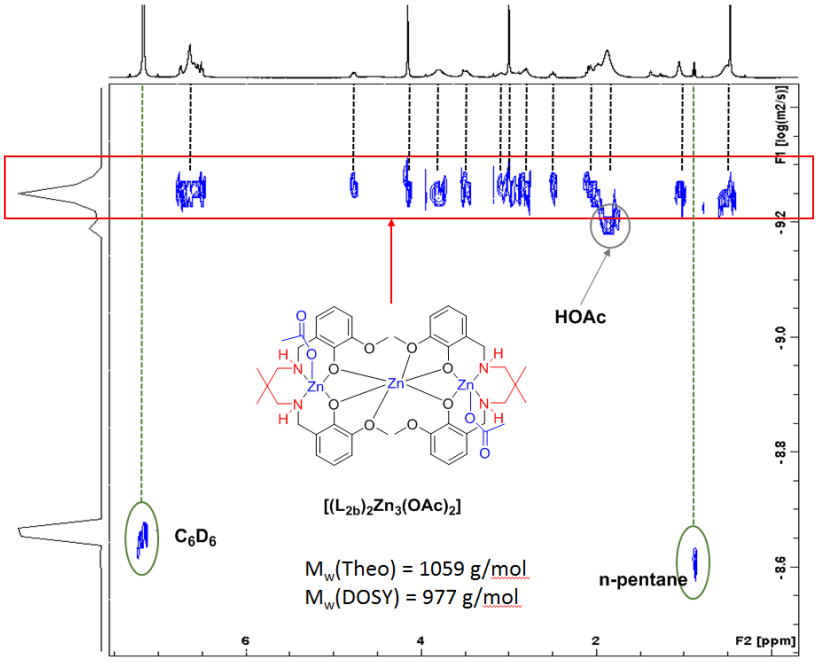

Figure B.17. DOSY spectrum of **$[(L_{2b})_2Zn_3(OAc)_2]$** (C_6D_6, 298 K).

Appendix C: Line Shape Analysis

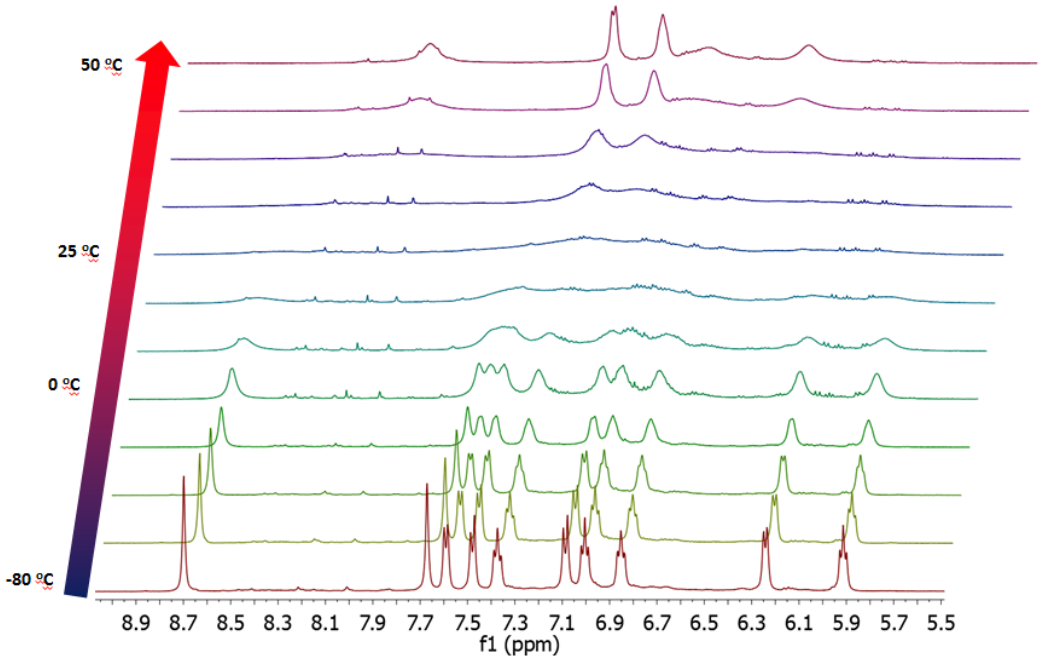

Figure C.1. Overlaid of ^{1}H NMR spectra of **[L^{Et}Zn$_2${N(SiMe$_3$)$_2$}]** from 193 K (bottom spectrum) to 333 K (top spectrum) with ΔT = 10 K (d_8-THF).

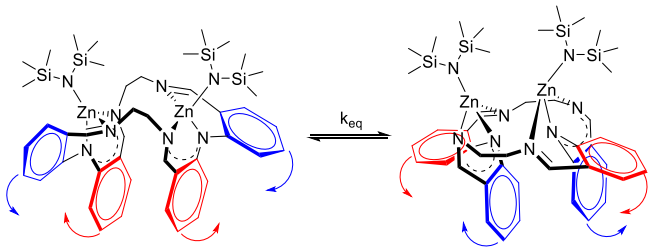

Figure C.2. Proposed equilibrium between two conformers of **[L^{Et}Zn$_2${N(SiMe$_3$)$_2$}$_2$]**.

Determination of the Gibbs free energy of the equilibrium illustrated in Figure C.2 from variable temperature ^{1}H NMR spectra analysis (Figure C.1).

$$\Delta G^{\neq} = RT_c[22.96 + ln\left(\frac{T_c}{\Delta\delta}\right)]$$

Where R is the gas constant [8.314 J(mol.K)$^{-1}$]; T_c is the coalescence temperature (273 K); Δδ is the chemical shift difference between the two imine signals at 173 K (408 Hz).

$$\Delta G^{\neq} = 8.314 * 283 * \left[22.96 + ln\left(\frac{283}{408}\right)\right] = 55'000\, J$$

With 1 kCal = 4.8314 KJ

$$\Delta G^{\neq} = 13\ kCal$$

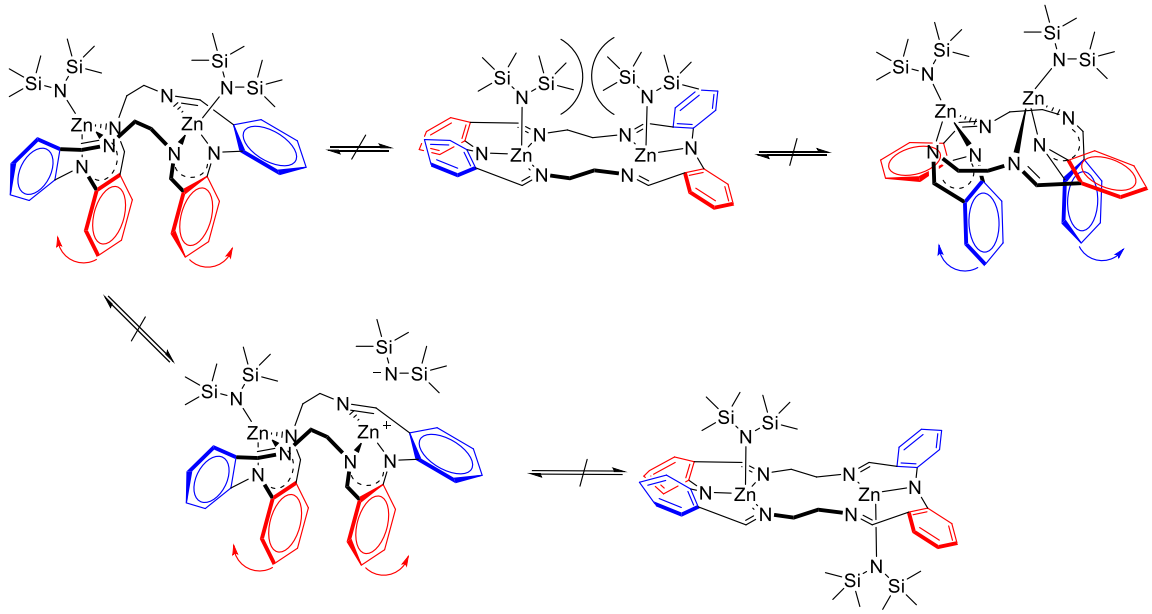

Figure C.3. Other, less favourable, equilibriums. The top route involves the formation of a planar geometry which is not favourable due to the bulk of the amido co-ligand and the loss of the π-π interaction between the two opposite phenyl units. The formation of a planar complex **[L^{Et}Zn$_2${N(SiMe$_3$)$_2$}]** as proposed in the second route would involve a dissociative procedure where first the breaking of the [Zn-N(SiMe$_3$)$_2$] bond occurs, then formation of a planar complex and finally re-coordination of the amido on the opposite face of the complex. The solid state structure of **[L^{Et}Zn$_2${N(SiMe$_3$)$_2$}$_2$]** indicates the [Zn-N(SiMe$_3$)$_2$] bonds {[Zn-N(SiMe$_3$)$_2$] = 1.941(2) Å} are larger than other BDI zinc amido complexes {[Zn-N(SiMe$_3$)$_2$] ≈ 1.890(2) Å}[1] but in the same range as other half salen and imine ligands {[Zn-N(SiMe$_3$)$_2$] = 1.940 Å}.[2] The dissociation is therefore considered to be unfavourable.

Appendix D: $^{13}C\{^1H\}$ NMR and DOSY NMR Spectra of Polymers

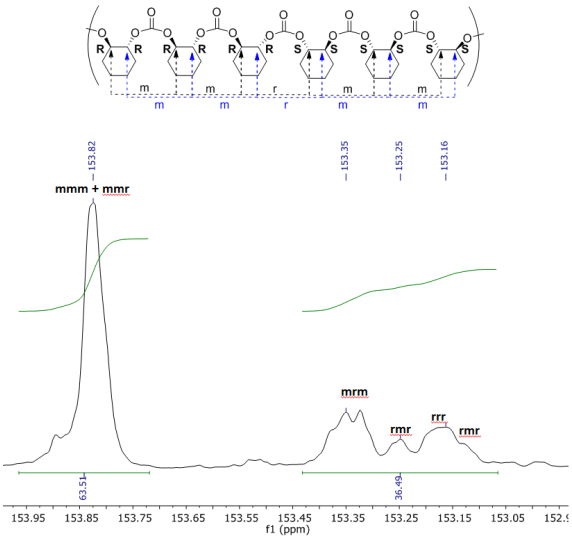

Figure D. 1. $^{13}C\{^1H\}$ NMR spectrum ($CDCl_3$, 298 K) of PCHC catalysed by **[LInO^{t}Bu]** expended in the carbonyl region. The sketch illustrates how each tetrad was assigned.

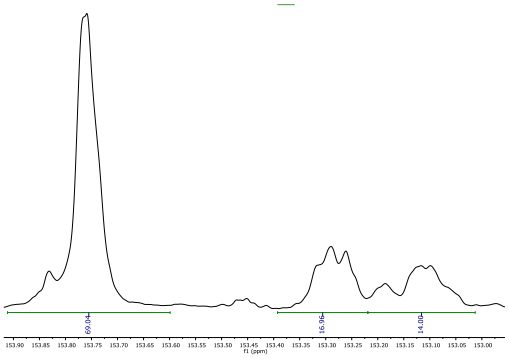

Figure D.2. $^{13}C\{^1H\}$ NMR spectra of PCHC (298 K, $CDCl_3$) catalysed by **[^{Amyl}LInO^{t}Bu]** expended in the carbonyl region.

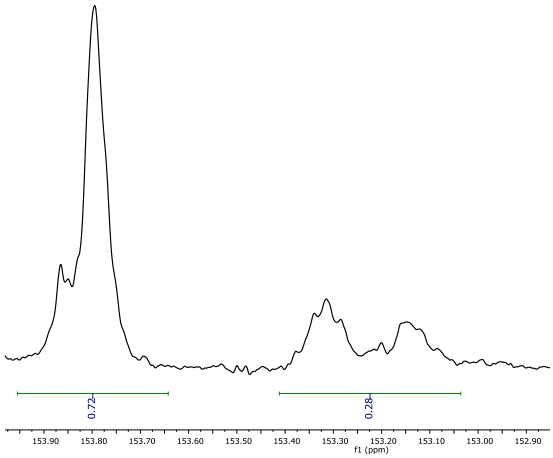

Figure D.3. $^{13}C\{^1H\}$ NMR spectrum of PCHC (298 K, $CDCl_3$) catalysed by **[^{Cumyl}LInO^{t}Bu]** expended in the carbonyl region.

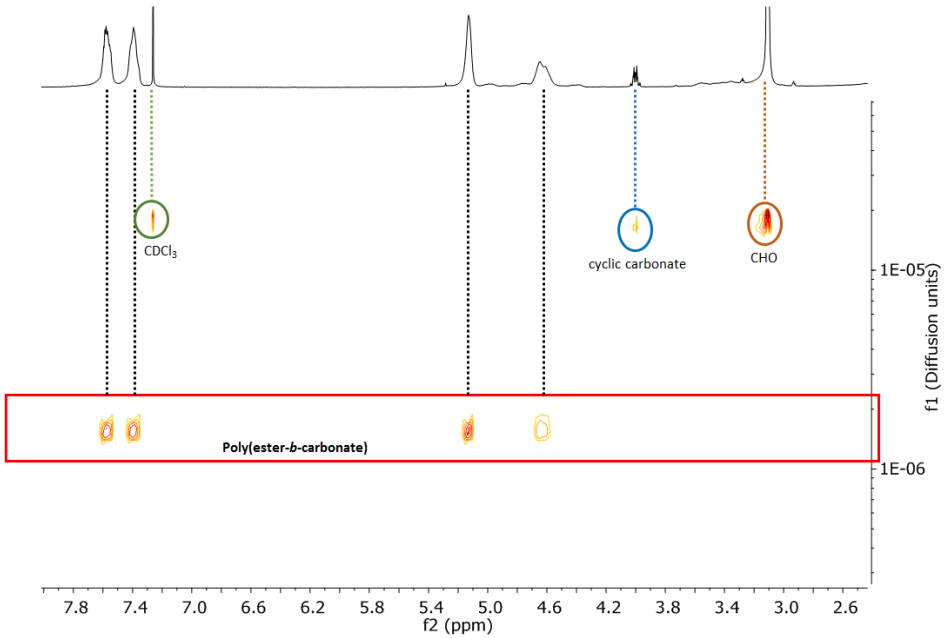

Figure D.4. DOSY NMR spectrum of the poly(ester-*b*-carbonate) catalysed by **[$L_{2a}Zn_2OAc_2$]** ($CDCl_3$, 298 K).

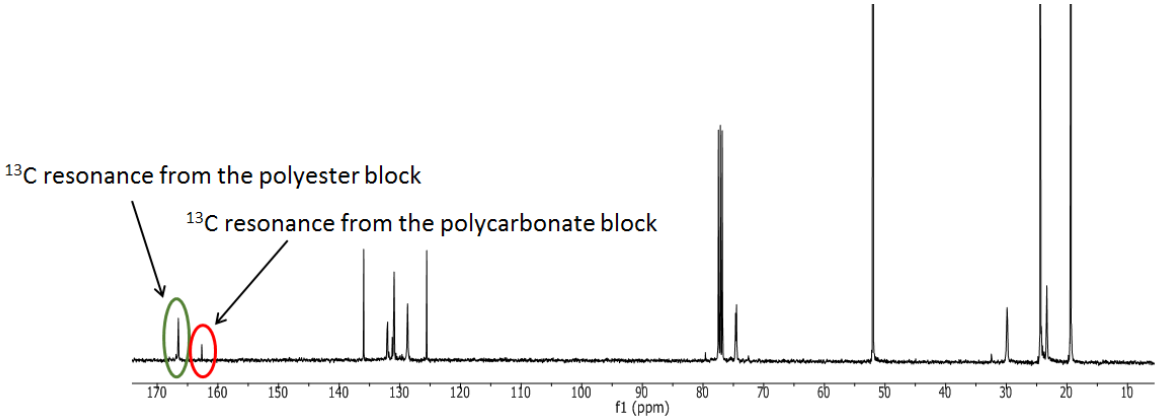

Figure D.5. ^{13}C NMR spectrum of the poly(ester-*b*-carbonate) catalysed by **[$L_{2a}Zn_2OAc_2$]** ($CDCl_3$, 298 K).

Appendix E: MALDI ToF Spectra of Polymers

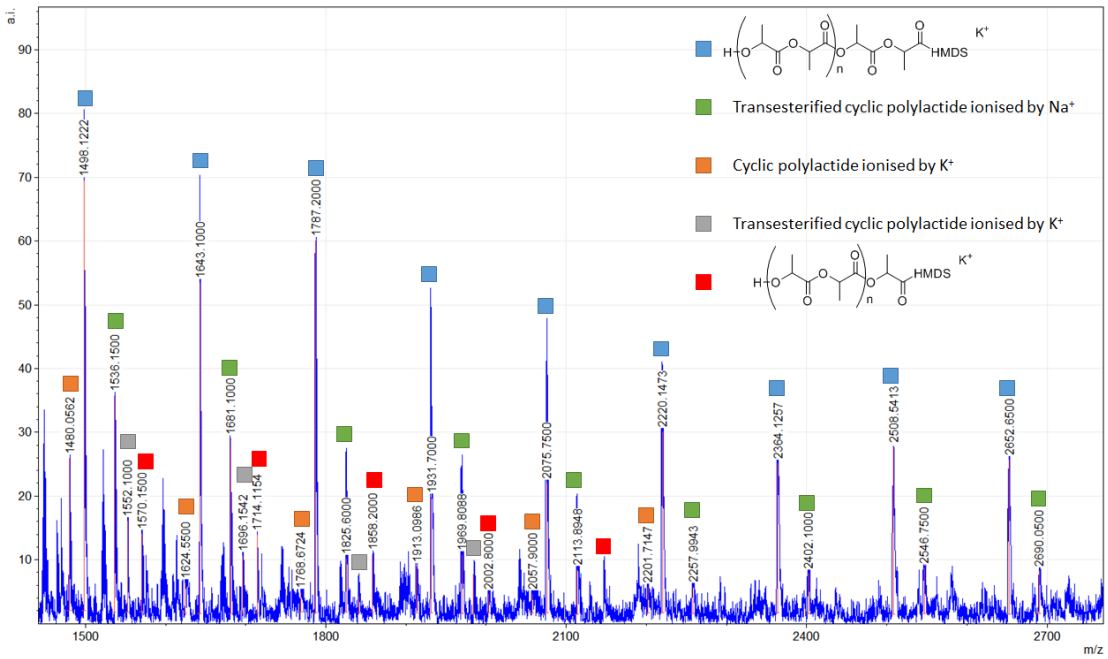

Figure E.1. Example of MALDI-ToF spectrum obtained for polylactide catalysed by zinc amido catalyst. In this case, the polymer was synthesised from **[L^{Pr}Zn$_2${N(SiMe$_3$)$_2$}]**, at 25 °C, in THF, in presence of 1000 equiv. of *rac*-LA.

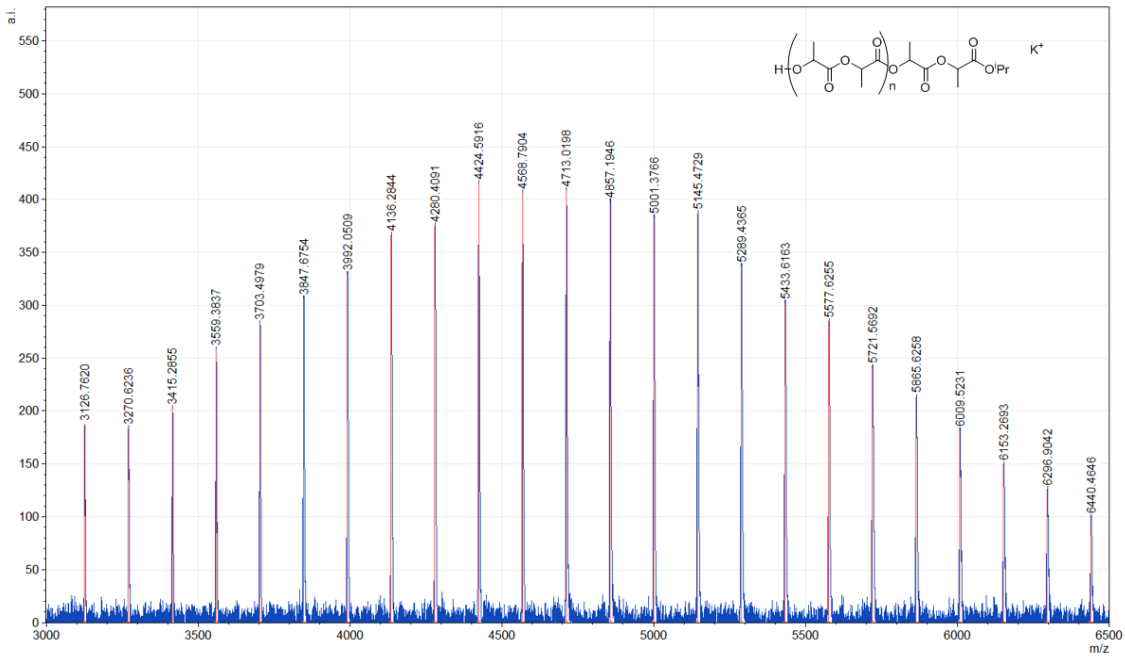

Figure E.2. Example of MALDI-ToF spectrum obtained for polylactide catalysed by an alkoxide catalyst. In this case, the polymer was synthesised using **[L^{Pr}Zn$_2$(OiPr)$_2$]**, at 25 °C, in THF, in presence of 1000 equiv. of rac-LA.

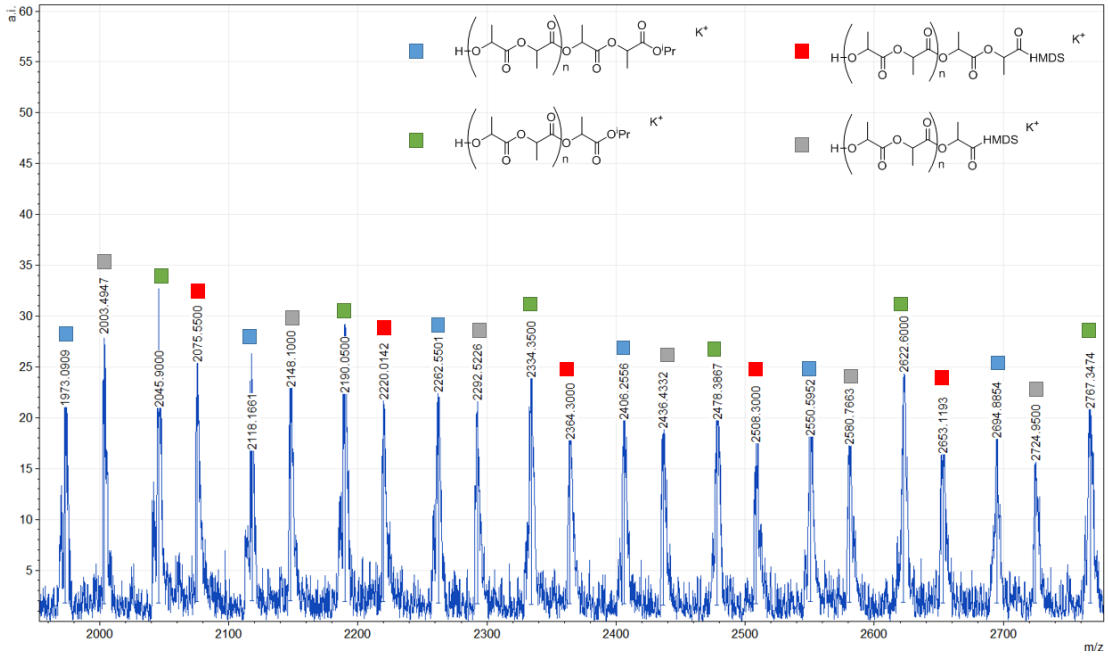

Figure E.3. Example of a MALDI-ToF spectrum obtained for an immortal polymerization reaction of *rac*-LA starting from a zinc amido pre-catalyst. In this case, the polymer was synthesised using **[L^{Open}Zn N(SiMe$_3$)$_2$]**, at 25 °C, in THF, with 10 equiv. of IPA, in presence of 1000eq of *rac*-LA.

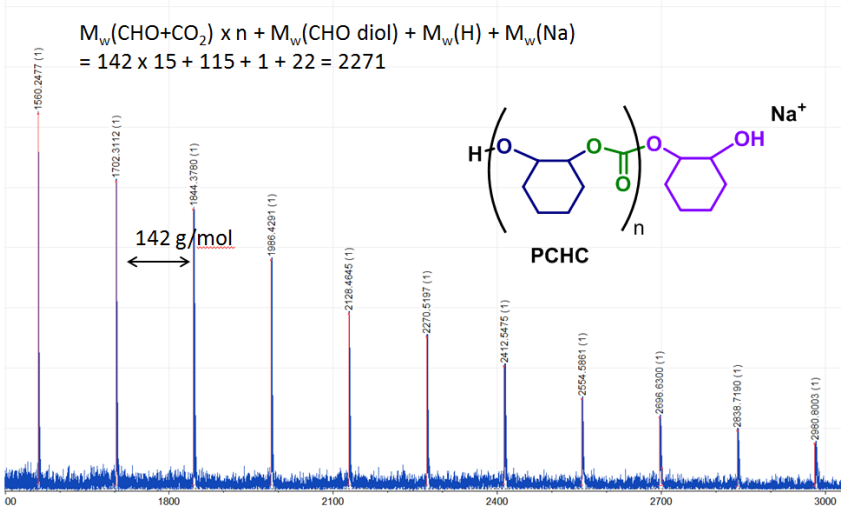

Figure E.4. Example of a MALDI-ToF spectrum of PCHC. In this case, the polymer has been synthesised using **[^{cumyl}LInO^{t}Bu]**, at 80 °C, 1 bar of CO_2, in CHO (neat).

Appendix F: SEC Traces

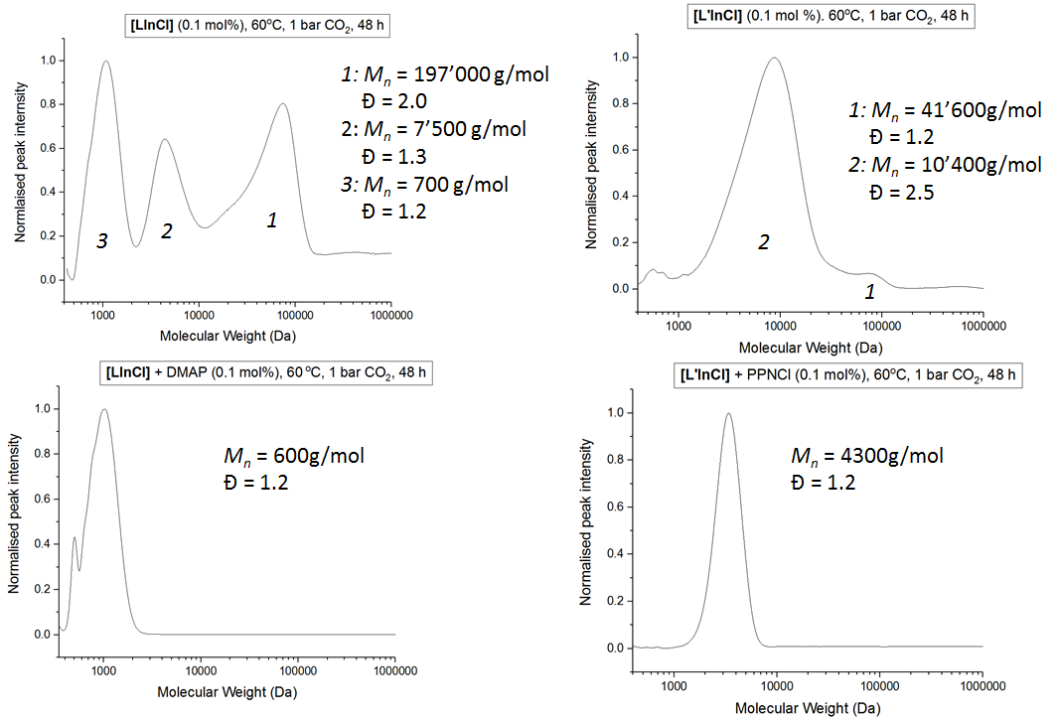

Figure F.1. SEC traces obtained for PCHC catalysed by **[LInCl]** (top left), **[L'InCl]** (top right), **[LInCl]** + DMAP (bottom left) and **[L'InCl]** + PPN-Cl (bottom right) at 60 °C, and 1 bar of CO_2, after 48 h of reaction.

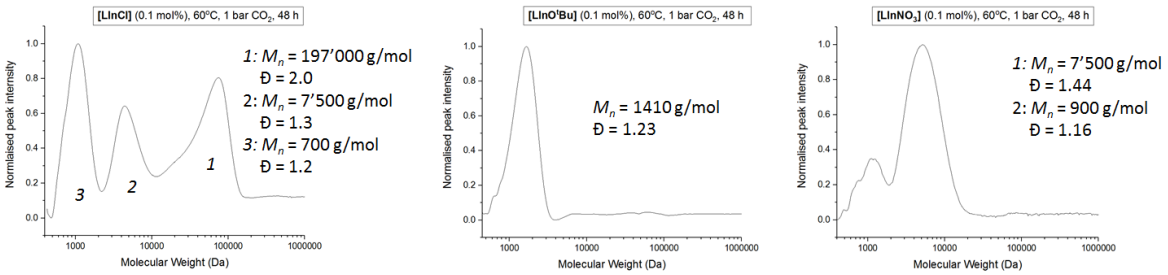

Figure F.2. SEC traces obtained for PCHC catalysed by **[LInCl]** (left), **[LInO^{t}Bu]** (middle) and **[LInNO$_3$]** (right) at 60 °C, and 1 bar of CO_2, after 48 h of reaction.

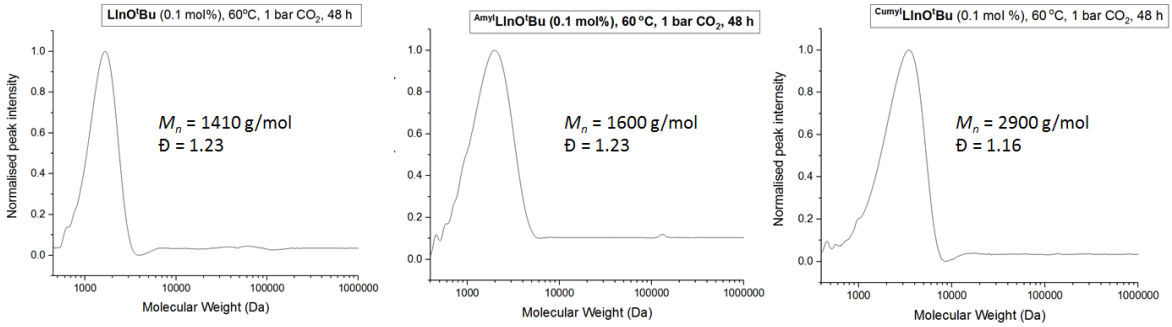

Figure F.3. SEC traces obtained for PCHC catalysed by **[LInO^{t}Bu]** (left,) **[^{Amyl}LInO^{t}Bu]** (middle) and **[^{Cumyl}LInO^{t}Bu]** (right) at 60 °C and 1 bar of CO_2 after 48 h of reaction.

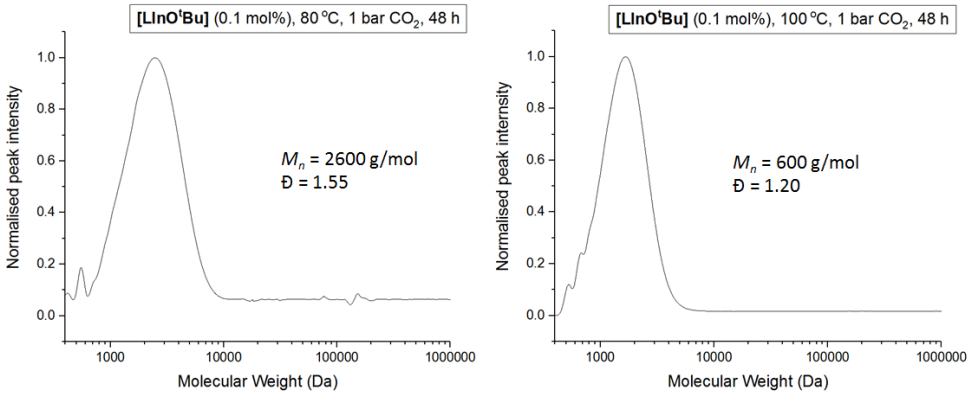

Figure F.4. SEC traces obtained for PCHC, catalysed by **[LInO^{t}Bu]**, at 80 °C (right spectrum) and 100 °C (left spectrum), for 48 h reaction, at 1 bar of CO_2 pressure.

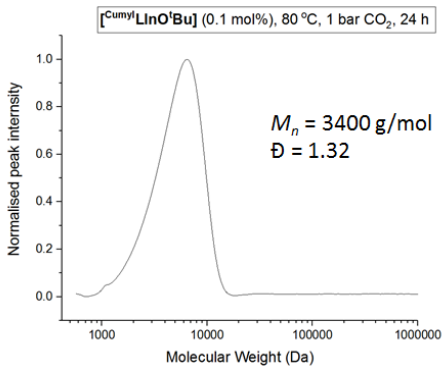

Figure F.5. SEC trace of PCHC, obtained using **[^{cumyl}LInO^{t}Bu]** (0.1 mol%), at 80 °C, at 1 bar of CO_2, after 24 h of reaction.

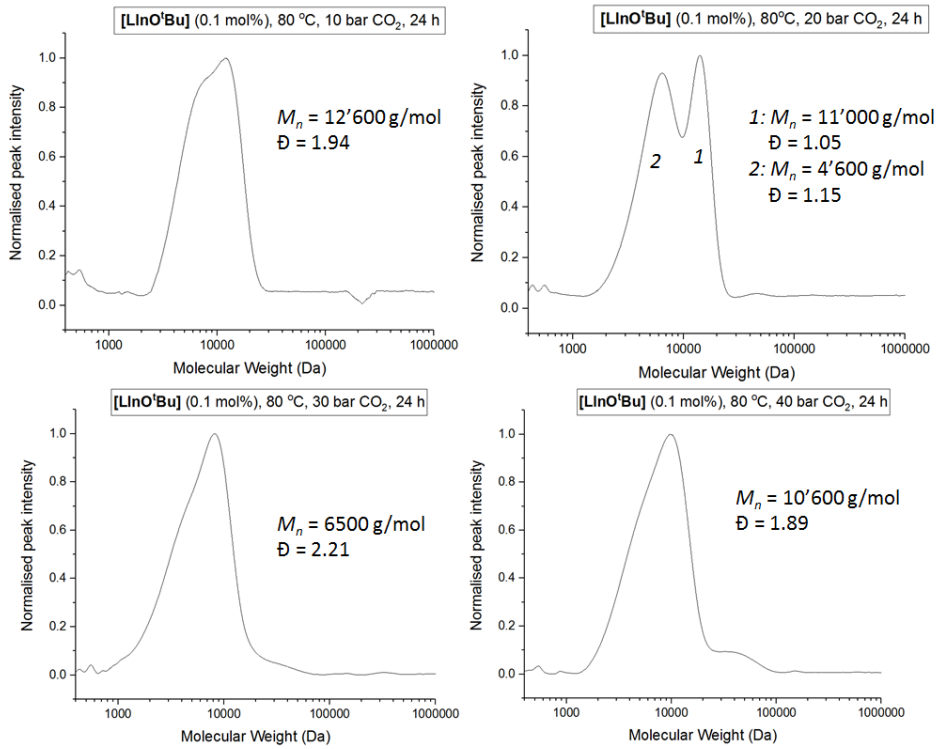

Figure F.6. SEC traces obtained for PCHC, catalysed by **[LInO^{t}Bu]** at 80 °C, for 24 h, at different CO_2 pressure: 10 bar (top left), 20 bar (top right), 30 bar (bottom left) and 40 bar (bottom right).

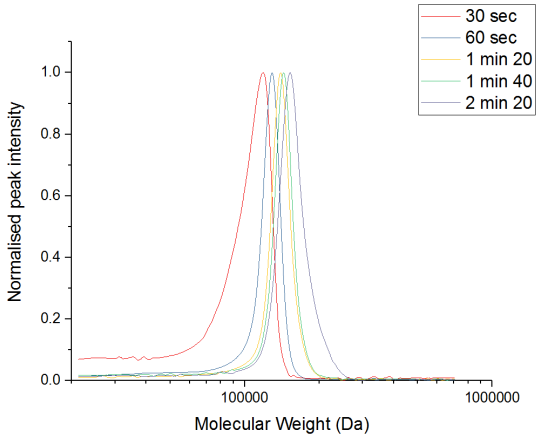

Figure F.7. Example of SEC obtained for polylactide catalysed by zinc amido initiator. In this case, the spectrum shows an overlap of SEC traces of polylactide catalysed by **[L^{Open}ZnN(SiMe$_3$)$_2$]** (0.1 mol%). Conditions: [rac-LA] = 1M, THF, 25 ^{o}C.

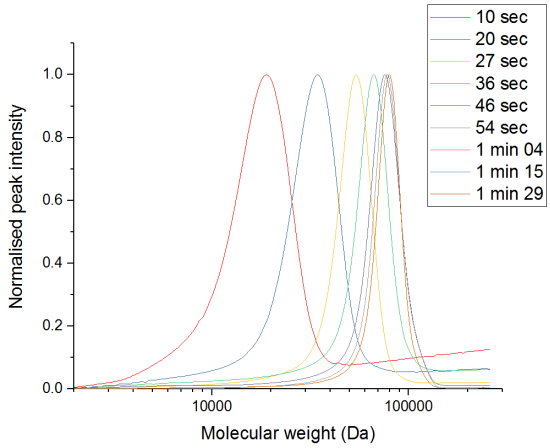

Figure F.8. Example of SEC obtained for polylactide catalysed by zinc alkoxide initiator. In this case, the spectrum shows an overlap of SEC traces of polylactide catalysed by **[L^{Open}Zn(O^{i}Pr)]** (0.1 mol%). Conditions: [rac-LA] = 1M, THF, 25 ^{o}C.

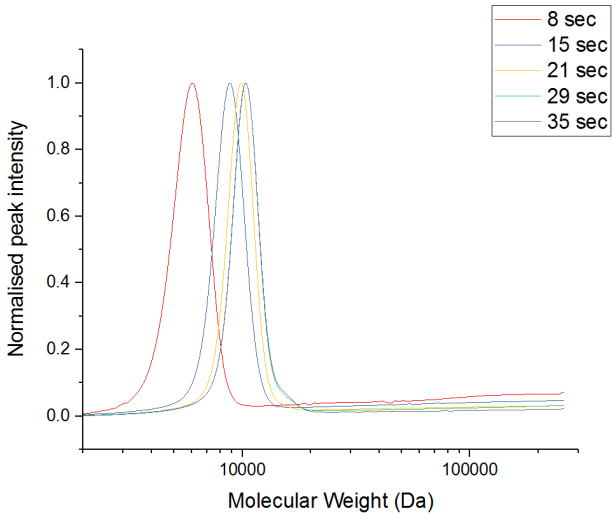

Figure F.9. Example of SEC obtained for polylactide catalysed by zinc amido initiator under immortal conditions. In this case, the spectrum shows an overlap of SEC traces of polylactide catalysed by **[L^{Et}Zn$_2${N(SiMe$_3$)}$_2$]** (Conditions: [cat] = 0.1 mol%, [rac-LA] = 1M, THF, 10 equiv isopropanol, 25 ^{o}C).

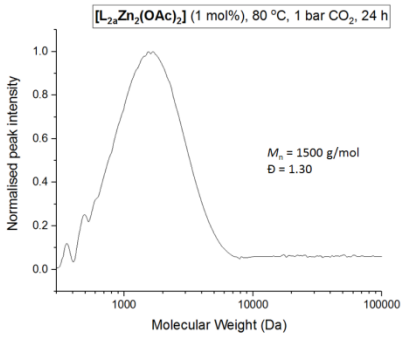

Figure F.10. Example of a SEC trace obtained for polycarbonate catalysed by dinuclear zinc complexes at low CO_2 pressure. In this case, PCHC has been catalysed by **$[L_{2a}Zn_2(OAc)_2]$**.

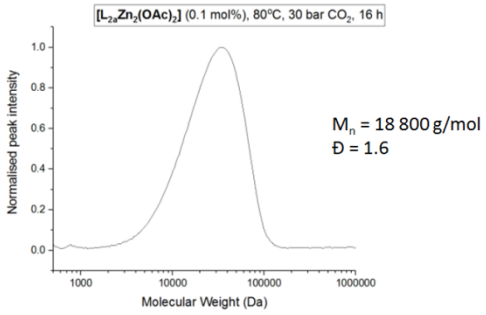

Figure F.11. Example of a SEC trace obtained for polycarbonate catalysed by dinuclear zinc complexes at high CO_2 pressure. In this case, PCHC has been catalysed by **$[L_{2a}Zn_2(OAc)_2]$**.

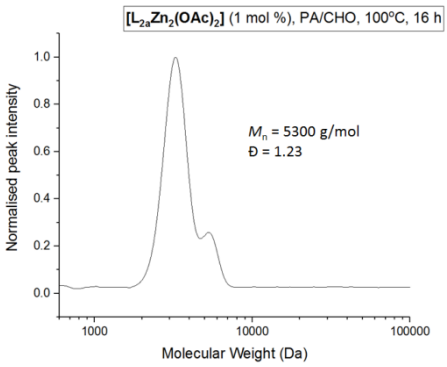

Figure F.12. Example of a SEC trace obtained for polyester (PA/CHO) catalysed by dinuclear zinc complexes, at 100 °C. In this case, the polyester has been catalysed by **$[L_{2a}Zn_2(OAc)_2]$**.

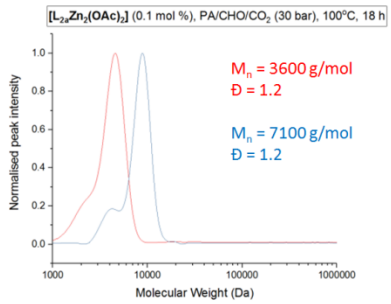

Figure F.13. Overlap of SEC traces corresponding to two aliquots taken after 2 h and 18 h during PA/CHO/CO_2 terpolymerization catalysed by **$[L_{2a}Zn_2(OAc)_2]$** (0.1 mol%), at 100 °C, 30 bar of CO_2.

Appendix G: Kinetic Plots

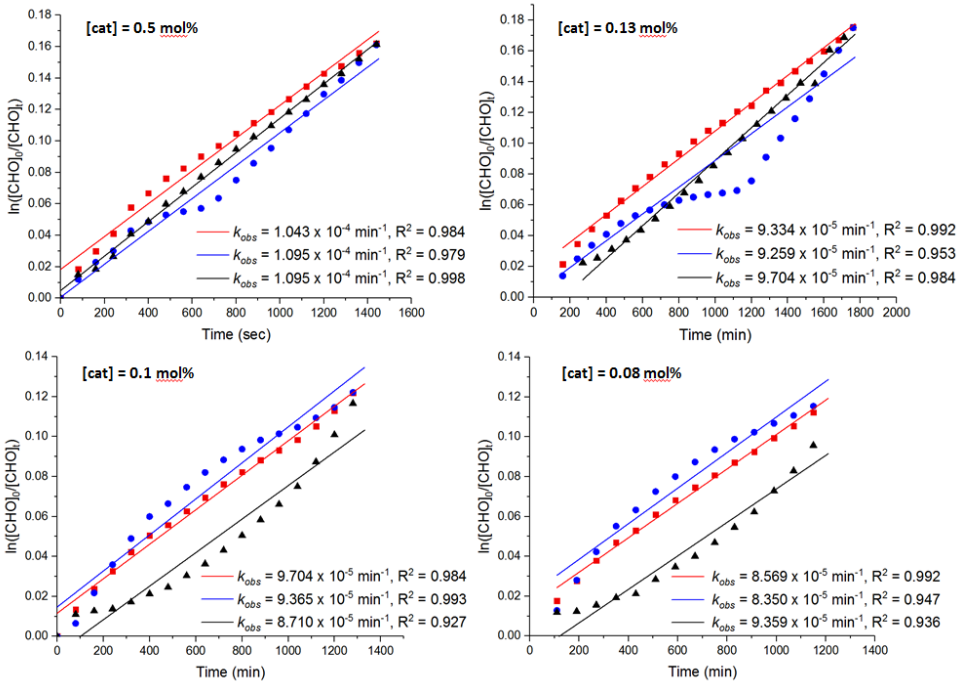

Figure G.1. Overlay of semi-logarithmic pseudo first-order plots for the copolymerization of CHO/CO_2 initiated from **LInO^{t}Bu** obtained at three different specific IR bands assigned to PCHC: C=O stretch at 1787-1731 cm^{-1} (▲), the C-O-C symmetric stretch at 1239-1176 cm^{-1} (●) and a polymer mode at 1014 cm^{-1} (■). Initial rates are determined from the slope of the linear fitting of each band and correspond to 0-20 % conversion.

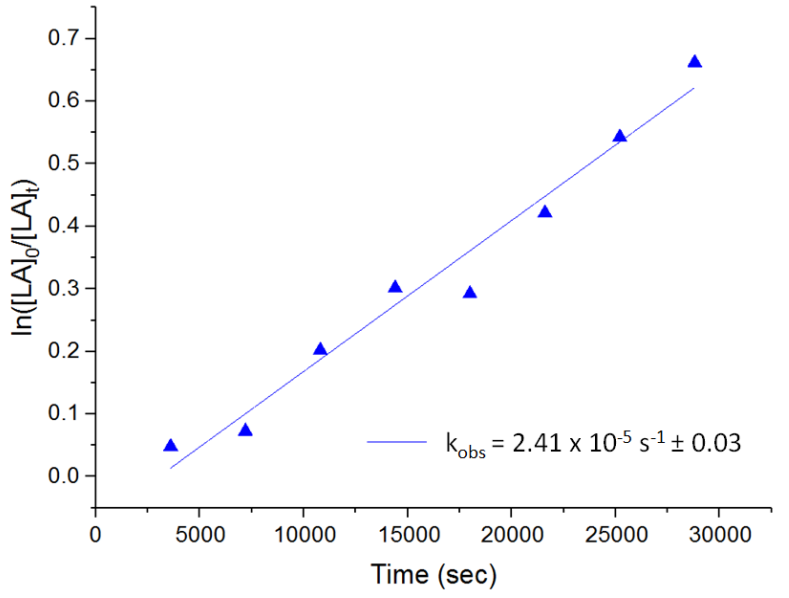

Figure G2. Plot of ln([LA_0]/[LA_t]) against time for **[$L^{Et}Zn_2(O^iPr)_2$]** (▲) with 1000 equivalents of *rac*-LA. Conditions: [rac-LA] = 1M, THF, 25 ^oC.

Appendix H: $^{1}H\{^{1}H\}$ NMR Spectrum

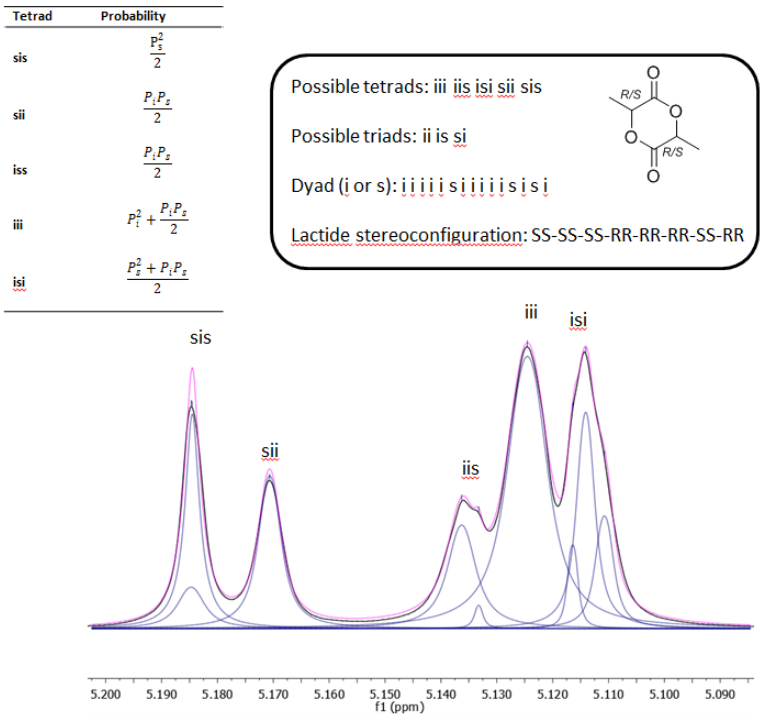

Figure H.1. General example of a $^{1}H\{^{1}H\}$ NMR spectrum zoomed in the methyne region of PLA in $CDCl_3$ at 298 K (in this case, $P_i = 0.54$).

References

[1] B. M. Chamberlain, M. Cheng, D. R. Moore, T. M. Ovitt, E. B. Lobkovsky, G. W. Coates, *J. Am. Chem. Soc.* **2001**, *123*, 3229-3238.

[2] a) S. Abbina, G. Du, *ACS Macro Letters* **2014**, *3*, 689-692; b) D. J. Darensbourg, W. Choi, O. Karroonnirun, N. Bhuvanesh, *Macromolecules* **2008**, *41*, 3493-3502.